FABAD

JOURNAL of PHARMACEUTICAL SCIENCES

CONTENTS

Research Articles

Review Articles

Evaluation of the Genotoxic Impurities of Selpercatinib Through HPLC and LC-MS/MS Identification of Selpercatinib Stress Degradation Products

Bheemireddy DIVYA*, J Murali PRAKASH**, Eevana Venkata CHIRANJEEVI***, Bhaskara Rao TADIBOINA*****°

Evaluation of the Genotoxic Impurities of Selpercatinib Through HPLC and LC-MS/MS Identification of Selpercatinib Stress Degradation Products

SUMMARY

The current investigation entails the characterization of five degradation products (DPs) formed in different stress conditions of selpercatinib employing liquid chromatography–tandem mass spectrometry (LC-MS/MS). Additionally, high-performance liquid chromatographic (HPLC) method was developed for precise quantifying genotoxic impurities of selpercatinib. To explore the stability profile of selpercatinib, it was subjected to forced degradation experiments including acidic, basic, oxidative, photolytic, and thermal stress. These experiments revealed the degradation of selpercatinib under basic, acidic, and photolytic conditions, resulting in the formation of five distinct DPs. The chromatographic resolution of selpercatinib and its impurities, along with DPs, was effectively attained on a Zorbax C18 (250 mm × 4.6 mm, 5 μm) column using aqueous ammonium acetate and methanol in 70:30 (v/v) at pH 4.5 with 0.1% formic acid as the mobile phase, pumped isocratically at 0.9 mL/min and 226 nm wavelength. The approach generates a precise calibration curve that accurately fits within the 15-120 μg/mL range for selpercatinib and LOQ (0.015 μg/mL) to 0.12 μg/mL for impurities with acceptable precision, accuracy, and recovery. The efficacy of this method was validated through LC-MS/MS, which allowed for the verification of the chemical structures of newly generated degradation products of selpercatinib. Hence, this approach can be appropriate for the resolution and quantification of genotoxic impurities in selpercatinib and can also be applicable for the evaluation of stress degradation products.

***Key Words:** Selpercatinib, HPLC method development, impurities quantification, forced degradation studies, degradation products, structural characterization.*

Selperkatinibin Genotoksik Safsızlıklarının HPLC ile Değerlendirilmesi ve Selperkatinib Stres Bozulma Ürünlerinin LC-MS/MS Tanımlaması

ÖZ

Mevcut araştırma, sıvı kromatografi-tandem kütle spektrometrisi kullanılarak selperkatinibin farklı stres koşullarında oluşan beş bozunma ürününün (DP'ler) karakterizasyonunu içerir. Ek olarak, selperkatinibin genotoksik safsızlıklarının kesin olarak ölçülmesi için yüksek performanslı sıvı kromatografisi (HPLC) yöntemi geliştirilmiştir. Selperkatinibin stabilite profilini araştırmak için asidik, bazik, oksidatif, fotolitik ve termal stres dahil olmak üzere zorunlu bozunma deneyleri yapılmıştır. Bu deneyler, selpercatinibin bazik, asidik ve fotolitik koşullar altında bozunduğunu ve bunun sonucunda beş farklı DP'nin oluştuğunu ortaya çıkarmıştır. Selperkatinib ve safsızlıklarının DP'lerle birlikte kromatografik ayrımı, mobil faz olarak %0.1 formik asit, izokratik olarak 0,9 mL/dak ve 226 nm dalga boyunda pompalanması ile pH 4.5'te 70:30 (h/h) sulu amonyum asetat ve metanol kullanılarak Zorbax C18 (250 mm x 4.6 mm, 5 μm) kolonunda etkin bir şekilde sağlanmıştır. Yaklaşım, selperkatinib için 15-120 μg/mL aralığına ve safsızlıklar için LOQ (0.015 μg/mL) 0.12 μg/mL aralığına kabul edilebilir hassasiyet, doğruluk ve geri kazanımla doğru bir şekilde uyan kesin bir kalibrasyon eğrisi oluşturmuştur. Bu yöntemin etkinliği, selperkatinibin yeni üretilen bozunma ürünlerinin kimyasal yapılarının doğrulanmasına olanak tanıyan LC-MS/MS aracılığıyla doğrulanmıştır. Dolayısıyla bu yaklaşım, selperkatinibin genotoksik safsızlıklarının ayrımı ve miktarının belirlenmesi için uygun olabilir ve aynı zamanda stres bozunma ürünlerinin değerlendirilmesi için de uygulanabilir.

***Anahtar Kelimeler:** Selperkatinib, HPLC yöntemi geliştirme, safsızlıkların ölçümü, zorunlu bozunma çalışmaları, bozunma ürünleri, yapısal karakterizasyon.*

* ORCID: , Department of Chemistry, Koneru Lakshmaiah Education Foundation, Vaddeswaram, Guntur - 522302, A.P., India
** ORCID: , Department of Chemistry, Koneru Lakshmaiah Education Foundation, Vaddeswaram, Guntur - 522302, A.P., India
*** ORCID: , Department of Organic Chemistry, Sri Y.N.M College (Autonomous), Narsapur - 534275, AP, India
**** ORCID: , Department of Chemistry, Koneru Lakshmaiah Education Foundation, Vaddeswaram, Guntur - 522302, A.P., India

° Corresponding Author; Bhaskara Rao Tadiboina
E-mail: tbhaskararao@gmail.com

INTRODUCTION

The therapeutic product includes both active pharmaceutical ingredients (API) and excipients. The API is responsible for pharmacological effects upon absorption into the systemic circulation within the living body (Gorog, 2006). However, in specific instances, the active ingredient or the excipients may not be entirely pure, potentially harboring additional substances from various sources, such as synthesis, excipient, residual solvent, or degradation products. These unwanted components, distinct from the API and excipients, are impurities (Gorog, 2018).

In a pharmaceutical product, when the occurrence of impurities are expected, it becomes essential to detect and characterize them using appropriate analytical methods. This systematic procedure is commonly known as impurity profiling. Impurity profiling is a comprehensive strategy aimed at identifying unknown impurities and elucidating their chemical structures. This process is crucial in ensuring that impurities in pharmaceutical substances are identified and quantified within acceptable limits, thus mitigating potential toxicological effects on the human body (Nagpal *et al.*, 2011).

Impurity profiling requires analytical techniques that are highly sensitive, selective, and efficient in detecting and quantifying trace amounts of impurities (Murali *et al.*, 2022). Traditional methods with lower sensitivity and accuracy are insufficient for quantification due to the nominal quantities in which impurities may exist within drug substances (Patel & Apte, 2016). Furthermore, the structural similarities between many impurities and the parent drug molecule highlight the necessity for advanced hyphenated analytical techniques. HPLC and LC-MS/MS are versatile methods extensively employed for evaluating trace-level impurities in pharmaceutical products (Kiran *et al.*, 2017).

Selpercatinib is a targeted cancer therapy designed to treat specific types of cancer associated with mutations in the RET gene. It belongs to the tyrosine kinase inhibitor class and is approved for treating advanced or metastatic non-small cell lung cancer, medullary thyroid cancer, and other RET fusion-positive solid tumors (Li *et al.*, 2019). RET gene mutations play a role in the development and progression of certain cancers. Selpercatinib works by specifically inhibiting the activity of the RET protein, which helps to slow down or stop the growth of cancer cells (Russo *et al.*, 2020). Selpercatinib can ability to cross the blood-brain barrier, potentially making it effective against tumors that have spread to the brain (Wirth *et al.*, 2020).

A review of the literature was conducted to identify various analytical methods reported for the quantification of selpercatinib. One HPLC (Singamsetty *et al.*, 2021) was reported for evaluation of selpercatinib in dosage forms, in contrast one HPLC-MS/MS (Gulikers *et al.*, 2023) bioanalytical method was reported for analyzing selpercatinib in combination with pralsetinib, brigatinib, and lorlatinib. Existing literature indicates a lack of reported analytical methods for quantifying genotoxic impurities in selpercatinib, and no author has characterized the stress degradation compounds of selpercatinib. Therefore, this paper introduces an optimized HPLC method for quantifying genotoxic impurities of selpercatinib and LC-MS/MS characterization of degradation products (DPs). The study involves genotoxic impurities, namely nitroso and N-oxide impurities based on their availability. Figure 1 provides a comprehensive overview of selpercatinib and its impurities.
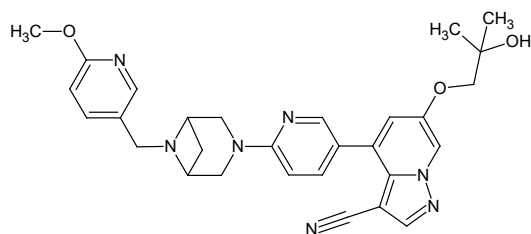
A) Selpercatinib

Systemic name: *6-(2-hydroxy-2-methylpropoxy)-4-*
(6-(6-((6-methoxypyridin-3-yl)methyl)-3,6-
diazabicyclo[3.1.1]heptan-3-yl)pyridin-3- yl)
pyrazolo[1,5-a]pyridine-3-carbonitrile
Formula: $C_{29}H_{31}N_7O_3$
Mass: 525.61 g/mol
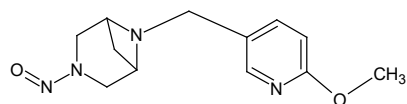
B) Nitroso impurity

Systemic name: *6-((6-Methoxypyridin-3-yl)*
methyl)-3-nitroso-3,6-diazabicyclo [3.1.1]heptane
Formula: $C_{12}H_{16}N_4O_2$
Mass: 248.3 g/mol
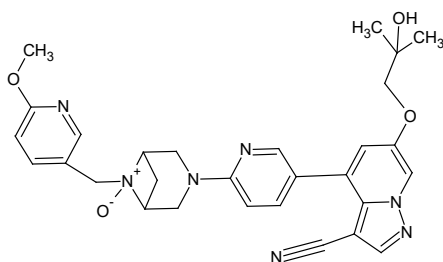
C) N-Oxide impurity

Systemic name: *3-(5-(3-Cyano-6-(2-hydroxy-2-methylpropoxy)pyrazolo[1,5-a]pyridin-4-yl)pyridin-2-yl)-6-*
((6-methoxypyridin-3-yl)methyl)-3,6-diazabicyclo[3.1.1]heptane 6-oxide
Formula: $C_{29}H_{31}N_7O_4$
Mass: 541.6 g/mol

Figure 1. Systemic details of Selpercatinib and its impurities in the study

MATERIAL AND METHOD

Chemicals and instruments

The 98.55 % pure API of Selpercatinib, along with nitroso impurity and N-Oxide impurity, were procured from Eli Lilly and Company (India) Private Limited, Hyderabad. The Retevmo® brand tablet with a 40 mg dose was obtained from the pharmacy. The water (milli-Q®), acetonitrile (HPLC purity), and methanol (HPLC purity), solvents along with filter papers (0.2 µ nylon), were brought from Merck Chemicals, Mumbai. Analytical reagent chemicals, i.e., potassium dihydrogen phosphate (KH_2PO_4), orthophosphoric acid (H_3PO_4), sodium hydroxide (NaOH), hydrogen

peroxide (H_2O_2), and hydrochloric acid (HCl), were brought from Fisher Scientific, Mumbai. The HPLC study was performed on a Waters 1100 (Japan) instrument with Agilent ChemStation software whereas as the Waters triple quadrupole LC-MS system (Japan) with MassLynx software was utilized for the LC-MS study.

Selpercatinib and impurity solution preparation

An accurately measured 25 mg of Selpercatinib API and the impurities were then individually placed in 25 mL flasks containing pure methanol as a diluent. Subsequently, the analytes were completely dissolved in the solvent using a sonicator. After dissolution, the

solutions were filtered through a 0.2μm filter. Adjustments to the volume in each flask were made using the same solvent to attain separate solutions of Selpercatinib and its impurities, each with a concentration of 1000 μg/mL. Additional dilutions were prepared from this stock solution whenever necessary.

Formulation solution preparation

The pharmaceutical formulation under the Retevmo® brand, containing 40 mg of Selpercatinib, was employed to prepare the formulation solution. Tablets were finely powdered, and 25 mg of pure drug equivalent powder was placed in a 25 mL flask filled halfway with methanol. The formulation analytes were dissolved in the solvent using a sonicator, and any undissolved formulation excipients were removed by filtration. The final volume was adjusted to achieve a concentration of 1000 μg/mL of Selpercatinib. Additional dilutions were made as necessary to obtain a Selpercatinib concentration equivalent to 100% precision level, and the solutions were analysed immediately after preparation.

Method development

The method development process commenced with the investigating of the optimal wavelength for detecting Selpercatinib and its impurities, utilizing a UV detector. Standard solutions, each containing Selpercatinib and impurities at a concentration of 10 μg/mL, were individually scanned across the range of 200 to 400 nm. Through the overlay of spectra, an iso-absorption wavelength was identified, ensuring accurate detection of both substances. Further, various stationary phase configurations from different manufacturers were systematically evaluated to achieve the highest resolution of analytes. Meticulous adjustments to the composition of the mobile phase were made through systematic experimentation, aiming to fine-tune the method conditions to separate Selpercatinib and its impurities successfully. The finalized conditions, meticulously selected to ensure optimal resolution, were subsequently employed in the following validation procedures, laying the foundation for robust and reliable analytical methodology.

Method Validation

The guidelines prescribed by ICH (ICH 1994; ICH 1996; ICH 2003) and authors reported in literature were utilized for conducting validation study of the proposed method (Varma *et al.*, 2022; Rajesh *et al.*, 2022; Varma *et al.*, 2023; & Rajesh *et al.*, 2023).

The method sensitivity for detecting the targeted impurities underwent rigorous assessment employing the signal-to-noise (S/N) ratio procedure. A S/N ratio of 10 and 3 was established as the quantification limit (LOQ) and detection limit (LOD) respectively. To construct a linear plot, each impurity's LOQ was considered the lower limit in the calibration curve. Subsequently, the concentration of Selpercatinib was meticulously adjusted to ensure that the standard solution contained 0.1% of the impurities, facilitating accurate quantification. Utilizing the correlation and regression results obtained from the linear curve, the range of analysis was derived, ensuring comprehensive coverage of analyte concentrations.

Method reproducibility was meticulously confirmed through precision experiments, encompassing interday (n=6), intraday (n=3 for each day), and ruggedness (n=3 for each analyte) assessments. In each precision study, the area response was meticulously recorded, and the percentage relative standard deviation (%RSD) was calculated. A %RSD of less than 2 was deemed adequate, demonstrating the robustness and reliability of the analytical methodology.

The method accuracy was rigorously evaluated through a comprehensive recovery experiment conducted at 50%, 100%, and 150% levels within the calibration range. The %RSD of the area values at each level was meticulously assessed during each analysis. Acceptability criteria were set for recovery results to fall within the range of 98-102%, alongside a %RSD of less than 2%, ensuring precise and reliable quantification. Furthermore, method reliability was systematically examined by varying the proposed method conditions, and analyses were conducted under each altered condition. Changes in the area response were

carefully scrutinized, with a % change of less than 2 deemed acceptable, demonstrating the robustness and consistency of the analytical methodology.

Stability studies

The stability profile of the drug was comprehensively assessed under diverse conditions, encompassing photolytic, dry heat, oxidative, and hydrolytic stress. To ensure a thorough evaluation, absorbance was recorded using an ultraviolet (UV) detector, while the LC–MS/MS technique was utilized to characterize DPs. In examining the effects of hydrolytic, oxidative, and photolytic stress, a solution of Selpercatinib with a precisely known concentration was meticulously prepared in HPLC-grade methanol. This approach facilitated the precise control and reproducibility necessary for accurately assessing the drug's stability under the specified conditions.

Hydrolytic degradation testing was meticulously carried out under both acidic and basic conditions to assess the drug's susceptibility to hydrolytic breakdown. In this evaluation, 1 mL of the Selpercatinib formulation solution was accurately measured and placed into 10 mL flasks. Subsequently, 1 mL of the respective stress-inducing solution (0.1 N NaOH or 0.1 N HCl) was added, and the flasks were left undisturbed for 24 hours. In addition, the samples were subjected to accelerated degradation by placing them in a water bath set at 70°C with the respective stress-inducing solution for 7 hours. Following the degradation period, the samples were neutralized, and the volume was adjusted with the mobile phase up to the mark. Subsequently, the samples were analyzed using appropriate analytical techniques to evaluate any changes or degradation products that may have occurred under the specified conditions.

Oxidative degradation testing was meticulously conducted using 15% hydrogen peroxide as the oxidizing agent. Initially, 1 mL of the Selpercatinib formulation solution was precisely measured and placed into 10 mL flasks. Following this, 1 mL of 15% hydro-gen peroxide was added to each flask, and the solutions were allowed to stand undisturbed for 24 hours. Additionally, accelerated degradation was induced by subjecting the samples to a water bath maintained at 70°C for 7 hours. After the degradation period, the samples were neutralized, and the volume was adjusted with the mobile phase up to the mark. Subsequently, the samples were meticulously analyzed using appropriate analytical techniques to assess any degradation products or changes resulting from oxidative stress. For thermal degradation testing, the samples were exposed to a temperature of 70°C for 7 days in an air oven. Conversely, photolytic degradation was performed by exposing Selpercatinib powder to UV light for 7 days within a photo-stability chamber.

The stress-induced Selpercatinib samples were then brought to a standard concentration and assessed using the proposed analytical method. This comprehensive approach ensured a thorough evaluation of the drug's stability under various conditions, providing valuable insights into its formulation and storage requirements.

LC-MS characterization of DPs

DPs formed during exposure to stress conditions were identified and characterized through analysis utilizing LC-MS/MS. Initially, the eluents from the column were detected using a UV detector, providing preliminary information on the compounds present. Subsequently, a portion of the eluents was carefully directed into the mass detector to generate mass spectra. To ensure optimal sensitivity and accuracy, approximately 40% of the eluents were directed into the mass detector with the assistance of a splitter. The resulting mass spectra and fragmentation patterns were meticulously analyzed and summarized to evaluate the nature and extent of degradation observed in the DPs. This comprehensive approach facilitated a detailed understanding of the stress-induced degradation pathways and provided valuable insights into the stability profile of the drug under investigation.

Method applicability

The proposed analytical HPLC method underwent thorough scrutiny to detect and quantify impurities present in Selpercatinib tablet formulations. To validate the method's efficacy, sample solutions derived from Retevmo˚ tablets were prepared and subjected to analysis. The method's robustness was evaluated through direct analysis of formulation sample solutions, as well as analysis after spiking formulation solution with known concentrations of the target impurities. Subsequent examination of the resulting chromatograms and their corresponding responses allowed for a comprehensive assessment of the method's applicability. The method's accuracy, precision, and sensitivity were thoroughly evaluated by meticulously comparing the peak responses and retention times of impurities in both the unspiked and spiked samples, ensuring its suitability for the intended analytical purpose.

RESULTS AND DISCUSSION

Due to lack of any published analytical method in existing literature for evaluating genotoxic impurities of Selpercatinib, this investigation aimed to develop a straightforward HPLC technique. The purpose of this method was facilitated with nitroso impurity and N-Oxide impurity of Selpercatinib. To achieve the best resolution of analytes, various optimization experiments were conducted using several column configurations. The optimization process also involved fine-tuning pH and composition. Various solvent ratios were explored, including various buffer strengths, to determine the most suitable mobile phase. This enabled us to effectively separate Selpercatinib and its impurities. Consequently, a wide range of buffers with varying pH levels was examined to achieve optimal resolution.

Selpercatinib and its impurities were resolved effectively on Zorbax C18 column (250mm×4.6mm,5μm), at 35°C Column temperature. The chromatographic conditions involved a mobile phase of aqueous ammonium acetate and methanol in 70:30 (v/v) at pH 4.5 with 0.1% formic acid, employing 0.9 mL/min isocratic elution and 226 nm wavelength. The blank and system suitability chromatogram noticed in the developed method is presented in Figure 2.

The blank chromatogram observed while analysing the diluent as sample was presented in Figure 2A, which clearly shows no chromatographic detections throughout the entire run time. The Selpercatinib solution spiked with 0.1 % of each impurity was also analysed. The chromatogram visualizes well-resolved and retained peaks corresponding to Selpercatinib and its impurities. The retention time (tR) was noticed as 8.41 min for Selpercatinib, whereas 4.52 min and 11.10 min respectively for the N-oxide impurity and nitroso impurity. The chromatogram doesn't visualize additional detections throughout the entire run time (Figure 2B), suggesting specificity for analyzing nitroso impurities of Selpercatinib.
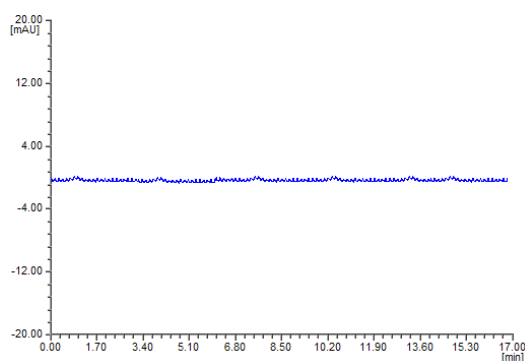
A
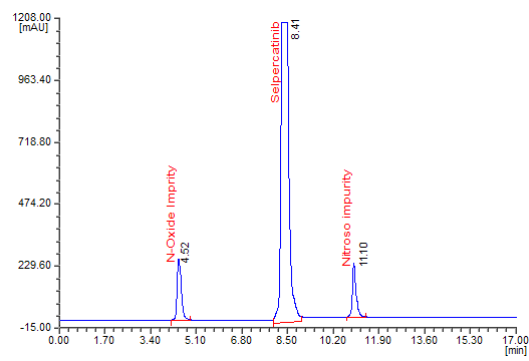
B

Figure 2. Specificity chromatograms in the optimized method

System suitability is a crucial aspect of the chromatographic method validation process, confirming the proposed method's capability to generate well-resolved peaks with high reproducibility consistently. This test is essential for assessing the HPLC system's performance and the procedure's ability to yield high-quality data. The evaluation of system suitability involved the assessment of several parameters, including resolution (Rs), USP tail factor (T), theoretical plates (N), relative standard deviation (RSD) of area, elution time (t_R), and relative retention time (RRT). The calculated RSD values for both t_R and area of Selpercatinib and its impurities were less than 1%, which falls within the acceptance limit. This suggests a high level of reproducibility of peaks representing Selpercatinib and its impurities, with approximately consistent area and retention time during each injection at the fixed concentration. Furthermore, the resolution (Rs) between first eluted peak and subsequent peaks was exceeded 2, indicating a satisfactory resolution of the proposed method. The system suitability results for Selpercatinib and its impurities were compared against regulatory permissible levels and were presented in Table 1. These results affirm that the method successfully meets system suitability criteria.

Table 1. System suitability results of Selpercatinib and its impurities

Parameter	Experiment results for			Acceptance criteria
	Selpercatinib	N-Oxide Impurity	Nitroso Impurity	
t_R (min)	8.41	4.52	11.10	--
RRT	--	0.54	1.32	< 2
RRF	--	0.829	0.038	--
R_s	7.99	--	5.73	> 2
A_s	0.99	0.96	0.91	< 2
N	7568	5234	9682	> 2000

The terms LOD and LOQ signify the method's capacity to accurately detect the smallest analyte amount and quantitate it, respectively. LOD of the impurities was identified as 0.004 µg/mL, and LOQ was finalized as 0.015 µg/mL for impurities. To assess the linearity of the developed method, a linear curve was constructed by plotting the area against various standard concentrations of Selpercatinib and its impurities separately. The standard concentrations range from 15-120 µg/mL for Selpercatinib and 0.015 µg/mL – 0.120 µg/mL for its impurities. The calibration plot, depicting analyte concentration versus peak area, exhibited a linear relationship across the specified concentration range. This linearity was established using the linear simple regression least square method. The regression equation for the line was tabulated in Table 2.

Precision of developed method was evaluated through examination of parameters encompassing both repeatability and intermediate precision. A minimum of six determinations were conducted daily by injecting and analyzing freshly prepared concentrations. This rigorous testing allowed us to evaluate both the within-day (intraday) and between-day (interday) variability, as well as ruggedness. These results indicate acceptable levels of both intraday and interday variability. The mean RSD values for the repeatability and reproducibility study across the studied concentration levels for Selpercatinib and its impurities were found to be acceptable (Table 2), suggesting that the method is reproducible.

To evaluate the method's accuracy, a recovery experiment was conducted. Standard concentrations were intentionally spiked at three levels corresponding to 50%, 100%, and 150% of the target concentration. These spiked samples, prepared in three replicates, were analysed to quantify Selpercatinib and its impurities. The calculated analyte concentrations were subsequently compared to the nominal concen-

trations, allowing us to calculate the % recovery. The results revealed that the mean % recovery values for all three levels, based on three replicates, comfortably fell within the acceptance limit of 98% to 102%, as outlined in regulatory guidelines. These findings af-

firm the method's accuracy as it consistently delivers results aligned with the expected analyte concentrations. Table 2 presents the summarized results of this study.

Table 2. Summary results noticed in linearity, precision, and accuracy study

Parameter	Results		
	Selpercatinib	N-oxide impurity	Nitroso impurity
Linearity			
Range (µg/mL)	15-120	0.015-0.120	0.015-0.120
Intercept	10310	605.54	- 1231.5
Slope	13369	741571	683092
r^2	0.9996	0.9996	0.9990
Precision$^{\$\$}$			
Intraday	0.43	0.61	0.58
Day 1 in interday	0.48	0.46	0.59
Day 2 in interday	0.41	0.12	0.40
Ruggedness	1.16	0.43	0.61
50 % accuracy level$^{\$}$			
Amount prepared (µg/mL)	45	0.045	0.045
Amount recovered (µg/mL)	44.70	0.045	0.045
% Recovery	99.33	99.66	99.97
% RSD	1.81	0.58	0.16
100 % accuracy level$^{\$}$			
Amount prepared (µg/mL)	60	0.06	0.06
Amount recovered (µg/mL)	59.13	0.060	0.060
% Recovery	98.54	100.10	100.02
% RSD	1.39	0.46	0.28
150 % accuracy level$^{\$}$			
Amount prepared (µg/mL)	75	0.075	0.075
Amount recovered (µg/mL)	74.64	0.074	0.075
% Recovery	99.52	99.30	99.63
% RSD	0.99		0.60

n=3 for experiments marked with $^{\$}$ whereas n = 6 for experiments marked with $^{\$\$}$

Several critical parameters were investigated to assess the method reliability for analysing impurities of Selpercatinib. These parameters included variations in the pH, mobile phase composition, and detector wavelength. The % change, shifts in retention time, and system suitability were closely monitored as responses to the deliberate changes in method parameters. Pertaining to the mobile phase composition, variations within ± 5%, ± 0.1 % factor variation in pH, and ± 5 nm variation in detector wavelength of the

specified method condition was performed. The comprehensive results of this study demonstrate that deliberate changes made within the specified parameter ranges don't affect the elution, retention time as well as system suitability. The mean % change remained stable across all conditions, exhibiting only slight variability within acceptable limits. These findings underscore the robustness of the proposed method, affirming its reliability under variations within the specified parameter ranges, as shown in Table 3.

456

Table 3. Robustness results of Selpercatinib and its impurities

S No	Changed condition	Parameter	Results observed		
			Selpercatinib	N-Oxide impurity	Nitroso impurity
1	MP 1	% change	0.93	0.95	0.73
		t_R	8.45	4.51	11.10
		N	7639	5129	9871
2	MP 2	% change	-0.08	-1.26	-0.22
		t_R	8.47	4.55	11.18
		N	7756	5276	9743
3	pH 1	% change	-0.25	0.65	-0.42
		t_R	8.44	4.59	11.13
		N	7987	5502	9604
4	pH 2	% change	0.35	-1.29	-0.15
		t_R	8.49	4.56	11.16
		N	8091	5678	9956
5	WL 1	% change	-0.44	-0.43	0.38
		t_R	8.43	4.55	11.11
		N	7566	5233	9612
6	WL 2	% change	-0.43	0.35	0.95
		t_R	8.41	4.52	11.18
		N	7590	5107	9987

MP (mobile phase) 1: 75:25 (v/v) of solvent A and B; MP 2: 65:35 (v/v) of solvent A and B; WL (wavelength) 1: 231 nm; WL 2: 221 nm; pH 1: 4.4; pH 2: 4.6

Following the ICH stability guidelines, a variety of forced conditions, namely thermal, basic, acidic, oxidative, and photolytic were employed to conduct degradation studies on the pharmaceutical product Selpercatinib. These studies led to the identification and characterization of five distinct degradation products, designated as DP1 to DP5, using HPLC/MS analysis. The outcomes of these investigations have furnished valuable insights into the conditions that render the drug susceptible to degradation, thus facilitating the implementation of appropriate preventive measures during the formulation process.

UV degradation conditions, minimal significant degradation was observed, with an assay percentage of 95.80%. Among the various degradation conditions, the most pronounced degradation was observed in the acid-induced degradation study, the degradation reached 9.51%. Figure 3A depicts the chromatogram from this study, revealing well-separated DPs with retention times of 1.59 minutes and 5.16 minutes, denoted as DP 1 and DP 4, respectively. Additionally, the chromatogram revealed the presence of nitroso impurity at a retention time of 11.10 minutes. In the base-induced degradation study, as depicted in Figure 3B, three distinct degradation products were resolved at retention times of 1.79 minutes, 3.79 minutes and 12.09 minutes, designated respectively as DP 1, DP 3 and DP 5. Percentage degradation under base degradation conditions was measured at 8.74%. In the peroxide degradation study, the assay percentage for Selpercatinib was 6.33%, with a 97.25% mass balance. Figure 3C Chromatogram for this study delineated a single degradation product with a retention time of 2.14 minutes, labelled DP 2. The outcomes of the purity study, conducted using the PDA detector, provided robust validation of the purity and consistency of the Selpercatinib peak across all stress samples under examination. The mass balance for these stressed samples was higher than 98%. These consistent results from the peak purity tests unequivocally affirmed the uniformity and purity of the Selpercatinib peak. Notably, the Selpercatinib assay showed remarkable stability, further attesting to the method's specificity and efficacy in detecting stability. Table 4 presents the recovery results and Figure 3 visualize the stress study chromatograms.

Table 4. Stress degradation results of Selpercatinib and its impurities

Stress	% degradation[#] of Selpercatinib	% assay[#] of Selpercatinib	% Mass balance[$]	Remark
Acidic	9.51	90.49	98.34	DP 1 and 4 were noticed
Basic	8.74	91.26	99.16	DP 1, 3 and 5 were noticed
Peroxide	6.33	93.67	97.25	DP 2 was noticed
Thermal	5.81	94.19	98.01	DP 5 was noticed
UV light	4.2	95.8	97.63	DP 1 and DP 3 were noticed

[#]n = 3; [$]sum of Selpercatinib, impurities and DPs
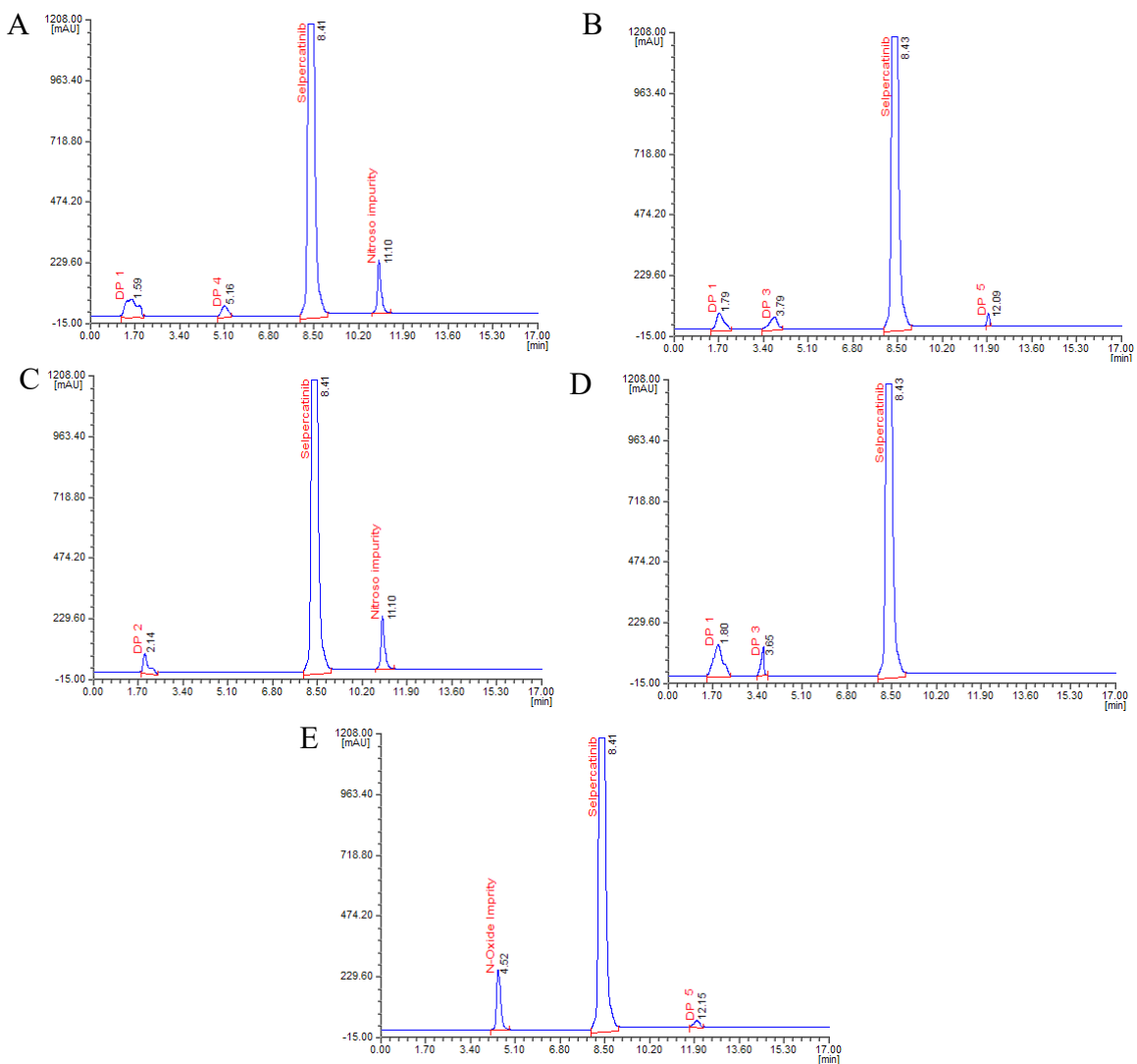
A) DP 1 and 4 visualized in acid degradation chromatogram; B) DP 1, 3 and 5 visualized in base degradation chromatogram; C) DP 2 visualized in peroxide degradation chromatogram; D) DP 1 and 3 visualized in UV degradation chromatogram; E) DP 5 visualized in thermal degradation chromatogram;

Figure 3. Forced degradation chromatograms of Selpercatinib and its impurities

Characterization of DPs by LC-MS/MS

Stress-induced DPs of Selpercatinib were subjected to characterization via LC-MS/MS analysis. The LC method remained unchanged, and the mass operating conditions were fine-tuned to maximize each mass fragment with minimized or no noise. The collision induced dissociation spectra of each DP along with its accurate mass measurements were noted for evaluated the structure of each DP formed in stress study.

Figure 4 illustrates the fragmentation mechanism of DP1, with the ESI spectrum (Figure 9A) revealing the most intense [M+H]⁺ ion at m/z 454 representing the molecular mass of DP 1 as 453.49 g/mol. The MS/MS spectrum of DP1 exhibited highly intense product ion peaks at m/z-125 (loss of $C_{19}H_{15}N_5O$), 161 (resulting by loss of $C_{17}H_{17}N_4O$ from m/z 454), and m/z 386 (loss of C_4HN_2O from m/z 454) and the accurate mass measurements suggest the molecular composition of these fragments. The DP 1 was identified as *chloromethyl11,17-dihydroxy-10,13-dimethyl-3-oxo-6,*

7, 8, 9, 10, 11, 12, 13, 14, 15, 16, 17- dodecahydro- 3H-cyclopenta [a] phenanthrene-17-carboxylate with molecular formula of $C_{25}H_{23}N_7O_2$ and molecular mass of 453.49 g/mol.

Figure 5 illustrates the fragmentation mechanism of DP 2 of Selpercatinib identified in peroxide induced stress study. The fragmentation spectra (Figure 9B) of DP 2 visualizes the parent ion with m/z of 472 (m+1) confirms molecular mass of DP 2. In the fragmentation spectra, there were notable product ions at m/z 139 (loss of $C_{19}H_{19}N_5O$), 221 (resulting by loss of $C_{14}H_{11}N_4O$), 191 (loss of $C_{15}H_{13}N_4O_2$ from parent ion), and m/z 100 (loss of $C_{21}H_{18}N_5O_2$ from parent ion). The MS/MS experiments, in conjunction with accurate mass assessments, provide strong support for the proposed fragmentation scheme. The DP 2 was identified as *17-(ethoxycarbonyloxy)-11-hydroxy-10,13-dimethyl-3-oxo-6,7,8,9,10,11,12,13,14,15,16,17-dodecahydro-3H-cyclopenta[a]phenanthrene-17-carboxylic acid* with molecular formula of $C_{26}H_{29}N_7O_2$ and molecular mass of 471 g/mol.
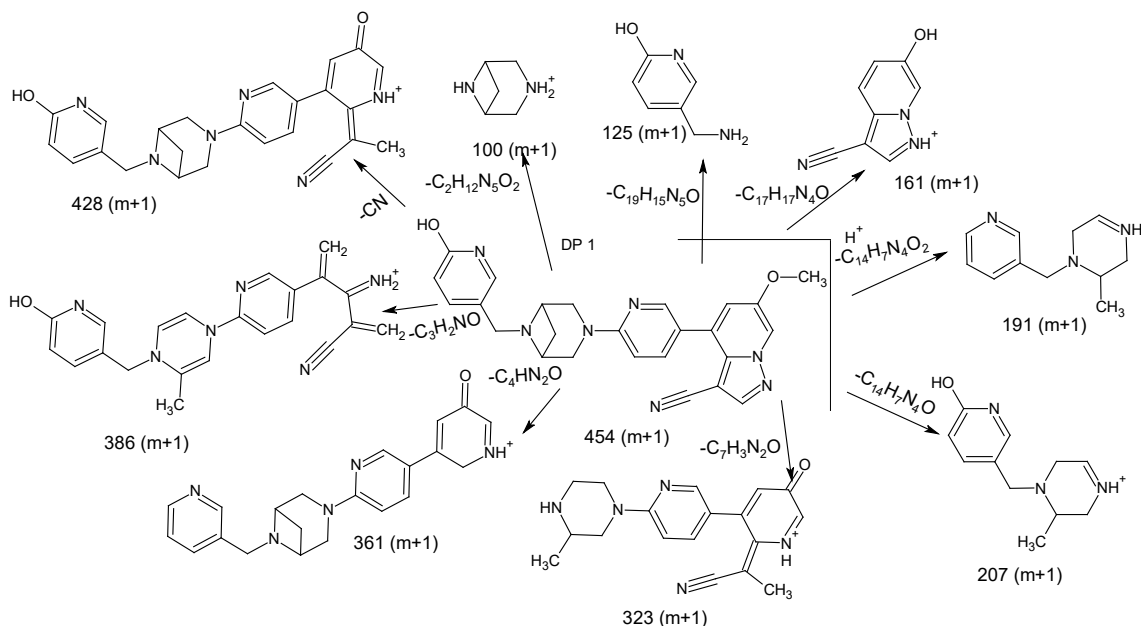
Figure 4. Fragmentation mechanism proposed for DP 1
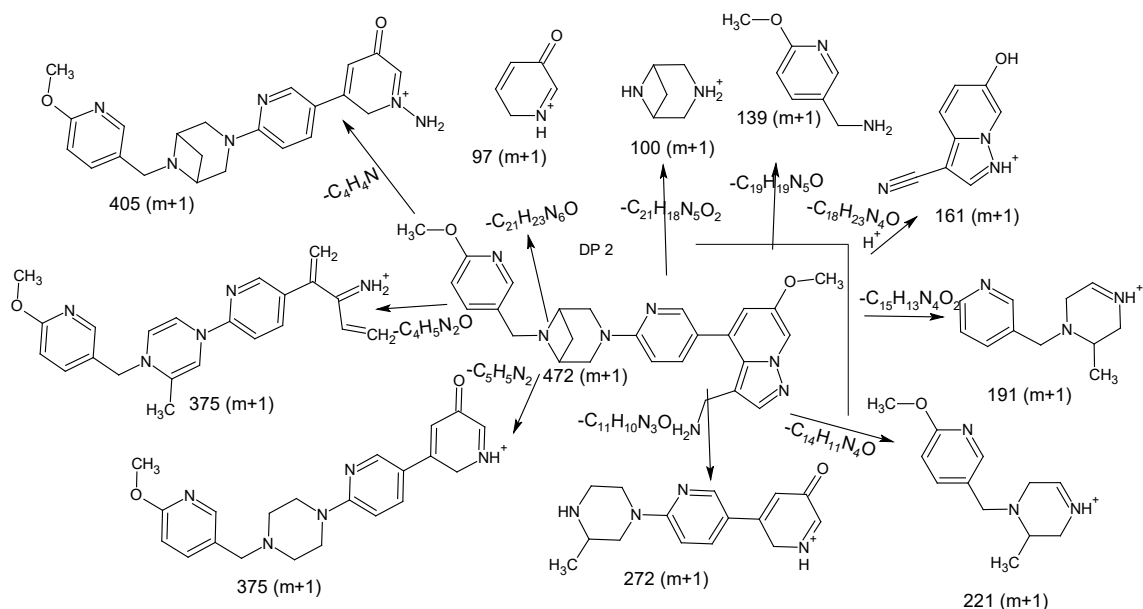
Figure 5. Fragmentation mechanism proposed for DP 2

Figure 6 illustrates the fragmentation mechanism of DP 3 of Selpercatinib which was noticed in base and UV induced stress study. The fragmentation spectra of DP 3 (Figure 9C) visualize parent ion with m/z of 266 (m+1) confirms the molecular mass of DP 3. In the fragmentation spectra, there were notable product ions at m/z 117 (loss of 2 different fragments i.e. -C_4H_4O and -C_4H_4) and m/z 250 (loss of H_2N from parent ion). The DP 3 was identified as *1,17-dihydroxy-10,13-di-methyl-6,7,8,9,10,11,12,13,14,15,16,17-dodecahy-dro-3H-cyclopenta[a] phenanthren-3-one* with molecular formula of $C_{14}H_{11}N_5O$ with 265 g/mol molecular mass.

The fragmentation spectrum of DP 4 identified at 5.16 minutes (Figure 9D), confirms parent ion at m/z 424 [M+H]⁺. The spectra show various that can helpful for elucidating the structure of DP 4 was noticed, notably at m/z 145 (m+1), 191 (m+1), 329 (m+1) and 109 (m+1). The pattern of fragmentation in correla-

tion with parent ion suggests DP 4 as *ethyl 11-hy-droxy-10,13-dimethyl-3-oxo-6,7,8,9,10,11,12,13,14,1 5,16,17-dodecahydro-3H-cyclopenta [a] phenanthren-17-yl carbonate*, with $C_{24}H_{21}N_7O$ as formula. The fragmentation pattern is presented in Figure 7.

The base and thermal degradation chromato-gram visualizes a please change as peak at 12.0 min and was designated as DP 5 which was not detected in other stress studied performed in the study. The prominent parent ion at m/z 415 (m+1) identified along with fragment ions at m/z 125 (m+1), which result by losing $C_{17}H_{14}N_4$. The acquired data (Figure 9E) proved DP 5 as *chloromethyl17-(carboxyoxy)-11-hydroxy-10,13-dimethyl-3-oxo-6, 7, 8, 9, 10, 11, 12, 13, 14, 15, 16, 17-dodecahydro-3H-cyclopenta[a]phenan-threne-17-carboxylate*, possessing a molecular formula of $C_{23}H_{22}N_6O_2$. The fragmentation pattern is present-ed in Figure 8.
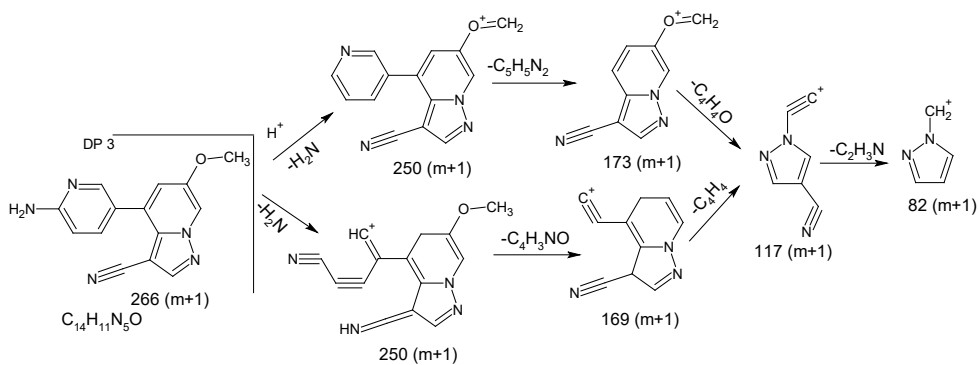
Figure 6. Fragmentation mechanism proposed for DP 3
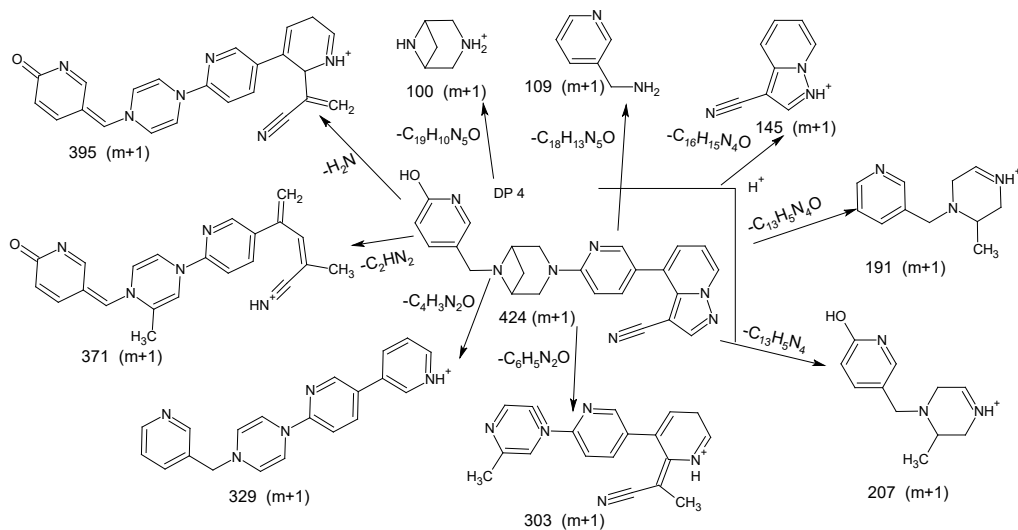
Figure 7. Fragmentation mechanism proposed for DP 4
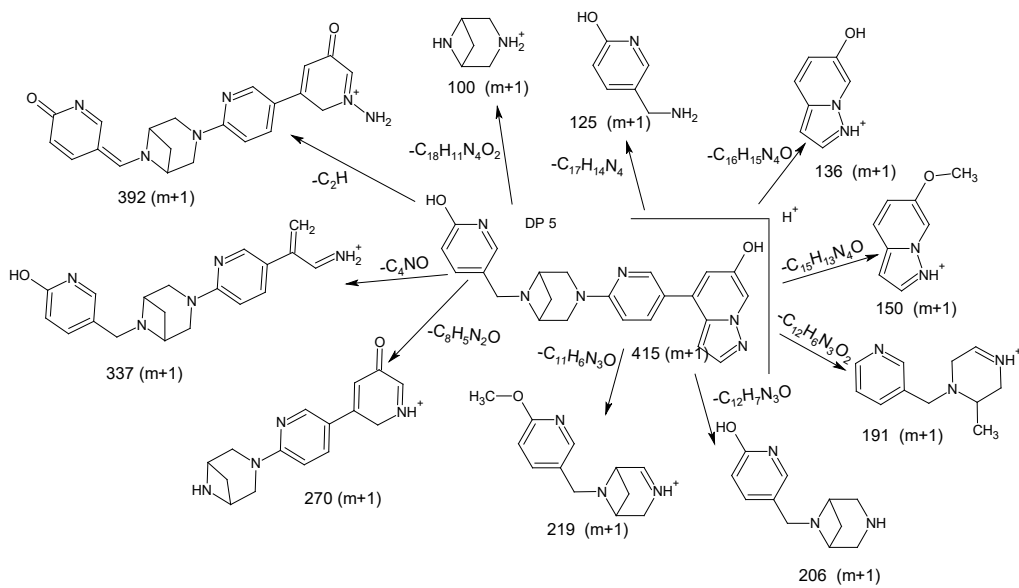
Figure 8. Fragmentation mechanism proposed for DP 5

DP 1 (A); DP 2 (B); DP 3 (C); DP 4 (D); DP 5 (E)
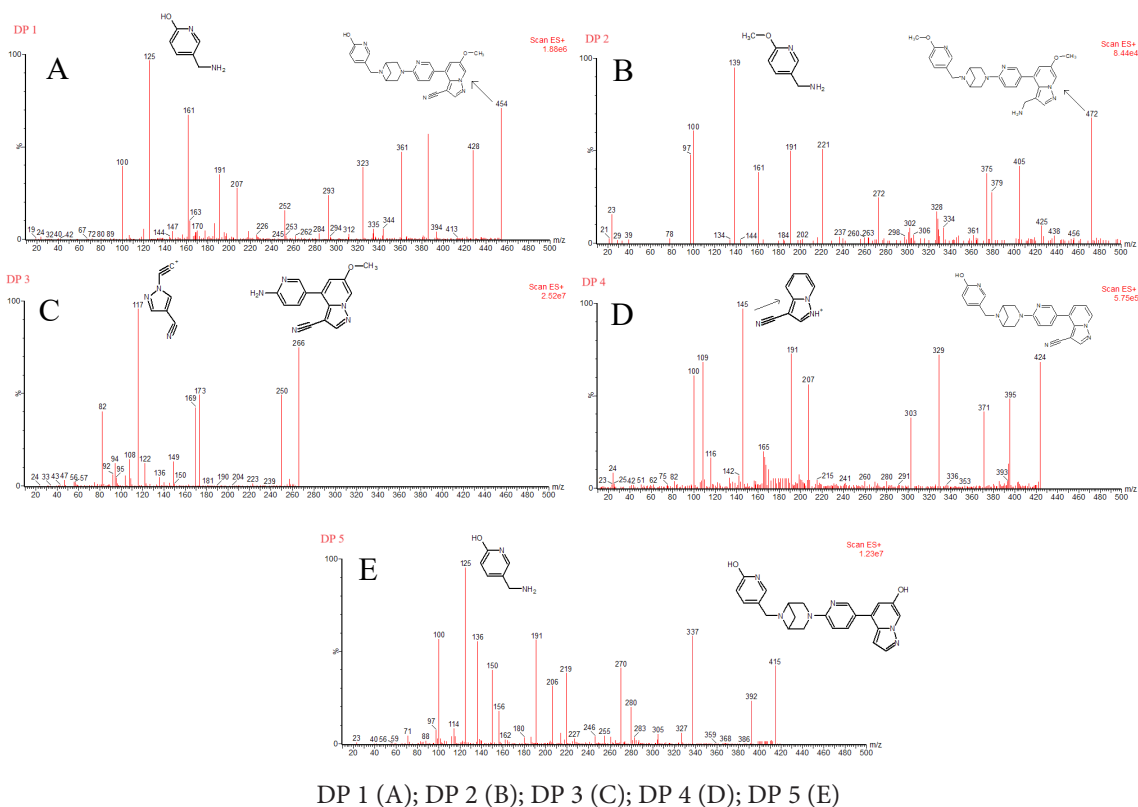
Figure 9. Mass spectra of DPs observed in forced degradation study

The established HPLC technique was employed to quantify the investigated impurities in formulations. The spiked sample analysis chromatogram visualizes well-retained peaks representing impurities and Selpercatinib (Figure 10A). Whereas direct formulation chromatogram doesn't visualize any peak representing impurities (Figure 10B) suggest that the impurities not detected in sample. This highlights that method was adequately fit for analyzing Selpercatinib impurities.

A = spiked formulation; B = Un-spiked formulation
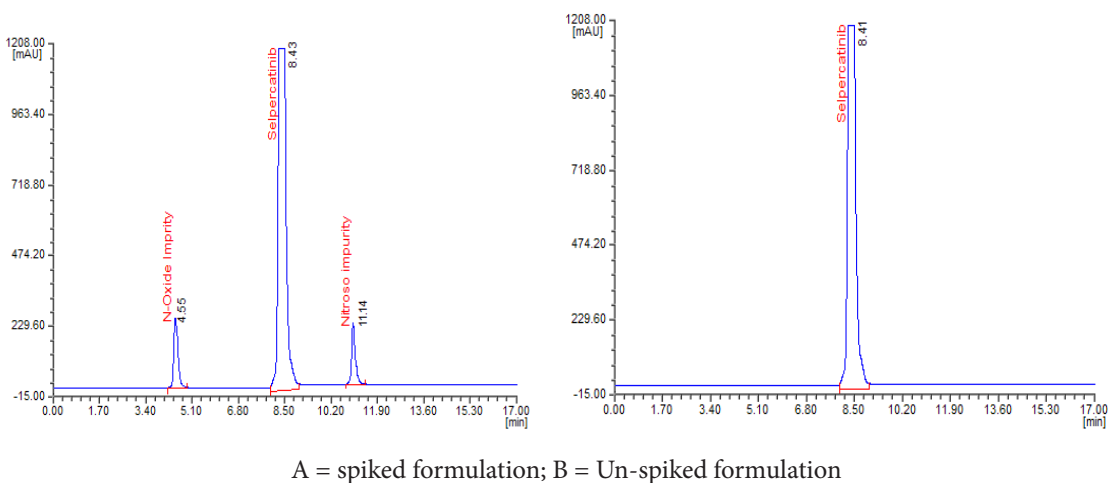
Figure 10. Formulation analysis chromatogram of Selpercatinib

The findings were correlated with literature and observed that the method reported by Singamsetty *et al.*, 2021 was applicable for quantification of selpercatinib in dosage forms whereas method published by Gulikers *et al.*, 2023 only applicable for quantification of selpercatinib in biological samples. No method is available for the quantification of process-related as well as degradation impurities, and hence this finding offers the best option for quantification of both process-related and degradation impurities in bulk drug and formulations.

CONCLUSION

This study aimed to develop a straightforward HPLC method for evaluating genotoxic impurities of Selpercatinib, addressing the absence of published analytical methods in existing literature. The method was specifically designed to target nitroso and N-oxide impurities of Selpercatinib. Extensive optimization experiments were conducted, including variations in column configurations, pH, and mobile phase composition, to achieve optimal resolution of analytes. The final method, employing a Zorbax C18 column with a mobile phase composed of aqueous ammonium acetate and methanol at a pH of 4.5, demonstrated effective separation of Selpercatinib and its impurities. The robustness and reliability of the method were further validated through system suitability testing, which confirmed consistent peak resolution and reproducibility. Additionally, the method exhibited excellent sensitivity, with LOD and LOQ values well below regulatory limits. Precision and accuracy assessments, including recovery experiments and linearity studies, further demonstrated the method's suitability for quantitative analysis of impurities in Selpercatinib formulations. Moreover, the method's reliability was confirmed through robustness testing, showing consistent performance under deliberate variations in method parameters. The degradation studies conducted under various stress conditions provided valuable insights into the drug's stability profile and susceptibility to degradation, further validating the efficacy and specificity of the developed method. Notably, our findings revealed that the drugs exhibited stability under UV hydrolysis conditions but underwent degradation in photolysis acidic and alkaline environments. This study effectively elucidated the fragmentation pathways and characterized the degradation products of Selpercatinib. Consequently, this developed method can serve not only for assessing the genotoxic impurities of Selpercatinib but also for the identification of stress-induced DPs.

AUTHOR CONTRIBUTION STATEMENT

Concept: BRT; Data Collection or Processing: BD; Analysis: BD, EVC; Interpretation: BD, JMP, Literature Search: BD, EVC; Writing: BD, EVC, JMP; Proof reading: BRT

CONFLICT OF INTEREST

Authors declare that there is no conflict of interest.

REFERENCES

Gorog, S. (2006). The importance and the challenges of impurity profiling in modern pharmaceutical analysis. TrAC Trends in Analytical Chemistry, 25(8), 755-757. https://doi.org/10.1016/j.trac.2006.05.011

Gorog, S. (2018). Critical review of reports on impurity and degradation product profiling in the last decade. TrAC Trends in Analytical Chemistry, 101, 2-16. https://doi.org/10.1016/j.trac.2017.09.012

Gulikers, J. L., van Veelen, A. J., Sinkiewicz, E. M. J., de Beer, Y. M., Slikkerveer, M., Stolk, L. M. L., ... van Geel, R. M. J. M. (2023). Development and validation of an HPLC-MS/MS method to simultaneously quantify brigatinib, lorlatinib, pralsetinib and selpercatinib in human K2-EDTA plasma. Biomed Chromatogr, 37(6), e5628. https://doi.org/ 10.1002/bmc.5628.

International Conference of Harmonisation. (1994). ICH. Q2(R1), Validation of analytical procedures: text and methodology. Geneva: International Conference on Harmonization.

International Conference of Harmonisation. (1996). ICH. Q1B, Stability testing: photostability testing of new drug substances and products. Geneva: International Conference on Harmonization.

International Conference of Harmonisation. (2003). ICH. Q1A(R2), Stability testing of new drug substances and products. Geneva: International Conference on Harmonization.

Kiran, R. D., Rakesh, B. J., Sanjay, J. S., & Atul, A. S. (2017). Impurity profiling of drugs towards safety and efficacy: theory and practice. Journal of the Chilean Chemical Society, 62(2), 3543-3557. http://dx.doi.org/10.4067/S0717-97072017000200024

Li, A. Y., McCusker, M. G., Russo, A., Scilla, K. A., Gittens, A., Arensmeyer, K., ... Rolfo, C. (2019). RET fusions in solid tumors. Cancer Treat Rev, 81, 101911. https://doi.org/10.1016/j.ctrv.2019.101911

Murali Krishnam Raju P., Shyamala, Venkata Narayana B., Dantuluri HSNR., Bhupatiraju RV., (2022). A fast, validated UPLC method coupled with PDA-QDa detectors for impurity profiling in betamethasone acetate and betamethasone phosphate injectable suspension and isolation, identification, characterization of two thermal impurities. Ann. Pharm. Fr. 80(6), 837-52. https://doi.org/10.1016/j.pharma.2022.03.003.

Nagpal, S., Karan, Upadhyay, A., Bhardwaj, T. R., & Thakkar, A. (2011). A Review on Need and Importance of Impurity Profiling. Current Pharmaceutical Analysis, 7(11), 62–70. http://dx.doi.org/10.2174/157341211794708749

Patel, S., & Apte, M. (2016). A Review on Significances of Impurity Profiling. Res J Pharm Dosage Form and Tech, 8(1), 31-36. https://doi.org/10.5958/0975-4377.2016.00005.7

Rajesh, V. B., Battula, S. R., Kapavarapu, M. V. N. R., & Mandapati, V. R. (2022). A novel Rivaroxaban degradation impurity detection by RP-HPLC extraction by preparative chromatography, and characterization by LC-MS, NMR and FT-IR: Analysis of novel impurity in batch samples and tablets of Rivaroxaban. Rasayan J. Chem., 15, 2373-2381. https://doi.org/10.31788/RJC.2022.1547008

Rajesh, V. B., Sreenivasa, R. B., Maruthi, V. N. R. K., & Varaprasad, R. M. (2023). Assessment of gas chromatography methodology approach for the trace evaluation of carcinogenic impurity. methyl chloride, in trimetazidine dihydrochloride. Ann. Pharm. Fr., 81, 64-73. https://doi.org/10.1016/j.pharma.2022.06.012

Russo, A., Lopes, A. R., McCusker, M. G., Garrigues, S. G., Ricciardi, G. R., Arensmeyer, K. E., ... Rolfo, C. (2020). New Targets in Lung Cancer (Excluding EGFR, ALK, ROS1). Curr Oncol Rep, 22(5), 48. https://doi.org/10.1007/s11912-020-00909-8

Singamsetty, N., Sundararajan, R., (2021). Analytical Method Development and Validation for Determination of Selpercatinib by Using RP-HPLC. Int. J. Res. Pharm. Sci., 12(1), 931-939.

Varma, B. H. R., & Rao, B. S. (2023). Gas Chromatography-Head Space-Mass Spectrometry Sensor based Quality Control of Dobutamine Hydrochloride Bulk Material for a mutagenic impurity. 2-bromopropane. Res. J. Chem. Environ., 27, 54-61. https://doi.org/10.25303/2702rjce054061

Varma, R. B., & Rao, B. S. (2022). Gas Chromatography-Head Space-Flame Ionization Sensor based assessment of four residuary solvents in rivaroxaban bulk medication. Res. J. Pharm. Technol., 15, 5158-5163. https://doi.org/10.52711/0974-360X.2022.00868

Wirth, L. J., Sherman, E., Robinson, B., Solomon, B., Kang, H., Lorch, J., ... et al. (2020). Efficacy of selpercatinib in RET-altered thyroid cancers. N Engl J Med, 383, 825-835.

The Local Anesthetic Activity of 4-(Naphthalen-1-yloxy)But-2-yn-1-yl)-Containing Piperidine Derivatives in Experimental Animal Models

Malika KHAIITOVA[*°], Yelena SYCHEVA[**°], Vasiliy TRUBACHEV[***], Elmira SATBAYEVA[****], Valentina YU[*****], Talgat NURGOZHIN[******], Edgaras STANKEVIČIUS[******], Yeskendir GASSANOV[*******], Zauresh UTELBAYEVA[********], Khaidar TASSIBEKOV[*********]

The Local Anesthetic Activity of 4-(Naphthalen-1-yloxy)but-2-yn-1-yl)-containing Piperidine Derivatives in Experimental Animal Models

4-(Naftalen-1-iloksi)but-2-in-1-il)-İçeren Piperidin Türevlerinin Deneysel Hayvan Modellerinde Lokal Anestezik Aktivitesi

SUMMARY

Piperidine derivatives are of interest to researchers considering piperidines as an effective scaffold for the synthesis of new compounds. This research aimed to investigate the acute toxicity and local anesthetic activity of new synthesized 4-(Naphthalen-1-yloxy)but-2-yn-1-yl)-containing piperidine derivatives as inclusion complexes with β-cyclodextrin. Moreover, there was hydrogen or 3-methoxyphenyl in position 1 of the substituent at the nitrogen atom of the piperidine ring. The acute toxicity tests were performed on outbred laboratory mice by subcutaneous injection of increasing concentrations of the test solutions. The initial investigation of local anesthetic activity during infiltration anesthesia was performed on guinea pigs using the Bulbring & Wajda animal model. An in-depth study of the efficacy of the most active compound was performed on a model of infiltration anesthesia of the rabbit's abdominal wall by determining the threshold of nociception during electrical stimulation. The new studied piperidine derivatives are low-toxic substances, which are confirmed by the results of an acute toxicity study. At the stage of the primary study of local anesthetic activity during infiltration anesthesia on the experimental Bulbring and Wajda model, the LAS-251 compound showed the greatest activity, surpassing the reference drugs in terms of anesthesia index, duration of full anesthesia and total duration of action. At the stage of in-depth study, despite a longer latency period, LAS-251 has a local anesthetic effect longer than procaine and is slightly inferior to lidocaine. Results of the present study are promising because complex 1-(4-(naphthalen-1-yloxy)but-2-yn-1-yl)-4-phenylpiperidine (LAS-251) with cyclodextrin showed high local anesthetic activity. The new piperidine derivative is future-oriented for prospective studies of other types of anesthesia as a potential medicinal substance for therapeutic use in the future.

***Key Words:** Piperidine derivatives, local anesthetic activity, acute toxicity, infiltration anesthesia*

ÖZ

Piperidin türevleri, piperidinleri yeni bileşiklerin sentezi için etkili bir iskelet olarak gören araştırmacıların ilgisini çekmektedir. Bu araştırma, yeni sentezlenen 4-(Naftalen-1-iloksi)but-2-in-1-il) içeren β-siklodekstrin ile inklüzyon kompleksleri halindeki piperidin türevlerinin akut toksisitesini ve lokal anestezik aktivitesini araştırmayı amaçlamaktadır. Ayrıca piperidin halkasının azot atomundaki substitüentin 1. konumunda hidrojen veya 3-metoksifenil bulunmaktadır. Akut toksisite testleri, artan konsantrasyonlarda test solüsyonlarının deri altına uygulanması yoluyla fareler üzerinde gerçekleştirildi. İnfiltrasyon anestezisi sırasında lokal anestezik aktiviteye ilişkin ilk çalışma, Bulbring & Wajda hayvan modeli kullanılarak kobaylar üzerinde gerçekleştirildi. Elektriksel stimülasyon sırasında nosisepsiyon eşiğinin belirlenmesiyle tavşanın karın duvarına uygulanan infiltrasyon anestezisi modelinde en aktif bileşiğin etkinliğine ilişkin derinlemesine bir çalışma gerçekleştirildi. İncelenen yeni piperidin türevlerinin düşük toksisiteli maddeler olduğu, bir akut toksisite çalışmasının sonuçlarıyla da doğrulandı. Deneysel Bulbring ve Wajda modelinde infiltrasyon anestezisi sırasında lokal anestezik aktivitenin birincil çalışması aşamasında, LAS-251 bileşiği, anestezi indeksi, tam anestezi süresi ve toplam anestezi süresi açısından referans ilaçlardan üstün olan en yüksek aktiviteyi gösterdi. Derinlemesine çalışma aşamasında, daha uzun bir gecikme süresine rağmen, LAS-251'in prokainden daha uzun süreli ve lidokainden biraz daha düşük bir lokal anestezik aktiviteye sahip olduğu görüldü. Bu çalışmanın sonuçları umut vericidir, çünkü 1-(4-(naftalen-1-iloksi)but-2-in-1-il)-4-fenilpiperidin (LAS-251) ile siklodekstrin kompleksi yüksek lokal anestezik aktivite gösterdi. Bu yeni piperidin türevi, gelecekte terapötik kullanım için potansiyel bir ilaç olarak diğer anestezi türleriyle ilgili ileriye yönelik çalışmalar yapılması için umut vericidir.

***Anahtar Kelimeler:** Piperidin türevleri, lokal anestezik aktivite, akut toksisite, infiltrasyon anestezisi*

[*] ORCID: 0000-0001-6775-4358, Department of Pharmacology, Faculty of General Medicine -1, Asfendiyarov Kazakh National Medical University, Almaty, Republic of Kazakhstan.
[**] ORCID: 0000-0002-8409-2672, Laboratory of Physiologically Active Compounds chemistry, A.B. Bekturov Institute of Chemical Sciences, Almaty, Republic of Kazakhstan.
[***] ORCID: 0000-0002-8317-7914, Department of Pharmacology, Faculty of General Medicine -1, Asfendiyarov Kazakh National Medical University, Almaty, Republic of Kazakhstan.
[****] ORCID: 0000-0002-5521-5776, Department of Pharmacology, Faculty of General Medicine -1, Asfendiyarov Kazakh National Medical University, Almaty, Republic of Kazakhstan.
[*****] ORCID: 0000-0001-6508-707X, Laboratory of Synthetic and Natural Medicinal Compounds Chemistry, A.B. Bekturov Institute of Chemical Sciences, Almaty, Republic of Kazakhstan.
[******] ORCID: 0000-0002-8036-604X, Department of Pharmacology, Faculty of General Medicine -1, Asfendiyarov Kazakh National Medical University, Almaty, Republic of Kazakhstan.
[*******] ORCID: 0000-0003-2210-708X, Institute of Physiology and Pharmacology, Lithuanian University of Health Sciences, Kaunas, Lithuania.
[********] Orcid: 0000-0002-4184-4758, Department of Pharmacology, Faculty of General Medicine -1, Asfendiyarov Kazakh National Medical University, Almaty, Republic of Kazakhstan.
[*********] ORCID: 0000-0003-4312-9093, Faculty of General Medicine -2, Asfendiyarov Kazakh National Medical University, Almaty, Republic of Kazakhstan.
[**********] ORCID: 0000-0002-1067-5162, Laboratory of Synthetic and Natural Medicinal Compounds Chemistry, A.B. Bekturov Institute of Chemical Sciences, Almaty, Republic of Kazakhstan.

° Corresponding Author;   Malika Khaiitova
              E-mail: khaiitova.m@kaznmu.kz

Yelena Sycheva
E-mail: yelena-sycheva@yandex.kz

INTRODUCTION

Every year, a large number of different surgical interventions and procedures are performed all over the world (Weiser et al., 2008). Thus, surgical biopsies, epidural anesthesia, dental procedures, blockage of major nerves are widespread in clinical practice (Becker et al., 2012). Pathological pain and pain are caused by hypersensitivity, while it is a common concomitant symptom. Therefore, it is necessary to use different methods of anesthesia (Woolf, 2010; Yu et al., 2019).

The methods of infiltration and conduction anesthesia are simple and safe to use, which allows them to be used instead of general anesthesia. The local effect is ensured due to the high concentration of the drug at the injection site of local anesthetics (Raithel et al., 2018). Local anesthesia methods can also be used after various operations to ensure adequate anesthesia in the postoperative period (Ma et al., 2017). The mechanism of action of local anesthetics is associated with a violation of the passage of Na^+ ions through the ionophores of the membrane of neurons, thereby interrupting neural conduction (Xie et al., 2022).

The use of local anesthetics avoids the occurrence of various side effects inherent in other painkillers, such as gastrointestinal bleeding, impaired blood clotting, functional disorders of the liver or kidneys, tolerance, dependence, and others. The use of modern anesthetics also has the advantage of minimising the risk of allergic reactions. However, the development of hypersensitivity is directly related to the frequency of drug use (Grzanka et al., 2016; Ilfeld et al., 2021; Yin et al., 2021).

Another essential problem with the use of local anesthetics is the development of local and systemic toxicity (Tsai et al., 2021). The local toxicity is a significant obstacle in the development of new anesthetic drugs. The majority of local anesthetics have neurotoxicity, chondrotoxicity, and myotoxicity observed after intramuscular and intra-articular injections

(Baker et al., 2012; Verlinde et al., 2016). Systemic toxicity develops rarely, but this complication is accompanied by agitation of the central nervous system, cardiovascular disorders, in particular, there is possible arrhythmia and methemoglobinemia. These side effects can be observed with frequent use of prilocaine, articaine, and benzocaine (Wadlund, 2017; Johansson et al., 2020). The anesthetics, which contain para-aminobenzoic acid contribute to the development of allergic reactions, as well as symptoms of numbness and paresthesia (McMahon et al., 2022).

When considering the issue of compliance of local anesthetics with the essential requirements, where rapid blockade of peripheral nerves, long-term effect, and absence of local and systemic reactions are of particular importance, it is worth noting the need to develop new drugs that meet the needs of doctors in modern clinical practice (Chahar et al., 2012; Chitilian et al., 2013).

Considering the above, preclinical studies of new drugs with local anesthetic activity are relevant and practically important. From among the various chemical structures, the piperidine ring is one of the important components in the molecule of local anesthetics such as bupivacaine and ropivacaine. Furthermore, piperidine and its derivatives have different pharmacological properties (Vitaku et al., 2014; Martins et al., 2017).

The studies conducted indicate the possibility of using piperidine molecules in various fields of medicine. Because of the availability of synthesis and ease of embedding into other structural frameworks of various biogenic residues, piperidine derivatives are of interest to researchers considering piperidines as an effective scaffold for the synthesis of new compounds (De et al., 2015).

Based on the description above, two new 4-(Naphthalen-1-yloxy)but-2-yn-1-yl)-containing piperidine derivatives were synthesized in the laboratory. Substituted naphthoxyamine derivatives

belong to the class of biologically active molecules with a broad spectrum of therapeutic effects (Zuffo et al., 2019; Kottapalle, Shinde, 2021). We have previously synthesized β-cyclodextrin (β-CD)complex with 1-[1-(2,5-dimethoxyphenyl)-4-(naphthalene-1-yloxy)but-2-ynyl]-4-methylpiperazine whose structure is presented in Figure 1. New potentially biologically active 4-phenylnaphthoxybutynylpiperidines were synthesized by reacting 1-(prop-2-ynyloxy)naphthalene with 4-phenylpiperidine and aldehydes (benzaldehyde, formaldehyde and 3-methoxybenzaldehyde) in absolute dioxane in the presence of catalytic amounts of copper (I) iodide at temperature 40 °C. The compound had a pronounced promoting effect on the CD4^{+}, CD8^{+} and myeloid cells during aseptic inflammation, even under the influence of heavy metal salts (Yu et al., 2023).
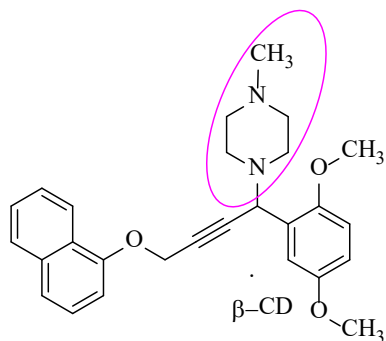
Figure 1. Chemical structure of β-cyclodextrin complex with 1-[1-(2,5-dimethoxyphenyl)-4-(naphthalene-1-yloxy)but-2-ynyl]-4-methylpiperazine.

The molecule contains a fragment of 4-(naphthalen-1-yloxy)but-2-yn-1-yl), however, the piperazine derivative group was decisive in increasing the immune status in previous studies. Therefore, it was exciting to study the type of biological action of substrates "devoid" of a single nitrogen atom. The purpose of present study was to perform experimental animal models to investigate acute toxicity and local anesthetic activity of new compounds, considering that piperidine is an important structure of the molecule of local anesthetics, like the objects of our study.

MATERIAL AND METHODS

Chemical research

The studied compounds that have been assigned the laboratory cipher LAS–251, LAS–252 (local anesthetic substance) were synthesised for the first time in the Laboratory of Chemistry of Synthetic and Natural Medicinal Compounds of Bekturov Institute of Chemical Sciences (Almaty). Total starting reagents used for the synthesis were purchased from Sigma-Aldrich and required no additional purification. The course of the reactions and the purity of the products were monitored by the TLC analysis on "Silufol UV-254" plates with the appearance of substances spots with iodine vapor. The eluent for TLC was a mixture acetone – hexane (1:2). The IR spectra were recorded on a Nicolet 5700 spectrometer in KBr tablets. The ^{1}H and ^{13}C NMR spectra of the samples were recorded on a JNM-ECA 400 (Jeol) spectrometer with operating frequencies 400 (^{1}H), 100 MHz (^{13}C) in deuterated chloroform (CDCl$_3$).

Currently, various molecular inclusion complexes with β-CDs are actively used in the pharmaceutical industry. The inclusion of this natural cyclic oligosaccharide makes it possible to convert liquid forms of low molecular weight substances into amorphous and crystalline powders. Also, such compounds become more stable in water, are less susceptible to oxidation in air, dehydration and evaporation. This method, it should be noted, eliminates the odor and taste of the original active substrate. The complexation of the active substance with cyclodextrin can increase bioavailability and reduce toxicity (Uekama, 2002; Barset al., 2003).

Synthesis 1-(4-(naphthalen-1-yloxy)but-2-yn-1-yl)-4-phenylpiperidine (1)

To a reaction mixture heated to 40° C consisting of 1.5 g (0.0082 mol) 1-(prop-2-iniloxy)naphthalene, 0.24 g (0.0082 mol) paraform, and 0.15 g (0.00078 mol) of copper iodide (I) in 20 ml of dioxane were mixed with 1.32 g (0.0082 mol) of 4-phenylpiperidine

in 10 ml of dioxane. 1-(4-(Naphthalen-1-yloxy)but-2-yn-1-yl)-4-phenylpiperidine (1) was isolated by column chromatography on Al_2O_3 by elution with an acetone mixture: hexane (1:3). The yield is 2.19 g (75%) in the form of oil, R_f 0.71.

Calculated, %: C 84.47; H 7.09; N 3.94 for $C_{25}H_{25}NO$. Found, %: C 84.59; H 7.18; N 4.07

IR (KBr, υ, cm^{-1}): 704, 805, 1319, 1419, 1583, 1681 (Ph), 2121 (C≡C).

^{1}H NMR (CDCl$_3$, δ, ppm): 1.85, 1.83 (dd, 4H, N-(CH$_2$)$_2$); 2.08-2.12 (m, 4H, N-(CH$_2$)$_2$(CH$_2$)$_2$); 2.56 (m, 1H, CH-piperidin); 3.39 (s 2H, CH$_2$-N); 4.97 (s, 2H, OCH$_2$); 6.99 (d, 1H, ArH^2); 7.40 (t, 1H, ArH^4); 7.50-7.53 (m, 3H, ArH^{3,6,7}); 7.82 (d, 1H, ArH^5); 8.29 (s, 1H, ArH^8); 7.25 (t, 2H, Ph-piperidine); 7.33 (t, 2H, Ph-piperidine); 7.38 (d, 1H, Ph-piperidine).

^{13}C NMR (CDCl$_3$, δ, ppm): 33.49 (N-(CH$_2$)$_2$(CH$_2$)$_2$); 42.23 (CH-piperidine); 47.69 (N-CH$_2$); 53.24 (N-(CH$_2$)$_2$); 56.22 (O-CH$_2$); 78.73, 80.08 (C≡C); 153.57 (C^1), 105.58 (C^2), 125.46 (C^3), 121.12 (C^4), 126.16 (C^5), 125.71 (C^6), 122.14 (C^7), 121.31 (C^8), 127.58 (C^9), 134.66 (C^{10}) (ArH); 126.98, 127.58, 128.58, 146.31 (Ph-piperidine).

Synthesis of Complex 1-(4-(naphthalen-1-yloxy)but-2-yn-1-yl)-4-phenylpiperidine with β-CD (LAS-251)

Solutions of 1 g 1-(4-(naphthalene-1-iloxy)but-2-inyl]-4-phenylpiperidine (1) in 20 ml of ethyl alcohol and 1 g of β-cyclodextrin in 20 ml of distilled water are mixed at a temperature of 45-50° C for 5 hours. After the end of the reaction, the aqueous ethanol solution is distilled and dried in a drying cabinet. The yield is 1.3 g (65%). The complex appeared as a light yellow powder, melting with decomposition above 240° C.

Calculated, %: C 53.99; H 6.42; N 0.94; O 38.64 for $C_{67}H_{95}NO_{36}$. Found, %: C 53.83; H 6.51; N 1.09.

Synthesis of 1-(1-(3-methoxyphenyl)-4-(naphthalen-1-yloxy)but-2-yn-1-yl)-4-phenylpiperidine (2)

1-(1-(3-Methoxyphenyl)-4-(naphthalen-1-yloxy)but-2-yn-1-yl)-4-phenylpiperidine (2) was synthesized similarly from 1-(prop-2-ynyloxy)naphthalene 2.0 g (0.0109 mol), 3-methoxybenzaldehyde 1.49 g (0.0109 mol) and 4-phenylpiperidine 1.76 g (0.0109 mol) in the presence of copper iodide (I) (0.15 g) in dioxane at 40 °C. The product was isolated by column chromatography on Al_2O_3 by elution with an acetone mixture: hexane (1:3). Yield 2.19 g (44%) oil, R_f (0.69).

Calculated, %: C 83.26; H 6.77; N 3.03 for $C_{32}H_{31}NO_2$. Found, %: C 83.35; H 6.87; N 3.15.

IR (KBr, υ, cm^{-1}): 705, 754, 1493, 1592, 1659 (Ph), 2125 (C≡C).

^{1}H NMR (CDCl$_3$, δ, ppm): 1.78-1.83 (m, 4H, N-(CH$_2$)$_2$); 2.08-2.15 (m, 4H, N-(CH$_2$)$_2$(CH$_2$)$_2$); 2.55 (m, 1H, CH-piperidin); 3.80 (s, 3H, OCH$_3$); 4.90 (s, 2H, OCH$_2$); 4.97 (s, 1H, CH-N); 6.81 (d, 1H, ArH^2); 6.94 (d, 1H, Ph); 7.06 (s, 1H, Ph); 7.17-7.20 (m, 2H, Ph); 7.41 (t, 1H, ArH^4); 7.47-7.50 (m, 3H, ArH^{3,6,7}); 7.80 (d, 1H, ArH^5); 8.29 (s, 1H, ArH^8); 7.25 (t, 2H, Ph-piperidine); 7.33 (t, 2H, Ph-piperidine); 7.37 (d, 1H, Ph-piperidine).

^{13}C NMR (CDCl$_3$, δ, ppm): 33.90 (N-(CH$_2$)$_2$(CH$_2$)$_2$); 42.59 (CH-piperidine); 53.02 (N-(CH$_2$)$_2$); 55.92 (OCH$_3$); 56.22 (O-CH$_2$); 61.60 (N-CH); 82.70, 84.11 (C≡C); 153.64 (C^1), 105.52, (C^2), 125.51 (C^3), 121.28 (C^4), 126.17 (C^5), 125.71 (C^6), 122.22 (C^7), 121.70 (C^8), 127.57 (C^9), 134.65 (C^{10}) (ArH); 126.98, 127.57, 128.47, 146.61 (Ph-piperidine); 113.42, 113.97, 129.16, 122.23, 139.66, 159.55 (Ph).

Synthesis of Complex 1-(1-(3-methoxyphenyl)-4-(naphthalen-1-yloxy)but-2-yn-1-yl)-4-phenylpiperidine with β-CD (LAS-252)

Solutions of 1 g 1-(1-(3-methoxyphenyl)-4-(naphthalen-1-yloxy)but-2-yn-1-yl)-4-phenylpiperidine (2) in 20 ml of ethyl alcohol and 1 β-cyclodextrin in 20 ml of distilled water are mixed at a temperature of 45-50 °C for 5 hours. After the end of the reaction, the aqueous ethanol solution is distilled and dried in a drying cabinet. The yield is 1.4 g (70%). The com-

plex appeared as a light yellow powder, melting with decomposition above 240 °C.

Calculated, %: C 55.67; H 6.38; N 0.88; O 37.08 for $C_{74}H_{101}NO_{37}$. Found, %: C 55.75; H 6.43; N 0.98.

Experimental animals and ethics approval

96 outbred laboratory male and female laboratory mice weighing 20-25 g were used to investigate acute toxicity. The primary study of local anesthetic activity during infiltration anesthesia was conducted on 30 mature male guinea pigs weighing 350-400 g. Mature outbred 24 male rabbits weighing 2500-3000 g were used in experiments to in-depth study the activity of the compounds. The experiments were carried out based on the Life Science laboratory of Asfendiyarov Kazakh National Medical University (KazNMU). Laboratory animals were provided by the KazNMU vivarium.

Laboratory animals were kept in specialized cages with a natural 12-hour day-night light regime with constant free access to clean water and standardized feed. Throughout the period of observation and experiments, the necessary hygienic conditions, a temperature regime of 25 ± 2 °C, a relative humidity of 55-60% and good air circulation were observed. Permanent dyes were used to label the laboratory animals of each group.

The experiments provided for in the protocol using laboratory animals were performed in accordance with the Order of the Minister of Health Care of the Republic of Kazakhstan "On approval of the rules for conducting preclinical (non-clinical) studies and requirements for preclinical bases for assessing the biological effect of medical devices". The care and maintenance of laboratory animals was carried out following the Guide for the Care and Use of Laboratory Animals (National Research Council (US) Committee, 2011). All described manipulations and procedures were carried out under the rules of the European Convention for the Protection of Vertebrate Animals and Directive 2010/63/EU. The research protocol was

approved by the Local Ethics Committee of Asfendiyarov Kazakh National Medical University (Decision Number: No. 14(120) and date October 28, 2021, with permission to extend the study - Decision Number: No. 1(137) and date January 31, 2023).

Acute toxicity study

Acute toxicity tests were conducted following the guidelines for preclinical studies of medicines (Mironov, 2012). Experiments were performed on healthy mature males and females of outbred laboratory mice. Laboratory animals were randomly divided into experimental and control groups of 6 mice (3 females and 3 males) each. The studied compounds dissolved in sterile water for injection (Novosibkhimpharm Company, Russia) in 3 increasing concentrations (100-1000 mg/kg) were injected once subcutaneously into the lateral surface of the body. Each animal in the group had one injection of the test compound at one concentration only. This route of administration corresponds to using substances as local anesthetics in the future. After the administration of solutions, laboratory animals were under constant supervision on the first day and then for 14 days. The general condition, changes in behavioural reactions, motor activity and metabolism, and toxic reactions from various organs and systems were recorded during observation. At the end of the experiment, the median lethal dose - LD_{50} was calculated for each compound, as well as LD_{16} and LD_{84}, to determine the standard error.

Local anesthetic activity study

The primary study of local anesthetic activity during infiltration anesthesia used the Bulbring and Wajda model (Bulbrıng and Wajda, 1945; Kuzenbayeva et al., 2000). Each experimental group included six male guinea pigs. The day before the experiment, all animals of the studied group had their hair removed in the back area. On the day of the test, 0.25 ml of 0.5% aqueous solutions were injected intradermally into 4 points corresponding to the corners of a square with a side of 3 cm. The method of administration is presented in Figure 2.

Figure 2. Intradermal administration of a solution (wheal method) on the back of a guinea pig according to the Bulbring and Wajda models (photograph).

Injections of solutions of the compounds were performed at the anterior and posterior points of the square. The solutions of the reference drugs were injected into the remaining parallel points. Following injection, the area of papule formation was marked with ink. The presence or absence of sensitivity at the injection site was assessed every 5 min by applying an irritation when touching the injection needle. The touches were carried out in a series of 6 touches at each point. An interval of 3-4 s was maintained between touches. In each series of experiments, the total number of needle touches that did not cause skin twitching in the area of the studied square on the animal's back for 30 min (anesthesia index), the duration of full anesthesia (absence of any reactions during exposure to an irritant) and the total duration of the anesthetic effect (the time during which the response reached the initial values) were recorded.

An in-depth study of the local anesthetic effect of the most active compound was carried out on a model of infiltration anesthesia of the abdominal wall of rabbits by determining the nociception threshold during electrical stimulation (Kuzenbayeva et al., 2000; Mironov, 2012). The experiments were performed on non-anesthetized male rabbits. The number of animals in each group was six animals. Prior to the start the experiment, the skin of the abdomen

on the side surfaces at the level of the middle third was freed from the fur of a rabbit fixed in a position on its back. The electrodes of an electrostimulator (Medistim Co, Russia) with moistened cotton swabs (0.9% NaCl) were applied to the prepared skin areas. First, we determined the threshold of pain sensitivity by applying minimal irritation with electric current pulses (duration 0.3 ms, frequency - 50Hz, amplitude 5-25V). The response to pain irritation was accompanied by a change in the rhythm and amplitude of the animal's breathing. These changes were recorded on the OLV-VM12 veterinary monitor (Zhengzhou Olive Electronic Technology Co, Ltd, China). The next stage of the experiment involved the injection of 0.5% aqueous solutions (solvent - sterile water for injection) of the studied substances intradermally in a volume of 0.5 ml and subcutaneously in a volume of 2 ml at the site of electrode application. Further tests were performed to determine the nociceptive reaction in response to a series of electrical stimulations after 3, 5, 10 min, etc. The process of the experiment is shown in Figure 3.

Figure 3. The test for determining the nociceptive reaction of a rabbit in the study of local anesthetic activity during infiltration anesthesia (photograph).

At the end of the experiment, the time of anesthesia development, depth (in percent), and duration were estimated. The assessment was performed by changing the threshold of the reaction to electrical irritation at the site of infiltration with a solution of the compound under study. Elimination of the response to threshold irritation was recorded as 20% anesthesia. An increase in stimulus threshold of 5 V was adopted as 40% anaesthesia. If the sensitivity threshold

was increased by 10V, the depth of anaesthesia was estimated to reach 60% and by 20V the depth of anaesthesia was estimated to reach 100%.

The obtained indicators were compared with local anesthetics widely used in clinical practice for infiltration anesthesia, characterized by varying degrees of efficiency and duration of action: procaine (HIM-PHARM JSC, Kazakhstan), lidocaine (BZMP JSC, Belarus), trimecaine (Zhaik-AS LLP, Kazakhstan).

Statistical analysis

The results of the current study are presented as Means±SE or SD. The online software "Quest Graph™ LD_{50} Calculator" was used to calculate the LD_{50}, LD_{16}, and LD_{84} indicators (AAT Bioquest, Inc., 19 Feb. 2023, /https://www.aatbio.com/tools/ld50-calculator/). The standard error was determined for LD_{50} (Randhawa, 2009). All experimental groups were compared with the control group. T-test and ANOVA were used to determine the statistical significance of differences in the compared groups. A value of $p<0.05$ was considered statistically significant. The statistical data analysis was performed using SPSS/27.0 software (IBM, USA) for Windows.

RESULTS AND DISCUSSION

Results of the synthesis of the new piperidine derivatives

Under the conditions of the Mannich reaction, the interaction of 1-(prop-2-iniloxy)naphthalene with heterocyclic amine (4-phenylpiperidine) and aldehydes (formaldehyde and 3-methoxybenzaldehyde) in the presence of catalytic amounts of CuI in an absolute dioxane medium at a temperature of 40 °C for 2 hours, 1-(4-(naphthalene-1-iloxy)but-2-inyl)-4-phenylpiperidine (1) (yield, 75%) and 1-(1-(3-methoxyphenyl)-4-(naphthalene-1-iloxy)but-2-inyl)-4-phenylpiperidine (2) (yield, 46%) were obtainedand presented in Scheme 1.
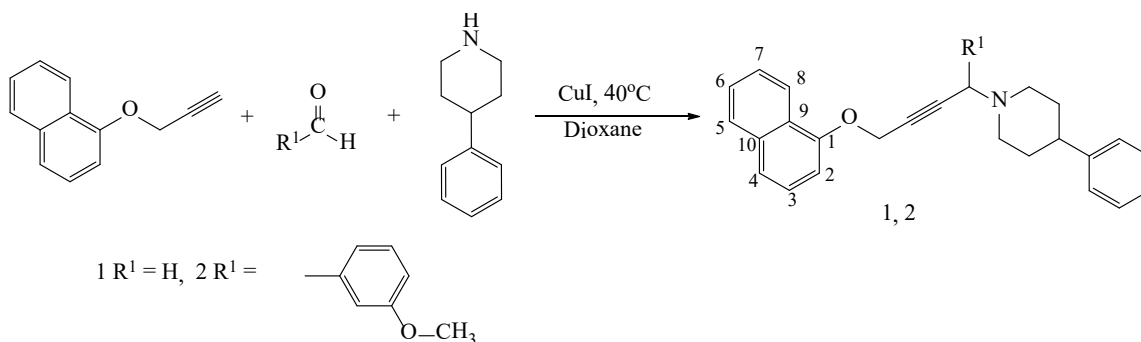
Scheme 1. Synthesis scheme of novel 4-phenylnaphthoxybutynylamines (1, 2).

The structure of the synthesized compounds was determined based on the analysis of IR spectra and NMR spectroscopy data of ^{1}H and ^{13}C.

In the IR spectra of compounds 1, 2 there is no absorption band in the 3309 cm^{-1} region, characteristic of the C-H terminal acetylene group of the initial 2-(prop-2-iniloxy)naphthalene, but there is a weak band in the region of 2121 and 2125 cm^{-1}, characteristic of a disubstituted C≡C bond, which confirms the formation of an aminomethylation product.

Signals of protons of the aminomethylene and aminomethine groups were detected in the NMR 1H 4-phenylnaphtoxybutinylamines 1, 2 in the region of 3.39 ppm and 4.97 ppm in the spectra of NMR. The chemical shift in the range δ 4.97 and 4.90 ppm is attributed to protons of the O-methylene group. The signals of the protons of the piperidine methylene groups are at 1.83-2.56 ppm. The strong-field chemical shift (3.80 ppm) is attributed to the protons of the methoxy group at the atom of the benzene cycle. In the weak field area δ 6.81-8.29 ppm, signals of protons of the naphthalene nucleus and Ph rings are detected.

In the NMR ^{13}C spectra of compounds 1, 2 in the range of 47.69 ppm and 61.60 ppm, signals of carbon atoms of the aminomethylene and aminomethine groups were detected. Carbon atoms of the C≡C triple bond resonate at 78.73, 80.08 ppm, and 82.70, 84.11 ppm. The signal with a chemical shift of 56.22 ppm is attributed to oxymethylene carbon. The signals of the atomic carbons of the phenyl rings are in the weak field (105.52-159.55 ppm) of the spectra. The carbon atoms of the piperidine cycle resonate in the range δ 33.49-53.24 ppm, and the signal of the OCH$_3$ group (55.92 ppm) is present in the spectrum of compound 2.

Hydrophilic natural polymers such as cyclodextrin are used as a matrix to produce water-soluble supramolecular complex systems. The most important property of CD is the ability to selectively bind organic and biological molecules, forming inclusion complexes of the "guest-host" type to obtain water-soluble forms. The complexes are formed by the interaction of ethanol solutions of 4-phenylnaphtoxybutinylamines (1, 2) with an aqueous solution of β-cyclodextrin taken in a mass ratio of 1:1, at a reaction temperature of 45-50 °C and conducting the reaction for 5 hours. After the end of the reaction, the aqueous ethanol solution is distilled. The resulting complexes are washed with 96% ethanol and dried in a drying cabinet. As a result, 1 and 2 inclusion complexes (LAS-251 and LAS-252) were obtained with yields of 65 and 70%, respectively (Scheme 2.). The progress of the reactions was monitored using thin-layer chromatography on silica gel until the disappearance of the starting products (R$_f$ 0.71 and R$_f$ 0.69) in an aqueous-alcohol solution. The products were collected after the slow evaporation of the solution by forming powder products. The complexes were identified through elemental analysis.
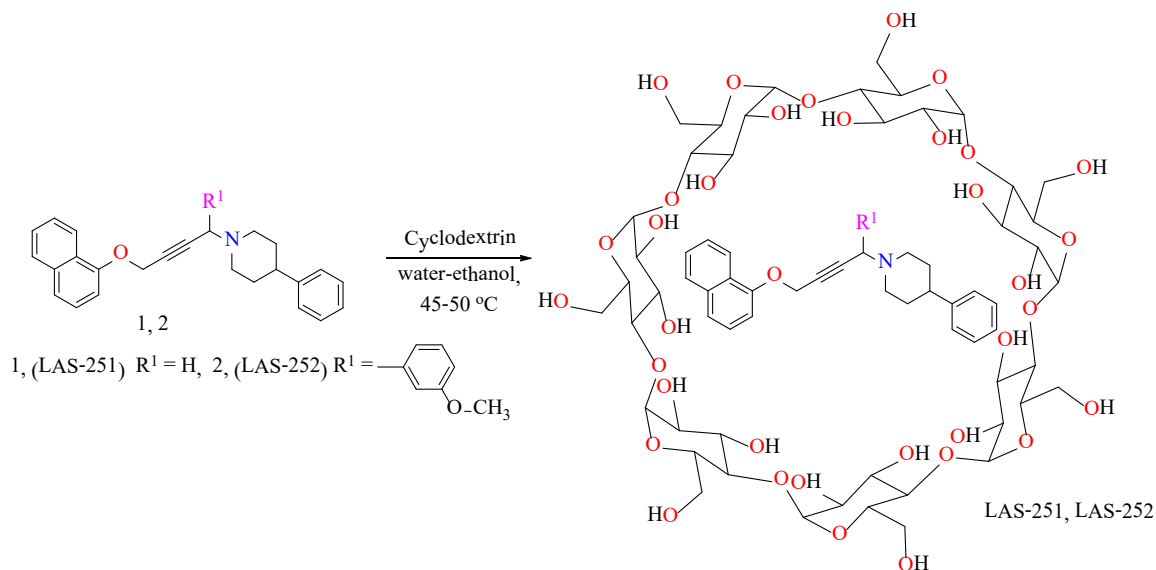
Scheme 2. Synthesis of β-cyclodextrin complex with 1-(4-(naphthalen-1-yloxy)but-2-yn-1-yl)-4-phenylpiperidine (LAS-251) and β-cyclodextrin complex with 1-(1-(3-methoxyphenyl)-4-(naphthalen-1-yloxy)but-2-yn-1-yl)-4-phenylpiperidine (LAS-252)

Acute toxicity assessment

Solutions of the studied compounds were administered to laboratory mice in 3 increasing concentrations following body weight, in a total volume of no more than 1 ml. As a result of observations with the administration of toxic doses, the clinical signs of intoxication of both compounds were similar. They differed in the rate of increase in symptoms of intoxication with an increase in dose.

After subcutaneous administration of high doses (500-700 mg/kg) of LAS-251 in the first 15 min, fading, muscle tremor with increased muscle tone, and increased breathing were observed in animals. The motor and research activity decreased in the following first hours of observation. Behavioural responses did not change, while responses to sound stimuli were preserved. From the second day onwards, symptoms of intoxication increased in several animals. Disturbances of motor activity with further developing adynamia and rapid breathing, lack of interest in food and water were revealed in laboratory animals. The animals took a lateral position, after which the death of laboratory animals in experimental groups was noted 2-3 days after administration.

The LAS-252 showed a variable range of symptoms in its poisoning pattern. The first signs of intoxication appeared in 2-4 min at a dose of 700 mg/kg.

Almost all animals had decreased motor and exploratory activity and a lack of response to sound stimuli. One animal suffered from seizures, followed by ataxia and subsequent death. The mortality of other animals in the group was recorded after 1-2 days. When the dosage was increased to 1000 mg/kg, this compound showed pronounced neurotoxicity, which was manifested by tonic-clinical seizures with a frequency of 30-40 s. The death of more than half of the mice in the experimental group occurred already in the first 1.5-2 hours of observation.

When studying the acute toxicity of new piperidine derivatives, the median lethal doses were determined. The tested compounds turned out to be less toxic than procaine, lidocaine, and trimecaine by subcutaneous administration. Considering the chemical structure, the LD_{50} values of LAS-251 and LAS-252 differed slightly (Table 1.).

Table 1. Values of LD_{50} piperidine derivatives in the study of acute toxicity.

Compound, reference drug	LD_{16}	LD_{50}, mg/kg	LD_{84}
LAS-251	245.6	531.5±156.3	792.57
LAS-252	352.2	508.5±101.9*	709.2
1. Lidocaine		230±35.7	
2. Procaine	-	480±1.0	-
3. Trimecaine		375±3.1	

Data were reported as means±SE (n=6). *P<0.05 compared to lidocaine (t-test). The differences in the indicators are statistically significant (p<0.05).

The LD_{50} of these compounds significantly exceeded those of lidocaine and trimecaine and were approximately comparable to procaine. However, the difference was statistically significant only in LAS-252 compared to lidocaine (p < 0.05).

Assessment of local anesthetic activity

The results of the primary study of local anesthetic activity during infiltration anesthesia (Bulbring and Wajda model) are presented in Figure 4.
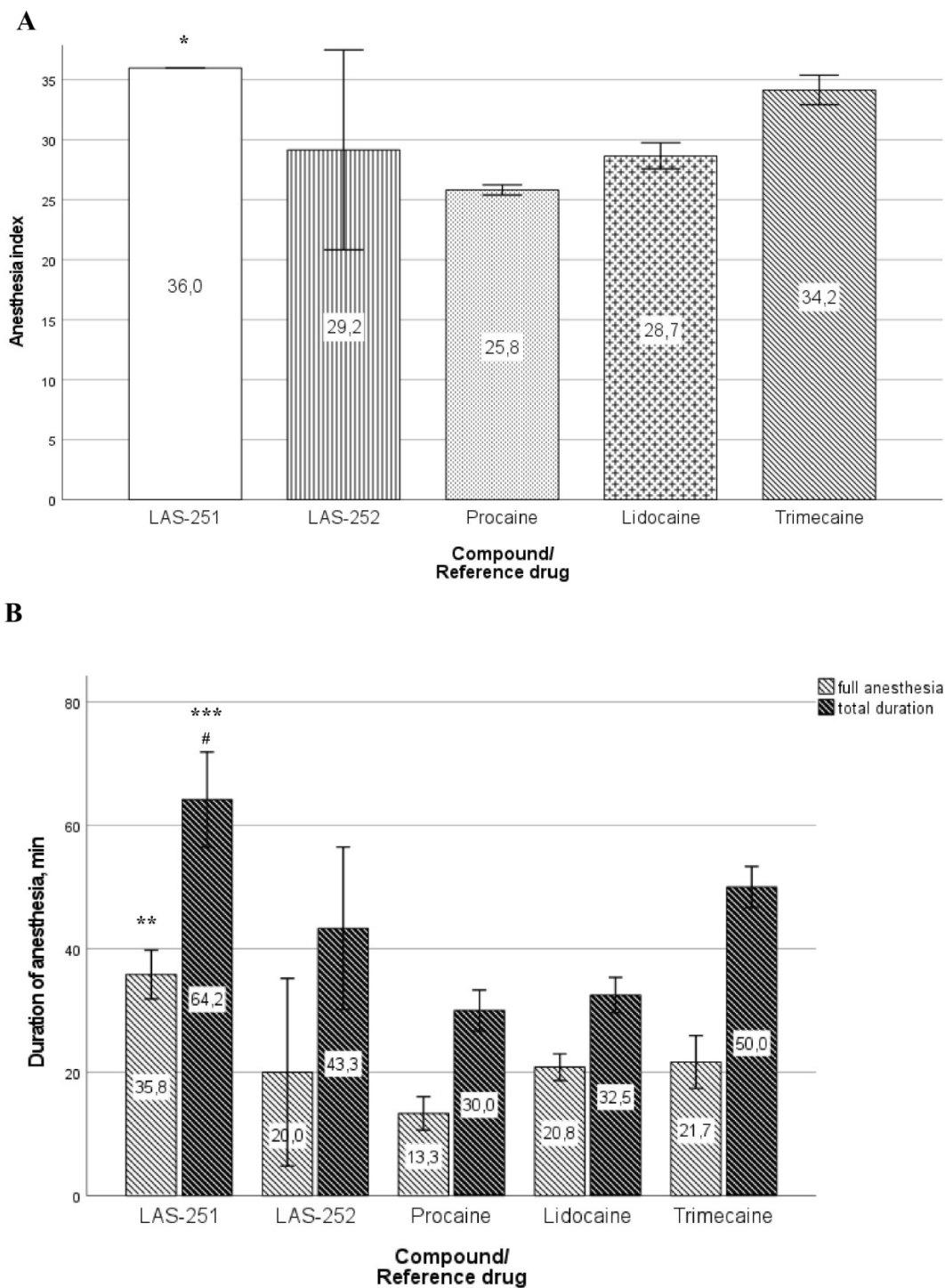
Figure 4. Indicators of the local anesthetic activity (0.5% aqueous solutions). Data are reported as means±SD (n=6), (ANOVA): A - Anesthesia index (max-36). *P<0.001 compared to procaine and lidocaine. B - Duration of anesthesia. **P<0.001 compared to all reference drugs, ***P<0.001 compared to procaine and lidocaine,#P<0.05 compared to trimecaine.

Of the two compounds studied, the piperidine derivative LAS-251 turned out to be the most active. A comparison of the indicators of local anesthetic activity of LAS-251 and reference drugs revealed statistically significant differences. The anesthesia index has reached its maximum value, which indicates the presence of pronounced local anesthetic activity superior to reference drugs, especially in comparison to procaine and lidocaine. According to the duration of full anesthesia, the studied compound was statistically significantly superior to the reference drugs, in particular: procaine - 2.7 times, lidocaine - 1.7 times, and trimecaine - 1.6 times. The total duration of anesthesia with the administration of LAS-251 lasted 64.2 min, which is 2 times longer than with procaine and lidocaine. The tested compound was superior to the

most active local anesthetic by 14.2 min.

LAS-252 had advantages over procaine in all parameters determined in the experiment, and in terms of the index and duration of complete anesthesia, it practically corresponded to those of lidocaine. The total duration of the local anesthetic effect of LAS-252 was higher than that of procaine. However, the differences identified with the comparison drugs were not statistically significant ($p > 0.05$).

Considering the initial experimental results, an in-depth study of local anaesthetic activity was carried out for compound LAS-251. In the conducted experiments, the rate of anesthesia onset, the duration of full anesthesia and the total duration of effect were determined (Table 2.).

Table 2. The local anesthetic activity of LAS-251 during the infiltration anesthesia of the abdominal wall in a rabbit (0.5% aqueous solutions).

Compound/ Reference drug	Anesthesia onset rate, min	Duration of full anesthesia, min	Total duration of anesthesia, min
LAS-251	9.7±2.0*	0	40.3±2.5**#
Procaine	3.0±0	0	23.8±1.5
Lidocaine	3.0±0	0	47.5±1.1
Trimecaine	3.0±0	5.0±0	86.6±2.1

Data reported as means±SE (n=6).*$P<0.05$ compared to all reference drugs, **$P<0.001$ compared to procaine and trimecaine, #$P<0.05$ compared to lidocaine (t-test). The differences in the indicators are statistically significant ($P<0.05$).

The local anesthetic effect of LAS-251 developed much slower, and the latency period was more than 3 times higher than the corresponding values of the reference drugs. Full anesthesia was not achieved, which was also typical for procaine and lidocaine. The experiments found that LAS-251 was significantly inferior to trimecaine and to a small extent to lidocaine in terms of total duration of infiltration anaesthesia, but exceeded this indicator of procaine by 16.5 min. Thus, the study confirmed the presence of local anesthetic activity with the achievement of anesthesia depth in laboratory animals by an average of 26.7%, with some advantage compared to procaine.

Currently, the piperidine cycle is quite a sought-after framework in pharmaceutics for developing new drugs. The chemical structure of piperidine can be found in more than twenty pharmacological groups and alkaloids (Frolov et al., 2023). A review of scientific research showed that several thousand different piperidine derivatives have been reported from preclinical and clinical studies over the last decade (Källström et al., 2008). There are not many studies on searching for compounds with local anesthetic activity among them, even though the piperidine ring is one of the components of the chemical structure of local anesthetics (Martins et al., 2017).

The results of our study revealed local anesthetic activity of previously unstudied new piperidine derivatives during infiltration anesthesia, expressed to varying degrees. The primary toxicity study demonstrated the safety of the substances in a further series of experiments to determine their efficiency, which also compares favorably with other studies. Another distinctive feature is the use of an in-depth research model, the conditions of which are as close as possible to clinical practice, which made it possible to obtain more reliable and expanded results. The local anesthetic indices presented in this article demonstrate the presence of local anesthetic activity of the piperidine derivative LAS-251, which correlates with the data of world studies. The lower activity of LAS-252 is probably due to the presence of a methoxyphenyl fragment, which affected solubility and, consequently, efficiency. The presence of a free hydrogen atom in the molecule LAS-251 apparently improved the solubility and increased its efficiency.

Earlier studies revealed local anesthetic activity of several new phenylpiperidine derivatives exceeding procaine, but the substances caused necrotic changes and exhibited higher toxicity in the cocaine range (Fellows et al., 1944). The findings of this review confirm the results of previous studies of different series of substances from the group of piperidines with local anesthetic activity in various types of anesthesia (Khaiitova et al., 2022). As in our study, the experimental drug kazcaine [1-(2-ethoxyethyl)-4-ethynyl-benzoyloxypiperidine hydrochloride], has high activity in infiltration anesthesia even in 0.1% solution (Kemelbekov U et al., 2010). In contrast to kazcaine, LAS-251 was effective in 0.5% and inferior in activity to lidocaine and trimecaine in a series of in-depth tests.

Another similar study [4-(benzoyloxy)-3-butoxy-piperidinium chloride] also showed marked activity not only for infiltration but also for conduction anesthesia with the effect enhanced by combination with epinephrine (Pichkhadze et al., 2016). The study of

potentiation of the efficacy of the compounds of the present research in interaction with vasoconstrictors is of interest in further tests. The activity of piperidine derivatives is also interesting in terminal anesthesia. In one study, the S-isomer of 2-{2-[N-(2-indanyl)-N-phenylamino]ethyl} piperdine was shown to be effective in local anesthetic action when applied to the surface of skin and mucous membranes (Gunnar et al., 2010).

The emergence of a new class of safer, highly active opioid analgesics and anesthetics is associated with the creation of several compounds containing 4-phenylpiperidine, found in morphine, in their structure (Kudzma et al., 1989). Verification of the analgesic activity of the compounds studied in this article may be a target for future studies. Considering that analgesic effects are also present in other piperidines with proven efficacy, such as promedol and fentanyl (Vasilyuk et al., 2021).

A comprehensive analysis of the results presented in this article allows us to conclude that the new piperidine derivative LAS-251 should be considered as a potential drug substance for the development of new highly effective drugs based on it. Preclinical studies of efficacy in other types of anesthesia, other pharmacological effects may become the subject of future studies.

CONCLUSION

In conclusion, it should be noted that the new 4-(Naphthalen-1-yloxy)but-2-yn-1-yl)-containing piperidine derivatives synthesized quite simply under the conditions of the Mannich reaction by the interaction of 1-(prop-2-ynyloxy) naphthalene with 4-phenylpiperidine and aromatic aldehydes in the presence of CuI are low-toxic substances, which are confirmed by the results of an acute toxicity tests. LAS-251 compound showed the greatest activity in the initial study of local anaesthetic activity during infiltration anaesthesia in the Bulbring and Wajda experimental model, surpassing the reference drugs in terms of anesthesia index, duration of full anesthesia and total duration

of action. The stage of in-depth study showed that, despite a longer latency period, LAS-251 has a local anesthetic effect longer than procaine and is slightly inferior to lidocaine. The results of the research suggest that the novel piperidine derivative LAS-251 is promising for further study in other types of anesthesia as a potential medicinal substance for therapeutic applications in the future.

AUTHOR CONTRIBUTION STATEMENT

Conduction of experiments, analysis of data and writing of original draft (MK), synthesis and structural analysis of compounds (YS), assistance with modelling of experiments and writing the manuscript (VT), design and direction of the project, editing of the pharmacological part (ES), writing and editing of chemical part (VY), review and supervision of the pharmacological part (TN), study conception and supervision of the pharmacological part (ES), data recording and assistance with experiments (YG), visualization and software (ZU), review and supervision of chemical part (KT)

CONFLICT OF INTEREST

The authors declare that there is no conflict of interest.

REFERENCES

Baker, J. F., & Mulhall, K. J. (2012). Local anaesthetics and chondrotoxicty: What is the evidence? *Knee surgery, sports traumatology, arthroscopy : official journal of the ESSKA*, *20*(11), 2294–2301. https://doi.org/10.1007/s00167-011-1804-6

Barse, B., Kaul, P., Banerjee, A., Kaul, C.L., & Banerjee, U.C. (2003). Cyclodextrins: emerging applications. *Chimicaoggi*, *21*(9), 48-53. https://eurekamag.com/research/004/093/004093661.php

Becker, D. E., & Reed, K. L. (2012). Local anesthetics: review of pharmacological considerations. *Anesthesia progress*, *59*(2), 90–103. https://doi.org/10.2344/0003-3006-59.2.90

Bulbrıng, E., & Wajda, I. (1945). Biological comparison of local anaesthetics. *The Journal of pharmacology and experimental therapeutics*, *85*(1), 78–84. https://jpet.aspetjournals.org/content/85/1/78

Chahar, P., & Cummings, K. C., 3rd (2012). Liposomal bupivacaine: a review of a new bupivacaine formulation. *Journal of pain research*, *5*, 257–264. https://doi.org/10.2147/JPR.S27894

Chitilian, H. V., Eckenhoff, R. G., & Raines, D. E. (2013). Anesthetic drug development: Novel drugs and new approaches. *Surgical neurology international*, *4*(Suppl 1), S2–S10. https://doi.org/10.4103/2152-7806.109179

De, S., Banerjee, S., Babu, M. N., & Keerithi, C. N. (2015). Importance of piperidone moiety in pharmaceutical chemistry: a review. *Journal of Applied Pharmaceutical Research*, *3*(2), 08-15. https://japtronline.com/index.php/joapr/article/view/52

Fellows, E. J. (1944) Local Anesthetic Activity of a Series of Phenyl Piperidine Derivatives. *Proceedings of the Society for Experimental Biology and Medicine*, *57*(2), 276-277. https://doi.org/10.3181/00379727-57-14781

Frolov, N. A., Vereshchagin, A. N. (2023). Piperidine Derivatives: Recent Advances in Synthesis and Pharmacological Applications. *International Journal of Molecular Sciences*, *24*(3), 2937. https://doi.org/10.3390/ijms24032937

Grzanka, A., Wasilewska, I., Śliwczyńska, M., & Misiołek, H. (2016). Hypersensitivity lo local anesthetics. *Anaesthesiology intensive therapy*, *48*(2), 128–134. https://doi.org/10.5603/AIT.a2016.0017

Gunnar, A., & Jan, L. Ch. (2010). S-Isomer of 2- piperidine and Other Dermal Anesthetic Agents. (US Patent No 2010/0179114A1). United States, Jul. 15. https://patents.google.com/patent/US20100179114A1/en?oq=US+2010%-2f0179114A1

Ilfeld, B. M., Eisenach, J. C., & Gabriel, R. A. (2021). Clinical Effectiveness of Liposomal Bupivacaine Administered by Infiltration or Peripheral Nerve Block to Treat Postoperative Pain. *Anesthesiology*, *134*(2), 283–344. https://doi.org/10.1097/ALN.0000000000003630

Johansson, K. S., Høgberg, L. C. G., Christensen, M. B., Petersen, T. S., Dalhoff, K., & Bøgevig, S. (2020). Local anaesthetic systemic toxicity. *Ugeskrift for laeger*, *182*(51), V11190656. https://ugeskriftet.dk/videnskab/systemisk-toksicitet-ved-lokalanalgetika

Källström, S., & Leino, R. (2008). Synthesis of pharmaceutically active compounds containing a disubstituted piperidine framework. *Bioorganic & Medicinal Chemistry*, *16*(2), 601-35. https://doi.org/10.1016/j.bmc.2007.10.018

Kemelbekov, U.S., Hagenbach, A., Lentz, D., Imachova, Sh.O., Pichkhadze, G.M., Rustembekov, Zh.I., Beketov, K.M., Praliyev, K.D., Gabdulkhakov, A., Guskov, A., & Saenger, W. (2010). Pharmacology and structures of the free base of the anaesthetic kazcaine and its complex with β-cyclodextrin. *Journal of Inclusion Phenomena and Macrocyclic Chemistry, 68*, 323-330. https://doi.org/10.1007/s10847-010-9791-7

Khaiitova, M., Seitaliyeva, A., Satbayeva, E., Serdalieva, D., & Nurgozhin, T. (2022) Experimental study of the pharmacological activity of new azaheterocycles derivatives: A literature review. *Journal of clinical medicine of Kazakhstan, 19*(1), 16-22. https://doi.org/10.23950/jcmk/11680

Kottapalle, G., & Shinde, A. (2021). Synthesis of 1-(2-substitutedphenyl-2,3-dihydro-1H-benzo[b][1,4]diazepin-4-yl)naphthalene-2-ol under different solvent conditions as a potent antimicrobial agent. *Chemical Data Collections*, *33*, 100690. https://doi.org/10.1016/j.cdc.2021.100690

Kudzma, L. V., Severnak, S. A., Benvenga, M. J., Ezell, E. F., Ossipov, M. H., Knight, V. V., Rudo, F. G., Spencer, H. K., & Spaulding, T. C. (1989). 4-Phenyl- and 4-heteroaryl-4-anilidopiperidines. A novel class of analgesic and anesthetic agents. *Journal of medicinal chemistry*, *32*(12), 2534–2542. https://doi.org/10.1021/jm00132a007

Kuzenbayeva, R.S., Rakhimov, K.D., Shin, S.N., & Chukanova, G.N. (2000). *Methodological guide: Preclinical study of local anesthetic activity of new biologically active substances*. Almaty: Kazakhstan, (available in Russian).

Ma, N., Duncan, J. K., Scarfe, A. J., Schuhmann, S., & Cameron, A. L. (2017). Clinical safety and effectiveness of transversus abdominis plane (TAP) block in post-operative analgesia: a systematic review and meta-analysis. *Journal of anesthesia*, *31*(3), 432–452. https://doi.org/10.1007/s00540-017-2323-5

Martins, M. L., Eckert, J., Jacobsen, H., Dos Santos, É. C., Ignazzi, R., de Araujo, D. R., Bellissent-Funel, M. C., Natali, F., Koza, M. M., Matic, A., de Paula, E., & Bordallo, H. N. (2017). Probing the dynamics of complexed local anesthetics via neutron scattering spectroscopy and DFT calculations. *International journal of pharmaceutics*, *524*(1-2), 397–406. https://doi.org/10.1016/j.ijpharm.2017.03.051

McMahon, K., Paster, J., & Baker, K. A. (2022). Local anesthetic systemic toxicity in the pediatric patient. *The American journal of emergency medicine*, *54*, 325.e3–325.e6. https://doi.org/10.1016/j.ajem.2021.10.021

Mironov, A.N. (2012). *Guidelines for conducting preclinical studies of medicines. Part one*. Grif & Co: Moscow, Russia, 944, (available in Russian).

National Research Council (US) Committee for the Update of the Guide for the Care and Use of Laboratory Animals (2011). *Guide for the Care and Use of Laboratory Animals (8th ed.)*. Washington (DC): National Academies Press (US).

Pichkhadze, G.M., Smagulova, G.S., Kadyrova, D.M., Praliev K.D., & Yu V.K. (2016). Local Anesthetic Activity of a Promising Piperidine Derivative (LAS-54) in Combination with Epinephrine. *Pharmaceutical Chemistry Journal, 50*, 600–602. https://doi.org/10.1007/s11094-016-1498-7

Raithel, S. J., Sapio, M. R., Iadarola, M. J., & Mannes, A. J. (2018). Thermal A-δNociceptors, Identified by Transcriptomics, Express Higher Levels of Anesthesia-Sensitive Receptors Than Thermal C-Fibers and Are More Suppressible by Low-Dose Isoflurane. *Anesthesia and analgesia*, *127*(1), 263–266. https://doi.org/10.1213/ANE.0000000000002505

Randhawa, M. A. (2009). Calculation of LD50 values from the method of Miller and Tainter, 1944. *Journal of Ayub Medical College, Abbottabad : JAMC*, *21*(3), 184–185. https://www.ayubmed.edu.pk/JAMC/PAST/21-3/Randhawa.pdf

Tsai, S. H. L., Yolcu, Y. U., Hung, S. W., Kurian, S. J., Alvi, M. A., Fu, T. S., & Bydon, M. (2021). The analgesic effect of intravenous lidocaine versus intrawound or epidural bupivacaine for postoperative opioid reduction in spine surgery: A systematic review and meta-analysis. *Clinical neurology and neurosurgery*, *201*, 106438. https://doi.org/10.1016/j.clineuro.2020.106438

Uekama, K. (2002). Recent aspekts of pharmaceutical applikation of cyclodextrins. *Journal of Inclusion Phenomena and Macrocyclic Chemistry*, *44*, 3-7. https://doi.org/10.1023/A:1023007032444

Vasilyuk, A. A., & Kozlovsky, V. I. (2021). Promising directions for the application of piperidine derivatives as structural components of neurotropic drugs (available in Russian). *Vestnik VGMU, 20*(2), 8-17. https://doi.org/10.22263/2312-4156.2021.2.8

Verlinde, M., Hollmann, M. W., Stevens, M. F., Hermanns, H., Werdehausen, R., & Lirk, P. (2016). Local Anesthetic-Induced Neurotoxicity. *International journal of molecular sciences*, *17*(3), 339. https://doi.org/10.3390/ijms17030339

Vitaku, E., Smith, D. T., & Njardarson, J. T. (2014). Analysis of the structural diversity, substitution patterns, and frequency of nitrogen heterocycles among U.S. FDA approved pharmaceuticals. *Journal of medicinal chemistry*, *57*(24), 10257–10274. https://doi.org/10.1021/jm501100b

Wadlund D. L. (2017). Local Anesthetic Systemic Toxicity. *AORN journal*, *106*(5), 367–377. https://doi.org/10.1016/j.aorn.2017.08.015

Weiser, T. G., Regenbogen, S. E., Thompson, K. D., Haynes, A. B., Lipsitz, S. R., Berry, W. R., & Gawande, A. A. (2008). An estimation of the global volume of surgery: a modelling strategy based on available data. *Lancet (London, England)*, *372*(9633), 139–144. https://doi.org/10.1016/S0140-6736(08)60878-8

Woolf C. J. (2010). What is this thing called pain? *The Journal of clinical investigation*, *120*(11), 3742–3744. https://doi.org/10.1172/JCI45178

Xie, Y. K., Luo, H., Zhang, S. X., Chen, X. Y., Guo, R., Qiu, X. Y., Liu, S., Wu, H., Chen, W. B., Zhen, X. H., Ma, Q., Tian, J. L., Li, S., Chen, X., Han, Q., Duan, S., Shen, C., Yang, F., & Xu, Z. Z. (2022). GPR177 in A-fiber sensory neurons drives diabetic neuropathic pain via WNT-mediated TRPV1 activation. *Science translational medicine*, *14*(639), eabh2557. https://doi.org/10.1126/scitranslmed.abh2557

Yin, Q., Zhang, W., Ke, B., Liu, J., & Zhang, W. (2021). Lido-OH, a Hydroxyl Derivative of Lidocaine, Produced a Similar Local Anesthesia Profile as Lidocaine With Reduced Systemic Toxicities. *Frontiers in pharmacology*, *12*, 678437. https://doi.org/10.3389/fphar.2021.678437

Yu, S., Wang, B., Zhang, J., & Fang, K. (2019). The development of local anesthetics and their applications beyond anesthesia. *International Journal of Clinical and Experimental Medicine,12*(12), 13203-13220. https://www.ijcem.com/files/ijcem0100790.pdf

Yu, V. K., Sycheva, Y. S., Kairanbayeva, G. K., Dembitsky, V. M., Balabekova, M. K., Tokusheva, A. N., Seilkhanov, T. M., Zharkynbek, T. Y., Balapanova, A. K., & Tassibekov, K. S. (2023). Naphthalene-oxypropargyl-Containing Piperazine as a Regulator of Effector Immune Cell Populations upon an Aseptic Inflammation. *Molecules (Basel, Switzerland)*, *28*(20), 7023. https://doi.org/10.3390/molecules28207023

Zuffo, M., Stucchi, A., Campos-Salinas, J., Cabello-Donayre, M., Martínez-García, M., Belmonte-Reche, E., Pérez-Victoria, J. M., Mergny, J. L., Freccero, M., Morales, J. C., & Doria, F. (2019). Carbohydrate-naphthalene diimide conjugates as potential antiparasitic drugs: Synthesis, evaluation and structure-activity studies. *European journal of medicinal chemistry*, *163*, 54–66. https://doi.org/10.1016/j.ejmech.2018.11.043

Assessment of the Antioxidant, Antiproliferative and Antityrosinase Potential of Unripe Fruit of *Prunus x domestica* L.

Zühal BAYRAKÇEKEN GÜVEN*°, Neslihan YUCE**, A. Ahmet BASARAN***

Assessment of the Antioxidant, Antiproliferative and Antityrosinase Potential of Unripe Fruit of Prunus x domestica L.

SUMMARY

Prunus x domestica L. is a valuable plant that belongs to the Rosaceae family and is distributed worldwide. The aim of this study is to investigate the biological effect of the unripe green fruits of P. domestica, which have only been studied to a limited extent so far. The antioxidant capacity of the fruit extracts and subfractions was investigated by DPPH, TEAC and CUPRAC assays. The antiproliferative effect was investigated against the cell lines L929, CaCo-2 and PC-3. While the highest antiproliferative effect against cancer cell lines was found in the unripe fruit ethyl acetate subfraction, extracts and fractions showed no cytotoxic effect on the healthy cell line L929. The fruit ethyl acetate fraction showed a strong inhibition of the enzyme tyrosinase with an IC50: 51.83 µg/mL compared to standard compound kojic acid (IC50: 21 µg/mL). It was found that the methanol extract from unripe fruits as well as the ethyl acetate and aqueous subfractions exhibited strong antioxidant activity, showed concentration-dependent cytotoxic activity on PC-3 and CaCo-2 cells, but had no cytotoxic effect on healthy L929 cells. The high antioxidant capacity of the fruits, their selective cytotoxic effect on prostate and colon cancer cells and their strong tyrosinase inhibitory activity suggest that they could be a new, safe and cost-effective source for the pharmaceutical and cosmeceutical industries.

***Key Words:** Prunus domestica L., unripe fruit, antioxidant, antiproliferative, tyrosinase inhibition.*

Prunus x domestica L. Olgunlaşmamış Meyvelerinin Antioksidan, Antiproliferatif ve Antitirozinaz Potansiyellerinin Değerlendirilmesi

ÖZ

Prunus x domestica L., Rosacea familyasına ait olan ve dünya çapında yaygın bulunan değerli bir bitkidir. Bu çalışmanın amacı; bugüne kadar sınırlı sayıda çalışılan P. domestica olgunlaşmamış yeşil meyvelerinin biyolojik etkisinin incelenmesidir. Meyve ekstraktlarının antioksidan kapasiteleri DPPH, TEAC, CUPRAC yöntemleriyle incelendi. Antiproliferatif aktivite L929, CaCo-2 ve PC-3 hücre hatlarına karşı araştırıldı. Kanser hücre hatlarına karşı en yüksek antiproliferatif etki meyve etilasetat alt fraksiyonunda bulunurken, tüm ekstreler L929 sağlıklı hücre hattında sitotoksik etki gösterdi. Meyve etilasetat fraksiyonu standart olarak kullanılan kojik asitle (IC50: 21 µg/mL) kıyaslandığında IC50: 51.83 µg/mL değeri ile güçlü tirozinaz enzim inhibisyonu gösterdi. Olgunlaşmamış meyve metanol ekstresi ile etilasetat ve sulu alt fraksiyonların güçlü antioksidan aktiviteye sahip olduğu, PC-3 ve CaCo-2 hücreleri üzerinde konsantrasyona bağlı olarak sitotoksik aktivite gösterdiği, ancak sağlıklı L929 hücreleri üzerinde sitotoksisite etkisi olmadığı görüldü. Meyvelerin yüksek antioksidan kapasitesi, prostat ve kolon kanser hücreleri üzerindeki seçici sitotoksik etkisi ve güçlü tirozinaz enzim inhibitör etkisi ile ilaç ve kozmesötik endüstrisi için yeni, toksik olmayan ve ucuz bir kaynak olabileceğini düşündürmektedir.

***Anahtar Kelimeler:** Prunus domestica L., olgunlaşmamış meyve, antioksidan, antiproliferatif, tirozinaz inhibisyonu.*

* ORCID: 0000-0003-3405-6996, Department of Pharmacognosy, Faculty of Pharmacy, Erzincan Binali Yıldırım University, Erzincan, Turkey
** ORCID: 0000-0001-6878-064, Department of Medical Biochemistry, Faculty of Medicine, Ataturk University, Erzurum, Turkey
*** ORCID: 0000-0001-8570-9649, Department of Pharmacognosy, Faculty of Pharmacy, Baskent University, Ankara, Turkey

° Corresponding Author; Zühal Bayrakçeken Güven
E-mail: zhlbayrakceken@gmail.com

INTRODUCTION

Nature has always been the leading supplier of compounds, which are the leading raw materials for medicines, important for disease prevention and cure, and the inspiration for medical developments. In addition to drug discovery, organic synthesis, and biotechnological research, research into the development of natural compounds is one of the most important contributions to drug discovery and is becoming increasingly important. For example, chemotherapeutics derived from natural sources are becoming increasingly crucial as better therapeutic options for the cancer treatment. In addition, plants with high antioxidant activity also show promising results in the prevention and treatment of various diseases. Fruit, which are mainly consumed as food, are considered a potential source of cosmetic products thanks to their rich content of phenolic substances and their safe use (Kabir et al., 2021; Lu et al., 2021; Madhuri & Pandey, 2009; Maheshwari & Sharma, 2023; Sharafan et al., 2023).

Interest in research on *P. domestica* fruits (plums) has increased significantly since the 1990s due to the high content of phenolic substances in plums, including anthocyanin and flavonoids. Studies have shown that plums fruits have many health benefits, including improving bone health, boosting memory, antioxidants, anti-inflammatory and anti-cancer effects, and relieving constipation. These positive effects on health can be attributed to the antioxidant effect of plums, which is linked to their high phenol content (Ayub et al., 2023; Igwe & Charlton, 2016).

Many epidemiological studies show that a diet rich in vegetables and fruit can improve health and reduce the risk of major diseases. Fruit and vegetables are rich in vitamins, minerals and antioxidants, they are a source of fiber and have a low energy density, which makes them valuable for health (Angelino et al., 2019; Ayub et al., 2023). In this respect, the rich content of minerals and phytochemicals of *P. domestica* fruits appears to be a promising species identifying

bioactive natural products. Fruit are an essential source of magnesium, calcium, and fiber in the daily diet. They contain various valuable phytochemicals such as abscisic acid, lignans anthocyanins and flavonoids, pectins and carotenoids, glycosides, and carbohydrates. Anthocyanins, flavonoids, and hydroxycinnamic acid, which are abundant in plums, are considered secondary metabolites responsible for the antioxidant effect (Ayub et al., 2023; Shukla, Shukla, & Singh, 2021; Usenik, 2021).

The studies carried out so far have shown that there are mainly studies on phytochemical and biological effects on ripe fruits, but very few studies have been found on unripe fruits. In this study, the antiproliferative effects of the methanol extract, ethyl acetate and aqueous fractions obtained from the unripe fruits of *P. domestica* were analyzed against L929, PC-3, CaCo-2 and the total antioxidant activity by DPPH, CUPRAC and TEAC methods. By studying the tyrosinase enzyme inhibition of the extracts, their effect on the healthy fibroblast cell line L929, and their antioxidant activity, their safe and effective potential cosmetic effects were investigated.

MATERIAL AND METHODS

Plant Material

The unripe green fruits of *Prunus x domestica* L. were collected in April 2022 at the Sıhhiye Campus of Hacettepe University. A voucher specimen was deposited in the Herbarium of the Faculty of Pharmacy, Hacettepe University, Ankara, Turkey [HUEF 22059]. The voucher specimen was identified by Prof Dr. A. Ahmet Basaran (Department of Pharmacognosy, Faculty of Pharmacy, Baskent University, Ankara, Turkey).

Preparation of extract and fractions from *Prunus x domestica* L.

Unripe fruits of *P. domestica* (20 g) were extracted three times with methanol (200 mL) at a temperature of not more than 40 °C. The three parts obtained were added to each other and evaporated with the

evaporator, yielding the main extract of methanol (0.95 g). The extract was then suspended in water and a liquid-liquid partitioning was performed with petroleum ether (PE) to separate lipophilic compounds, especially chlorophylls. The aqueous fraction was then extracted with 2x100 mL ethyl acetate (EtOAc), the solvents were evaporated, and the ethyl acetate (0.11 g) and aqueous subfractions (0.54 g) were recovered separately. These were stored at 4 °C to be used for biological effect studies.

Mushroom tyrosinase enzyme inhibition assay

Inhibition of tyrosinase enzyme assay was performed with some modifications to the method developed by Kim et al.(Güven et al., 2022; Güven, Saracoglu, Nagatsu, Yilmaz, & Basaran, 2023; Kim et al., 2017). In this method, in which L-tyrosine was used as a substrate, the absorbance of the dopachrome formed during the reaction between the substrate and the enzyme was measured spectrophotometrically at a wavelength of 475 nm and compared with the blank value. Kojic acid was applied as a standard compound (positive control).

DPPH radical scavenging effect

The DPPH radical scavenging effect was determined by spectroscopic evaluation of the color change from purple to yellow in the reaction mixture of methanolic 2,2-diphenyl-1-picrylhydrazyl (DPPH) solution (Harput, Genc, & Saracoglu, 2012). All analyses were performed in triplicate. Gallic acid was used as a standard compound to compare the results, and the values obtained were expressed as gallic acid equivalents.

ABTS scavenging activity

The ABTS [2,2'-azino-bis(3-ethylbenzothiazoline-6-sulfonic acid)] radical scavenging activity of the extracts and fractions was evaluated spectrophotometrically by the decolorization assay, with absorbance measured at 734 nm. Trolox was used as the standard compound, and the total antioxidant activity was calculated as equivalent to Trolox and expressed as mg Trolox/g extract (Re et al., 1999).

Copper Reducing Antioxidant Capacity (CUPRAC)

The antioxidant capacity that reduces copper ions was determined by the method developed by Özyürek et al., and the experimental results were calculated by measuring the absorbance values at 450 nm (Ozyurek, Bektasoglu, Guclu, & Apak, 2009). Standard curve was prepared with different Trolox concentrations. The unit of total antioxidant activity was expressed as mg Trolox/g extract.

Antiproliferative activity

The effect of different extracts of *P. domestica* fruit, such as methanol, ethyl acetate, and water on cell viability was examined using Cell Viability Detection Kit-8 (CVDK8, Ecotech Biotechnology, Erzurum, Türkiye) following the manufacturer's protocol (Barlak et al., 2021). Cell viability was measured every 24 hours for two days. The L929 (CRL-2148, ATCC), PC-3 (CRL-1435, ATCC) and CaCo-2 (HTB-37, ATCC) cells obtained from the American Type Culture Collection (ATCC). *P. domestica* fruit extracts were prepared at different concentrations (800-400-200-100-50 µg/mL) with serum medium. PC-3, CaCo-2, and L929 cells were treated with these extracts for 24 and 48 hours. PC-3, CaCo-2 cells were seeded in 96-well plate wells with 4.5 x10^3 cells per well, while L929 cells were seeded in 96-well plate wells with 4.2x10^3 cells per well. They were incubated for 24 and 48 hours. At the end of the incubation period, the medium in the wells was removed and the medium was added to each well as a 10% CVDK-8 solution. The cells were incubated again in the incubator for 3 hours. The viability of the cells was determined by measuring the optical density at 450 nm using a Benchmark Plus microplate spectrophotometer (Biorad, Segrate-Milano, Italy). The change in cell viability was calculated by comparing the absorbance values of the control groups. Experiments were performed with at least three replicates.

Statistical analysis

The data were analyzed using the Statistical Package for Social Science (SPSS) program. The Kolmogorov-Smirnov test was used to determine

whether the data were normally distributed. Since the data showed normal distribution, the results were expressed as mean ± standard deviation. One-way analysis of variance (ANOVA) followed by Tukey's post hoc test was applied to the results, and the differences were considered significant at p < 0.001. Two-way analyses of variance (ANOVA) were used to evaluate both factors. The results were assessed at 95% confidence interval and p<0.001 was considered statistically significant.

RESULTS AND DISCUSSION

Evaluation of the antiproliferative potential of the extract and fractions

The main methanol extract of *P. domestica* fruits, and the remaining EtOAc and H_2O subfractions were prepared separately. To evaluate the cytotoxicity of the obtained extracts and fractions their effects on cell proliferation of two cancer cell lines PC-3 (human prostate carcinoma), CaCo-2 (human colorectal adenocarcinoma) and normal L929 (murine fibroblast) cells were determined using the CVDK method.

The results showed a dose-dependent cytotoxicity of the EtOAc fraction against the cell lines PC-3 and CaCo-2 in concentration ranges of 50-800 μg/mL (Figures 1 and 2). The ethyl acetate fraction inhibited PC-3 cells by 41.36 % at the highest concentration (Figure 1.). The cytotoxic effect was found to be limited against all cell lines in the aqueous fractions. The main fruit extract and fractions showed negligible antiproliferative activity in the L929 cell line (Figure 3). Cell viability was 93.84%, even at the highest concentration of the ethyl acetate fraction (800 μg/mL) Miljic et al. tested the cytotoxic effects of fruit wines obtained from three plum varieties common in Serbia on Hep2c, RD and L2OB cancer cell lines. A significant decrease in cell viability was observed with an $IC_{50} < 50$ μg/mL value against all three cell lines (Miljić et al., 2016).
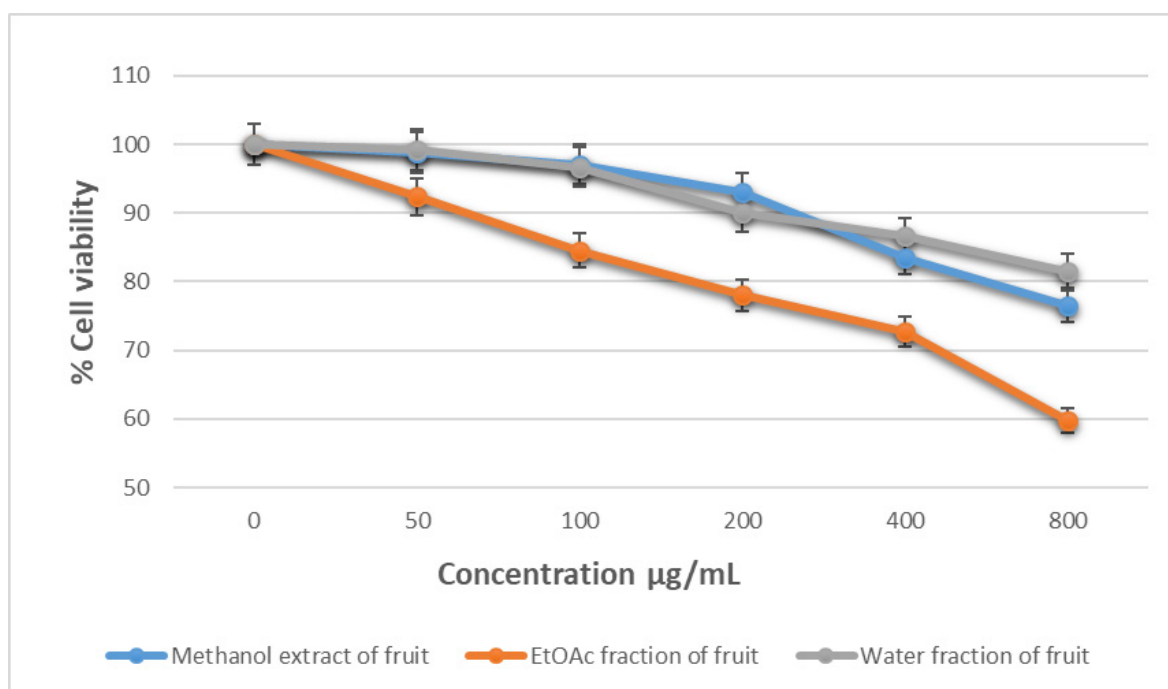
Figure 1. Antiproliferative activities of the *P. domestica* unripe fruit extract and fractions against PC-3 cell line
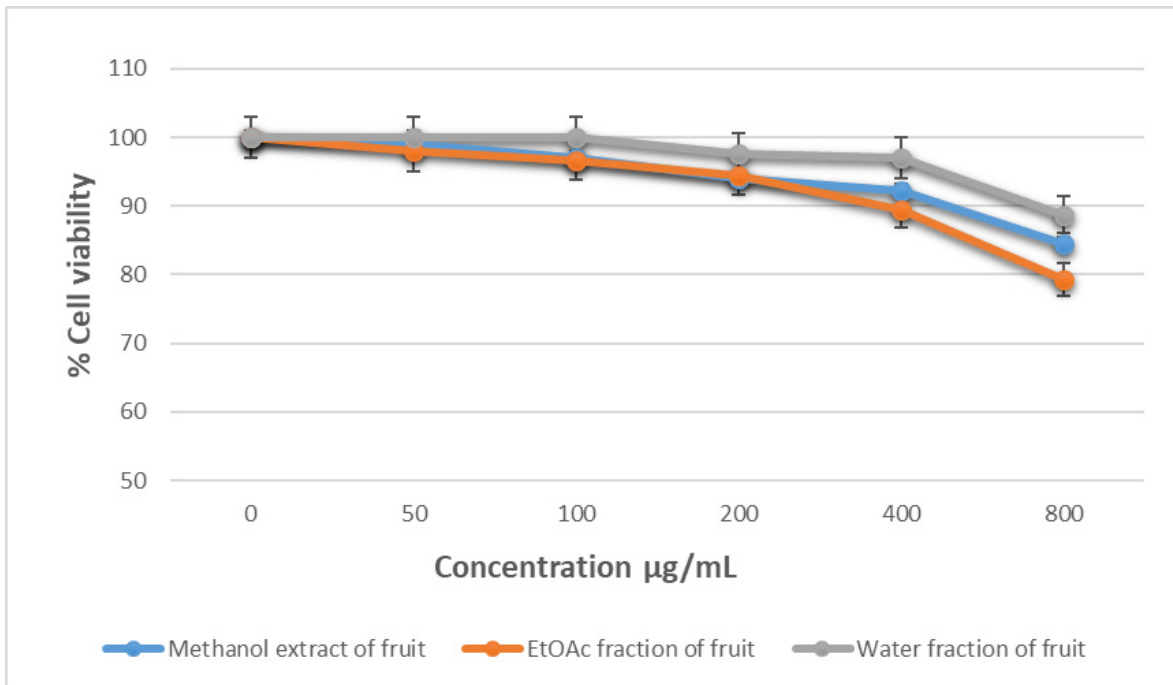
Figure 2. Antiproliferative activities of the *P. domestica* unripe fruit extract and fractions against CaCo-2 cell line
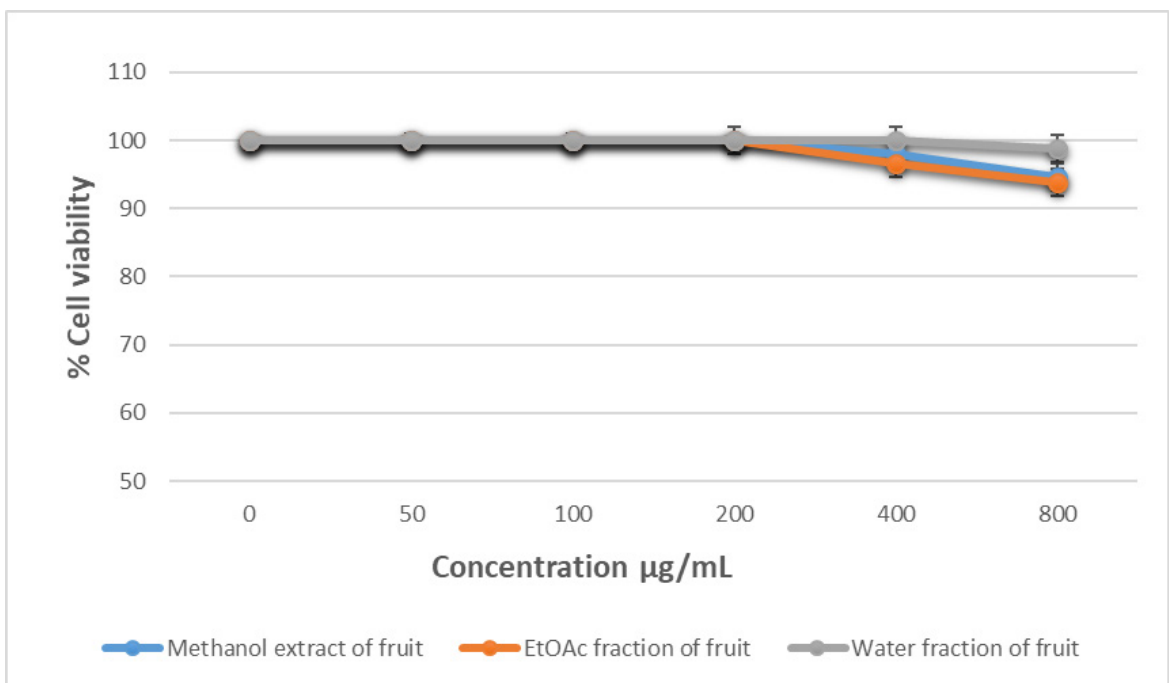
Figure 3. Antiproliferative activities of *P. domestica* unripe fruit extract and fractions against L929 cell line

Antioxidant capacity of the extract and the fractions

Antioxidant activity was determined using CUPRAC, TEAC and DPPH assays. While the EtOac fraction proved to most effective in all methods, the aqueous fractions showed weak antioxidant activity (Table 1). Gallic acid was used as the standard compound to determine DPPH radical scavenging activity and the results were expressed as equivalent to gallic acid. For the TEAC and CUPRAC methods, the results are expressed as Trolox equivalent.

Table 1. Antioxidant capacity of unripe fruit of *P. domestica* extract and fractions

	DPPH[a]	TEAC[b]	CUPRAC[b]
Methanol extract of fruit	101.65 ±1.98	179.16 ±2.68	212.06 ±2.85
EtOAc fraction of fruit	120.64 ±2.07	180.45 ±2.56	251.43 ±1.84
Water fraction of fruit	64.36 ±1.08	78.44 ±1.36	107.18 ±1.24

Data are presented as mean ± SD, n=3 experiments, (p < 0.001)
a: mg gallic acid/g extract
b: mg trolox/g extract

In this study, the ethyl acetate fractions of the unripe fruits of *P. domestica* were the most effective fraction according to the antioxidant capacity studies tested. The fruit water fraction showed the least activity. When comparing the antioxidant capacity of the extracts and fractions, the ethyl acetate fraction showed the highest effect for all methods, which was 251.43 and 180.45 mg Trolox/g extract for the CUPRAC and TEAC methods, respectively.

The antioxidant capacity and tyrosinase enzyme inhibition results were found to be parallel. The ethyl acetate fraction of the fruits showed the highest tyrosinase of the enzyme tyrosinase with IC_{50}: 51.83 µg/mL, and the antioxidant effect was also the highest for all tested methods.

In a study, the antioxidant effects of methanol extracts of flowers of *P. domestica* were analyzed by ABTS (65 µmol TE g^{-1}), DPPH (47.50 µmol TE g^{-1}) and CUPRAC (1.04 mmol TE g^{-1}) (Dundar, Sahin, Parlak, & Saricaoglu, 2023). The DPPH radical scavenging activity of plum wines produced from two varieties of *P. domestica,* Crvena ranka and Požegača, was investigated, and the results were determined to be 0.94 and 1.33 mg Trolox L^{-1}, respectively (Ljekocevic et al., 2019).

There are numerous studies in the literature comparing the antioxidant capacity of ripe and unripe fruit (Benmohamed et al., 2023; Hwang, Kim, & Shin, 2020; Yang et al., 2024). In a study comparing the antioxidant effect of ripe and unripe fruits of *P. persica*, it was found that the antioxidant capacity of the unripe fruits was higher (Giovanoudis et al., 2023). In another study the change in antioxidant capacity and chemical content of *Prunus persica* fruits during the ripening period was investigated. Both ascorbic acid and polyphenol contents and antioxidant activities decreased significantly during the ripening period (Liu, Cao, & Jiang, 2015).

Mushroom tyrosinase enzyme inhibition

The antityrosinase potential of the main methanol extract of the fruit, ethyl acetate, and aqueous fractions was investigated using L-tyrosine as a substrate. The IC_{50} values of the extract, the fractions, and the kojic acid (positive control) are shown in Table 2. It was found that all extracts and fractions showed very potent inhibition compared to the standard compound. The ethyl acetate subfraction showed higher antityrosinase effects than the others with IC_{50}: 51.83 µg/mL value.

Table 2. Mushroom tyrosinase enyme inhibition of unripe fruit of *P. domestica* extract and fractions (IC$_{50}$ μg/mL)

Methanol extract	EtOAc fraction	Water fraction	Kojic acid
102.034 ±1.28	51.83±0.82	121.06±1.08	21±0.28

Data are presented as mean ± SD, n=3 experiments, (p < 0.001).

A study by Wahyuningsih et al. evaluated the effect of 2% plum extract application on preventing the expression of tyrosinase enzyme and the increase in the amount of melanin in the skin of male guinea pigs exposed to UV-B light. According to the results, it was found that the expression of the enzyme tyrosinase in the skin of guinea pigs decreased and the increase in the amount of melanin was prevented (Wahyuningsih, Pangkahila, & Winarti, 2023).

In another study, the effect of plum leaf extracts on the enzyme tyrosinase was investigated. The extracts showed weak tyrosinase inhibition (from 0.0 to 11.6%) compared to licorice extract (91.6%) and kojic acid (78.9%), which were used as standards. The highest activity was found in EtOAc extracts (Stierlin, Azoulay, Massi, Fernandez, & Michel, 2018).

Mocan et al. showed that the tyrosinase enzyme inhibition of leaf samples from different cultivars of *P. domestica* between 23.07 mg KAE/g extract for cultivar Ialomita and up to 8.90 mg KAE/g extract for the cultivar Minerva (Mocan et al., 2018).

CONCLUSION

P. domestica is a globally widespread species that has always been consumed as food and is characterised by its fruits with a high nutrient content. In this study the antiproliferative, antioxidant, and antityrosinase effects of extracts and fractions of different polarities of the unripe fruits of *P. domestica* were investigated. The extracts, which showed no significant cytotoxic effect on healthy L929 fibroblast cells even at high concentrations, exhibited a cytotoxic effect on PC-3 (human prostate carcinoma) and CaCo-2 (human colorectal adenocarcinoma) cancer cells, depending on the concentration. Unripe fruits of *P. domestica* are a natural source that has no toxic effect on normal cells, has a selective cytotoxic effect on cancer cells, has a strong antioxidant effect in DPPH, TEAC, and CUPRAC methods, and has a strong antityrosinase effect compared with kojic acid. Therefore, it can be a safe and effective source for developing new natural products for the cosmetics and pharmaceutical industries. So far, studies have mainly focused on ripe fruits, but there are few studies on unripe fruits. Therefore, unripe fruits can be considered as a source of bioactive natural compounds and have economic value.

AUTHOR CONTRIBUTION STATEMENT

Concept: Z.B.G., A.A.B.; Design: Z.B.G., A.A.B.., Control: Z.B.G., A.A.B., Sources: Z.B.G., N.Y., A.A.B., Materials: Z.B.G., A.A.B.., Data Collection and/or Processing: Z.B.G., N.Y.; Analysis and/or Interpretation: Z.B.G., N.Y.; Literature Review: Z.B.G., N.Y., Manuscript Writing: Z.B.G.; Critical Review: Z.B.G., N.Y., A.A.B.

CONFLICT OF INTEREST

The authors declare that there is no conflict of interest.

REFERENCES

Angelino, D., Godos, J., Ghelfi, F., Tieri, M., Titta, L., Lafranconi, A., . . . Sciacca, S. (2019). Fruit and vegetable consumption and health outcomes: An umbrella review of observational studies. *International journal of food sciences and nutrition, 70*(6), 652-667.

Ayub, H., Nadeem, M., Mohsin, M., Ambreen, S., Khan, F. a., Oranab, S., . . . Zarlasht, M. (2023). A comprehensive review on the availability of bioactive compounds, phytochemicals, and antioxidant potential of plum (*Prunus domestica*). *International Journal of Food Properties, 26*(1), 2388-2406.

Barlak, N., Capik, O., Kilic, A., Sanli, F., Aytatli, A., Yazici, A., . . . Karatas, O. F. (2021). MicroRNA-145 transcriptionally regulates Semaphorin 3A expression in prostate cancer cells. *Cell Biology International, 45*(5), 1082-1090.

Benmohamed, M., Guenane, H., Messaoudi, M., Zahnit, W., Egbuna, C., Sharifi-Rad, M., . . . Boubekeur, S. (2023). Mineral profile, antioxidant, anti-inflammatory, antibacterial, anti-urease and anti-α-amylase activities of the unripe fruit extracts of pistacia atlantica. *Molecules, 28*(1), 349.

Dundar, A. N., Sahin, O. I., Parlak, M. E., & Saricaoglu, F. T. (2023). Drying kinetics and change in bioactive compounds of edible flowers: *Prunus domestica. Journal of Food Process Engineering, 46*(10), e14405.

Giovanoudis, I., Athanasiadis, V., Chatzimitakos, T., Kalompatsios, D., Mantiniotou, M., Bozinou, E., . . . Lalas, S. I. (2023). Antioxidant Capacity in Two Different Cultivars of Ripe and Unripe Peaches Utilizing the Cloud-Point Extraction Method. *AgriEngineering, 5*(4), 2139-2154.

Güven, Z. B., Dogan, Z., Saracoglu, I., Picot, L., Nagatsu, A., & Basaran, A. A. (2022). Food plant with antioxidant, tyrosinase inhibitory and antimelanoma activity: Prunus mahaleb L. *Food Bioscience, 48*, 101804.

Güven, Z. B., Saracoglu, I., Nagatsu, A., Yilmaz, M. A., & Basaran, A. A. (2023). Anti-tyrosinase and antimelanogenic effect of cinnamic acid derivatives from Prunus mahaleb L.: Phenolic composition, isolation, identification and inhibitory activity. *Journal of Ethnopharmacology, 310*, 116378.

Harput, U. S., Genc, Y., & Saracoglu, I. (2012). Cytotoxic and antioxidative activities of Plantago lagopus L. and characterization of its bioactive compounds. *Food Chem. Toxicol., 50*(5), 1554-1559. doi:10.1016/j.fct.2012.01.019

Hwang, H., Kim, Y.-J., & Shin, Y. (2020). Assessment of physicochemical quality, antioxidant content and activity, and inhibition of cholinesterase between unripe and ripe blueberry fruit. *Foods, 9*(6), 690.

Igwe, E. O., & Charlton, K. E. (2016). A systematic review on the health effects of plums (*Prunus domestica* and Prunus salicina). *Phytotherapy Research, 30*(5), 701-731.

Kabir, M. T., Rahman, M. H., Akter, R., Behl, T., Kaushik, D., Mittal, V., . . . Abdel-Daim, M. M. (2021). Potential Role of Curcumin and Its Nanoformulations to Treat Various Types of Cancers. *Biomolecules, 11*(3), 392. Retrieved from https://www.mdpi.com/2218-273X/11/3/392

Kim, J. H., Yoon, J.-Y., Yang, S. Y., Choi, S.-K., Kwon, S. J., Cho, I. S., . . . Choi, G. S. (2017). Tyrosinase inhibitory components from Aloe vera and their antiviral activity. *J. Enzyme Inhib. Med. Chem., 32*(1), 78-83. doi:10.1080/14756366.2016.1235568

Liu, H., Cao, J., & Jiang, W. (2015). Evaluation of physiochemical and antioxidant activity changes during fruit on-tree ripening for the potential values of unripe peaches. *Scientia Horticulturae, 193*, 32-39.

Ljekocevic, M., Jadranin, M., Stankovic, J., Popovic, B., Nikicevic, N., Petrovic, A., & Tesevic, V. (2019). Phenolic composition and DPPH radical scavenging activity of plum wine produced from three plum cultivars. *J. Serb. Chem. Soc., 84*(2), 141-151. doi:10.2298/jsc180710096l

Lu, W., Shi, Y., Wang, R., Su, D., Tang, M., Liu, Y., & Li, Z. (2021). Antioxidant activity and healthy benefits of natural pigments in fruits: A review. *International journal of molecular sciences, 22*(9), 4945.

Madhuri, S., & Pandey, G. (2009). Some anticancer medicinal plants of foreign origin. *Curr. Sci., 96*(6), 779-783.

Maheshwari, N., & Sharma, M. C. (2023). Anticancer properties of some selected plant phenolic compounds: future leads for therapeutic development. *Journal of Herbal Medicine*, 100801.

Miljić, U., Puškaš, V., Velićanski, A., Mašković, P., Cvetković, D., & Vujić, J. (2016). Chemical composition and in vitro antimicrobial and cytotoxic activities of plum (*Prunus domestica* L.) wine. *Journal of the Institute of Brewing, 122*(2), 342-349.

Mocan, A., Diuzheva, A., Carradori, S., Andruch, V., Massafra, C., Moldovan, C., . . . Zara, S. (2018). Development of novel techniques to extract phenolic compounds from Romanian cultivars of *Prunus domestica* L. and their biological properties. *Food and chemical toxicology, 119*, 189-198.

Ozyurek, M., Bektasoglu, B., Guclu, K., & Apak, R. (2009). Measurement of xanthine oxidase inhibition activity of phenolics and flavonoids with a modified cupric reducing antioxidant capacity (CUPRAC) method. *Anal. Chim. Acta, 636*(1), 42-50. doi:10.1016/j.aca.2009.01.037

Re, R., Pellegrini, N., Proteggente, A., Pannala, A., Yang, M., & Rice-Evans, C. (1999). Antioxidant activity applying an improved ABTS radical cation decolorization assay. *Free Radical Biol. Med., 26*(9/10), 1231-1237. doi:10.1016/S0891-5849(98)00315-3

Sharafan, M., Malinowska, M. A., Ekiert, H., Kwaśniak, B., Sikora, E., & Szopa, A. (2023). Vitis vinifera (Vine Grape) as a Valuable Cosmetic Raw Material. *Pharmaceutics, 15*(5), 1372.

Shukla, R. K., Shukla, A., & Singh, R. (2021). Evaluation of nutritive value, phytochemical screening, total phenolic content and in-vitro antioxidant activity of the seed of *Prunus domestica* L. *Plant Science Today, 8*(4), 830–835-830–835.

Stierlin, E., Azoulay, S., Massi, L., Fernandez, X., & Michel, T. (2018). Cosmetic potentials of *Prunus domestica* L. leaves. *J. Sci. Food Agric., 98*(2), 726-736. doi:10.1002/jsfa.8520

Usenik, V. (2021). The influence of the production system on the composition of phytochemicals in *Prunus domestica* L. fruit. *Journal of Food Composition and Analysis, 95*, 103701.

Wahyuningsih, M. D., Pangkahila, W., & Winarti, N. W. (2023). The Administration of 2% Plum (*Prunus domestica* L.) Extract Cream Inhibited the Increase of Tyrosinase Enzyme Expression and the Amount of Skin Melanin in Male Guinea Pigs (Cavia porcellus) Skin Exposed to UV B Light. *European Journal of Biomedical Research, 2*(3), 12-16.

Yang, Q.-N., Deng, W., Wu, D.-T., Li, J., Liu, H.-Y., Yan, H.-L., . . . Huang, J.-W. (2024). Characterization, Antioxidant Capacity, and Anti-Inflammatory Activity of Polyphenol-Enriched Extracts Obtained from Unripe, Mature, and Overripe Fruits of Red-Fleshed Kiwifruit Cultivars. *Foods, 13*(18), 2860.

^{99m}Tc-Labeled Microsized Liposomes

Helin HEKIMOGLU[*+], Merve KARPUZ[**o+], Emre OZGENC[***],
Evren GUNDOGDU[****]

---

^{99m}Tc-Labeled Microsized Liposomes

SUMMARY

Respiratory diseases can cause the death of the patient if not diagnosed at the early stages. Imaging techniques in nuclear medicine are frequently preferred for diagnosing of these diseases. Radiopharmaceuticals can be used to evaluate the perfusion or ventilation capacity of the lung. Liposomes, formed by lipid layers and an aqueous core, are micro- or nanometer-sized vesicular systems. They can be passively accumulated in lung capillaries due to their surface and physicochemical properties. In light of this information, in our study, liposome formulations with micrometer particle sizes containing DTPA-PE chelating agent for radiolabeling with ^{99m}Tc were designed for the imaging of lung diseases. After the preparation of liposomes, the optimum formulation exhibits proper particle size (~5 µm) and zeta potential (~-6 mV) values, and the vesicular integrity was imaged with SEM in characterization studies. Liposomes were dried by lyophilization to obtain cold-kit formulations for radiolabeling. The effect of the lyophilization process on the characterization properties of the vesicles was evaluated. All liposome formulations were radiolabeled with high efficiency in the optimal radiolabeling conditions comprising 1 mCi of radioactivity, 250 µg.ml⁻¹ of stannous chloride, and 15 min incubation period. In addition, the radiolabeled liposomes were found to be stable, with radiolabeling efficiencies of over 90% for 6 hours. As a result, the developed Tc-99m labeled formulation has the potential to be used as a lung perfusion imaging agent following in vitro and in vivo studies and clinical trials.

Key Words: *Technetium-99m, liposome, lung perfusion imaging, capillary blockade*

^{99m}Tc İşaretli Mikro Boyutlu Lipozomlar

ÖZ

Solunum yolu hastalıkları erken teşhis edilmediği takdirde hastanın ölümüne neden olabilir. Nükleer tıp görüntüleme teknikleri bu hastalıkların tanısında sıklıkla tercih edilmektedir. Radyofarmasötikler akciğerin perfüzyon veya ventilasyon kapasitesinin değerlendirilmesinde kullanılabilmektedir. Lipid katmanlar ve sulu bir çekirdekten oluşan lipozomlar, mikro veya nanometre boyutuna sahip veziküler sistemlerdir. Yüzey ve fizikokimyasal özellikleri nedeniyle akciğer kılcal damarlarında pasif olarak birikebilirler. Bu bilgiler ışığında çalışmamızda, akciğer hastalıklarının görüntülenmesinde ^{99m}Tc ile radyoişaretleme için DTPA-PE şelatör ajanı içeren, mikrometre partikül büyüklüğünde lipozom formülasyonları tasarlanmıştır. Lipozomların hazırlanmasından sonra, karakterizasyon çalışmalarında, optimum formülasyon uygun partikül boyutu (~5 µm) ve zeta potansiyeli (~-6 mV) değerlerini sergilerken, veziküler bütünlük SEM ile görüntülenmiştir. Radyoaktif işaretlemeye uygun soğuk kit formülasyonları elde etmek için lipozomlar liyofilizasyon yoluyla kurutulmuş ve liyofilizasyon işleminin veziküllerin karakterizasyon özellikleri üzerindeki etkisi değerlendirilmiştir. Tüm lipozom formülasyonları, 1 mCi radyoaktivite, 250 µg.ml⁻¹ kalay klorür ve 15 dakikalık inkübasyon süresi içeren optimal radyoaktif işaretleme koşullarında yüksek verimle işaretlenmiştir. Ayrıca radyoişaretli lipozomların 6 saat boyunca %90'ın üzerinde radyoişaretleme verim değerlerine sahip olması nedeniyle stabil olduğu bulunmuştur. Sonuç olarak geliştirilen Tc-99m işaretli formülasyon, in vitro ve in vivo çalışmalar ve klinik deneylerin ardından, akciğer perfüzyon için potansiyel bir görüntüleme ajanı olma potansiyeline sahiptir.

Anahtar Kelimeler: *Teknesyum-99m, lipozom, akciğer perfüzyon görüntüleme, kapiller blokaj*

---

[*] ORCID ID: 0009-0001-7119-6878. Izmir Katip Celebi University Faculty of Pharmacy, Izmir, Turkey.
[**] ORCID ID: 0000-0001-6681-2448. Izmir Katip Celebi University Faculty of Pharmacy, Department of Radiopharmacy, Izmir, Turkey.
[***] ORCID ID: 0000-0002-7586-8520. Ege University Faculty of Pharmacy, Department of Radiopharmacy, Izmir, Turkey.
[****] ORCID ID: 0000-0003-2111-101X. Ege University Faculty of Pharmacy, Department of Radiopharmacy, Izmir, Turkey.

[+] These authors contributed equally.

[o] Corresponding Author; Merve KARPUZ,
e-mail: merve.karpuz@ikcu.edu.tr

INTRODUCTION

Respiration begins from the nostril, passes through the pharynx and larynx, and continues to the main bronchi leading to the two lungs and from the bronchi to the bronchioles, at the ends of which are the alveoli. Airflow through the bronchial system is called ventilation. The blood flow in the pulmonary arterial system is called pulmonary perfusion. Respiratory diseases, the leading causes of death in the world, comprise serious diseases such as chronic obstructive pulmonary disease (COPD), pneumonia, lung cancer, bronchitis, tuberculosis, or asthma (Labaki & Han, 2020). These diseases, affecting lung ventilation or perfusion, can cause the death of the patient if not diagnosed at the early stages.

In routine clinics, to diagnose these diseases, lung and respiratory system diseases can be noninvasively imaged through radiological (chest radiography, computed tomography (CT), magnetic resonance imaging (MRI)), or nuclear medicine [Positron Emission Tomography (PET), single-photon emission computed tomography (SPECT)] imaging techniques (Hollings & Shaw, 2002). Chest radiography is used to diagnose or monitor the prognosis of the diseases affecting the thorax.

Thorax CT is a superior imaging modality to plain chest radiography due to its much higher contrast resolution and ability to prevent tissue superposition. Thorax CT examinations are performed with multi-slice spiral CT (MDCT) systems today. Although MRI is not a primary method of choice in the evaluation of chest diseases, it is preferred for the assessment of lesions in chest wall and mediastinal tumors thanks to its main advantages such as high soft tissue contrast, ability to perform multiplanar examination and image tumors and vessels without contrast agent. Compared to other methods, nuclear medicine techniques are often preferred because they can obtain three-dimensional images containing metabolic information with high precision.

Radiopharmaceuticals, containing pharmaceutical and radionuclide parts, are used for diagnostic or therapeutic purposes in nuclear medicine. The pharmaceutical part is responsible for delivering the radionuclide to the target tissue and is not responsible for any pharmacological activity. Radiopharmaceuticals accumulate in the desired organs or tissues depending on the physical, chemical, and biological properties of the pharmaceutical part. Radionuclide part is responsible for imaging or treatment thanks to the rays emitted by the radionuclide. Alpha- and beta-emitting radionuclides are used for therapeutic applications. Radiopharmaceuticals are used in SPECT or PET imaging depending on gamma or positron emission. Radiopharmaceuticals can be used to determine the perfusion or ventilation capacity of the lung. Lung perfusion imaging, used in the diagnosis of pulmonary embolism, pulmonary artery stenosis, hepatopulmonary syndrome, is based on the capture of particles larger than 10 μm in the capillary bed of the lung. Particles larger than 10 μm size accumulate in capillaries during the first pass through the pulmonary artery following the intravenous administration. Radionuclide ventilation studies of the lungs can be performed to determine any airway obstruction using aerosols (Elgazzar, 2011). In clinics, lung capacity is determined by performing perfusion and ventilation imaging using radiopharmaceuticals such as ^{99m}Tc-labeled macroaggregate albumin particles (^{99m}Tc-MAA), ^{99m}Tc-labeled DTPA aerosols, ^{67}Ga-citrate, and ^{18}F-labeled 18-Fluoro-2-deoxy-D-glucose (^{18}F-FDG). ^{99m}Tc-MAA and ^{99m}Tc-DTPA aerosols are used for lung perfusion and ventilation imaging, respectively, while ^{67}Ga-citrate and ^{18}F-FDG are used for imaging tumor or infection in the lung (Jacobson et al., 2015; Saha, 2018). ^{99m}Tc-MAA is one of the most frequently utilized radiopharmaceuticals in nuclear medicine clinics. Its applications include the evaluation of lung perfusion and the determination of patient characteristics before the administration of selective internal radiation therapy (Sancho et al., 2017). Nevertheless, in certain instances, in addition to minor adverse

effects such as hypersensitivity, dyspnea, dizziness, and rash, various types of serious adverse events, including angioedema, cardiac arrest, bradycardia, and respiratory arrest, have been documented in patients undergoing 99mTc-MAA imaging (Schreuder et al., 2019). Therefore, the development of alternative agents to ^{99m}Tc-MAA is a necessity.

Liposomes are spherical vesicles formed by one or more biological membrane-like lipid layers with an aqueous phase in between. The phospholipid molecules that form liposomes are amphiphilic and consisting of a hydrophilic head and hydrophobic hydrocarbon chains. Liposomes are biocompatible, non-pyrogenic, non-antigenic and biodegradable systems due to their similarity to the cell membrane. They are used in the diagnosis and/or treatment of many diseases and offer advantages such as slow and controlled drug release, entrapment of drugs with different physicochemical properties, surface modification and conjugation of different ligands or radioisotopes. Liposomes can be classified as multilamellar vesicles (MLV), small unilamellar vesicles (SUV), large unilamellar vesicles, and multivesicular liposomes (MVL) depending on the number of layers and particle sizes (Šturm & Poklar Ulrih, 2021). MVL, containing MLV and/or SUV liposomes in its structure, have particle sizes between 500 nm and 100 μm. They have a high encapsulation capacity due to their high water content (95%) and large particle size.

Some studies have been carried out in the literature using MVL-type liposome formulations for a variety of diseases. Jain et al. prepared acyclovir-loaded MVL-type liposomes with a particle size of 7-16 μm for the treatment of diseases caused by the herpes simplex virus. They reported that the drug encapsulation efficiency of MVL was 3 to 6 times higher and the drug release lasted longer compared to MLV-type liposomes (Jain et al., 2005). Another MVL type liposome formulations with particle sizes ranging from 1-10 μm were prepared and radiolabeled with [177]Lu (a beta-emitting radionuclide) by Cvjetinovic et al. for the radiosynovectomy, which is a treatment method

applied by intra-articular injection of therapeutic radiopharmaceuticals. According to the scintigraphy images obtained from the knee joints of rats, liposomes were localized in the joint until the 30th day. Additionally, it was reported in the biodistribution study that no free Lu-177 or Lu-177 labeled liposome formulation was detected outside the joint tissue (Cvjetinovic et al., 2021).

Targeting drug delivery systems is essential to overcome the shortcomings of conventional imaging techniques and treatment methods, especially in complex diseases such as cancer. Targeting increases the concentration of the drug in the diseased area and reduces the concentration of the drug in other parts of the body. This reduces the risk of side effects on healthy tissue and allows better pharmacological effects to be achieved with the same or lower drug concentration. Additionally, drug can be delivered more effectively to intracellular areas and hard-to-reach organs such as the brain. Passive targeting is achieved by altering the particle size and/or surface properties of liposomes. In contrast, specific ligands or polymers or lipids that are sensitive to physical changes in the disease are used for active targeted liposomes (Karpuz et. al, 2018). Particle size affects the biodistribution, the half-life, the drug encapsulation efficiency, the drug release behavior, the toxic profile, the stability properties, and the tissue to reach the formulation. After intravenous injection, drug carrier systems with particle sizes between 5-15 μm are captured by the lung's capillary network and distributed widely in the lung tissue. Therefore, it is possible to passively target drug carrier systems to the lungs by using particles of this size (SreeHarsha et al., 2019).

In the light of the above information, in our study, MVL-type liposome vesicles, as an alternative to the ^{99m}Tc-MAA, are designed and formulated to radiolabel with ^{99m}Tc, for the imaging of lung diseases by gamma camera or SPECT. It is designed to passively accumulate vesicles in the lungs thanks to their 5-15 μm particle size. After preparation, the liposomes were lyophilized and the effect of lyophilization on

characterization profiles of the vesicles was evaluated. Last but not least, the optimum radiolabeling conditions were determined. Our study has a novelty due to preparation and radiolabeling of liposome vesicles with micrometer particle size for imaging of lung diseases.

MATERIALS AND METHODS

Materials

Lecithin from soybean 90 (PC) was obtained from PanReac Applichem. Cholesterol (Chol), stannous chloride (SnCl$_2$), diethylenetriaminepentaacetic acid anhydride (DTPA), and Tris(hydroxymethyl) aminomethane, and 1,2-Dioleoyl-sn-glycero-3-phosphoethanolamine (PE) to synthesize DTPA-PE were purchased from Sigma-Aldrich.

Methods

Preparation of Liposomes

After obtaining DTPA-PE, a chelating conjugate for radiolabeling with ^{99m}Tc, based on our previous studies (Karpuz et al., 2024; Karpuz et al., 2020), liposome formulations were prepared by two different techniques (thin-film hydration and reverse-phase evaporation). In the Bangham technique (Bangham, Standish, & Watkins, 1965), a lipid mixture containing PC, Chol, and DTPA-PE was dissolved in chloroform.

After the evaporation of organic solvent at 45°C using vacuum and heating bath (BUCHI R100, Switzerland), dried film was hydrated using Tris buffer (20 mM, pH:7.4). In reverse-phase evaporation technique (Cvjetinović et al., 2021), after the solving of lipid phase in chloroform-methanol (4:1, v/v), Tris buffer (20 mM, pH:7.4) was added dropwise on the lipid-organic solvent mixture. The organic solvent was evaporated at 80°C using a vacuum and heating bath (BUCHI R100, Switzerland), and after evaporation of the organic solvent, the liposome dispersion was kept in a fume hood for 1 h at room temperature to remove residual organic solvents. The rate for lipids in the preparation of liposomes is given in Table 1. After the preparation, optimum liposome dispersions were lyophilized to obtain cold-kit formulations. To that end, the vials were sealed with parafilm to prevent contamination and loss of substance, and a needle was used to puncture the parafilm to allow for lyophilization. The formulations were subjected to a freezing process at -80 °C for 24 hours. Subsequently, the formulations were subjected to freeze-drying using a Christ Alpha 1-2 LD Freeze Dryer apparatus, with a pressure of 1 Pa maintained at -45 °C for 48 hours (Glavas-Dodov et al., 2005).

Table 1. Liposomes and their lipid contents.

Formulations	Lipid Conc. (mM)	PC (% M)	Chol (% M)	DTPA-PE (mg.mL^{-1})	Preparation Technique	Lyophilization
Lipo-1	40	80	20	5	Bangham	Not implemented
Lipo-2	40	70	30	5	Bangham	Not implemented
Lipo-3	40	80	20	5	Reverse phase evaporation	Not implemented
Lipo-3L	40	80	20	5	Reverse phase evaporation	Implemented
Lipo-4	40	70	30	5	Reverse phase evaporation	Not implemented
Lipo-4L	40	70	30	5	Reverse phase evaporation	Implemented

Imaging and Characterization of Liposomes

The mean particle size and zeta potential of liposomes were measured by Malvern Mastersizer and Malvern Zetasizer, respectively. According to the particle size analysis, optimal formulations were selected and, the morphology of optimal liposome vesicles was imaged by scanning electron microscopy (ZEISS Sigma 300 VP SEM, Germany) under high vacuum (Quorum Q150R ES, UK) after drying the formulations in a glass lamella at 37°C.

Radiolabeling of Liposomes with ^{99m}Tc

All formulations were radiolabeled with ^{99m}Tc using the chelating agent DTPA-PE, which provides a stable complex between the bilayer of the liposome

and the radionuclide (Karpuz et al., 2020). The tin-reduction technique was used in the radiolabeling, and the optimum concentration of $SnCl_2$ solution in 0.01 N HCl (10, 250, 500 μg.ml^{-1}) and incubation time (5 and 15 min) were evaluated to obtain the highest radiolabeling yield. For this purpose, 1 ml of formulations were radiolabeled with ^{99m}Tc solution after the reducing of Na^{99m}TcO$_4$ with 1 mCi radioactivity using $SnCl_2$ solution, then this mixture was vortexed, and incubated for different periods at the room temperature. The radiation dose was determined according to the previous studies in the literature (Gharepapagh et al., 2021; Karpuz et al., 2024; Ozgenc et al., 2022). Radiolabeled liposomes were dialyzed by using a regenerated cellulose membrane with a 3500-Da cut-off size for 5h at 4°C against Tris buffer (20 mM, pH 7.4) to remove free ^{99m}Tc and hydrolyzed ^{99m}Tc, which are radiochemical impurities for ^{99m}Tc radiopharmaceuticals (Silindir-Gunay et al., 2019). A control sample containing Na^{99m}TcO$_4$ solution was used to eliminate the decrease of radioactivity as a function time and dilution.

Evaluation of Radiolabeling Efficiency and Stability

For quality control of radiolabeling, the percentage of radiolabeling efficiency (RE %) was determined by radio-thin-layer chromatography (RTLC) through separation of radiochemical impurities. To this end, radiolabeled liposomes were applied to a silica gel plate, as a stationary phase. At the end of development, radioactivity values in the cut plates were measured by RTLC (Bioscan AR 2000) for 6 h. Hydrolyzed Tc-99m (R_f = 1.0) and free Tc-99m (R_f = 1.0) were identified as radioactive contaminants using pyridine: acetic-acid: water (3: 5: 1.5 v/v/v) and saline mobile phases, respectively (De Silva et al., 2019; Métayé & Desmarquet, 2001; Métayé et al., 2001). RE % was calculated using the following equation (Eq. 1):

RE %=100 -[Free Tc-99m (%)+Hydrolized Tc-99m (%)] (Eq. 1)

In the study of radiolabeling stability, after the radiolabeling of liposomes using optimum conditions,

100 μL of radiolabeled liposomes were incubated in 900 μL of saline at 37°C. The stability was checked using RTLC by calculating of RE % up to 6 h.

Statistical analysis

All measurements were performed at least in triplicates, and the data was shown using mean ± standard deviation (SD). Two-way analysis of variance with Tukey's or Sidak's multiple comparisons tests were used to determine whether there was a statistical difference between the groups. Differences were considered as significant when $p < 0.05$ (*).

RESULTS AND DISCUSSION

Preparation, Characterization, and SEM Imaging of Liposomes

A literature review revealed the occurrence of anaphylactic and allergic reactions to ^{99m}Tc-MAA (Schreuder et al., 2019a; Schreuder et al., 2019b). Due to their cell-membrane-like structures, liposomes are biocompatible and non-allergic drug delivery systems. Accordingly, the objective of this study was to develop micro-sized liposome formulations as the pharmaceutical component of a radiopharmaceutical with the intention of emulating the ^{99m}Tc-MAA.

In the liposome formulations, lecithin and cholesterol were used to obtain bilayer vesicles and to increase the stability, respectively. In addition, DTPA-PE, a chelating agent between radioisotope and liposome bilayer, was added to the formulation for the radiolabeling procedure. The preparation technique is chosen according to the intended use of the vesicles. In this study, it is aimed that liposomes having in the range of 5-10 micrometer particle size are obtained as a passively targeted formulation to lung capillaries. Therefore, liposome formulations were successfully prepared using lipid-hydration and reverse phase evaporation techniques.

As shown in Table 2, liposome vesicles with the desired particle size could not be obtained using the Bangham technique. This finding agrees with the literature where MLV type liposomes with a particle size of ~1 μm were obtained by the Bangham

technique (Has & Sunthar, 2020). However, the liposomes prepared by the reverse phase evaporation technique showed more suitable particle sizes. MVL type formulations in the range of 1-16 µm particle size were prepared in the literature using a technique similar to that used in this study (Cvjetinovic et al., 2021; Fadel & Kassab, 2011; Jain et al., 2005). The reverse phase evaporation technique has been employed by various studies to formulate liposomes, with the resulting particle size of MVL-type liposome vesicles being found to be greater than 1 µm (Chen et al., 2014; Shi & Qi, 2018). Our findings align with this observation. In the study performed by Ko et al., after obtaining liposomes by reverse phase evaporation technique, the particle size of vesicles was reduced using extrusion (Ko & Bickel, 2012). In addition, the histograms are given in Figure 1 to show the particle size distribution. The SEM images and the particle size distribution graphs agree in showing a wide distribution of particle sizes. Liposome vesicles have a broad particle distribution range because no process such as extrusion or sonication has been used to reduce the particle size and achieve uniform distribution. As seen in Figure 2, although Lipo-3 and Lipo-4 have a lower mean particle size than desired, the histograms show that there are liposomes with larger particle sizes in the formulation. Therefore, Lipo-3 and Lipo-4 were lyophilized to not only increase the stability of the liposomes but also to provide a ready-to-use cold kit for radiolabeling with Tc-99m (Yu et al., 2021). After the lyophilization process, no statistically significant change was observed in the particle size of the Lipo-4 formulation, while the particle size of Lipo-3 decreased. Chen et al. observed a similar decrease in particle size of liposomes after freeze- drying process (Chen et al., 2014). However, this difference was not found to be statistically significant. Similarly, no significant change in particle size of 5-fluorouracil-loaded liposomes after lyophilization has been reported in the literature (Glavas-Dodov et al., 2005). Furthermore, the use of a cryoprotectant is usually recommended to avoid potential adverse effects

such as disruption of vesicle integrity or changes in particle size that may occur during lyophilization (Arshinova et al., 2012). Therefore, for further studies, a cryoprotectant agent can be added to the liposome formulations.

The zeta potential refers to the difference in electrical potential between the layer and the fluid surrounding a charged particle (Clogston & Patri, 2011). Formulations with a high zeta potential exhibit a more stable profile due to the repulsive forces between highly electrically charged particles, which reduces the possibility of aggregation. The zeta potential values are given in Table 2. Statistically essential differences were found between the zeta potential values of the formulations depending on the preparation technique, as shown in Table 2 ($p < 0.05$). Some factors such as preparation technique, hydration medium, lipids influence the zeta potential of liposomes (Smith et al., 2017). In this study, the preparation technique may be the reason for this difference in zeta potential. Furthermore, a study evaluated the impact of particle size on zeta potential. It was reported that using ultrasonication and an elevated ultrasonic probe power contributed to an augmentation in zeta potential value, which was attributed to a reduction in particle size (Nakatuka et al., 2015). As the particle size of the vesicles decreases, the probability of aggregation in liposome dispersions decreases. Therefore, it can be said that another possible reason is differences in particle size. Although Lipo-1 and Lipo-2 formulations exhibited high stability due to zeta potential values higher than 30 mV, their small particle sizes were less suitable for accumulation in pulmonary capillaries. No statistically significant alterations were observed in the zeta potential values of the liposomes before and after the lyophilization process. In addition, it can be said that Lipo-3 and Lipo-3L formulations were more stable compared to Lipo-4 and Lipo-4L formulations due to their higher zeta potential values. Therefore, Lipo-3 and Lipo-3L formulations were chosen for SEM imaging. The vesicle integrity of Lipo-3 and Lipo-3L can be seen in

Figure 2. The images of vesicles are compatible with particle size results. In the present study, the vesicles can be observed using the 1,000-magnification due to their micrometer particle sizes. Although more sensitive techniques are preferred, in some studies, SEM was used for this purpose (Karpuz et al., 2024; Lujan et al., 2019)

Table 2. Characterization properties of liposome formulations (n=6).

Formulation	Particle Size (μm ± SD)	Zeta Potential (mV ± SD)
Lipo-1	1.48 ± 0.49	-35.30 ± 0.62
Lipo-2	1.06 ± 0.26	-56.50 ± 0.55
Lipo-3	5.00 ± 1.34	-6.33 ± 0.59
Lipo-3L	3.31 ± 1.13	-8.42 ± 1.24
Lipo-4	3.06 ± 0.95	0.57 ± 0.31
Lipo-4L	3.29 ± 1.20	0.26 ± 0.27
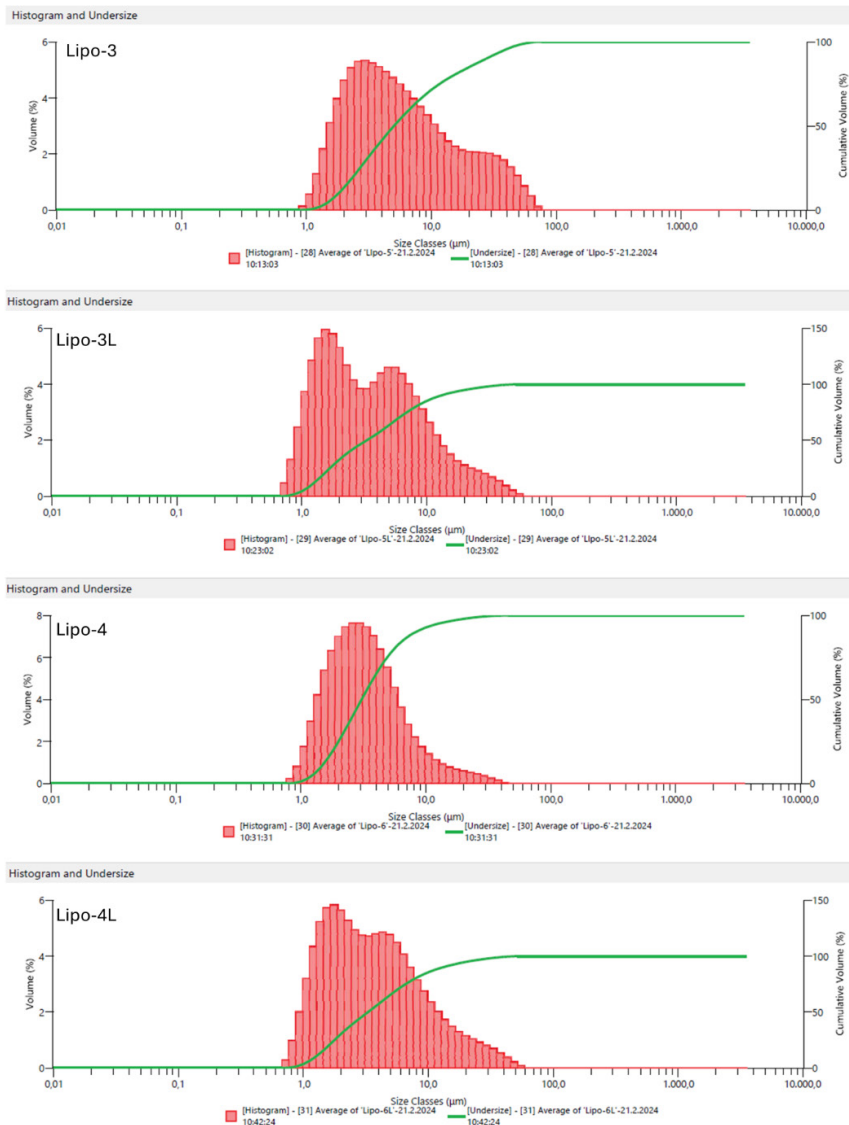
Figure 1. Particle size distribution histograms of liposome formulations.
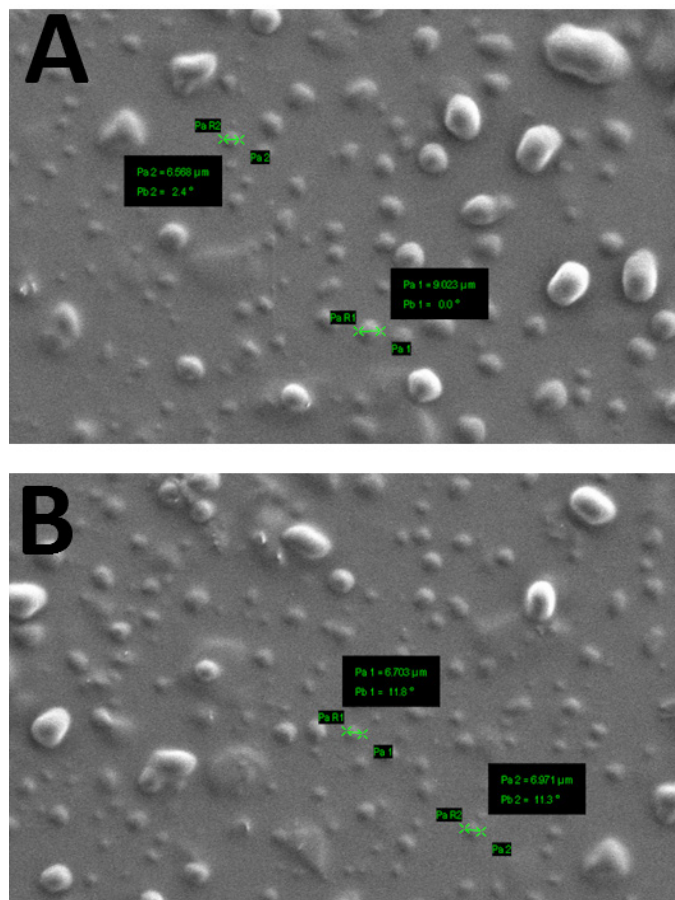
Figure 2. SEM images of Lipo-3 (A) and Lipo-3L (B) formulations in 1.00 KX magnification.

Radiolabeling Efficiency and Stability

Liposomes prepared by reverse phase evaporation technique were radiolabeled with ^{99m}Tc due to the DTPA-PE content in the formulations. Based on previous studies and radiation safety principles, a radiation dose of 1 mCi was chosen (Karpuz et al., 2023). Liposomes can be radiolabeled by different methods including chelation. The DTPA and PE parts of the chelator are bound to the radiometal and bilayer of liposome vesicles, respectively (Silindir Günay, 2020). The radiolabeling stability of this method is higher than other techniques such as radioisotope encapsulation or direct surface labeling (Bentivoglio et al., 2023). In this radiolabeling procedure, an inducing agent such as $SnCl_2$, ascorbic acid, or ferrous ions is essential for reducing the oxidation state of ^{99m}Tc^{+7} to ^{99m}Tc^{+5} (Mushtaq et al., 2021). $SnCl_2$ was used as the inducing agent, and statistically significant differences were found among experiment groups that used different amounts of inducing agent ($p < 0.05$). As given in Figure 3, the highest RE % values were obtained when 250 µg.ml^{-1} of $SnCl_2$ was used. All formulations were radiolabeled with higher than 85% RE at this concentration. After determining the optimum inducing agent amount, the effect of incubation time on RE% was evaluated. As seen in Figure 4, statistically higher RE % values were obtained when a 15 min incubation time was applied compared to 5 min ($p < 0.05$). This finding is similar to the study in which ^{99m}Tc-MAA was prepared (Hunt et al., 2006). Therefore, the optimum $SnCl_2$ concentration and incubation time were detected as 250 µg.ml^{-1} and 15 min, respectively, to reach the highest RE %.

In addition, for radiopharmaceuticals, the bond between the radionuclide and the pharmaceutical parts should be stable until the purpose of application

in the desired area of the body is achieved. Therefore, the radiolabeling stability of radiolabeled liposomes was tested by evaluating RE % values during the physical half-life of ^{99m}Tc (6 h). As seen in Figure 5, the RE % values of all liposome formulations were found to be higher than 80% during 6 h thanks to the use of optimal radiolabeling conditions and chelation technique.
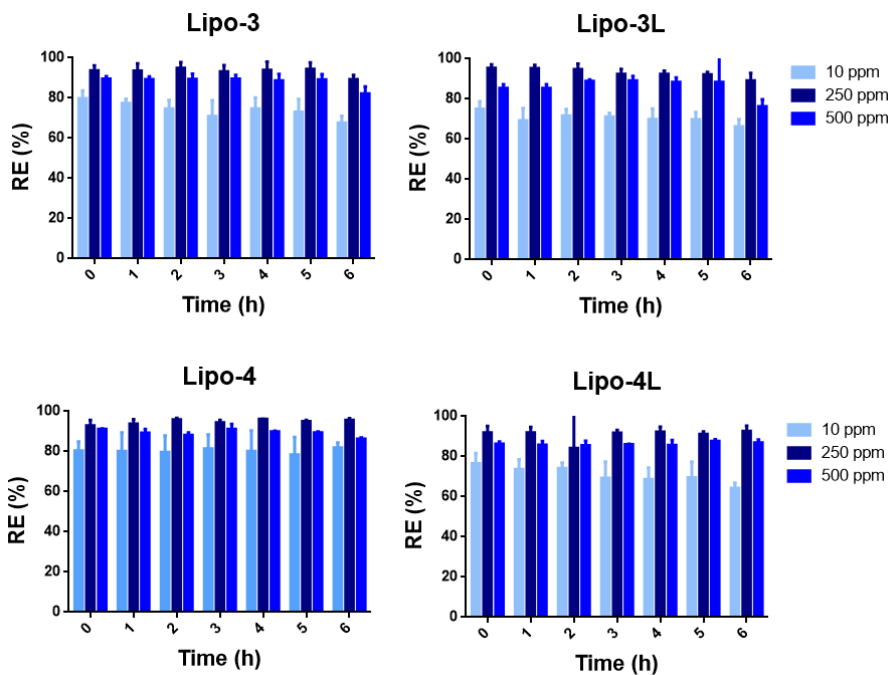
Figure 3. The effect of SnCl$_2$ concentration on RE % of liposome formulations (n=3) (ppm: parts per million, μg.mL^{-1}).
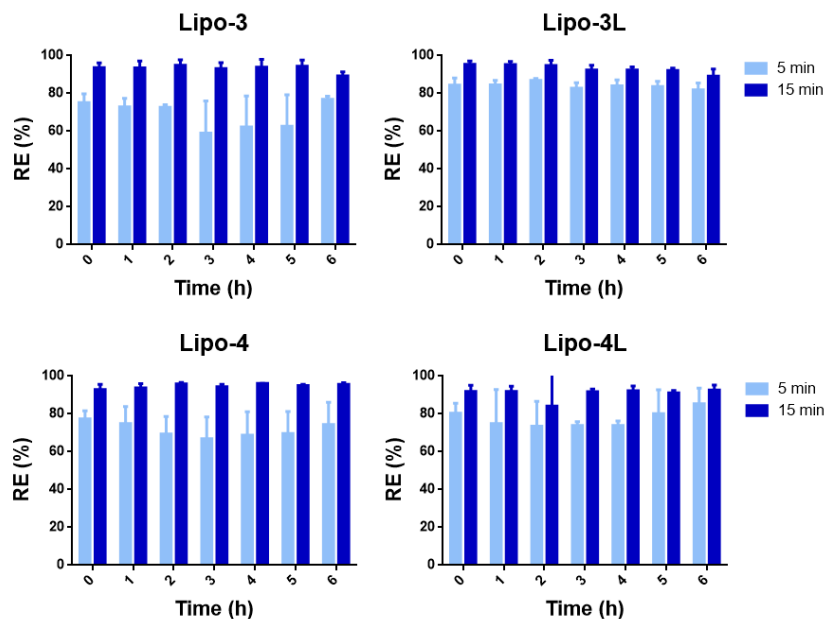
Figure 4. The effect of incubation time on RE % of liposome formulations (n=3). SnCl$_2$ was used at the concentration of 250 μg.ml^{-1})
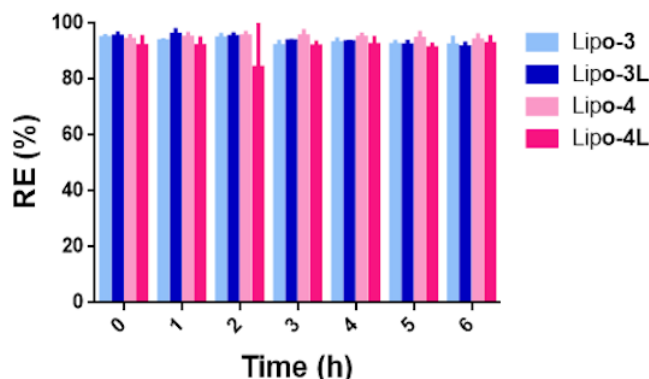
Figure 5. Stability of *in vitro* radiolabeling of formulations in PBS (n=3).

CONCLUSION

Respiratory diseases such as chronic obstructive pulmonary disease, pneumonia, lung cancer, bronchitis, tuberculosis, or asthma are the leading causes of death in the world. These diseases can cause death of the patient because of their effect on lung ventilation or perfusion. Nuclear imaging techniques have some superiorities, such as their ability to obtain three-dimensional images containing metabolic information with high precision compared to radiological ones. Liposomes are the most preferred drug delivery system thanks to their biocompatible profiles. They may vary in number of bilayers and particle size due to preparation technique and lipid content. Liposomes with particle sizes in the range of 5-15 μm can be passively targeted to the lung capillary.

In this study, micro-sized liposome formulations were prepared using two different techniques to radiolabel with ^{99m}Tc due to their DTPA-PE contents. According to the results of characterization studies, formulations prepared by the reverse phase evaporation technique (Lipo-3 and Lipo-4) exhibit more proper particle size distribution compared to liposomes prepared by the Bangham technique. No significant change in physicochemical properties was observed in these liposomes after the lyophilization process to obtain cold-kit formulations. In addition, the highest values of RE % were obtained in the radiolabeling conditions comprising 250 μg.ml^{-1} of SnCl$_2$ concentration and 15 min of incubation time. Also, the radiolabeling stability of formulations remained for 6 h.

Therefore, it was concluded that the Lipo-3 formulation and its lyophilized form (Lipo-3L) are more suitable as the pharmaceutical part of a radiopharmaceutical for radiolabeling with ^{99m}Tc in the lung perfusion imaging.

AUTHOR CONTRIBUTION STATEMENT

Conception and design (MK), data collection and processing (HH, MK, EO, EG), analysis and interpretation (MK, EO, EG) literature search (HH, MK), preparing the study text (HH, MK), critical reviews (EO, EG).

CONFLICT OF INTEREST

The authors declare that there is no conflict of interest

REFERENCES

Arshinova, O. Y., Sanarova, E. V., Lantsova, A. V., & Oborotova, N. A. (2012). Lyophilization of liposomal drug forms (Review). *Pharmaceutical Chemistry Journal, 46*(4), 228-233. doi:10.1007/s11094-012-0768-2

Bangham, A. D., Standish, M. M., & Watkins, J. C. (1965). Diffusion of univalent ions across the lamellae of swollen phospholipids. *Journal of Molecular Biology, 13*(1), 238-IN227. doi:10.1016/S0022-2836(65)80093-6

Bentivoglio, V., Nayak, P., Varani, M., Lauri, C., & Signore, A. (2023). Methods for Radiolabeling Nanoparticles (Part 3): Therapeutic Use. *Biomolecules, 13*(8), 1241. doi:10.3390/biom13081241

Chen, G., Li, D., Jin, Y., Zhang, W., Teng, L., Bunt, C., & Wen, J. (2014). Deformable liposomes by reverse-phase evaporation method for an enhanced skin delivery of (+)-catechin. *Drug Development and Industrial Pharmacy, 40*(2), 260-265. doi:10.3109/03639045.2012.756512

Clogston, J. D., & Patri, A. K. (2011). Zeta Potential Measurement. In S. E. McNeil (Ed.), *Characterization of Nanoparticles Intended for Drug Delivery* (pp. 63-70). Totowa, NJ: Humana Press. doi: 10.1007/978-1-60327-198-1_6

Cvjetinovic, D., Jankovic, D., Milanovic, Z., Mirkovic, M., Petrovic, J., Prijovic, Z., . . . Vranjes-Duric, S. (2021). (177)Lu-labeled micro liposomes as a potential radiosynoviorthesis therapeutic agent. *International Journal of Pharmaceutics, 608*, 121106. doi:10.1016/j.ijpharm.2021.121106

De Silva, L., Fu, J. Y., Htar, T. T., Muniyandy, S., Kasbollah, A., Wan Kamal, W. H. B., & Chuah, L. H. (2019). Characterization, optimization, and in vitro evaluation of Technetium-99m-labeled niosomes. *International Journal of Nanomedicine, 14*, 1101-1117. doi:10.2147/ijn.S184912

Elgazzar, A. H. (2011). Respiratory System. In A. H. Elgazzar (Ed.), *A Concise Guide to Nuclear Medicine* (pp. 79-87). Berlin, Heidelberg: Springer Berlin Heidelberg. doi:10.1007/978-3-642-19426-9_6

Fadel, M., & Kassab, K. (2011). Evaluation of the Photostability and Photodynamic Efficacy of Rose Bengal Loaded in Multivesicular Liposomes. *Tropical Journal of Pharmaceutical Research, 10*(3). doi:10.4314/tjpr.v10i3.5

Gharepapagh, E., Fakhari, A., Firuzyar, T., Shomali, A., & Azimi, F. (2021). Preparation, biodistribution and dosimetry study of Tc-99m labeled N-doped graphene quantum dot nanoparticles as a multimodular radiolabeling agent. *New Journal of Chemistry, 45*(8), 3909-3919. doi:10.1039/D0NJ04762G

Glavas-Dodov, M., Fredro-Kumbaradzi, E., Goracinova, K., Simonoska, M., Calis, S., Trajkovic-Jolevska, S., & Hincal, A. A. (2005). The effects of lyophilization on the stability of liposomes containing 5-FU. *International Journal of Pharmaceutics, 291*(1), 79-86. doi:https://doi.org/10.1016/j.ijpharm.2004.07.045

Has, C., & Sunthar, P. (2020). A comprehensive review on recent preparation techniques of liposomes. *Journal of Liposome Research, 30*(4), 336-365. doi:10.1080/08982104.2019.1668010

Hollings, N., & Shaw, P. (2002). Diagnostic imaging of lung cancer. *European Respiratory Journal, 19*(4), 722-742. doi:10.1183/09031936.02.00280002

Hunt, A. P., Frier, M., Johnson, R. A., Berezenko, S., & Perkins, A. C. (2006). Preparation of Tc-99m-macroaggregated albumin from recombinant human albumin for lung perfusion imaging. *European Journal of Pharmaceutics and Biopharmaceutics, 62*(1), 26-31. doi:https://doi.org/10.1016/j.ejpb.2005.06.005

Jacobson, O., Kiesewetter, D. O., & Chen, X. (2015). Fluorine-18 radiochemistry, labeling strategies and synthetic routes. *Bioconjugate Chemistry, 26*(1), 1-18. doi:10.1021/bc500475e

Jain, S. K., Jain, R. K., Chourasia, M. K., Jain, A. K., Chalasani, K. B., Soni, V., & Jain, A. (2005). Design and development of multivesicular liposomal depot delivery system for controlled systemic delivery of acyclovir sodium. *AAPS PharmSciTech, 6*(1), E35-41. doi:10.1208/pt060108

Jain, S. K., Jain, R. K., Chourasia, M. K., Jain, A. K., Chalasani, K. B., Soni, V., & Jain, A. (2005). Design and development of multivesicular liposomal depot delivery system for controlled systemic delivery of acyclovir sodium. *AAPS PharmSciTech, 6*(1), 8. doi:10.1208/pt060108

Karpuz, M., Aydin, H. H., Ozgenc, E., Erel-Akbaba, G., Atlihan-Gundogdu, E., & Senyigit, Z. (2024). (99m)Tc-labeled, tofacitinib citrate encapsulated chitosan microspheres loaded in situ gel formulations for intra-articular treatment of rheumatoid arthritis. *Drug Development Research, 85*(5), e22247. doi:10.1002/ddr.22247

Karpuz, M., Ozgenc, E., Oner, E., Atlihan-Gundogdu, E., & Burak, Z. (2024). 68Ga-labeled, imatinib encapsulated, theranostic liposomes: Formulation, characterization, and in vitro evaluation of anticancer activity. *Drug Development Research, 85*(1), e22136. doi:10.1002/ddr.22136

Karpuz, M., Silindir-Gunay, M., Kursunel, M. A., Esendagli, G., Dogan, A., & Ozer, A. Y. (2020). Design and in vitro evaluation of folate-targeted, co-drug encapsulated theranostic liposomes for non-small cell lung cancer. *Journal of Drug Delivery Science and Technology, 57*, 101707. doi:10.1016/j.jddst.2020.101707

Karpuz, M., Silindir-Gunay, M., & Ozer, A. Y. (2018). Current and Future Approaches for Effective Cancer Imaging and Treatment. *Cancer Biotheraphy and Radiopharmaceuticals, 33*(2), 39-51. doi:10.1089/cbr.2017.2378

Karpuz, M., Temel, A., Ozgenc, E., Tekintas, Y., Erel-Akbaba, G., Senyigit, Z., & Atlihan-Gundogdu, E. (2023). 99mTc-Labeled, Colistin Encapsulated, Theranostic Liposomes for Pseudomonas aeruginosa Infection. *AAPS PharmSciTech, 24*(3), 77. doi:10.1208/s12249-023-02533-8

Ko, Y. T., & Bickel, U. (2012). Liposome-Encapsulated Polyethylenimine/Oligonucleotide Polyplexes Prepared by Reverse-Phase Evaporation Technique. *AAPS PharmSciTech, 13*(2), 373-378. doi:10.1208/s12249-012-9757-8

Labaki, W. W., & Han, M. K. (2020). Chronic respiratory diseases: a global view. *The Lancet Respiratory Medicine, 8*(6), 531-533. doi:10.1016/S2213-2600(20)30157-0

Lujan, H., Griffin, W. C., Taube, J. H., & Sayes, C. M. (2019). <p>Synthesis and characterization of nanometer-sized liposomes for encapsulation and microRNA transfer to breast cancer cells</p>. *International Journal of Nanomedicine, Volume 14*, 5159-5173. doi:10.2147/ijn.s203330

Métayé, T., & Desmarquet, M. (2001). Rapid quality control for testing the radiochemical purity of 99Tcm-tetrofosmin. *Nuclear Medicine Communications, 22*(10). doi:10.1097/00006231-200110000-00014

Métayé, T., Desmarquet, M., Rosenberg, T., Guilhot, J., & Bouin-Pineau, M. H. (2001). Rapid quality control for testing the radiochemical purity of 99Tc(m)-tetrofosmin. *Nuclear Medicine Communications, 22*(10), 1139-1144. doi:10.1097/00006231-200110000-00014

Mushtaq, S., Bibi, A., Park, J. E., & Jeon, J. (2021). Recent Progress in Technetium-99m-Labeled Nanoparticles for Molecular Imaging and Cancer Therapy. *Nanomaterials (Basel), 11*(11). doi:10.3390/nano11113022

Nakatuka, Y., Yoshida, H., Fukui, K., & Matuzawa, M. (2015). The effect of particle size distribution on effective zeta-potential by use of the sedimentation method. *Advanced Powder Technology, 26*(2), 650-656. doi:10.1016/j.apt.2015.01.017

Ozgenc, E., Karpuz, M., Arzuk, E., Gonzalez-Alvarez, M., Sanz, M. B., Gundogdu, E., & Gonzalez-Alvarez, I. (2022). Radiolabeled Trastuzumab Solid Lipid Nanoparticles for Breast Cancer Cell: in Vitro and in Vivo Studies. *ACS Omega, 7*(34), 30015-30027. doi:10.1021/acsomega.2c03023

Saha, G. B. (2018). Diagnostic Uses of Radiopharmaceuticals in Nuclear Medicine. In G. B. Saha (Ed.), *Fundamentals of Nuclear Pharmacy* (pp. 269-354). Cham: Springer International Publishing. doi:10.1007/978-3-319-57580-3_13

Sancho, L., Rodriguez-Fraile, M., Bilbao, J. I., Beorlegui Arteta, C., Iñarrairaegui, M., Moran, V., & Sangro, B. (2017). Is a Technetium-99m Macroaggregated Albumin Scan Essential in the Workup for Selective Internal Radiation Therapy with Yttrium-90? An Analysis of 532 Patients. *Journal of Vascular and Interventional Radiology, 28*(11), 1536-1542. doi:10.1016/j.jvir.2017.07.019

Schreuder, N., de Hoog, Q., van der Bruggen, W., & van Puijenbroek, E. P. (2019a). Anaphylactic Reaction to Tc-99m Macrosalb. *Drug Safety - Case Reports, 6*(1), 4. doi:10.1007/s40800-019-0097-4

Schreuder, N., Koopman, D., Jager, P. L., Kosterink, J. G. W., & van Puijenbroek, E. (2019b). Adverse Events of Diagnostic Radiopharmaceuticals: A Systematic Review. *Seminars in Nuclear Medicine, 49*(5), 382-410. doi:10.1053/j.semnuclmed.2019.06.006

Shi, N.-Q., & Qi, X.-R. (2018). Preparation of Drug Liposomes by Reverse-Phase Evaporation. In W.-L. Lu & X.-R. Qi (Eds.), *Liposome-Based Drug Delivery Systems* (pp. 37-46). Berlin, Heidelberg: Springer Berlin Heidelberg. doi:10.1007/978-3-662-49231-4_3-1

Silindir-Gunay, M., Karpuz, M., Ozturk, N., Yekta Ozer, A., Erdogan, S., & Tuncel, M. (2019). Radiolabeled, folate-conjugated liposomes as tumor imaging agents: Formulation and in vitro evaluation. *Journal of Drug Delivery Science and Technology, 50*, 321-328. doi:10.1016/j.jddst.2019.02.003

Silindir Günay, M. (2020). The Formulation of Methylene Blue Encapsulated, Tc-99m Labeled Multifunctional Liposomes for Sentinel Lymph Node Imaging and Therapy. *Turkish Journal of Pharmaceutical Sciences, 17*(4), 381-387. doi:10.4274/tjps.galenos.2019.86619

Smith, M. C., Crist, R. M., Clogston, J. D., & McNeil, S. E. (2017). Zeta potential: a case study of cationic, anionic, and neutral liposomes. *Analytical and Bioanalytical Chemistry, 409*(24), 5779-5787. doi:10.1007/s00216-017-0527-z

SreeHarsha, N., Venugopala, K. N., Nair, A. B., Roopashree, T. S., Attimarad, M., Hiremath, J. G., . . . Tratrat, C. (2019). An Efficient, Lung-Targeted, Drug-Delivery System To Treat Asthma Via Microparticles. *Drug Design, Development and Therapy, 13*, 4389-4403. doi:10.2147/DDDT.S216660

Šturm, L., & Poklar Ulrih, N. (2021). Basic Methods for Preparation of Liposomes and Studying Their Interactions with Different Compounds, with the Emphasis on Polyphenols. *International journal of molecular sciences, 22*(12), 6547. doi:10.3390/ijms22126547

Yu, J. Y., Chuesiang, P., Shin, G. H., & Park, H. J. (2021). Post-Processing Techniques for the Improvement of Liposome Stability. *Pharmaceutics, 13*(7), 1023. doi:10.3390/pharmaceutics13071023

A Novel Method for The Simultaneous Determination of Olanzapine and Escitalopram in Artificial Saliva by High Performance Liquid Chromatography

Aysun DİNÇEL*°, Selin ŞAMİL**, E. Damla GÖK-TOPAK***

A Novel Method for the Simultaneous Determination of Olanzapine and Escitalopram in Artificial Saliva by High Performance Liquid Chromatography

SUMMARY

Monitoring of the drug levels can be very important for efficient drug treatment. For this purpose, studies on drug analysis from various biological fluids (especially plasma) are carried out in analytical chemistry. For many drugs, determination of drug concentration in saliva can be used alternatively for drug level monitoring. Patients with cognitive dysfunction have difficulty in maintaining usual living standards and adapting to society. Individuals with such disorders need to be treated with an appropriate medication regimen. Generally, treatment is provided orally and the most commonly used antipsychotic drugs are olanzapine (OLZ) and escitalopram (ESC). Measurement of saliva drug concentration of OLZ and ESC can be helpful for the treatment of diseases. In this study, it is aimed at developing a novel HPLC method that will allow OLZ and ESC to simultaneously be determined in artificial saliva. The separation was achieved on XBridge, C18 column with diode array detector (DAD) (240 nm) and isocratic elution of mobile phase containing acetonitrile and phosphate buffer mixture (20 mM NaH_2PO_4, pH 4.6) (35:65, v/v) containing mobile phase at a flow rate of 0.9 mL/min. Drug extraction from artificial saliva was applied using a methanol and acetonitrile (1:1; v/v) mixture. The recoveries were found in the range of 97.508% and 104.49% (mean) for OLZ and ESC, respectively, from artificial saliva.

Key Words: *Olanzapine, Escitalopram, Saliva, HPLC, Validation.*

Olanzapin ve Essitalopramın Yapay Tükürükte Yüksek Performanslı Sıvı Kromatografisi ile Eşzamanlı Tayini için Yeni Bir Yöntem

ÖZ

İlaç seviyelerinin izlenmesi, etkili ilaç tedavisi için çok önemli olabilir. Bu amaçla analitik kimyada başta plazma olmak üzere çeşitli biyolojik sıvılardan ilaç analizine yönelik çalışmalar yürütülmektedir. Birçok ilaç için tükürük, ilaç konsantrasyonu tayini, ilaç seviyesi takibi için alternatif olarak kullanılabilir. Bilişsel işlev bozukluğu olan hastalar normal yaşam standartlarını sürdürmekte ve topluma uyum sağlamakta zorluk çekerler. Bu tür bozuklukları olan bireylerin uygun bir ilaç rejimi ile tedavi edilmesi gerekir. Genellikle tedavi ağız yoluyla sağlanır ve en yaygın kullanılan antipsikotik ilaçlar olanzapin (OLZ) ve essitalopramdır (ESC). OLZ ve ESC'nin tükürük ilaç konsantrasyonunun ölçülmesi hastalıkların tedavisi için yararlı olabilir. Bu çalışmada, OLZ ve ESC'nin yapay tükürükte eş zamanlı olarak belirlenmesini sağlayacak yeni bir HPLC yönteminin geliştirilmesi amaçlanmıştır. Ayırma işlemi XBridge, C18 kolonunda diyot dizi dedektör (DAD) (240 nm) ve asetonitril ve fosfat tampon karışımı (20 mM NaH_2PO_4, pH 4.6) 35:65 (h/h) içeren mobil fazın izokratik elüsyonu ile 0,9 mL/dak akış hızında gerçekleştirilmiştir. Yapay tükürükten ilaç ekstraksiyonu, metanol ve asetonitril (1:1; v/v) karışımı kullanılarak uygulanmıştır. Yapay tükürükten geri kazanım değerleri OLZ ve ESC için sırasıyla %97.508 ve %104.49 (ortalama) aralığında bulunmuştur.

Anahtar Kelimeler: *Olanzapin, Essitalopram, Tükürük, HPLC, Validasyon*

---

* ORCID: 0000-0002-1986-6862: Lokman Hekim University, Faculty of Pharmacy, Department of Analytical Chemistry, 06510, Ankara, Türkiye
** ORCID: 0009-0005-0650-5477: Lokman Hekim University, Faculty of Pharmacy, Department of Analytical Chemistry, 06510, Ankara, Türkiye
*** ORCID: 0000-0002-2586-8207: Lokman Hekim University, Faculty of Pharmacy, Department of Analytical Chemistry, 06510, Ankara, Türkiye

° Corresponding Author; Aysun DİNÇEL
E-mail: aysun.dincel@lokmanhekim.edu.tr

INTRODUCTION

Cognitive dysfunction is one of the most critical health problems that reduce the quality of life and can affect both the individual and their environment. Patients with cognitive dysfunction (psychotic disorder) have difficulties living as healthy and adapting to society, if they cannot access appropriate treatment, the quality of life of the patient and the patient's environment decrease. The most essential treatment method for psychotic disorders is the use of antipsychotic drugs. The two most commonly used drugs are olanzapine (OLZ) and escitalopram (ESC).

OLZ is an atypical antipsychotic drug approved by the US Food and Drug Administration (FDA) for the treatment of schizophrenia, and bipolar disorder. It is also recommended for patients with anorexia nervosa, autism spectrum disorders, Tourette syndrome and tic disorders. OLZ is also used to treat resistant depression and depressive episodes in bipolar disorder (Dziurkowska et al., 2020). Molecular formula is $C_{17}H_{20}N_4S$ and chemically named 2-methyl-4-(4-methylpiperazin-1-yl)-10*H*-thieno[2,3-b][1,5]benzodiazepine (Figure 1).
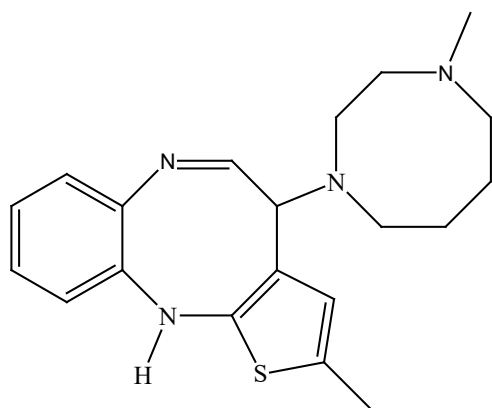
Figure 1. Chemical structure of olanzapine

ESC is a widely used antidepressant approved by the US Food and Drug Administration (FDA) in 2001 and prescribed to more than 240 million patients to date. ESC is an oral serotonin reuptake inhibitor (SSRI). It is effective in the treatment of moderate to severe generalized anxiety disorder, panic attacks

(agoraphobia), and obsessive-compulsive disorder and is generally well tolerated (Garnock-Jones et al., 2010). Molecular formula is $C_{20}H_{21}FN_2O$ and chemically named (1*S*)-1-[3-(dimethylamino)propyl]-1-(4-fluorophenyl)-3H-2-benzofuran-5-carbonitrile (Figure 2).
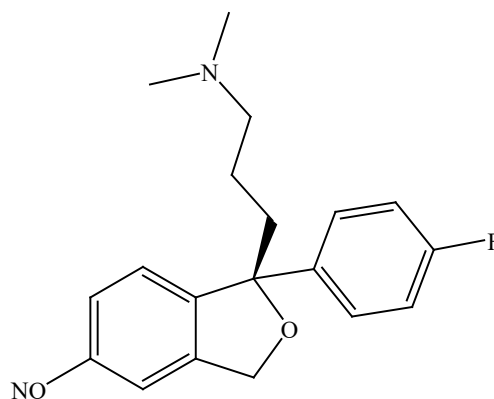
Figure 2. Chemical structure of escitalopram

Determination of adequate drug levels of antipsychotic drugs plays a very important role in the course and treatment of the diseases. For this reason, developing methods for drug analysis in various biological fluids is one of the most important fields of study in analytical chemistry. Analytical methods for the determination of antipsychotic drugs need to be highly sensitive and selective for accurate and precise quantification.

High-performance liquid chromatography (HPLC) methods are generally preferred for determining of drug levels in plasma or other biological materials as they provide sensitive and accurate results.

With the methods developed with HPLC, it is possible to reach the analysis result in a very short time. In this study, it is aimed to develop a validated HPLC method that allows simultaneous analysis of OLZ and ESC in artificial saliva.

Few studies have been published in the literature for the simultaneous determining of ESC and OLZ. The method developed by Alasabashi et al. did not include stability studies, and the analysis of ESC and OLZ in

biological fluids was not performed (Alasabashi et al., 2022). A method for the simultaneous analysis of OLZ and ESC in saliva by HPLC is not yet available.

In the studies conducted, OLZ and ESC are usually quantified in blood. Monitoring serum and plasma levels to determine drug concentrations and monitor patient treatment is still one of the most commonly used methods in routine controls. However, drug determination methods in serum and plasma can pose many problems in practice due to various difficulties in the collection of diagnostic material (Chiu & Franklin 1996; Raggi et. al., 2000; Boulton et al., 2001; Bhimanadhuni et al., 2012; Teichert et al., 2020). For example, drawing blood from a patient can have adverse effects such as fear, pain, skin irritation, and infection. In addition, professional medical personnel are required to obtain serum or plasma for analytical research. For this reason, alternative sample options are being developed to reduce the amount of work and risk involved.

The advantage of choosing saliva as the matrix, which can be an alternative to plasma and serum, is related to the non-invasive nature of the collection procedure, which requires fewer safety precautions must be taken and the health professional gathering the sample needs to possess less training. The amount of drugs detected in saliva is reported to reflect the concentration of a free, non-protein-bound drug in plasma. Given that only the free form of the drug exerts pharmacologic activity, the importance of saliva analysis in pharmacokinetic studies is evident. However, further research is needed before saliva analysis can replace plasma analysis for each drug (Abad 1983). For these reasons, this study aimed to develop a sensitive, accurate, and rapid HPLC method to determine the levels of OLZ and ESC from artificial saliva, an easily accessible diagnostic material.

MATERIAL AND METHOD

Chemicals and reagents

Analytical standards of OLZ, % purity 99.8, and ESC, % purity 99.7 were obtained from Ali Raif İlaç Sanayi A.Ş., Quercetin (Q; internal standard, IS) was purchased from Merck, (Darmstadt, Germany). Acetonitrile (HPLC grade, CARLO ERBA, Italy), methanol (HPLC grade, CARLO ERBA, Italy), NaH_2PO_4, KCl, NaCl, NaOH, $CaCl_2$ KSCN, NH_2CONH_2, and Na_2S were purchased from Sigma-Aldrich (USA). OLZ, ESC and Q stock solutions were prepared with methanol at 1 mg/mL. The solutions to be used in the analysis were prepared daily by diluting the stock solutions with methanol to the desired concentration values. Stock solutions were stored at -20 °C for 1 week.

Instrumentation and chromatographic conditions

The chromatographic system consisted of a Shimadzu liquid chromatograph equipped with a pump (LC-10AT VP), a controller (SCL-10A VP) connected to a computer using software (Class-VP 5.03), an autosampler (SIL-10AD VP), 10 μL injection loop and Diode Array Detector (DAD, SPD-10A VP). The system was controlled through a system controller (SCL-10A), a personal computer using a CLASS-VP 5.0 workstation with a data processing system (Shimadzu, Kyoto, Japan) installed on it. The separation was performed on a XTerra, C_{18} (100 x 4.6 mm i.d., 3.5 μm), and XBridge, C_{18} (250 x 4.6 mm, particle size 5 μm) analytical columns (Waters, Milford, MA, USA). The column temperature was set to 24 °C. The mobile phase consisted of 20 mM NaH_2PO_4 (pH adjusted to 4.6 with NaOH), and acetonitrile in the ratio of 35:65 (v/v) in isocratic mode and the DAD detector was set to the wavelength of 240 nm. 10 μL of sample solutions was injected into the HPLC system at the flow rate of 0.9 mL/min. Quercetin was chosen as the internal standard as its peak was very well resolved from two drug peaks, showing any interfering peaks. All solutions were prepared in type 1 water (Simplicity 185 Water System, Millipore Corp., Bedford, MA, USA). The mobile phase was filtered through a membrane filter with a pore diameter of 0.45 μm and kept in an ultrasonic bath for 15 min to remove the soluble gases. At end of the analysis, column was flushed with approximately

20 times of column volume of a mixture with HPLC grade water and methanol (50:50, v/v). Finally, the column was stored in pure methanol. This procedure was applied for every analysis.

Drug analysis in artificial saliva

The development of the method of simultaneous analysis of OLZ and ESC in artificial saliva by HPLC was carried out using the standard addition method of active substance components into artificial saliva. For this purpose, artificial saliva was prepared by dissolving the components given in Table 1 in 1 L of pure water (J Pytko-Polonczyk et al; 2017).

Artificial saliva was used to prepare solutions of OLZ and ESC at the desired concentration values, and Q was spiked to the concentration value of 0.5 µg/mL. 1 mL of a solution that was prepared with artificial saliva was taken in a 2 mL Eppendorf tube, then 0.5 mL of a mixture of methanol and acetonitrile (1:1; v/v) was added to the solutions, and then the solutions were mixed with a vortex mixer for 15 s and then centrifuged at 6000 rpm for 6 min. After centrifugation, approximately 300 µL aliquot was taken from the top of the tube without shaking. Aliquot was filtrated by a 0.45 µm nylon injector filter, and then 10 µL of a solution was injected into the HPLC system. This procedure was repeated two times for each sample. The developed method was validated according to International Conference on Harmonization (ICH) requirements (Validation of Analytical Procedures: Text and Methodology Q2 (R1), 2014; Validation of Analytical Procedures Q2(R2), 2022).

Table 1. Artificial saliva content (for 1 L, pH=6.5)

Compound	Quantity (mg)
KCl	400
NaCl	400
$NaH_2PO_4.H_2O$	690
$CaCl_2.2H_2O$	795
$Na_2S.9H_2O$	5
KSCN	300
CH_4N_2O	1000

Method validation

Validation studies were performed according to ICH requirements. Within the scope of the validation studies carried out, retention time, capacity factor, tailing factor, and theoretical number of plates for each drug were calculated. The system suitability test was performed with six repeated injections of the standard mixture solution at a concentration of 1 µg/mL. In the method, the calibration curve was obtained by the peak area under the analyte peak being divided by the peak area of the IS peak area, and the obtained values were plotted against the concentration value of each drug. The method linearity was evaluated by examining the correlation coefficient (r) values from the obtained curves. The linearity was calculated using the regression equation (y = mx + n) data, including concentration ranges, correlation coefficients, and the standard error of intercept. In addition, sensitivity, selectivity, accuracy, recovery and precision studies were performed at three different concentration values (1, 2 and 3 µg/mL, n=6) and intra-day and inter-day repeated analysis results were evaluated. The limit of detection (LOD) value was taken as the signal-to-noise (S/N) value equal to 3 for repeated (n=6) different standard solution analyses. The limit of quantification (LOQ) value was taken as the value where the RSD value was less than or equal to 5% for repeated (n=6) different solution analyses and the signal-to-noise (S/N) value equal to 10 for repeated (n=6) different standard solution analyses (Jenke 1996; Jenke 1996).

RESULTS AND DISCUSSION

To determine the optimum chromatographic separation conditions, various mobile phase compositions and different stationary phases were tested. For this purpose, the effect of the ratio of organic composition as acetonitrile and methanol in the mobile phase was investigated at different concentrations and different elution applications. For this purpose, XTerra, C_{18} (250 x 4.6 mm, particle size 3.5 µm) and XBridge, C_{18} (250 x 4.6 mm, particle size

5 µm) analytical columns were tested as stationary phase and the best separation was achieved with XBridge, C_{18} column. Again, the optimization studies of the mobile phase composition were carried out with buffer solutions at different pH values; the effects of pH values between 3.5 and 5.0 on the capacity factor and peak symmetry ratios for separation were examined. Also, the concentration of buffer solution was investigated according to the capacity factor. The best separation was obtained for OLZ, ESC, and Q in isocratic elution with the mobile phase composition of acetonitrile and phosphate buffer (20 mM, pH 4.6)

35:65 (v/v) at a flow rate of 0.9 mL/min (24°C).

For validation studies, specificity, LOD, LOQ, selectivity, linearity, accuracy, sensitivity, intra-day and inter-day precision were investigated for developed method.

The method was linear in the range of 0.8-3 µg/mL for OLZ and ESC. The r^2 (regression coefficient) values from the curve equations obtained were close to 1 (Table 2). The LOD and LOQ values for OLZ and ESC in artificial saliva were to be 0.3 µg/mL and 0.8 µg/mL, respectively.

Table 2. Calibration curve parameters

Drug	Slope	Intercept	r^2	Slope SE*	Intercept SE*	LOD (µg/mL)
OLZ	2.0151	0.5992	0.9981	0.084	0.093	0.3
ESC	1.4639	0.603	0.9914	0.079	0.078	0.3

SE*: Standard Error (n=6)

As a result of the studies carried out to determine the selectivity of the method, it was determined that there was no interference peak in the retention times

of OLZ, ESC, and IS peaks caused by artificial saliva, mobile phase, or HPLC system (Figure 3).

(a)

(b)
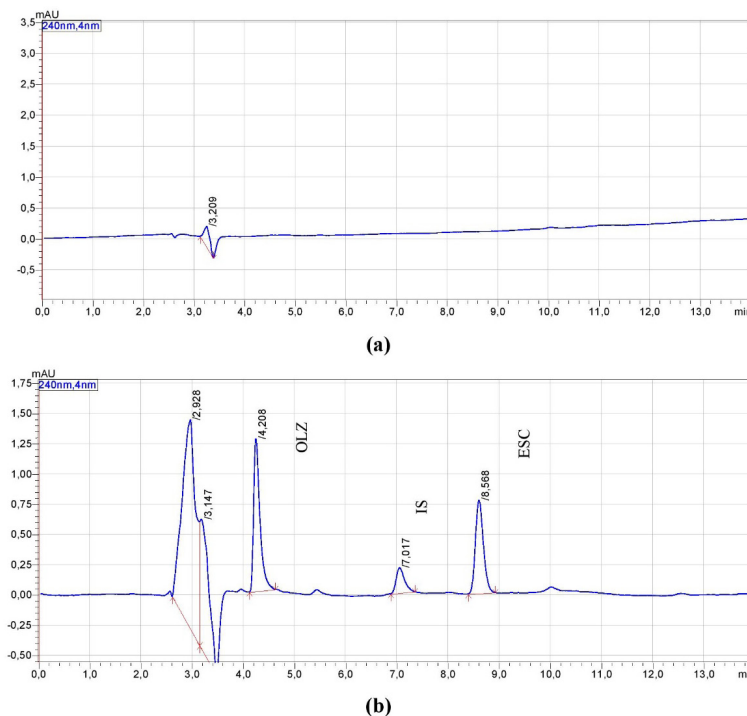
Figure 3. (a) Chromatogram of artificial saliva without drugs, (b) Chromatogram of artificial saliva extraction containing 1.5 µg/mL OLZ and ESC

Suitability parameters including retention time, capacity factor, tailing factor, theoretical number of plates were investigated (Table 3).

HPLC-DAD system suitability for the developed method was evaluated based on retention time, injection repeatability, capacity factor, tailing factor and the theoretical number of plates. The data obtained from 6 replicate experiments were used for the investigated parameters. The values obtained (Table 3) meet the accepted conditions of capacity factor k values for good separations, tailing factor≤1.5, and the theoretical number of plates>2000, and the system was found to be suitable for analyzing targeted drugs. Calculated % RSD values of retention time and capacity factor, tailing factor parameters were also determined (Jenke 1996; Jenke 1996).

Table 3. System suitability parameters

Active ingredients	Retention time* (min)	Capacity factor, k*	Tailing factor*	The Theoretical number of plates
OLZ	4.25 ± 0.21	0.34 ± 0.07	1.65 ± 0.17	2742.97
ESC	8.52 ± 0.05	1.66 ± 0.02	1.21 ± 0.04	24545.31
IS	7.01 ± 0.11	1.19 ± 0.04	1.46 ± 0.16	9618.06

*n=6, results are given by mean ± relative standard deviation

Within the precision studies, intra-day, inter-day repeated (n=6) analyses were performed at concentrations of 1, 2 and 3 µg/mL. In the extraction studies, the effects of methanol, acetonitrile and extraction solutions individually or in different mixture combinations on the analysis were examined. The best extraction solvent mixture was selected as a mixture of methanol and acetonitrile (1:1; v/v). The data obtained after extraction were analyzed by calculating the mean, relative standard deviation, and standard deviation values (Table 4).

Table 4. Inter-day and intra-day precision and accuracy results (n=6)

Added (µg/mL)	Parameters	OLZ		ESC	
		Inter-day	Intra-day	Inter-day	Intra-day
1	Found	0.981	0.979	1.027	1.045
	Precision RSD (%)	1.282	0.430	0.982	1.363
	RE	-0.509	-0.487	-0.511	-0.478
	Accuracy Bias (%)	-1.865	-2.130	2.684	4.490
	Recovery (%)	98.135	97.870	102.684	104.490
2	Found	2.051	2.016	2.047	2.056
	Precision RSD (%)	1.370	0.912	0.256	0.205
	RE	-0.487	-0.496	-0.488	-0.486
	Accuracy Bias (%)	2.536	0.815	2.331	2.802
	Recovery (%)	102.536	100.815	102.331	102.802
3	Found	2.925	3.069	3.053	3.288
	Precision RSD (%)	2.495	0.985	2.401	2.343
	RE	-0.483	-0.483	-0.490	-0.388
	Accuracy Bias (%)	-2.492	1.778	3.339	2.019
	Recovery (%)	97.508	101.778	103.33	102.019

$\bar{x}$: Mean value, RE: Relative error, RSD**:** Relative Standard Deviation,

Bias**:** ((amount found - amount added)/amount found) x100

The studies carried out to investigate the recovery values of OLZ and ESC from artificial saliva (n=6), from the data obtained, the recovery values were found in the range of 97.508% and 104.49%.

It is crucial to establish a method for choosing saliva as an alternative for analyzing serum and plasma levels to ascertain drug concentrations and for patient therapy. Saliva sample collection is more accessible to implement as it requires fewer safety precautions and is a non-invasive sampling procedure. The HPLC method developed for OLZ and ESC analysis in artificial saliva is presented as an easily applicable method when the recovery and accuracy parameters are examined. The developed method is sensitive, with a LOD of 0.3 µg/mL. It has short retention times with a separation time of approximately 10 minutes. In addition, proposed practical extraction procedure for drug determination can be helpful further analysis procedures. The developed method is superior to the existing methods in the literature regarding precision and easy applicability.

CONCLUSION

Analyzing of drugs in biological material is critical in determining an effective treatment regimen. In this study, a new method for OLZ and ESC analysis in artificial saliva was developed. Due to ethical limitations, the study could not be performed in patient saliva samples. OLZ and ESC analysis in blood and saliva samples from patients may give more precise results in terms of the usability of saliva in determining drug levels. In addition, this can be said in light of previous studies on the usability of saliva as a substitute for plasma drug levels. In this study, a novel easy, simple, selective and validated chromatographic method was developed for OLZ and ESC in artificial saliva allowing simultaneous analysis in HPLC-DAD system. The developed method may be necessary as it has not been done in the literature and can be presented as a new and applicable approach and method in drug treatment processes. The developed analysis method can be applied as a new, simple method in drug-level monitoring and different applications.

AUTHOR CONTRIBUTION STATEMENT

Idea (EDGT, AD), planning and method development of HPLC analyses (AD), the manuscript designing and editing (AD), performing experiments (AD, SŞ), investigation and literature review (AD, SŞ, EDGT).

CONFLICT OF INTEREST

Authors declare that there is no conflict of interest.

REFERENCES

Abad, F. (1983). İlaç Etken Maddelerinin Plazma. Seviyelerini Yansıtan Bir Sıvı: Tükrük. *FABAD Journal of Pharmaceutical Sciences*, *8*, 121-131. Retrieved from https://dergi.fabad.org.tr/pdf/volum8/Issue3/1.pdf

Alasabashi, M., Ževžikovienė, A., Marksa, M., Rimkienė, L., Ževžikovas, A. (2022). The validated method for the analysis of a mixture of psychotropic medicines olanzapine, clorazepate and escitalopram using a high-performance liquid chromatography method, *Chemija*, *33*(2), 35-39. doi:10.6001/chemija.v33i2.4706.

Bhimanadhuni, C.N., Garikapati, D.R., Usha, P. (2012). Development and validation of an RP-HPLC method for the simultaneous determination of Escitalopram Oxalate and Clonazepam in bulk and its pharmaceutical formulations. *International Current Pharmaceutical Journal*, *1*(8), 193-198. doi:10.3329/icpj.v1i8.11249

Boulton, D.W., Markowitz, J.S., DeVane, C.L. (2001). A high-performance liquid chromatography assay with ultraviolet detection for olanzapine in human plasma and urine. *Journal of Chromatography B Biomedical Science Application*, *759*(2), 319-323. Doi: 10.1016/s0378-4347(01)00240-7.

Chiu, J.A., Franklin, R.B. (1996). Analysis and pharmacokinetics of olanzapine (LY170053) and two metabolites in rat plasma using reversed-phase HPLC with electrochemical detection. *Journal of Pharmaceutical and Biomedical Analysis*. *14*(5), 609-615. doi:10.1016/0731-7085(95)01651-1.

Dziurkowska, E., Jiménez-Morigosa, C., López-Rivadulla, M., & Wesolowski, M. (2020). Development and validation of solid-phase extraction coupled with a liquid chromatography-tandem mass spectrometry method for quantitation of olanzapine in saliva. *Journal of chromatography. B, Analytical technologies in the biomedical and life sciences*, *1136*, 121896. doi: 10.1016/j.jchromb.2019.121896

Garnock-Jones, K.P., McCormack, P.L. (2010). Escitalopram: a review of its use in the management of major depressive disorder in adults. *CNS Drugs*, *24*(9), 769-96. doi: 10.2165/11204760-000000000-00000. PMID: 20806989.

ICH, (2022). Harmonized Tripartite Guideline, on validation of analytical procedures Q2(R2), ICH Steering Committee, Retrieved from https://database.ich.org/sites/default/files/ICH_Q2-R2_Document_Step2_Guideline_2022_0324.pdf Access date: 21 August 2024.

ICH, (2014). Harmonized Tripartite Guideline, Validation of analytical procedures: Text and Methodology Q2(R1), ICH Steering Committee, Retrieved from https://database.ich.org/sites/default/files/Q2%28R1%29%20Guideline.pdf Access date: 21 August 2024.

Jenke, D.R. (1996). Chromatographic method validation: A review of current practices and procedures. II. Guidelines for primary validation parameters. *Journal of Liquid Chromatography and Related Technologies, 19* (5), 737-757. doi:10.1080/10826079608005534

Jenke, D.R. (1996). Chromatographic method validation: A review of current practices and procedures. III. Ruggedness, re-validation and system suitability. *Journal of Liquid Chromatography and Related Technologies, 19* (12), 1873-1891. doi:10.1080/10826079608014012

J Pytko-Polonczyk, J., Jakubik, A., Przeklasa-Bierowiec, A., & Muszynska, B. (2017). Artificial saliva and its use in biological experiments. *Journal of physiology and pharmacology : an official journal of the Polish Physiological Society, 68*(6), 807–813. Retrieved from https://pubmed.ncbi.nlm.nih.gov/29550792/

Raggi, M., Casamenti, G., Mandrioli, R., Fanali, S., De Ronchi, D., Volterra, V. (2000). Determination of the novel antipsychotic drug olanzapine in human plasma using HPLC with amperometric detection. *Chromatographia, 51*(9), 562-566. doi:10.1007/BF02490813

Teichert, J., Rowe, J.B., Ersche. K.D., Skandali. N., Sacher. J., Aigner, A. (2020). Determination of Atomoxetine or Escitalopram in human plasma by HPLC. Applications in Neuroscience Research Studies. *International Journal of Clinical Pharmacology and Therapeutics, 58*(8), 426-438. doi:10.5414/CP203705.

Does Functionality of Perivascular Adipose Tissue Decrease in the Adult Rat Thoracic Aorta?

Gaye OZTURK*, Melike Hacer OZKAN**°

Does Functionality of Perivascular Adipose Tissue Decrease in the Adult Rat Thoracic Aorta?

SUMMARY

Perivascular adipose tissue (PVAT) regulates vascular tone with anticontractile effects by releasing paracrine factors. Aging is considered an independent risk factor that impairs vascular function in humans and rodents. There are limited studies examining the effects of aging on PVAT. In this study, we investigated the contractions to noradrenaline and the relaxations to acetylcholine in the presence and absence of PVAT in isolated thoracic aortas of 10-12-week-old young and 52-week-old adult Wistar rats. Noradrenaline contractions were lower in aortas with PVAT compared to rings without PVAT in both young and adults. The amplitude of contractions in adult rat aorta in the absence of PVAT was significantly higher compared to young rats. However, when PVAT was left intact, the amplitude and sensitivity of noradrenaline contractions were low in young and adults, indicating continued anticontractile effect of PVAT. Noradrenaline contractions were significantly potentiated by L-NAME, a nitric oxide (NO) synthase inhibitor, in young rat aortas, and this increase was lower in the presence of PVAT. However, the potentiating effect of L-NAME in the adults did not change with PVAT. Acetylcholine-induced endothelium-dependent relaxations were reduced in the adult rats compared with young. Acetylcholine relaxations were not affected by PVAT in young rats, whereas the decreased acetylcholine relaxations were further reduced in the aged aortas with PVAT. As a result, the anticontractile function of PVAT continues in adult rats and limits the contraction with a tonic inhibitory effect. However, PVAT does not seem to protect endothelium-dependent relaxations that decrease with aging.

Key Words: *Anticontractile, aorta, endothelium, NO, PVAT, rat.*

Erişkin Sıçan İzole Torasik Aortunda Perivasküler Adipoz Doku Fonksiyonu Azalır mı?

ÖZ

Perivasküler adipoz doku (PVAD) parakrin faktörler salıvererek kasılma-karşıtı etki ile damar tonusunu düzenler. Yaşlanma, insanlarda ve kemirgenlerde damar yapısını ve işlevini bozan bağımsız bir risk faktörü olarak kabul edilir. Yaşlanmanın PVAD işlevi üzerine etkilerini inceleyen sınırlı sayıda çalışma vardır. Biz bu çalışmada, 10-12 haftalık genç ve 52 haftalık erişkin Wistar erkek sıçanların izole torasik aortasında PVAD varlığında ve yokluğunda noradrenalin kasılmalarını ve asetilkolin ile elde edilen endotele bağlı gevşemeleri inceledik. Noradrenalin kasılmaları hem genç hem de erişkin gruba ait PVAD'ı sağlam torasik aorta halkalarında PVAD'ı sıyrılmış olanlara göre düşüktü. PVAD yokluğunda erişkin sıçan torasik aortunda elde edilen noradrenalin kasılmalarının boyu genç sıçan aortuna kıyasla anlamlı derecede yüksekti. Ancak bu arterlerde PVAD sağlam bırakıldığında, noradrenalin kasılma boyu ve duyarlılığı genç ve erişkin grupta benzerdi, bu da PVAD'ın erişkin sıçanlarda kasılma-karşıtı işlevinin devam ettiğini gösterdi. Genç sıçan torasik aortunda noradrenalin kasılmaları, nitrik oksit (NO) sentaz inhibitörü L-NAME varlığında güçlenerek arttı ve bu artış oranı PVAD varlığında daha düşüktü. Ancak, L-NAME'in erişkin grupta noradrenalin -aracılı kasılmalardaki güçlendirici etkisi PVAD varlığında değişmedi. Asetilkolin-kaynaklı ve endotel-bağımlı gevşemeler erişkin grupta genç gruba kıyasla önemli ölçüde azaldı. PVAD'ın sağlam bırakılması genç sıçan aortunda endotele bağlı gevşemeleri etkilemezken, yaşlı sıçan aortunda azalmış asetilkolin gevşemeleri daha da azaldı. Sonuç olarak, PVAD'ın kasılma-karşıtı işlevinin erişkin sıçanlarda devam ettiği ve tonik inhibitör etkiyle damardaki kasılmayı sınırladığı belirlenmiştir. Ancak PVAD'ın yaşlanmayla birlikte azalan endotele bağlı gevşemeleri geri çeviremediği söylenebilir.

Anahtar Kelimeler: *Kasılma-karşıtı, aorta, endotel, NO, PVAT, sıçan.*

---

* ORCID: 0000-0002-2073-7865, Private Mim Hospital, Cankaya, Ankara, Turkiye
** ORCID: 0000-0003-1339-2616, Department of Pharmacology, Faculty of Pharmacy, Hacettepe University, Sihhiye, Ankara, Turkiye

° Corresponding Author; Melike Hacer OZKAN
E-mail: melikeo@hacettepe.edu.tr

INTRODUCTION

Perivascular adipose tissue (PVAT) covers the outer surface of the vascular wall where it is located without being separated by any elastic lamina from the tunica adventitia (Siegel-Axel & Haring, 2016) (Gil-Ortega, Somoza, Huang, Gollasch, & Fernandez-Alfonso, 2015). Previously, PVAT was thought to be only a barrier that protects the vessel from mechanical injury; further studies have revealed that bioactive molecules released from PVAT can also affect neighboring vascular smooth muscle by endocrine and paracrine functions (Rajsheker et al., 2010). Similarly, molecules released from the vascular components such as endothelium can also diffuse into PVAT and modulate its function on vascular homeostasis (Margaritis et al., 2013). Healthy PVAT participates in a number of modulatory processes including anti-inflammatory properties, anti-oxidative defense, vasodilation or anticontractile action (Hu, Garcia-Barrio, Jiang, Chen, & Chang, 2021).

The anticontractile function of PVAT has been demonstrated by its inhibiting effect on contraction to various agonists in isolated vascular tissues mounted to organ bath system or wire myograph (Gao et al., 2005). PVAT secretes a wide range of adipocytokines, including adipokines and cytokines, which are involved in the regulation of vascular tone. Adiponectin is the most abundant molecule produced and released by PVAT (Chang, Garcia-Barrio, & Chen, 2020). Adiponectin binds to the receptor of the endothelial cells and leads to the phosphorylation of AMP-activated protein kinase and then to the activation of the endothelial NO synthase, promoting NO production (Cheng et al., 2007). PVAT can act as two sides of the same coin, cardiovascular risk factors as well as vascular aging may alter the structure and functionality of PVAT which leads to the loss of its vascular protective properties, and the release of contractile factors from PVAT affecting the vascular tone (Wang et al., 2024). However, little is known

about the impact of age on PVAT and how PVAT modulates the vascular reactivity in aged vasculature.

In this study, we aimed to investigate how PVAT and its paracrine action on vascular reactivity alter in isolated thoracic aortic rings of young and adult rats. Contractile responses to noradrenaline, and endothelium-dependent relaxations to acetylcholine were evaluated in isolated thoracic aortic rings of young (10-12-week-old) and adult (52-week-old) Wistar albino male rats in the absence and presence of PVAT.

MATERIAL AND METHODS

In the current study, Wistar Albino male rats weighing 180-200 g and 8 to 10-week-old were acquired from Kobay DHL Inc. Co. (Ankara, Turkiye). The animals were housed in the laboratory for two weeks to be accustomed to the laboratory environment with unlimited access to standard food and water under a 12-hour light/dark cycle. The rats were included in the experiments when they were 10-12- or 52-week-old. Hacettepe University Animal Experiments Local Ethics Committee authorized all animal procedures (Ethics Committee No: 2022/08-04).

On the day of the experiment, body weights (g) of the rats were measured. After that, rats were stunned with carbon dioxide (CO_2) inhalation and decapitated with a guillotine. Thorax was opened, thoracic aorta was isolated and put into a petri dish containing a cold Krebs-Henseleit Solution (KHS). One group of the vessels isolated from young and adult rats were left PVAT intact (PVAT+) and the other group of the vessels were removed from PVAT (PVAT-). The PVAT was cleaned around the thoracic aorta with small incisions using an appropriate cataract scissor. To ensure that the PVAT volume was the same in all rings, a fat layer of approximately 2 mm was left on the outer surface of the rings when preparing the tissues (Cacanyiova et al., 2021). The volumetric ratio between PVAT and endothelium was kept similar in

all groups. The vessels with or without PVAT were made into 3-4 mm ring preparations and placed in isolated organ baths of 5 mL containing KHS, which was continuously gassed (95% O_2 - 5% CO_2) at 37°C. In some experiments, the endothelium was mechanically damaged with a sterile syringe needle that was rubbed into the vascular lumen. Endothelial function was assessed by relaxations to acetylcholine (10 μM) after phenylephrine pre-contraction. Tissues that relaxed 10% or less were considered endothelium-removed.

At the beginning of the experiment, 2 g of basal tension were applied to the preparations. Immediately after, they were primed with 100 μM phenylephrine and then washed at 15-minute intervals for 1.5 hours. Tension changes were recorded on the computer via the isometric force transducer using the BIOPAC MP35 amplifier and Student Lab program (BIOPAC MP35 Data Acquisition System, Goleta, CA, USA). In the preliminary experiments, contraction responses to KHS containing 80 mM KCL were obtained twice in succession in all preparations. The second contractions to 80 mM KCL were accepted as the maximum contraction of each tissue. After wash out and resting period vascular reactivity was evaluated as mentioned below.

Experimental protocol

To demonstrate the anticontractile action of PVAT in 10-12-week-old young and 52-week-old adult rats, cumulative contraction responses were obtained with α- and β-receptor agonist noradrenaline (0.1 nM-100 μM) in the thoracic aortic rings in which PVAT was left intact or removed. After an hour of wash-out and resting period, the same tissues were incubated for 45 minutes with N^W-nitro-L-arginine methyl ester (L-NAME; 100 μM), a NO synthase inhibitor, and noradrenaline contractions were repeated. In this way, it was investigated the contribution of NO to anticontractile response of PVAT in young rats and how this contribution changes with aging.

In another set of experiments, the possible influence of the endothelium on the anticontractile function of the PVAT was examined by eliciting norepinephrine contractions in the absence of endothelium in aortic rings with or without PVAT in young rats.

Endothelium-dependent vasodilation was also examined in thoracic aortic rings belong to both age groups in the presence and absence of PVAT. After pre-contraction with phenylephrine (0.1 or 1 μM) cumulative relaxation responses to muscarinic agonist acetylcholine (1 nM-10 μM) were obtained.

At the end of the experiments dry tissue weights of both PVAT-intact or -removed aortas from young and adult rats were measured.

Statistical analysis

Data are seen as Mean ± Standard Error of Mean (SEM). In the organ bath experiments, contractions were shown as a percentage (%) of contractions to 80 mM KCL. Relaxations were shown as % of precontraction induced by phenylephrine. E_{max} is the maximum response (%) of an agonist-induced concentration-dependent response. pD_2 (-$logEC_{50}$) is the negative logarithm of drug concentration which constitutes half-maximum response of a concentration-response curve. Area Under the Curve (AUC, a.u) was calculated from each response-curve. Analysis of two concentration-response curves was done by 2-way ANOVA. Multiple comparisons (for pD_2, E_{max} and AUC values) were done by one-way ANOVA. All analyses were conducted using GraphPad Prism-9, and $p<0.05$ was considered to be significantly different.

Chemicals and solutions

Acetylcholine chloride, L-NAME, and L-phenylephrine hydrochloride (Sigma Chemical Co., St. Louis, MO, USA) were dissolved in distilled water. Indomethacin (Sigma Chemical Co., St. Louis, MO, USA) was prepared in distilled water containing 0.7% Na2CO3 (w/v). KHS had the following composition (mM): NaCL 118.0, KCL 4.7, $MgSO_4$ 1.2, $CaCL_2$ 2.5, KH_2PO_4 1.2, $NaHCO_3$ 25.0, and glucose 11.1. Eighty

mM KCL solution was prepared by substitution of KCL with equimolar NaCL.

RESULTS AND DISCUSSION

Body weights of the rats and dry tissue weights of isolated thoracic aorta rings with and without PVAT are shown in Table 1. Body weights of the adult group and tissue weights of aortic rings having PVAT increased significantly compared to those measured in the young group ($p<0.0001$). Aortic tissue weights without PVAT were similar in both young and adult rats (Table 1).

Contractile responses to noradrenaline (0.1 nM-100 μM) were evaluated in PVAT-intact and PVAT-removed aortic rings from young (10-12-week-old) and adult (52-week-old) rats. The amplitude of noradrenaline contractions (E_{max}) in the PVAT-intact rings was significantly lower than in PVAT-removed rings in both young and older rats, indicating the persistent anticontractile function of PVAT in both aged rats (Figure 1) (Table 2).

Table 1. Body weights (g) of 10-12-week-old young and 52-week-old adult rats (A), and dry tissue weights (mg/cm) of isolated thoracic aorta rings with and without PVAT in both age groups (B).

A

Wistar Rats	Body Weights (g)	n
10-12-week-old	337.90±11.58	10
52-week-old	620.69±15.96****	13

****$p<0.0001$ Student's *t* test (Mean ± SEM).

B

Thoracic Aorta Rings	Tissue Weights (mg/cm)	n
10-12-week-old (PVAT-)	3.17±0.19	10
10-12-week-old (PVAT+)	15.13±1.07	10
52-week-old (PVAT-)	4.72±0.20	7
52-week-old (PVAT+)	28.6±2.92****	6

****$p<0.0001$ 52-week-old (PVAT+) vs 12-week-old (PVAT+) Student's *t* test (mean ± SEM).
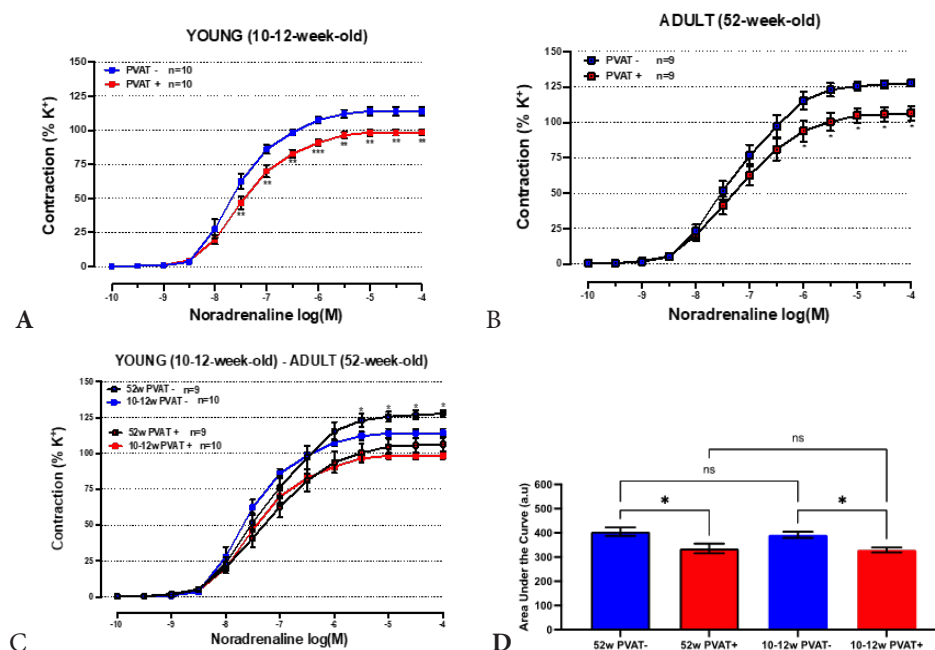
Figure 1. Cumulative contraction responses elicited by noradrenaline (0.1 nM-100 μM) in the presence and absence of perivascular adipose tissue (PVAT) in isolated thoracic aortas of 10-12-week-old young (A and C) and 52-week-old adult rats (B and C), and Area Under the Curves (AUC) of cumulative concentration-response curves of both age groups (D). Values are expressed as a percentage of contraction with 80 mM KCL containing KHS (mean ± SEM) (A and B: *$p<0.05$; PVAT+ group vs. PVAT- group, two-way ANOVA; C: p*<0.05; PVAT- old group vs. PVAT- young group, two-way ANOVA; D: *$p<0.05$; PVAT+ group vs. PVAT- group; one-way ANOVA).

To evaluate smooth muscle reactivity changing with aging, noradrenaline contractions in isolated thoracic aortic rings were compared together in young and adult groups. In the absence of PVAT, noradrenaline efficacy slightly but significantly increased in 52-week-old rats compared to 10-12-week-old rats without a significant difference in the sensitivity of noradrenaline contractions (Figure 1 and Table 2).

Interestingly, if PVAT was left intact, both efficacy and sensitivity of noradrenaline contractions were similar in the young and older rats (Figure 1C) (Table 2). Contractions obtained with 80 mM KCL did not change in two age groups regardless of the presence of PVAT (Figure 2). These data indicate that increased noradrenaline contractions are suppressed by the presence of reactive PVAT in adult rats.

Table 2. Efficacy (E_{max}) and pD_2 of noradrenaline and acetylcholine in isolated aortic rings with PVAT (PVAT+) or without PVAT (PVAT-) of 10-12-week-old young and 52-week-old adult rats.

		Young Rat Aorta			Adult Rat Aorta		
		PVAT- (n=10)	PVAT+ (n=10)	*P* value	PVAT- (n=9)	PVAT+ (n=9)	*P* value
NA	E_{max} (%)	114.12±3.13%	98.52±2.21%**	**$p<0.01$	127.78±2.55%#	106.44±5.11%*	*,#$p<0.05$
	pD_2	7.55±0.10	7.42±0.11	ns	7.21±0.15	7.16±0.12	ns
		PVAT- (n=6)	PVAT+ (n=5)	*P* value	PVAT- (n=7)	PVAT+ (n=6)	*P* value
ACh	E_{max} (%)	92.43±1.46%	85.30±2.33%	ns	68.03±4.95%	53.26±4.50%	ns
	pD_2	7.09±0.11	6.94±0.12	ns	7.49±0.09	7.18±0.14*	*$p<0.05$
L-NAME- **(n=5)**		Young Rat Aorta PVAT-			Young Rat Aorta PVAT+		
		L-NAME+ (n=5)	*P* value	L-NAME- (n=5)	L-NAME+ (n=5)	*P* value	
NA	E_{max} (%)	123.33±4.64%	136.63±8.2%**	$p<0.01$	108.49±5.29%	113.45±7.56%*	$p<0.05$
	pD_2	7.56±0.06	8.12±0.13**	$p<0.01$	7.52±0.14	8.06±0.18*	$p<0.05$
		Adult Rat Aorta PVAT-			Adult Rat Aorta PVAT+		
Noradrenaline **(0.1 nM-100 μM)**		L-NAME- (n=5)	L-NAME+ (n=5)	*P* value	L-NAME- (n=5)	L-NAME+ (n=5)	*P* value
E_{max} (%)		129.18±2.71%	160.19±5.34%***	***$p<0.001$	114.85±3.34%	140.78±4.76% **	**$p<0.01$
pD_2		7.25±0.10	7.74±0.08**	**$p<0.01$	7.09±0.15	7.74±0.11**	**$p<0.01$

NA: noradrenaline, ACh: acetylcholine, PVAT: perivascular adipose tissue, E*max*: maximum response, pD2: negative logarithm of half-maximum response.

**$p<0.01$ PVAT+ vs PVAT- in young rat aorta; * $p<0.05$ PVAT+ vs PVAT- in adult rat aorta; #$p<0.05$ adult rat aorta vs young rat aorta (PVAT-) *(Student's t test)*.
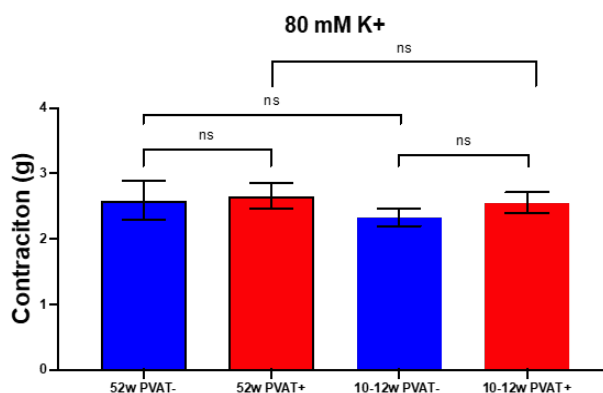
80 mM K+

Figure 2. Contractile responses to KHS containing 80 mM KCL in the presence and absence of perivascular adipose tissue (PVAT) in isolated thoracic aortas of 10-12-week-old young and 52-week-old adult rats (mean ± SEM) (one-way ANOVA).

Noradrenaline contractions in isolated thoracic aortas of the young and older rats were repeated after incubation with L-NAME (100 μM), the NO synthase inhibitor. Contractile responses to noradrenaline in the aortas of young rats were significantly potentiated with L-NAME in both PVAT-intact and PVAT-removed groups (Figure 3). When AUC values were examined, the increase rate of noradrenaline contractions with L-NAME was significantly greater in arteries without PVAT than those with PVAT (Figure 3 and Table 2). When the endothelium was damaged in isolated aortic rings with intact PVAT of young rats, the presence of L-NAME (100 μM) did not potentiate noradrenaline contractions (Figure 3).

A

B

C
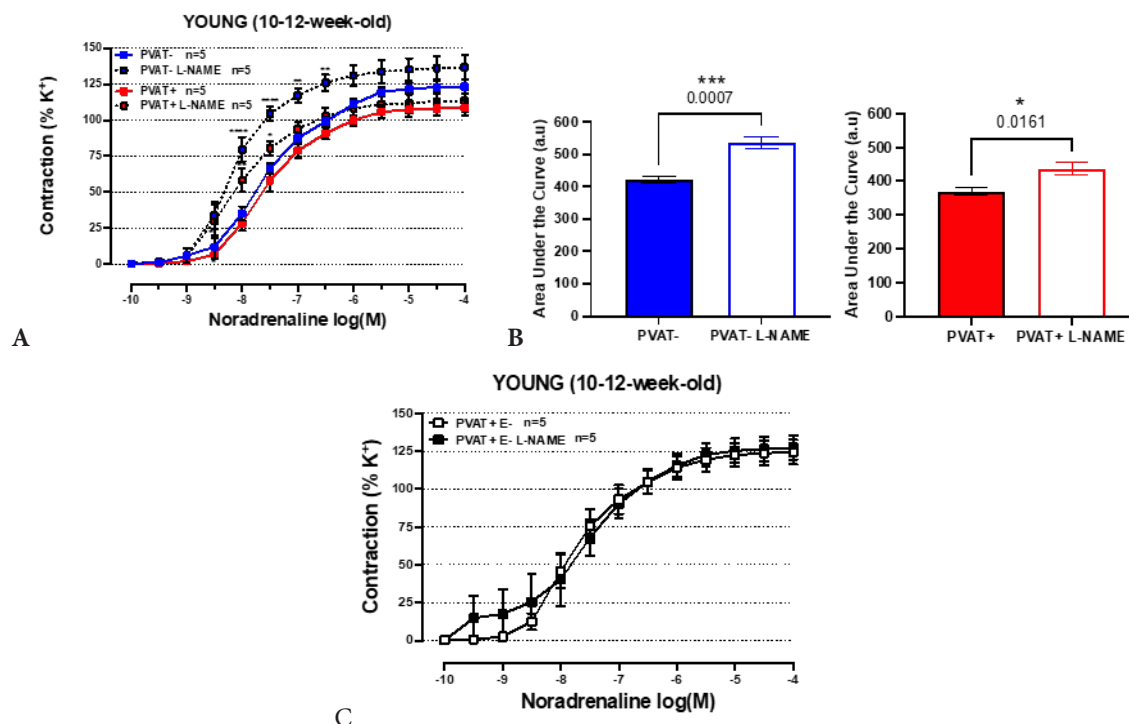
Figure 3. Cumulative contraction-response curves obtained with noradrenaline (0.1 nM-100 μM) and area under the curve (AUC) values in the presence and absence of L-NAME (100 μM) in isolated aortic rings of 10-12-week-old young rats with or without PVAT (A and B), or in endothelium-removed rings with PVAT (C). Values are expressed as a percentage of contraction of 80 mM KCL, and AUC's are expressed as arbitrary units (a.u.) (mean ± SEM) (A: *$p<0.05$, **$p<0.01$, ***$p<0.001$; ****$p<0.0001$ L-NAME+ vs. L-NAME-, two-way ANOVA) (B: *$p<0.05$, ***$p<0.001$ L-NAME+ vs. L-NAME-, Student's *t* test).

Noradrenaline contractions in the absence and presence of L-NAME were also evaluated in the 52-week-old adult rats. Noradrenaline contractions in both PVAT- and PVAT+ rings were also significantly but similarly potentiated with L-NAME as in young rats (Figure 4). Interestingly, when AUC values were examined, the potentiation obtained with L-NAME was the same in the tissues with and without PVAT (Figure 4 and Table 2).

A

B
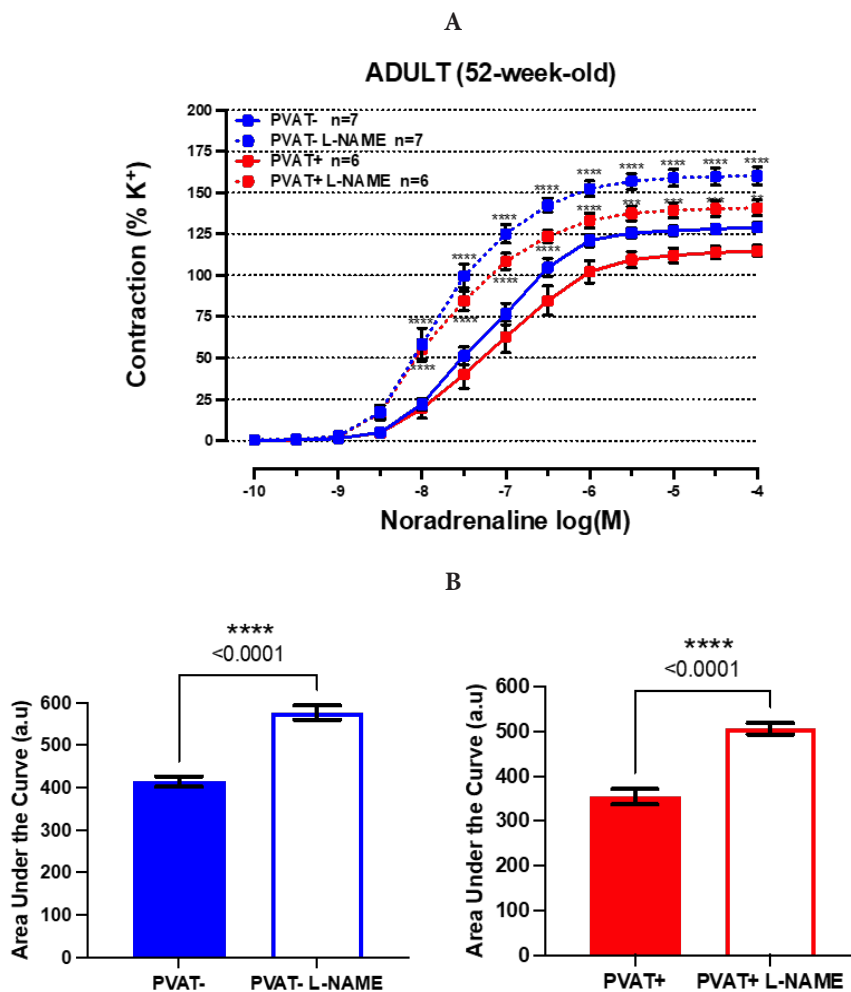
Figure 4. Cumulative contraction-response curves obtained with noradrenaline (0.1 nM-100 μM) (A) and area under the curve (AUC) values (B) in the presence and absence of L-NAME (100 μM) in isolated aortic rings of 52-week-old adult rats with or without PVAT. Values are expressed as a percentage of contraction of 80 mM KCL, and AUCs are expressed as arbitrary units (a.u.) (mean ± SEM) (A: **$p<0.01$, ***$p<0.001$, ****$p<0.0001$ L-NAME+ vs. L-NAME-, two-way ANOVA) (B: ****$p<0.0001$ L-NAME+ vs. L-NAME-, Student's *t* test).

Endothelium-dependent vasorelaxation was also examined in young and adult rats. Concentration-dependent relaxation responses were obtained with the muscarinic agonist acetylcholine (1 nM-10 μM) after precontraction with phenylephrine (0.3 μM or 1 μM) in isolated thoracic aorta rings. Endothelium-dependent relaxations in PVAT-removed arteries of the adult group were significantly decreased compared to the young group (Table 2). While the endothelium-dependent relaxations were preserved in the presence of PVAT in the young group, these relaxations further decreased in the older rats (Figure 5).
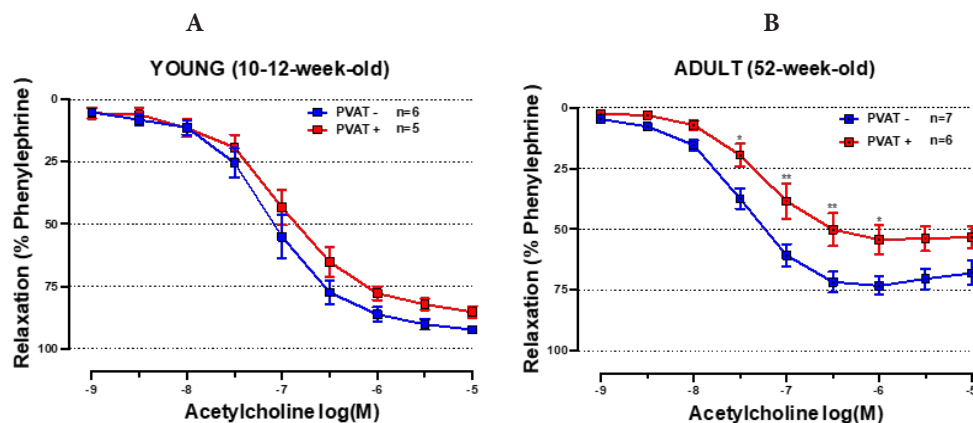
Figure 5. Cumulative relaxation-response curves obtained with acetylcholine (1 nM-10 μM) in PVAT- and PVAT+ isolated thoracic aortas of 10-12-week-old young (A) and 52-week-old adult rats (B). Values are expressed as % of phenylephrine precontraction (mean ± SEM) (*p<0.05, **p<0.01, 52 week PVAT+ vs 52 week PVAT-, two-way ANOVA).

Aging is considered an independent risk factor for cardiovascular and metabolic disorders. The regulatory function of PVAT on the vasculature may be affected by the aging process, contributing to the development of vascular dysfunction. In this study, we examined age-related changes in the anticontractile response of PVAT in thoracic aorta rings isolated from young and adult Wistar Albino rats.

The anticontractile activity of PVAT has been experimentally demonstrated in isolated thoracic aorta rings of rats (Soltis & Cassis, 1991). In this study, we show that vasoconstriction elicited by noradrenaline in isolated thoracic aortas of both 10-12-week-old young and 52-week-old adult rats is reduced in the presence of PVAT. Our data suggest that PVAT is functional in adult rats and that its tonic anticontractile effect contributes to the regulation of vascular tone in this age group.

Fifty-two-week-old adult rats were included in the study to evaluate how PVAT functionality changes with aging. The significant increase in noradrenaline contractions in isolated thoracic aortas of adult rats compared to the young group in the absence of PVAT was a suggested finding consistent with the literature. In general, as arteries age, inflammation and oxidative stress in the adventitia increase, leading to vascular wall remodeling and vasoconstriction (Queiroz &

Sena, 2020). However, noradrenaline contractions in isolated aortas of adult rats with intact PVAT were significantly suppressed and they reached a similar level to those in young rat aortas with intact PVAT, suggesting that the age-related increase in noradrenaline sensitivity can be compensated by PVAT.

In humans, PVAT abundance has been associated with decreased insulin sensitivity and decreased vascular reactivity regulation (Rittig et al., 2008). We detected that dry tissue weight with PVAT and body weights increased in the adult rats in comparison to the young group. However, the phenotypic characteristics of PVAT are also an essential factor in determining the modulation process of PVAT on the vascular structure. Thoracic aorta of rats has a brown adipose tissue phenotype whereas abdominal aorta has mostly a white adipose tissue-like phenotype (Kim, Shi, Winkler, Lee, & Weintraub, 2020; Li, Ma, & Zhu, 2021). While endothelial dysfunction can be observed with age in the isolated thoracic aorta of rats (13-month-old), it has been reported that regional changes in the PVAT phenotype (whitening) occur mainly in the abdominal aorta and more dominantly than in the thoracic aorta (Padilla, Jenkins, Vieira-Potter, & Laughlin, 2013). In other words, although endothelium-dependent vasodilation decreases in

adult rats, PVAT in the thoracic region may continue to exhibit anticontractile function with a brown adipose tissue phenotype. However, we also obtained experimental evidence that the cross-signaling interaction between PVAT and endothelium may be impaired in the advanced age group.

Endothelium and PVAT are considered vital paracrine tissues that regulate the contractile state of smooth muscle through the production of diffusible mediators. Some studies have reported that endothelium-derived NO contributes to the anticontractile response of PVAT in rat isolated thoracic aorta. In contrast, some others have suggested that it is independent from the endothelium. Indeed, agents such as adiponectin and angiotensin 1–7 released from PVAT can relax vascular smooth muscle by direct action, while they can also stimulate NO production when they diffuse to the endothelium (Chen, Montagnani, Funahashi, Shimomura, & Quon, 2003; Sampaio et al., 2007). In our study, the anticontractile response of PVAT was preserved in endothelium-stripped thoracic aortas isolated from young rats, which suggests that the anticontractile response of PVAT is independent of the endothelium. Since PVAT in the thoracic aorta is known to continuously express endothelial and neuronal NO synthase, different physiological stimuli may cause NO release from PVAT and NO-related vasorelaxation even in the absence of endothelial contribution. In the rat mesenteric arteries, it has been suggested that β3-adrenoceptors in perivascular fat cells are stimulated by noradrenaline and that NO derived from fat cells mediates the anticontractile response of PVAT in these arteries (Bussey et al., 2018). However, in our study, noradrenaline contractions obtained in endothelium-removed aortic tissues with intact PVAT were not changed after incubation with L-NAME, indicating that fat cell-derived relaxing factor is not a NO or NO-related substance in rat thoracic aorta. The differential sensitivity of anticontractile responses of PVAT to NO synthase inhibition in different vascular beds suggests that endothelial NO synthase expression in

perivascular fat cells varies according to the vascular tissue or anatomical region examined (Victorio, Fontes, Rossoni, & Davel, 2016; Barp, Bonaventura, & Assreuy, 2021). In this study, we did not aim to elucidate the molecular nature of the factor released from PVAT, but evidence in the literature suggests that PVAT-derived hydrogen peroxide (H_2O_2) may be one of the candidate molecules that causes endothelium-independent relaxation in rat isolated thoracic aorta (Gao, Lu, Su, Sharma, & Lee, 2007). Noradrenaline contractions in the aortic rings (with endothelium) of young rats were increased in the presence of L-NAME. The increase in contractions could be explained by inhibition of basal NO release from the endothelium. Interestingly the inhibitory effect of L-NAME was significantly less in the tissues with PVAT than in those without PVAT. This may be due to PVAT acting synergistically with the endothelium to limit vascular contraction, and the presence of PVAT limits NO release from the endothelium. Another possibility is that the anticontractile response of PVAT is potentiated to compensate for the increased noradrenaline contractions and endothelial NO inhibition by L-NAME.

Similar to young rats, noradrenaline contractions in isolated aortic rings with the endothelium of 52-week-old adult rats were sensitive to the inhibitory effect of L-NAME. However, when the AUC levels were evaluated, unlike the young group, the potentiation detected in noradrenaline contractions in the presence of L-NAME was independent of PVAT. This finding indicates that the anticontractile response of PVAT in adult rats could not compensate for the inhibitory effect of L-NAME on endothelial NO release as in the young group. However, the decrease in endothelium-dependent relaxations obtained with acetylcholine in the adult group compared to the young group means that endothelial NO release or bioavailability also decreases with age. Therefore, it can be speculated that adipocyte-derived NO release is also triggered due to the production of various adipokines in PVAT during noradrenaline contractions in adult rats. Although

this view can speculatively explain the increased sensitivity of noradrenaline contractions to L-NAME in the presence of PVAT in the adult group, the effect of L-NAME should also be examined in endothelium-removed tissues in adult rats to support this point of view.

When the literature is reviewed, endothelium-mediated acetylcholine relaxations in isolated rat aortas are either unchanged or reduced in the presence of PVAT (Soltis & Cassis, 1991; Lee, Chen, Tsao, & Wu, 2014). In our study, the relaxations obtained with acetylcholine in the young group were unaffected by the presence of PVAT. However, in adult rats, it was found that endothelium-dependent vasodilation in arteries devoid of PVAT was partially reduced compared to the young group, and interestingly, this was further reduced when PVAT was left intact in adult rats. The findings obtained in the young and adult groups indicate that PVAT does not make an additional contribution to endothelium-dependent relaxations. In addition, the bidirectional signaling interaction between the endothelium and PVAT may have changed in old age. Adipokines including adiponectin and leptin stimulate the activation of endothelial NO synthase and then contribute to vasodilation through the enhanced NO production in endothelial cells. It has been previously shown that perivascular-derived adiponectin partly compensates for age-related decline in NO-mediated vasodilation in rat isolated thoracic aorta (Juttner et al., 2024). However, PVAT also produces PVAT-derived contracting factors, including superoxide anion, prostaglandins, angiotensin II, and resistin, which contribute to counteract the effects of perivascular-derived relaxing factors, primarily reducing NO bioavailability and thus inducing endothelial dysfunction (Cheng, Bakar, Gollasch, & Huang, 2018). Although we did not aim to examine cellular pathways of PVAT-derived molecules affecting endothelial function, any of these contractile agents could be responsible for decreased endothelium-dependent vasorelaxations in adult rats in the presence of PVAT.

The biological age of 52-week-old rats corresponds to the average age range of a human adult (30-35 years) (Sengupta, 2013). Therefore, structural and phenotypic changes associated with cardiovascular aging in 52-week-old rats (such as inflammation, oxidative stress, smooth muscle cell proliferation, loss of elasticity and endothelial dysfunction) may not be fully reflected in vascular function. However, age-related endothelial dysfunction has been previously reported in 52-week-old mice or 59-week-old Sprague-Dawley rats (Nakladal et al., 2022). Although the findings obtained in this study are valuable regarding the regulatory role of PVAT on vascular tone in adult rats, repeating similar experiments in 18-24-month-old rats to make inferences about aging and changes in PVAT function is among our future research goals.

CONCLUSION

These data suggest that the anticontractile function of PVAT persists in adult rats and limits vascular contractions through its tonic inhibitory effect. However, PVAT does not protect endothelium-dependent relaxations that decrease with aging.

AUTHOR CONTRIBUTION STATEMENT

Data collection (GO), Data presentation (GO), supervision (MHO), writing manuscript (MHO).

CONFLICT OF INTEREST

The authors declare that they have no conflict of interest.

REFERENCES

Barp, C. G., Bonaventura, D., & Assreuy, J. (2021). NO, ROS, RAS, and PVAT: More Than a Soup of Letters. *Frontiers in Physiology, 12*, 640021. doi:10.3389/fphys.2021.640021

Bussey, C. E., Withers, S. B., Saxton, S. N., Bodagh, N., Aldous, R. G., & Heagerty, A. M. (2018). beta(3) -Adrenoceptor stimulation of perivascular adipocytes leads to increased fat cell-derived NO and vascular relaxation in small arteries. *British Journal of Pharmacology, 175*(18), 3685-3698. doi:10.1111/bph.14433

Cacanyiova, S., Golas, S., Zemancikova, A., Majzunova, M., Cebova, M., Malinska, H., . . . Berenyiova, A. (2021). The Vasoactive Role of Perivascular Adipose Tissue and the Sulfide Signaling Pathway in a Nonobese Model of Metabolic Syndrome. *Biomolecules, 11*(1). doi:10.3390/biom11010108

Cheng, C. K., Bakar, H. A., Gollasch, M., & Huang, Y. (2018). Perivascular Adipose Tissue: the Sixth Man of the Cardiovascular System. *Cardiovascular Drugs and Therapy, 32*(5), 481-502. doi:10.1007/s10557-018-6820-z

Cheng, K. K., Lam, K. S., Wang, Y., Huang, Y., Carling, D., Wu, D., . . . Xu, A. (2007). Adiponectin-induced endothelial nitric oxide synthase activation and nitric oxide production are mediated by APPL1 in endothelial cells. *Diabetes, 56*(5), 1387-1394. doi:10.2337/db06-1580

Chang, L., Garcia-Barrio, M. T., & Chen, Y. E. (2020). Perivascular Adipose Tissue Regulates Vascular Function by Targeting Vascular Smooth Muscle Cells. *Arteriosclerosis, Thrombosis and Vascular Biology, 40*(5), 1094-1109. doi:10.1161/ATVBAHA.120.312464

Chen, H., Montagnani, M., Funahashi, T., Shimomura, I., & Quon, M. J. (2003). Adiponectin stimulates production of nitric oxide in vascular endothelial cells. *Journal of Biological Chemistry, 278*(45), 45021-45026. doi:10.1074/jbc.M307878200

Gao, Y. J., Lu, C., Su, L. Y., Sharma, A. M., & Lee, R. M. (2007). Modulation of vascular function by perivascular adipose tissue: the role of endothelium and hydrogen peroxide. *British Journal of Pharmacology, 151*(3), 323-331. doi:10.1038/sj.bjp.0707228

Gao, Y. J., Zeng, Z. H., Teoh, K., Sharma, A. M., Abouzahr, L., Cybulsky, I., . . . Lee, R. M. (2005). Perivascular adipose tissue modulates vascular function in the human internal thoracic artery. *The Journal of Thoracic and Cardiovascular Surgery, 130*(4), 1130-1136. doi:10.1016/j.jtcvs.2005.05.028

Gil-Ortega, M., Somoza, B., Huang, Y., Gollasch, M., & Fernandez-Alfonso, M. S. (2015). Regional differences in perivascular adipose tissue impacting vascular homeostasis. *Trends in Endocrinology* & *Metabolism, 26*(7), 367-375. doi:10.1016/j.tem.2015.04.003

Hu, H., Garcia-Barrio, M., Jiang, Z. S., Chen, Y. E., & Chang, L. (2021). Roles of Perivascular Adipose Tissue in Hypertension and Atherosclerosis. *Antioxidants* & *Redox Signaling, 34*(9), 736-749. doi:10.1089/ars.2020.8103

Juttner, A. A., Ataei Ataabadi, E., Golshiri, K., de Vries, R., Garrelds, I. M., Danser, A. H. J., . . . Roks, A. J. M. (2024). Adiponectin secretion by perivascular adipose tissue supports impaired vasodilation in a mouse model of accelerated vascular smooth muscle cell and adipose tissue aging. *Vascular Pharmacology, 154*, 107281. doi:10.1016/j.vph.2024.107281

Kim, H. W., Shi, H., Winkler, M. A., Lee, R., & Weintraub, N. L. (2020). Perivascular Adipose Tissue and Vascular Perturbation/Atherosclerosis. *Arteriosclerosis, Thrombosis and Vascular Biology, 40*(11), 2569-2576. doi:10.1161/ATVBAHA.120.312470

Lee, M. H., Chen, S. J., Tsao, C. M., & Wu, C. C. (2014). Perivascular adipose tissue inhibits endothelial function of rat aortas via caveolin-1. *PLoS One, 9*(6), e99947. doi:10.1371/journal.pone.0099947

Li, X., Ma, Z., & Zhu, Y. Z. (2021). Regional Heterogeneity of Perivascular Adipose Tissue: Morphology, Origin, and Secretome. *Frontiers in Pharmacology, 12*, 697720. doi:10.3389/fphar.2021.697720

Margaritis, M., Antonopoulos, A. S., Digby, J., Lee, R., Reilly, S., Coutinho, P., . . . Antoniades, C. (2013). Interactions between vascular wall and perivascular adipose tissue reveal novel roles for adiponectin in the regulation of endothelial nitric oxide synthase function in human vessels. *Circulation, 127*(22), 2209-2221. doi:10.1161/CIRCULATIONAHA.112.001133

Nakladal, D., Sijbesma, J. W. A., Visser, L. M., Tietge, U. J. F., Slart, R., Deelman, L. E., . . . Buikema, H. (2022). Perivascular adipose tissue-derived nitric oxide compensates endothelial dysfunction in aged pre-atherosclerotic apolipoprotein E-deficient rats. *Vascular Pharmacology, 142*, 106945. doi:10.1016/j.vph.2021.106945

Padilla, J., Jenkins, N. T., Vieira-Potter, V. J., & Laughlin, M. H. (2013). Divergent phenotype of rat thoracic and abdominal perivascular adipose tissues. *American Journal of Physiology-Regulatory, Integrative and Comparative Physiology, 304*(7), R543-552. doi:10.1152/ajpregu.00567.2012

Queiroz, M., & Sena, C. M. (2020). Perivascular adipose tissue in age-related vascular disease. *Aging Research Reviews, 59*, 101040. doi:10.1016/j.arr.2020.101040

Rajsheker, S., Manka, D., Blomkalns, A. L., Chatterjee, T. K., Stoll, L. L., & Weintraub, N. L. (2010). Crosstalk between perivascular adipose tissue and blood vessels. *Current Opinion in Pharmacology, 10*(2), 191-196. doi:10.1016/j.coph.2009.11.005

Rittig, K., Staib, K., Machann, J., Bottcher, M., Peter, A., Schick, F., . . . Balletshofer, B. (2008). Perivascular fatty tissue at the brachial artery is linked to insulin resistance but not to local endothelial dysfunction. *Diabetologia, 51*(11), 2093-2099. doi:10.1007/s00125-008-1128-3

Sampaio, W. O., Souza dos Santos, R. A., Faria-Silva, R., da Mata Machado, L. T., Schiffrin, E. L., & Touyz, R. M. (2007). Angiotensin-(1-7) through receptor Mas mediates endothelial nitric oxide synthase activation via Akt-dependent pathways. *Hypertension, 49*(1), 185-192. doi:10.1161/01.HYP.0000251865.35728.2f

Sengupta, P. (2013). The Laboratory Rat: Relating Its Age With Human's. *International Journal of Preventive Medicine, 4*(6), 624-630. Retrieved from https://www.ncbi.nlm.nih.gov/pubmed/23930179

Siegel-Axel, D. I., & Haring, H. U. (2016). Perivascular adipose tissue: An unique fat compartment relevant for the cardiometabolic syndrome. *Reviews in Endocrine and Metabolic Disorders, 17*(1), 51-60. doi:10.1007/s11154-016-9346-3

Soltis, E. E., & Cassis, L. A. (1991). Influence of perivascular adipose tissue on rat aortic smooth muscle responsiveness. *Clinical and Experimental Hypertension, 13*(2), 277-296. doi:10.3109/10641969109042063

Victorio, J. A., Fontes, M. T., Rossoni, L. V., & Davel, A. P. (2016). Different Anti-Contractile Function and Nitric Oxide Production of Thoracic and Abdominal Perivascular Adipose Tissues. *Frontiers in Physiology, 7*, 295. doi:10.3389/fphys.2016.00295

Wang, Y., Wang, X., Chen, Y., Zhang, Y., Zhen, X., Tao, S., . . . Jiang, G. (2024). Perivascular fat tissue and vascular aging: A sword and a shield. *Pharmacological Research, 203*, 107140. doi:10.1016/j.phrs.2024.107140

Evaluation of Antioxidant, Cytotoxic Effects and Phytochemical Profiles of Galls Caused by Eriophyidae mite in *Juglans regia* Leaves

Semih BULUT**°, Burçin ÖZÜPEK***, Sultan PEKACAR****, Aysun ÖZDEMİR****,
Didem DELİORMAN ORHAN*****

Evaluation of Antioxidant, Cytotoxic Effects and Phytochemical Profiles of Galls Caused by Eriophyidae mite in Juglans regia Leaves

SUMMARY

This research presents the first study findings on the phytochemical contents and anticancer and antioxidant activities of galls caused by Eriophyidae mites on the leaves of Juglans regia L. Gall extracts collected from different localities in Turkey and prepared with solvents of different polarity were investigated for both antioxidant and cytotoxic activity. Cytotoxic activity studies showed that MCF-7 cancer cells were more sensitive to WLAA extract at a concentration of 100 μg/mL compared to healthy HUVEC cell lines. LC-QTOF-MS analysis results showed that all extracts contain chlorogenic acid, quercetin 4'-O-glucoside/quercetin 3-O-galactoside, quercetin 7-xyloside/quercetin 3-O-arabinoside, quercetin 7-O-rhamnoside, kaempferol 3-O-xyloside/kaempferol 3-O-arabinoside, and kaempferol derivatives. It was concluded that polyphenolic extracts obtained from galls formed in J. regia leaves can be considered as a new potential natural source for drug development studies due to their antioxidant and cytotoxic effects.

Key Words: *Antioxidant, cytotoxicity, galls, Juglans regia, phytochemical profile*

Juglans regia Yapraklarında Eriophyidae Akarının Neden Olduğu Gallerin Antioksidan, Sitotoksik Etkileri ve Fitokimyasal Profillerinin Değerlendirilmesi

ÖZ

Bu araştırma Juglans regia L. yapraklarında Eriophyidae akarlarının neden olduğu gallerin fitokimyasal içerikleri ile antikanser ve antioksidan aktivitelerine ilişkin ilk çalışma bulgularını sunmaktadır. Türkiye'nin farklı bölgelerinden toplanan ve farklı polaritedeki çözücüler ile hazırlanan gal ekstrelerinin hem antioksidan hem de sitotoksik aktiviteleri araştırılmıştır. Sitotoksik aktivite çalışmaları, MCF-7 kanser hücrelerinin, sağlıklı HUVEC hücre hatlarına kıyasla 100 μg/mL konsantrasyondaki WLAA ekstresine daha duyarlı olduğunu göstermiştir. LC-QTOF-MS analiz sonuçları tüm ekstrelerin klorojenik asit, kersetin 4'-O-glukozit/kersetin 3-O-galaktozit, kersetin 7-ksilozit/kersetin 3-O-arabinozit, kersetin 7-O-ramnozit, kemferol 3-O-ksilozit/kemferol 3-O-arabinozit ve kemferol türevleri içerdiğini göstermiştir. J. regia yapraklarında oluşan gallerden elde edilen polifenolik ekstrelerin, antioksidan ve sitotoksik etkileri nedeniyle ilaç geliştirme çalışmaları için yeni bir potansiyel doğal kaynak olarak değerlendirilebileceği sonucuna varılmıştır.

Anahtar Kelimeler: *Antioksidan, sitotoksisite, galler, Juglans regia, fitokimyasal profil*

---

* ORCID: 0000-0002-4098-0221, Department of Pharmacognosy, Faculty of Pharmacy, Suleyman Demirel University, Isparta, Turkiye
** ORCID: 0000-0003-2159-9860, Department of Pharmacognosy, Faculty of Pharmacy, Gazi University, Ankara, Turkiye
*** ORCID: 0000-0002-7782-9832, Department of Pharmacognosy, Faculty of Pharmacy, Gazi University, Ankara, Turkiye
**** ORCID: 0000-0003-0311-0507, Department of Pharmacology, Faculty of Pharmacy, Gazi University, Ankara, Turkiye
***** ORCID: 0000-0003-3916-4048, Department of Pharmacognosy, Faculty of Pharmacy, Gazi University, Ankara, Turkiye

° Corresponding Author; Semih BULUT
E-mail: semihbulut@sdu.edu.tr

INTRODUCTION

Cancer is a disease that occurs when normal cells in the body transform into tumor cells in a multi-stage process and multiply uncontrollably. In the next stage, these cells, which multiply uncontrollably, can spread to the surrounding and distant organs. Authorities reported that 9.6 million people died from cancer worldwide in 2018. Lung, breast, stomach, prostate, colorectal, liver, and cervical cancers are common today (WHO, 2024). The majority (90-95%) of all cancer cases are related to environmental factors, while a small amount (5-10%) is related to genetic causes (Anand et al., 2008). Approximately 33.3% of cancer deaths are due to behavioral and nutritional risk factors. These risk factors include obesity, insufficient physical activity, and tobacco use (Republic of Türkiye Ministry of Health, 2024).

Antioxidants interact with free radicals by eliminating free radicals in the body and reduce oxidative stress. In addition, they prevent cancer development by stopping uncontrolled cell division. Therefore, endogenous and exogenous antioxidants are important in cancer prevention. Medicinal plants and foods are among the sources of exogenous antioxidants (Alzeer et al., 2017). Numerous studies have shown that natural polyphenols (apigenin, luteolin, quercetin, kaempferol, resveratrol, etc.) can be used for the prevention and treatment of cancer through their antioxidant and anti-inflammatory effects (Zhou et al., 2016). The main methods used in cancer treatment today are radiotherapy, surgery, and chemotherapy. Chemotherapy has unpleasant side effects such as vomiting, nausea, diarrhea, hair loss, loss of appetite, fever, constipation, pain, fatigue, mouth sores, the formation of bruises on the skin, and bleeding. Medicinal plants, traditional folk medicines, and natural compounds are being evaluated for new opportunities in cancer prophylaxis and treatment (Greenwell & Rahman 2015; Altun & Sonkaya 2018).

Juglans regia L., a species belonging to the Juglandaceae family, is known as walnut in Anatolia.

It is a tree that naturally spreads throughout the world from the Balkans to the Himalayas and Southwest China. Its fruits are a strong source of nutrients owing to their high amount of fixed fat, as well as protein, carbohydrate, and mineral content. On the other hand, leaves of the plant contain carbohydrates, fatty acids, naphthalene derivatives (juglone), tannin, phenolic compounds, and ascorbic acid (Delaviz et al., 2017). It has been determined by researchers that *J. regia* leaf extracts show strong cytotoxic activities in colon, lung, breast adenocarcinoma, prostate, and human oral cancer cells (Salimi et al., 2012; Delaviz et al., 2017; Ara et al., 2023).

Pests that infest trees such as walnuts, pears, pistachios, almonds, and figs can have negative effects on the fruit shape, fruit productivity, and leaves of these species. Agricultural control methods are applied against this type of pest. The Eriophyidae mites, which infest walnut leaves and fruits, feed by sucking the sap of these parts, and the harmful substances they secrete during this time cause deterioration in the plant tissues and the formation of blisters. These blisters formed on the leaf are light green at first, then gradually become darker, turning from red to brown and finally to black. These blisters are known as galls. This pathological formation causes early shedding of leaves and deformation of fruits. Research should be carried out for the use of these galls in the development of some products with added value (medicine, cosmetics, etc.) (Denizhan & Çobanoğlu 2009; T.C. Gıda Tarım ve Hayvancılık Bakanlığı, 2017). Based on traditional knowledge, the ideas that form the basis for discovering pharmaceutical raw materials have emerged from the principles of sometimes similarities and sometimes contrasts. Semi-parasitic plants such as *Viscum album* L. (European mistletoe) damage the tree by absorbing all the minerals and water of the host tree with their haustorium. In this way, the tree, which dries up day by day, is likened to the spread of cancer in the human body. For this reason, European mistletoe has been included in cancer research for many years. Today,

fermented extracts of European mistletoe are used as an anticancer drug in anthroposophical medicine (Davis, 1982; Tennakoon & Pate 1996; Deliorman et al., 2000; Dela et al., 2015; Delebinski et al., 2015).

With the same approach, the polyphenolic extracts prepared from these pathological structures (gall) formed by Eriophyidae mites from the leaves of walnut trees in two different localities (Sinop and Ankara) in Turkey were investigated for cytotoxic activity in MCF-7 and HUVEC cell lines in this study. In addition to antioxidant activities of these polyphenolic extracts, analyses of polyphenolic substances were carried out by LC-QTOF/MS. The current research is original as it is the first report of phytochemical analysis and activity screening studies on galls caused by Eriophyidae mites on walnut leaves.

MATERIAL AND METHODS

Plant material

Walnut leaves were collected from Boyabat, Sinop, Turkey and Çankaya, Ankara, Turkey in July and August 2019. The plant materials were identified by Gülsen Kendir (Department of Pharmaceutical Botany, Suleyman Demirel University, Isparta, Turkey). Voucher specimens were stored in the GUL Herbarium, Suleyman Demirel University (GUL 111/1/1-2 and GUL 111/1/1-3).

Extraction

The galls on the walnut leaves were carefully removed with a scalpel and dried at 25°C. 50 mL of 80% acetone (WLSA) and 80% ethanol (WLSET) were added to the separately weighed two gall samples (1.32 g and 1.37 g, respectively) collected from Sinop and macerated at room temperature. 50 mL of 80% acetone (WLAA) was added to 0.51 g of gall sample collected from Ankara. Since the sample amount was insuffcient, an 80% ethanol extract could not be prepared. These samples were extracted for 14-18 hours on a shaker at 25°C, and then the extracts were filtered. The same procedures were repeated three times by adding solvents again. All solvents were evaporated using a rotary evaporator.

Chemical composition analysis of plant extracts

Total phenolic content

Folin-Ciocalteu reagent (10% v/v) was first added to the 20 µL extracts and kept at 25°C for 5 minutes. Then sodium carbonate (Na_2CO_3) solution (7.5% w/v) was mixed to the extract-folin mixture. The absorbance of the resulting mixture was measured at a wavelength of 735 nm. Total phenolic content was shown as gallic acid equivalent (GAE) mg/g extract (Zongo et al., 2010). The calibration equation was found as y = 6.1419x and calculated as r^2 = 0.9982.

Analysis of phenolic compounds by LC-QTOF-MS method

LC-QTOF-MS was used for qualitative analysis. Analyses were performed on Agilent 1260 series HPLC system and Agilent 6550 iFunnel High Resolution Mass Spectrometer device connected to this system. Analyses were made in negative mode. MS operating mode is 2 GHz Extended Dynamic Range. Agilent Zorbax Extend C-18 column was used in the analysis. Agilent MassHunter Software B06.00 and Metlin Metabolite database were used for analysis and data evaluation. LC-QTOF-MS analysis parameters of phenolic compounds: Column: Agilent Zorbax Extend C-18 (4.6 mm x 150 mm x 3.5 µm); Column oven: 35°C; Injection volume: 5 µL; Analysis Time: 25 min.; Mobile phase A: water-acetic acid (0.1%); Mobile phase B: Acetonitrile; Flow: 0.65 mL/min; Method; At the beginning of the analysis, the ratio of solvent B was 5% and isocratic flow was applied for one minute. Between 1-4 minutes, the solvent B rate has a 10% gradient flow. Between 4-10 minutes, solvent B 70% gradient flow was reached. Solvent B 90% gradient flow was applied between 10-11 minutes. 90% isocratic flow was applied between 11-16 minutes. Solvent B was decreased gradually to 5% between 16-16.1 minutes. Solvent B reached 55% with gradient flow between 16.1-20 minutes.

Antioxidant activity

In antioxidant activity studies, extracts and reference compounds in all methods were dissolved in methanol.

DPPH radical scavenging activity

The mechanism of 2,2-diphenyl-1-picrylhydrazyl (DPPH) radical scavenging activity method is based on the hydrogen atom and electron donating capacity of the extract to bleach the purple color of DPPH solution (Orhan et al., 2011). DPPH solution (1 mM) was added to the 80 μL extracts. The resulting mixture was left for 30 minutes. The absorbance values of the extracts and ascorbic acid were measured at 520 nm. The standard compound in the experiment was ascorbic acid (Jung et al., 2011).

Metal chelating capacity

The mechanism of action of metal chelating capacity is based on the inhibition of Fe^{2+}-ferrozine complex formation after reaction of the extracts with Fe^{2+} (Gülçin, 2010). The first $FeCl_2$ solution (2 mM) was added to the extracts, then ferrozine solution (5 mM) was added. The experiment was performed with a final volume of 130 μL. After this process, the absorbance of the extracts at 562 nm wavelength was measured with a microplate reader. Ethylene diamine tetra acetic acid (EDTA) was used as the standard compound in the experiment (Dinis et al., 1994).

Ferric-reducing antioxidant power

The mechanism of action of the reducing power of the extracts is based primarily on the reduction of $Fe^{3+}(CN)^6$ to $Fe^{2+}(CN)^6$ and then on the absorbance measurement of the blue-colored complex formed after the addition of excess Fe^{3+} (Gülçin, 2010). All test samples (50 μL) and quercetin (50 μL) were mixed with sodium phosphate buffer (pH = 7.2, 0.1 mol/L). Then, potassium ferricyanide solution (1% w/v) was added to the mixtures and the microplate was placed in an oven at 37°C. Then, trichloroacetic acid solution (10% w/v) was added to the mixture. The experiment was performed with a final volume of 210 μL. Results were measured at a wavelength of 700 nm. $FeCl_3$ (0.1% w/v) was added to the mixture, and the wavelength was measured again (Orhan et al., 2017).

Cytotoxic Activity

Cell culture

Breast cancer cells (MCF-7) and human umbilical vein endothelial cells (HUVEC) were cultured in an incubator in Dulbecco's Modified Eagle's medium (DMEM) containing 10% fetal bovine serum and 100 U/mL penicillin/streptomycin. Incubation conditions are set at 37 °C, with 5% CO_2. The extracts were dissolved in dimethyl sulfoxide (DMSO) and applied to the cells in increasing logarithmic concentrations (18, 30, 56, 100, and 180 μg/mL). Cells were treated with 0.2% DMSO.

Cytotoxic activity

The cytotoxic activity of the extracts was determined against MCF-7 cancer cells and HUVEC cell lines using the MTT assay. 10000 MCF-7 and HUVEC cells were transferred to each well of 96-well plates. The next day, cells were replaced with fresh medium in DMEM without phenol red (200 μL), and then extracts were added. After 72 hours of incubation, media containing 0.5 g/l MTT 50 μL (Life Technologies) was added to each well. Subsequently, formazan crystals were dissolved with DMSO (160 μL). Absorbances were measured at a wavelength of 570 nm. The cell viability (CV) percentage was calculated as follows (Özdemir et al., 2017). CV% = (Absorbance of extract group/absorbance of control group) x 100.

Statistical analysis

In cytotoxic activity studies, all values were evaluated using a one-way analysis of variance (ANOVA), followed by the Tukey post hoc test to analyze multi-group comparisons. The GraphPad Software Instat program was used to calculate the standard errors from the values found in other studies.

RESULTS AND DISCUSSION

The yields of acetone and ethanol extracts prepared from galls in walnut leaves collected from two different localities (Sinop and Ankara) in Turkey are

given in Table 1. Since the amount of gall formed on the walnut tree grown in Ankara is low and acetone is the solvent that can extract polyphenolic compounds from plants, especially tannins, only acetone extract was prepared from this plant sample. The extract yields of all three extracts were found to be quite close to each other. The chemical profile of the tested extracts was analyzed by the Folin-Ciocalteu method and LC-QTOF-MS methods. According to the results of the total phenol content determination using UV spectroscopy, it was determined that the acetone extract (WLSA; 177.31 ± 6.99 GAE mg/g extract) of the sample collected from Sinop had the highest total phenol content (Table 1).

Table 1. Yields and total phenolic contents of extracts

Extracts	Yield%	Total phenol content (GAE) mg/g extract ± SD[d]
WLSA[a]	14.67	177.31 ± 6.99
WLAA[b]	14.82	109.47 ± 1.24
WLSET[c]	15.29	157.12 ± 13.14

[a]WLSA: walnut leaves acetone Sinop, [b]WLAA: walnut leaves acetone Ankara,

[c]WLSET: walnut leaves ethyl alcohol Sinop, [d]SD: Standard deviation

The extracts were analyzed by LC-QTOF-MS in the negative mode. Total ion chromatograms of the extracts are given in Figure 1.
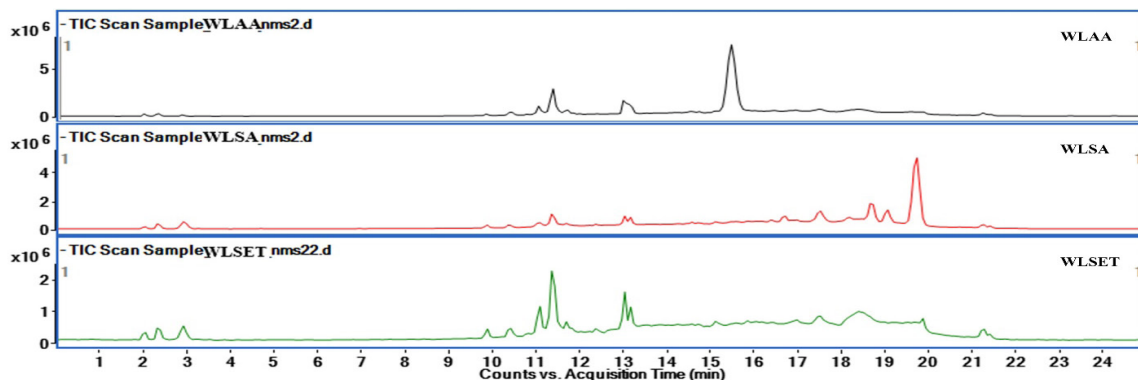
Figure 1. Total ion chromatograms of the extracts

Compounds with molecular weights of the chlorogenic acid 354.09508; - Quercetin 4'-O-glucoside / Quercetin 3-O-galactoside 464.09548; - Quercetin 7-xyloside / quercetin 3-O-arabinoside 434.08491; - Quercetin 7-O-rhamnoside 448.10056; - Kaempferol 3-O-xyloside / Kaempferol 3-O-arabinoside 418.09000; - Kaempferol derivative 578.14243 and - Kaempferol derivative 578.14243 of phenolic compounds with retention times of 9.85, 11.06, 11.33, 11.46, 11.73, 13.05 and 13.20 minutes in the chromatogram of the three extracts (Table 2, Figure 2).
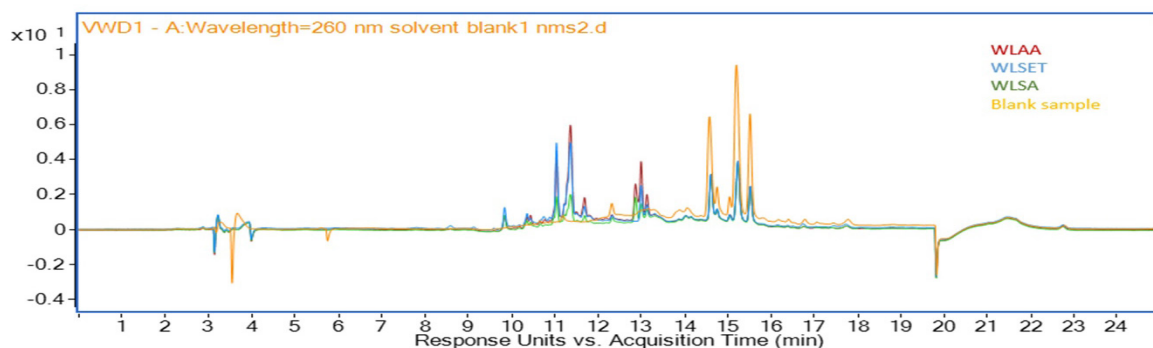
Figure 2. RP-HPLC chromatogram connected to LC-QTOF (260 nm) of the extracts and solvent. (Solvent and sample signals overlapped)

In addition, when the fragment ions of the compounds thought to have this molecular weight and the fragment ions belonging to the peaks thought to belong to these compounds in the extracts were compared, it was predicted that these compounds could be chlorogenic acid, quercetin 4'-*O*-glucoside/quercetin 3-*O*-galactoside, quercetin 7-xyloside/quercetin 3-*O*-arabinoside, quercetin 7-*O*-rhamnoside, kaempferol 3-*O*-xyloside/kaempferol 3-*O*-arabinoside, and kaempferol derivatives, respectively.

Interestingly, in the DPPH free radical scavenging activity method, it was observed that the effect was stronger in all extracts with decreasing doses. Similarly, in a different study, *J. regia* dichloramethane leaf extract showed stronger DPPH radical scavenging activity at 0.5 mg/mL concentration compared to 1 mg/mL (Erdogan Orhan et al., 2011). In another study, DPPH radical scavenging activity increased as the concentration of leaf essential oil of *J. regia* increased, but **β**-pinene, the major constituent of the essential oil, showed higher activity at 80 μg/mL concentration than at 100 μg/mL concentration (Rather et al., 2012). In this respect, there are differences in the literature, and our research results are similar to those of Erdoğan Orhan et al. WLSA, WLAA and WLSET extracts at 0.5 mg/mL concentration (85.90 ± 0.62, 86.95 ± 0.77 and 87.76 ± 0.21%, respectively) showed as potent radical scavenging effects as the reference compound ascorbic acid (91.80 ± 0.31%). The ferric reducing power was 2.517 ± 0.090, 1.925 ± 0.010 and 1.969 ± 0.070 in the extracts respectively, at a concentration of 2 mg/mL, with an absorbance value of 1.874 ± 0.030

for the reference compound quercetin. In the ferric reducing power test, on the contrary to the extracts, a decrease was observed in the absorbance values of the reference compound quercetin, on the contrary to the increase in the dose. It was determined that only WLAA extract had a very high metal chelating capacity (74.17 ± 11.06%) at 2 mg/mL concentration. On the other hand, the metal binding capacity of EDTA used as a reference at 2 mg/mL was found to be 100 ±0.00% (Table 3).

MCF-7 and HUVEC cell lines were used to test the cytotoxic activities of the extracts. The extracts were incubated with the cells for 72 hours. As a result of subsequent colorimetric assays, none of the WLSET and WLSA extracts changed the viability of MCF-7 cancer cells, while WLAA extracts reduced cell viability at concentrations of 100 and 180 μg/mL compared to the control group. WLAA extract reduced cell viability to 83.66 ± 3.84% at a concentration of 100 μg/mL, and the same extract reduced cell viability to 81.45±2.75% (p < 0.05) at a concentration of 180 μg/mL (Table 4, Figure 3).

In order to understand whether the induced cytotoxic effect is specific to cancer cells, the effects of the extracts on the healthy cell line HUVEC were also evaluated. It was determined that only WLSET and WLSA extracts cause a significant cytotoxic effect on HUVEC cell lines at a concentration of 180 μg/mL (Figure 4).

All these results showed that MCF-7 cancer cells were more sensitive to WLAA extract at a concentration of 100 μg/mL compared to healthy HUVEC cell lines.

Table 2. Mass fragments of phenolic compounds detected in extracts by LC-QTOF-MS

Retention time (min)	Molecular formula	Molecular weight	[M-H]⁻	Theoretical ion	Fragment ions	Ppm (Δ)	Compound	Determination methods
9.85	$C_{16}H_{18}O_9$	354.0951	353.0908	353.0881	191, 135, 173, 85	2.7	Chlorogenic acid	PubChem
11.06	$C_{21}H_{20}O_{12}$	464.0955	463.0914	463.0000	301, 300, 271, 255, 179, 151	9.1	Quercetin 4'-O-glucoside / Quercetin 3-O-galactoside	PubChem
11.33	$C_{20}H_{18}O_{11}$	434.0849	433.0812	433.0800	301, 300, 271, 179, 151	1.2	Quercetin 7-xyloside / Quercetin 3-O-arabinoside	PubChem
11.46	$C_{21}H_{20}O_{11}$	448.1006	447.0968	447.0927	301, 300, 271, 255, 151	4.1	Quercetin 7-O-rhamnoside	PubChem
11.73	$C_{20}H_{18}O_{10}$	418.090	417.0856	417.0899	285, 255, 227	4.3	Kaempferol 3-O-xyloside / Kaempferol 3-O-arabinoside	Metlin
13.05	$C_{30}H_{26}O_{12}$	578.1424	577.1402	577.1424	413, 285, 255, 227, 163	2.2	Kaempferol derivative	Metlin
13.20	$C_{30}H_{26}O_{12}$	578.1424	577.1402	577.1424	413, 285, 255, 227, 163	2.2	Kaempferol derivative	Metlin

Table 3. Antioxidant activity results of the extracts

Extracts	Metal chelating capacity inhibition% ± S.D.[b]			Ferric-reducing power absorbance ± S.D.			DPPH radical scavenging activity inhibition% ± S.D.		
	2 mg/mL	1 mg/mL	0.5 mg/mL	2 mg/mL	1 mg/mL	0.5 mg/mL	2 mg/mL	1 mg/mL	0.5 mg/mL
WLSA	8.80 ± 2.23	-	-	2.517 ± 0.090	1.681 ± 0.260	1.336 ± 0.030	75.39 ± 0.44	82.67 ± 0.32	85.90 ± 0.62
WLAA	74.17 ± 11.06	31.06 ± 8.10	16.16 ± 4.17	1.925 ± 0.010	1.446 ± 0.060	0.756 ± 0.010	73.05 ± 2.09	83.11 ± 2.49	86.95 ± 0.77
WLSET	54.58 ± 9.66	32.13 ± 8.17	-	1.969 ± 0.070	1.594 ± 0.100	1.134 ± 0.060	80.53 ± 1.21	85.86 ± 0.71	87.76 ± 0.21
Reference	2 mg/mL	1 mg/mL	0.5 mg/mL	2 mg/mL	1 mg/mL	0.5 mg/mL	2 mg/mL	1 mg/mL	0.5 mg/mL
EDTA	100 ± 0.00	99.86 ± 0.48	99.68 ± 0.08	NT	NT	NT	NT	NT	NT
Quercetin	NT[a]	NT	NT	1.874 ± 0.030	2.296 ± 0.010	2.931 ± 0.150	NT	NT	NT
Ascorbic acid	NT	NT	NT	NT	NT	NT	94.75 ± 0.71	95.23 ± 0.14	91.80 ± 0.31

[a]NT: Not tested, [b]SD: Standard deviation, -: No activity

Table 4. Cytotoxic activity of the extracts

Cell Line	Concentration (µg/mL)	Cell viability% ± SEM		
		WLSET	WLSA	WLAA
MCF- 7	18	94.41±1.29	99.94±3.08	95.64±2.79
	30	98.48 ± 2.53	104.40±2.00	100.20±2.36
	56	96.68±1.03	100.50±2.21	89.32±0.95
	100	97.76±1.33	106.40±1.77	83.66±3.84*
	180	108.30±2.97	112.40±6.14	81.45±2.75*
HUVEC	18	99.05 ± 5.90	98.27±2.95	103.40±2.12
	30	106.80±3.01	100.70±2.94	103.60±2.51
	56	94.95±1.58	99.29±1.83	95.69±3.21
	100	97.76±2.21	102.60±1.60	97.46±1.99
	180	64.11±1.65*	84.23±1.19*	92.81±3.43

n = 4; * $p < 0.05$; SEM: Standard error meaning
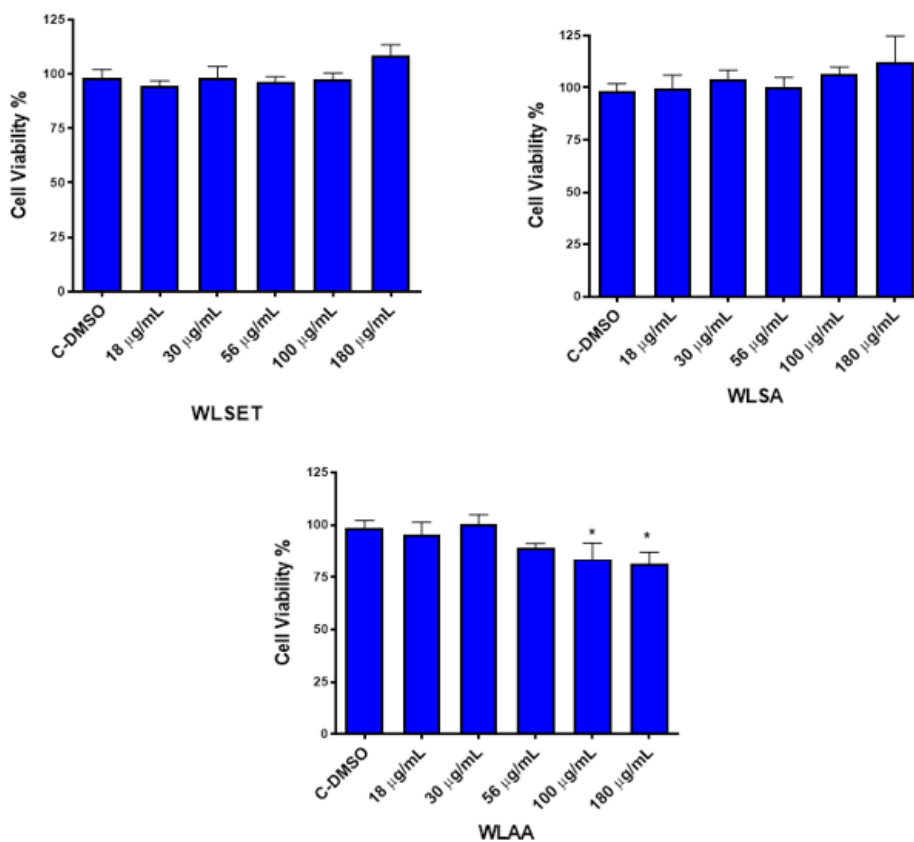
Figure 3. Cytotoxic effects of WLSET, WLAA, and WLSA extracts in MCF- 7 cell lines (n = 4 tested, One-Way ANOVA, * $p < 0.05$ vs. control DMSO)
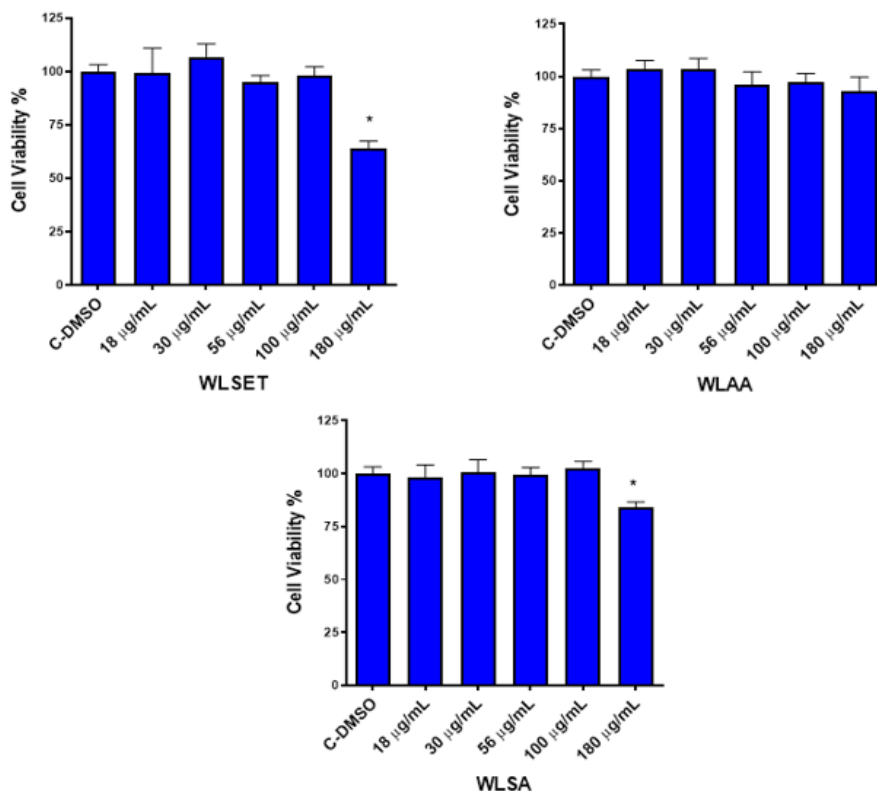
Figure 4. Cytotoxic effects of WLSET, WLAA, and WLSA extracts in HUVEC cell lines (n= 4 tested, One-Way ANOVA, * p < 0.05 vs. control DMSO).

One of the cells in the cancer microenvironment is the endothelial cell and endothelium plays important roles in cancer diseases (Sobierajska et al., 2020). Thus we also evaluated the cytotoxic effects of walnut leaves extracts on endothelial cells. Among the extracts examined in this study, it was determined that only WLAA extract exerted cytotoxic activity in MCF-7 cancer cell lines, on the other hand, it did not show any cytotoxic effect on healthy cell lines. A compound and/or extract evaluated for cytotoxic effect should not be cytotoxic to healthy cell lines. In addition, it is important that the extract is effective in terms of both cytotoxic and antioxidant effects, and when the WLAA extract is evaluated from this point of view, it is considered extremely promising.

Due to of the differences in the phenolic content of the extracts and LC-QTOF-MS analyses were performed to determine the phenolic content of the extracts. In LC-QTOF-MS analysis, fragmentation ions belonging to molecules thought to be derivatives of chlorogenic acid, quercetin 4'-*O*-glucoside/quercetin 3-*O*-galactoside, quercetin 7-xyloside/quercetin 3-*O*-arabinoside, quercetin 7-*O*-rhamnoside, kaempferol 3-*O*-xyloside/ kaempferol 3-*O*-arabinoside, and kaempferol derivatives were detected in all extracts. As seen in the chromatograms, it was not determined which phenolic compounds belonged to the main peaks observed at the 15th and 16th minutes in the WLAA extract, which was thought to be particularly effective.

As a result of our literature survey, it was concluded that scientific studies were also carried out on the galls formed in different plants. Gall, which is formed by an insect named *Adleria gallae* tinctoria on the branches, leaves, and buds of *Quercus species* (Oak), contains secondary metabolites in

tannin, phenolic acid, flavonoid, triterpenoid, and steroid structure, and depending on these contents, cholinesterase and monoamine oxidase inhibitor, antitumor, antihypertensive has been determined that they show antioxidant, antimicrobial, insecticidal, anti-inflammatory, and antiparasitic effects (Mirpour et al., 2015; Arina & Harisun 2019; Mahboubi 2020; Sukor et al., 2020; Elham et al., 2021).

Similarly, in the galls formed by a Pemphigus insect on the leaves and petioles of *Pistacia integerrima* Stewart from the Anacardiacae family; it has been reported that flavonoids, monoterpene, triterpenoid, sterol, triterpenic acid, fatty esters, ketoalcohol structured compounds, and dihydromalvalic acid are present. Scientific studies have also been published on the fact that the extracts obtained from these galls have antihyperalgesic, anti-inflammatory, antidepressant, and antihyperuricemic effects (Ahmad et al., 2010; Rauf et al., 2016).

It has been reported that the galls formed by the aphid *Schlechtendalia chinensis* on the leaves of *Rhus chinensis* Mill. are also rich in hydrolyzed tannins and gallotannins and display alpha glucosidase enzyme inhibitory, anticancer, antiviral, antimicrobial, and anti-inflammatory activities (Shim et al., 2003; Liu et al., 2014; Kwak et al., 2014).

In a study on oak galls caused by Eriophyidae, galls parts of the plant were found to be rich in gallotanene and gallic acid (Patni et al., 2012). In this context, it is thought that the biological activities of galls belonging to different plant species with different phytochemical content may also be different.

As a result of our literature studies, no phytochemical or activity studies were found on galls caused by Eriophyidae mites on *J. regia* leaves. For the first time in this study, the chemical compositions of polyphenol extracts obtained from galls were analyzed, and their antioxidant and cytotoxic activities were investigated.

Hakimuddin et al., evaluated the cytotoxic effects of the flavonoid fraction obtained from red wine on MCF-7 cell lines. Due to the strong selective cytotoxic effect of the fractions, the effects of some flavonoids (catechin, quercetin, and naringenin) in these fractions were tested again in the same cell line. All three flavonoids showed dose-dependent cytotoxic effects on the proliferation of MCF-7 cells. The IC_{50} values of quercetin, naringenin and catechin are listed as follows; 13, 51, and 150 µg/mL (Hakimuddin et al., 2004). In a study by Silva et al., it was reported that the ethanol extract of *Mimosa caesalpiniifolia* leaves had a cytotoxic effect on MCF-7 cell lines and that this extract was rich in flavonoids (Silva et al., 2014). These literature data showed that the cytotoxic effect of WLAA extract on MCF-7 cells may be due to the fact that it contains more catechins than other extracts. On the other hand, it can be predicted that the identified/unidentified phenolic compounds in this extract may also cause synergistic effects in both antioxidant and cytotoxic activities. LC-QTOF-MS analyses showed that some secondary metabolites in walnut leaves are also present in galls, and some compounds identified in galls have not been identified in walnut leaves so far. In other words, these findings suggest that walnut leaves contain some phenolic compounds (quercetin 4'-*O*-glucoside, quercetin 7-xyloside, quercetin 7-*O*-rhamnoside, kaempferol 3-*O*-xyloside, and kaempherol 3-*O*-arabinoside) that have not been detected until now.

CONCLUSIONS

In this report, the phytochemical contents, antioxidant and anticancer effect potentials of galls caused by *Eriophyidae* mites on *J. regia* leaves were investigated for the first time. While eight phenolic compounds were defined by LC-QTOF-MS. While it was observed that MCF-7 breast cancer cell lines were more sensitive to the polyphenolic extract of galls collected from the Ankara region, it was also concluded that this extract had a high antioxidant potential. When approached from a different perspective, the galls formed on the leaves of the trees both damage the trees and cause negative economic effects in terms of affecting fruit productivity.

Therefore, the results obtained in this study showed that these galls are worth examining in terms of anticancer, antioxidant, and many other activities, and in this way, a pathogenic condition for the tree can be a source for the discovery of new and natural drug raw materials. Future studies will continue to test the cytotoxic activities of the fractions obtained from the polyphenolic extracts of these galls formed on walnut leaves in different cancer cell lines and to determine the active compound or compounds.

ACKNOWLEDGEMENTS

AUTHOR CONTRIBUTION STATEMENT

Concept: SB, SP, DDO; Design: SB, BÖ, DDO; Control: SB, BÖ, AÖ, SP, DDO; Sources: SB, SP; Materials: SB, BÖ, SP, AÖ, DDO; Data Collection and/or processing: SB, SP, BÖ, SP, AÖ, DDO; Analysis and/or interpretation: SB, SP, AÖ, DDO; Literature review: SB, BÖ, DDO; Manuscript writing: SB, BÖ, SP, DDO; Critical review: SB, DDO; Other: SB, BÖ, SP

CONFLICT OF INTEREST

The authors declare that there is no conflict of interest.

REFERENCES

Ahmad, S., Ali, M., Ansari, S. H., & Ahmed, F. (2010). Phytoconstituents from the galls of Pistacia integerrima Stewart. *Journal of Saudi Chemical Society, 14*(4), 409-412. https://doi.org/10.1016/j.jscs.2010.05.003

Altun, I., & Sonkaya, A. (2018). The most common side effects experienced by patients were receiving first cycle of chemotherapy. *Iranian Journal of Public Health, 47*(8), 1218-1219.

Alzeer, J., Arafeh, R., & Al-Gubory, K. H. (2017). Antioxidants in the prevention and treatment of cancer. *Nutritional Antioxidant Therapies: Treatments and Perspectives* (pp. 493-521)

Anand, P., Kunnumakara, A. B., Sundaram, C., Harikumar, K. B., Tharakan, S. T., Lai, O. S., . . . Aggarwal, B. B. (2008). Cancer is a preventable disease that requires major lifestyle changes. *Pharmaceutical Research, 25*, 2097-2116.

Ara, T., Shafi, S., Ghazwani, M., Mir, J. I., Shah, A. H., Qadri, R. A., . . . Wahab, S. (2023). In vitro potent anticancer, antifungal, and antioxidant efficacy of Walnut (Juglans regia L.) Genotypes. *Agronomy, 13*(5), 1232. https://doi.org/10.3390/agronomy13051232

Arina, M. Z. I., & Harisun, Y. (2019). Effect of extraction temperatures on tannin content and antioxidant activity of Quercus infectoria (Manjakani). *Biocatalysis and Agricultural Biotechnology, 19*, 101104. https://doi.org/10.1016/j.bcab.2019.101104

Davis, P. H. (1982). Flora of Turkey and the East Aegean Islands 7. *Edinburgh University Press*, Edinburgh.

Dela, Cruz, J. F., Kim, Y. S., Lumbera, W. M., & Hwang, S. G. (2015). Viscum album var hot water extract mediates anti-cancer effects through G1 phase cell cycle arrest in SK-Hep1 human hepatocarcinoma cells. *Asian Pacific Journal of Cancer Prevention, 16*, 6417-6421.http://dx.doi.org/10.7314/APJCP.2015.16.15.6417

Delaviz, H., Mohammadi, J., Ghalamfarsa, G., Mohammadi, B., & Farhadi, N. (2017). A review study on phytochemistry and pharmacology applications of Juglans regia plant. *Pharmacognosy Review, 11*(22), 145-152. https://doi.org/10.4103/phrev.phrev_10_17

Delebinski, C. I., Twardziok, M., Kleinsimon, S., Hoff, F., Mulsow, K., Rolff, J., . . . Seifert, G. (2015). A natural combination extract of Viscum album L. containing both triterpene acids and lectins is highly effective against AML in vivo. *PLoS One*, *10*, e0133892. https://doi.org/10.1371/journal.pone.0133892

Deliorman, D., Caliş, I., Ergun, F., Doğan, B. S., Buharalioğlu, C. K., & Kanzik, I. (2000). Studies on the vascular effects of the fractions and phenolic compounds isolated from Viscum album ssp. album. *Journal of Ethnopharmacology*, *72*(1-2), 323-329. https://doi.org/10.1016/s0378-8741(00)00251-8

Denizhan, E., & Çobanoğlu, S. (2009) Eriophyid Mites of Walnut Trees (Juglans regia L.) and Their Predators in Ankara. *Yüzüncü Yıl University Journal of Agricultural Sciences*, *19*(1), 33-37.

Dinis, T. C., Maderia, V. M., & Almeida, L. M. (1994). Action of phenolic derivatives (acetaminophen, salicylate, and 5-aminosalicylate) as inhibitors of membrane lipid peroxidation and as peroxyl radical scavengers. *Archives of Biochemistry and Biophysics*, *315*(1), 161-169. https://doi.org/10.1006/abbi.1994.1485

Elham, A., Arken, M., Kalimanjan, G., Arkin, A., & Iminjan, M. (2021). A review of the phytochemical, pharmacological, pharmacokinetic, and toxicological evaluation of Quercus Infectoria galls. *Journal of Ethnopharmacology*, *273*, 113592. https://doi:10.1016/j.jep.2020.113592

Erdogan Orhan, I., Suntar, I. P., & Akkol, E. K. (2011). In vitro neuroprotective effects of the leaf and fruit extracts of Juglans regia L.(walnut) through enzymes linked to Alzheimer's disease and antioxidant activity. *International Journal of Food Sciences and Nutrition*, *62*(8), 781-786.

Greenwell, M., & Rahman, P. K. S. M. (2015). Medicinal plants: their use in anticancer treatment. *International Journal of Pharmaceutical Sciences and Research*, *6*(10), 4103-4112. https://doi: 10.13040/IJPSR.0975-8232.6(10).4103-12

Gülçin, I. (2010). Antioxidant properties of resveratrol: A structure–activity insight. *Innovative Food Science & Emerging Technologies*, *11*(1), 210-218.

Hakimuddin, F., Paliyath, G., & Meckling, K. (2004). Selective cytotoxicity of a red grape wine flavonoid fraction against MCF-7 cells. *Breast Cancer Research and Treatment*, *85*, 65-79. https://doi.org/10.1023/B:BREA.0000021048.52430.c0

Jung, H. A., Jin, S. E., Choi, R. J., Manh, H. T., Kim, Y. S., Min, B. S., . . . Choi, J. S. (2011). Anti-tumorigenic activity of sophoflavescenol against Lewis lung carcinoma in vitro and in vivo. *Archives of Pharmacal Research*, *34*, 2087-2099. https://doi: 10.1007/s12272-011-1212-y

Kwak, H., Hegeman, A. D., & Park, S. (2014). Seasonal changes in metabolic profiles of galls and leaves of Rhus chinensis using gas chromatography mass spectrometry and liquid chromatography quadrupole time-of-flight mass spectrometry. *Journal of Plant Biology*, *57*, 127-135. https://doi:10.1007/s12374-013-0498-3

Liu, P., Yang, Z. X., Chen, X. M., & Foottit, R. G. (2014). The effect of the gall-forming aphid Schlechtendalia chinensis (Hemiptera: Aphididae) on leaf wing ontogenesis in Rhus chinensis (Sapindales: Anacardiaceae). *Annals of the Entomological Society of America*, *107*(1), 242-250. https://doi.org/10.1603/AN13118

Mahboubi, M. (2020). Quercus infectoria fruit hulls and galls and female genital disorders. *Clinical Phytoscience*, *6*, 44. https://doi.org/10.1186/s40816-020-00194-9

Mirpour, M., Gholizadeh Siahmazgi, Z., & Sharifi Kiasaraie, M. (2015). Antibacterial activity of clove, gall nut methanolic and ethanolic extracts on Streptococcus mutans PTCC 1683 and Streptococcus salivarius PTCC 1448. *Journal of Oral Biology and Craniofacial Research*, *5*(1), 7-10. https://doi: 10.1016/j.jobcr.2015.02.002

Orhan, N., Deliorman Orhan, D., Gökbulut, A., Aslan, M., & Ergun, F. (2017). Comparative analysis of chemical profile, antioxidant, in-vitro and in-vivo antidiabetic activities of Juniperus foetidissima Willd. and Juniperus sabina L. *Iranian Journal of Pharmaceutical Research*, *16*, 64-74.

Orhan, N., Erdogan Orhan, I., & Ergun, F. (2011). Insights into cholinesterase inhibitory and antioxidant activities of five Juniperus species. *Food and Chemical Toxicology*, *49*(9), 2305-2312.

Özdemir, A., Yildiz, M., Senol, F. S., Şimay, Y. D., Ibişoglu, B., Gokbulut, A., … Ark, M. (2017). Promising anticancer activity of Cyclotrichium niveum L. extracts through induction of both apoptosis and necrosis. *Food and Chemical Toxicology*, *109*, 898-909. https://doi: 10.1016/j.fct.2017.03.062

Patni, V., Sharma, N., & Mishra, P. (2012). Oak (Quercus leucotrichophora) Galls, as an intense source of natural gallic acid. *LS International Journal of Life Sciences*, *1*(3), 186-191. https://doi: 10.5958/j.2319-118X.1.3.013

Rather, M. A., Dar, B. A., Dar, M. Y., Wani, B. A., Shah, W. A., Bhat, B. A., . . . Qurishi, M. A. (2012). Chemical composition, antioxidant and antibacterial activities of the leaf essential oil of Juglans regia L. and its constituents. *Phytomedicine*, *19*(13), 1185-1190.

Rauf, A., Uddin, G., Siddiqui, B. S., Khan, H., Shah, S. U., Ben, Hadda, T., . . . Khan, A. (2016). Antinociceptive and anti-inflammatory activities of flavonoids isolated from Pistacia integerrima galls. *Complementary Therapies in Medicine*, *25*, 132-138. https://doi: 10.1016/j.ctim.2016.02.002

Republic of Türkiye Ministry of Health, Early diagnosis saves lives. https://www.saglik.gov.tr/EN-102478/early-diagnosis-saves-lives.html, accessed 22 April 2024.

Salimi, M., Majd, A., Sepahdar, Z., Azadmanesh, K., Irian, S., Ardestaniyan, M. H., . . . Rastkari, N. (2012). Cytotoxicity effects of various Juglans regia (walnut) leaf extracts in human cancer cell lines. *Pharmaceutical Biology*, *50*(11), 1416-1422. https://doi.org/10.3109/13880209.2012.682118

Shim, Y. J., Doo, H. K., Ahn, S. Y., Kim, Y. S., Seong, J. K., Park, I. S., & Min, B. H. (2003). Inhibitory effect of aqueous extract from the gall of Rhus chinensis on alpha-glucosidase activity and postprandial blood glucose. *Journal of Ethnopharmacology* 2003, *85*(2-3), 283-287. https://doi: 10.1016/s0378-8741(02)00370-7

Silva, M. J. D., Carvalho, A. J. S., Rocha, C. Q., Vilegas, W., Silva, M. A., & Gouva, C. M. C. P. (2014). Ethanolic extract of Mimosa caesalpiniifolia leaves: Chemical characterization and cytotoxic effect on human breast cancer MCF-7 cell line. *South African Journal of Botany*, *93*, 64–69. https://doi.org/10.1016/j.sajb.2014.03.011

Sobierajska, K., Ciszewski, W. M., Sacewicz-Hofman, I., & Niewiarowska, J. (2020). Endothelial cells in the tumor microenvironment. *Advances in Experimental Medicine and Biology*, *1234*, 71-86. https://doi.org/10.1007/978-3-030-37184-5_6

Sukor, N. F., Jusoh, R., Kamarudin, N. S., Abdul Halim, N. A., Sulaiman, A. Z., & Abdullah, S. B. (2020). Synergistic effect of probe sonication and ionic liquid for extraction of phenolic acids from oak galls. *Ultrasonics Sonochemistry*, *62*, 104876. https://doi: 10.1016/j.ultsonch.2019.104876

T.C. Gıda Tarım ve Hayvancılık Bakanlığı. (2017). Ceviz entegre mücadele teknik talimatı. *Tarımsal Araştırmalar ve Politikalar Genel Müdürlüğü Gıda ve Kontrol Genel Müdürlüğü*, Ankara (in Turkish).

Tennakoon, K. U., & Pate, J. S. (1996). Effects of parasitism by a mistletoe on the structure and functioning of branches of its host. *Plant, Cell Environment*, *19*(5), 517-528. https://doi.org/10.1111/j.1365-3040.1996.tb00385.x

WHO, World Health Organization Cancer. https://www.who.int/health-topics/cancer#tab=tab_1, accessed 15 March 2024.

Zhou, Y., Zheng, J., Li, Y., Xu, D. P., Li, S., Chen, Y. M., & Li, H. B. (2016). Natural polyphenols for prevention and treatment of cancer. *Nutrients*, *8*(8), 515. https://doi.org/10.3390/nu8080515

Zongo, C., Savadogo, A., Ouattara, L., Bassole, I. H. N., Ouattara, C. A. T., Ouattara, A. S., . . . TraoreI, A. S. (2010). Polyphenols content, antioxidant and antimicrobial activities of Ampelocissus grantii (Baker) Planch.(Vitaceae): a medicinal plant from Burkina Faso. *International Journal of Pharmacology*, *6*(6), 880–887. https://doi: 10.3923/ijp.2010.880.887

A (hetero)arylidene-(4-substituted-thiazol-2-yl) hydrazine As New Potential MAO-B inhibitors. Computational Study and In-Silico Prediction

Moulay Ahfid El ALAOUY[*], Marwa ALAQARBEH[**°], Abdelouahid SBAI[***], Hamid MAGHAT[****], Tahar LAKHLIFI[*****], Mohammed BOUACHRINE[******]

A (hetero)arylidene-(4-substituted-thiazol-2-yl) hydrazine As New Potential MAO-B inhibitors. Computational Study and In-Silico Prediction

SUMMARY

The inhibitory effect of 44 hydrazine derivatives (4-substituted-thiazole-2-yl) compounds against hMAO-B was evaluated to understand the structure-activity-relationship. The results show that the CoMFA/SE model has high stability and predictability (Q2 = 0.608; R2 = 0.933; R2 Test = 0.70). Contour maps derived from the CoMFA/SE vacuum field and the electrostatic field provide more information about the modulation of these inhibitors.
The interactions were investigated by molecular docking and showed a conventional hydrogen bond with residues Ile14, Ser15, Gln206, Met436, Tyr435, Tyr60, and Ser59, which play essential roles in the biological field. The MD binding free energies for compound 26 and proposed compound M1 with hMAO-B of -134.288 kJ/mol and -150.506 kJ/mol, respectively, were -134.288 kJ/mol and -150.506 kJ/mol, respectively. Therefore, compound M1 is more active than compound 26 at the active site of the hMAO-B receptor.

Key Words: *ADMET, 3D-QSAR, Molecular Docking, Molecular Dynamics, hMAO-B.*

Yeni Bir Potansiyel MAO-B İnhibitörü Olarak Bir (hetero) ariliden-(4-sübstitüe-tiyazol-2-il) hidrazin. Hesaplamalı Çalışma and in-Silico Tahmin

ÖZ

Yapı-aktivite-ilişkisini anlamak amacıyla 44 hidrazin türevi (4-sübstitüe-tiyazol-2-il) bileşiğin hMAO-B'ye karşı inhibitör etkisi değerlendirilmiştir. Sonuçlar CoMFA/SE modelinin yüksek kararlılığa and tahmin edilebilirliğe sahip olduğunu göstermektedir (Q2 = 0.608; R2 = 0.933; R2 Test = 0.70). CoMFA/SE vakum alanı and elektrostatik alandan elde edilen sınır haritaları, bu inhibitörlerin modülasyonu hakkında daha fazla bilgi sağlar.
Etkileşimler moleküler yerleştirme yöntemi ile incelenmiş and biyolojik alanda önemli roller oynayan Ile14, Ser15, Gln206, Met436, Tyr435, Tyr60 and Ser59 kalıntılarıyla geleneksel bir hidrojen bağının varlığı gösterilmiştir. Bileşik 26 and önerilen bileşik M1'in hMAO-B ile MD bağlanma serbest enerjileri sırasıyla -134.288 kJ/mol and -150.506 kJ/mol'dür. Bu nedenle, M1 bileşiği hMAO-B reseptörünün aktif bölgesinde bileşik 26'dan daha aktiftir.

Anahtar Kelimeler: *ADMET, 3D-QSAR, Moleküler Yerleştirme, Moleküler Dinamik, hMAO-B*

[*] ORCID: 0009-0005-1593-1486 Molecular Chemistry and Natural Substances Laboratory, Faculty of Science, University Moulay Ismail, Meknes, Morocco
[**] ORCID: 0000-0002-0879-5077 Basic Science Department, Prince Al Hussein bin Abdullah II Academy for Civil Protection, Al-Balqa Applied University, Al-Salt 19117, Jordan
[***] ORCID: 0000-0002-7140-9853 Molecular Chemistry and Natural Substances Laboratory, Faculty of Science, University Moulay Ismail, Meknes, Morocco
[****] ORCID: 0000-0002-7731-330X Molecular Chemistry and Natural Substances Laboratory, Faculty of Science, University Moulay Ismail, Meknes, Morocco
[*****] ORCID: 0000-0003-4917-475X Molecular Chemistry and Natural Substances Laboratory, Faculty of Science, University Moulay Ismail, Meknes, Morocco
[******] ORCID: 0000-0002-8901-047X Molecular Chemistry and Natural Substances Laboratory, Faculty of Science, University Moulay Ismail, Meknes, Morocco

° Corresponding Author; Marwa Alaqarbeh,
marwaqarbh@hotmail.com; marwa.aqarbeh@bau.edu.jo

INTRODUCTION

Monoamine oxidase (MAO) is an oxidoreductase enzyme that catalyze monoamine neurotransmitters, and they belong to flavin adenine dinucleotide (FAD)-dependent protein (Yang et al., 2017). The deamination of neurotransmitters and biogenic amines is catalyzed by the flavoproteins MAO(Yücel and Özdemir, 2023), which has two distinct isoforms, A and B (MAO A and MAO B) (Chimenti et al., 2007). MAO-A metabolizes the ample endogenous amine serotonin, while MAO-B metabolizes small amines such as phenylethylamine, the precursor of dopamine and norepinephrine, a precursor to dopamine and norepinephrine. As a result, human MAO inhibitors (hMAO-Is) play a significant role in managing neurological and psychiatric illnesses. In particular, hMAO-A inhibitors are employed as antidepressants and anxiolytics, whereas hMAO-B inhibitors are adjuncts in treating PD (Secci et al., 2012a). MAO-B kinetics gets stronger with age in the brain, along with the increase of the catalytic process of oxidative deamination, which produces aldehydes and hydrogen peroxide as by-products (Lu et al., 2018)nanostructured NS. Since oxidative stress and the development of neuronal damage are linked, inhibition of MAO-B will likely prevent the brain from metabolizing monoamines, thereby counteracting the degenerative consequences (Vicente-Zurdo et al., 2023). The hMAO-B inhibitors are helpful and successful in reducing motor fluctuations in people with early and advanced Parkinson's disease (PD) by improving dopamine levels and reducing the side effects of PD treatments (Kondeva-Burdina et al., 2022a). In this regard, using specific hMAO-B inhibitors to treat PD is warranted because oxidative deamination of the primary monoamine by hMAO produces toxic NH_3, aldehyde, and H_2O_2 agents(Dhiman, Malik, Sobarzo-Sánchez, Uriarte and Khatkar, 2019). Because of the increase in hMAO activity and the consequent increase in H_2O_2 production by hMAO-B, age-related degenerative disease processes, Parkinson's may also be related to oxidative stress. Therefore, inhibitors of hMAO-B could work by reducing free radical production and increasing monoamine levels in the brain (Kondeva-Burdina et al., 2022b). In treating PD, MAO-B inhibitors play a crucial role in preserving dopamine levels in the brain and alleviating the symptoms of the disease (Bozbey, Taşkor Önel, Türkmenoğlu, Gürsoy and Dilek, 2022). Several heterocyclic compounds have been studied to investigate the potential MAO-B enzyme inhibition activity. 4-substituted thiazol-2-yl hydrazines belong to thiazole heterocyclic derivative and have been shown to bind to MAO-B enzyme and block its activity, thus helping preserve dopamine levels (Anastassova et al., 2022; Chimenti et al., 2010). Also, benzimidazoles and isoquinolines, other heterocyclic compounds, have interesting therapeutic targets for treating Parkinson's disease (Anastassova et al., 2022; Nagatsu, 1997). Further research has examined MAO-B inhibitors such as selegiline and rasagiline for their neuroprotective effects in PD by preserving dopamine levels (Fiddian-Green and Silen, 1975). Discovering and designing new MAO-B inhibitors as potential drugs to treat Parkinson's disease using computer-aided methods such as three-dimensional quantitative structure-activity relationship (3D-QSAR), molecular docking, ADMET predictions, and molecular dynamics (MD) simulations have been used to design potential candidate drugs (Aanouz et al., 2021). In this work, comparative molecular domain analysis (CoMFA) was performed on 44 hydrazine (4-substituted-thiazole-2-yl) derivatives synthesised by Daniela Secci *et al.* to relate the characteristic structure to the inhibitory activity of the hMAO-B enzyme (Secci et al., 2012). Molecular docking and ADMET studies facilitate the identification of new drug candidates. Finally, molecular dynamics simulation at 100 ns was performed to estimate the binding stability of 44 candidates within the target protein to confirm the docking results.

MATERIALS AND METHODS

Data collection

This study investigated 44 (hetero)arylidene-(4-substituted-thiazol-2-yl) hydrazine derivatives synthesised by Secci et al. were investigated as potential selective inhibitors of human MAO-B inhibitors. (Secci et al., 2012). The inhibitory activities of compounds IC$_{50}$ (M) values were changed to a logarithmic scale (pIC$_{50}$ = -log IC$_{50}$), as shown in (Table 1) and (Figure 1.). 35 compounds were used as a training set, and the remaining 9 inhibitors were used to validate the developed model. 3D-QSAR modeling was performed using Sybyl software, and the Gasteiger-Huckel method was used to add the partial atomic charges after the Tribe force field lowered the resulting energy. The convergence value of the Powell gradient energy was set to 0.005 kcal/mol A, and the maximum number of iterations was 1000 to produce an efficient 3D-QSAR model (Fiddian-Green and Silen, 1975).
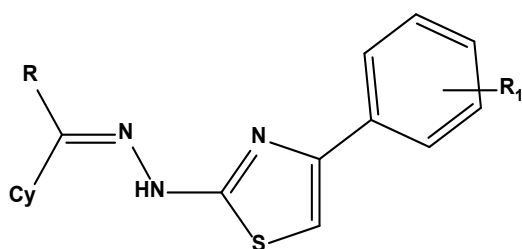
Figure 1. The chemical formula of the studied compounds.

Table 1. Activities and structures of (hetero) arylidene-(4-substituted-thiazol-2-yl) derivatives.

No	Cy	R	R1	IC$_{50}$ hMAO-B	pIC$_{50}$ hMAO-B
1		H	4-CN	1.49μM	5.827
2		H	4-CN	152.86nM	6.815
3*		CH$_3$	4-CN	3.11 μM	5.507
4		CH$_3$	4-CN	2.00 μM	8.699
5		CH$_3$	4-CN	995.94 nM	6.001
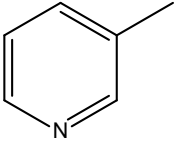
6	(3-methylpyridine)	H	4-CN	946.62 nM	6.023
7	(3-methylpyridine)	CH$_3$	4-CN	2.09 nM	8.68
8	(4-methylpyridine)	H	4-CN	6.75 µM	5.17
9*	(4-methylpyridine)	CH$_3$	4-CN	435.91 nM	6.36
10	(1-methylnaphthalene)	H	4-CN	1.10 µM	5.958
11	(3-methylindole)	H	4-CN	762.37nM	6.118
12	(5-methylbenzodioxole)	H	4-CN	301.10 nM	6.521
13	(2-methylfuran)	CH$_3$	4-NO$_2$	3.59 µM	5.445
14	(2-methylthiophene)	CH$_3$	4-NO$_2$	297.91 nM	6.526
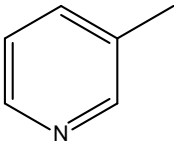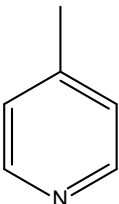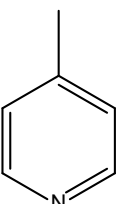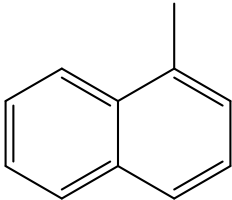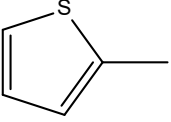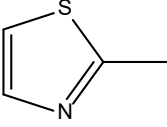
15		CH₃	4-NO₂	366.21 nM	6.436
16*		CH₃	4-NO₂	26.67 nM	7.574
17*		CH₃	4-NO₂	13.12 nM	7.882
18		H	4-F	652.80 nM	6.185
19		CH₃	4-F	319.82 nM	6.495
20		H	4-F	338.35 nM	6.47
21		CH₃	4-F	15.49 nM	7.81
22*		CH₃	4-F	1.21 μM	5.917
23		CH₃	4-F	350.70 nM	6.455
24*		CH₃	4-F	24.31 nM	7.614
25		H	4-F	482.16 nM	6.316
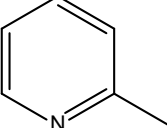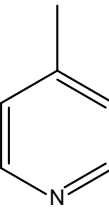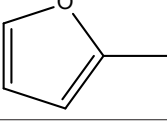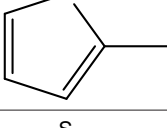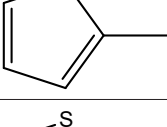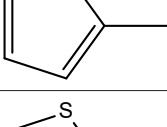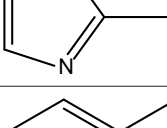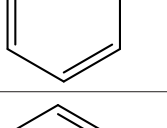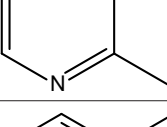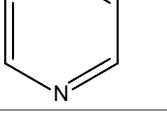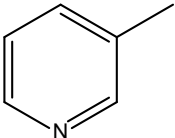
26		CH$_3$	4-F	1.70 nM	8.769
27*		H	4-F	12.82 µM	4.892
28		H	4-F	112.36 nM	6.95
29		H	4-F	577.99 nM	6.238
30		H	4-F	1.08 µM	5.966
31*		H	2,4-F	216.58 nM	6.664
32		CH$_3$	2,4-F	40.08 nM	7.397
33		H	2,4-F	16.58 nM	7.78
34		CH$_3$	2,4-F	3.01 nM	8.521
35		CH$_3$	2,4-F	12.96 nM	7.887
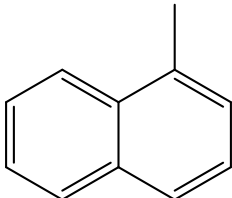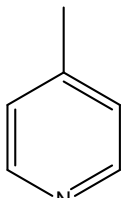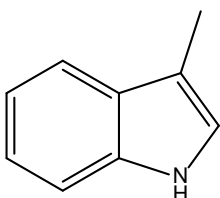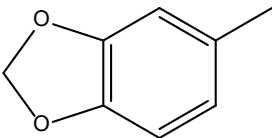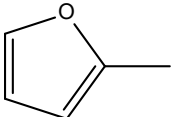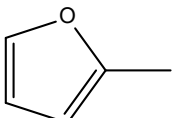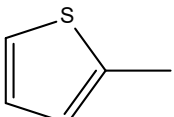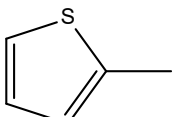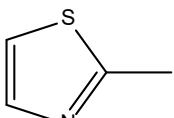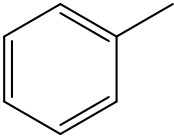
36		CH$_3$	2,4-F	90.26 nM	7.044
37 *		H	2,4-F	198.50 nM	6.702
38		CH$_3$	2,4-F	18.40 nM	7.735
39		H	2,4-F	548.85 nM	6.26
40		CH$_3$	2,4-F	16.68 nM	7.777
41		H	2,4-F	137 .6 nM	6.861
42		H	2,4-F	529.48 nM	6.276
43		H	2,4-F	1.17 µM	5.931
44		CH$_3$	2,4-F	1.42 µM	5.847
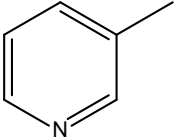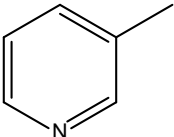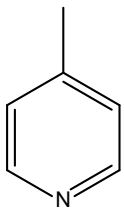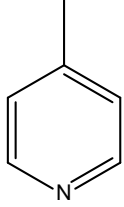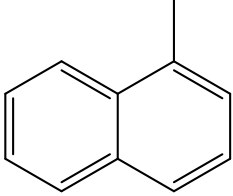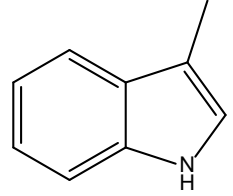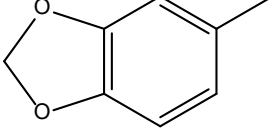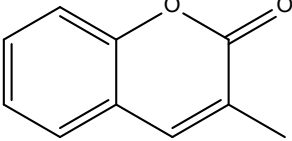
* Test set

Alignment of the inhibitors

One of the most critical aspects of the structural alignment of target compounds significantly impacts the predictive ability and accuracy of 3D QSAR models and the reliability of contour maps. In this paper, the least energetic conformation of the most active compound 26 has been considered as the superposition model (Stamm, Latscha, Janecek and Campana, 1976). The other inhibitors were aligned with the common backbone, and the alignment results are shown in (Figure 2).

Aligned compounds   core
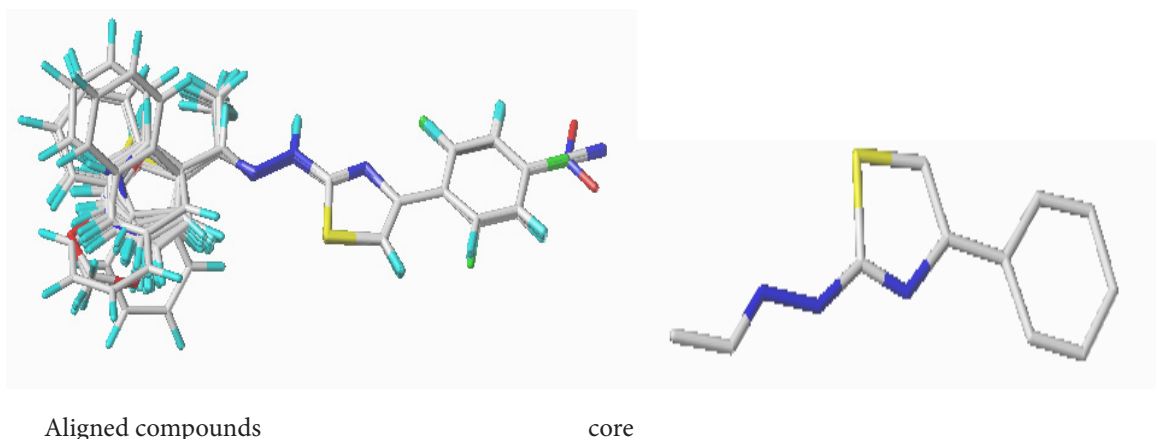
Figure 2. Overlay and alignment of the **44** molecules using Molecule **26** as a model.

Generation of 3 D-QSAR models

CoMFA and CoMSIA are three-dimensional quantitative structure-activity relationship (3D-QSAR) methods used to describe the properties of receptor interactions and chemical bonds. Carbon sp3 with a charge of +1 was used as a probe with a van der Waals radius of 1.52 and default energy cut-off values of over 30 kcal mol^{-1} to determine field energies. In addition, Gasteiger-Huckel charges were calculated. CoMFA and CoMSIA fields were automatically calculated using the standard Sybyl method for each molecule, using the Tripos force field in a cubic grid in all directions.

Partial least square (PLS) statistical analysis

The PLS approach was employed to construct the CoMFA and CoMSIA models, with the activity of the 35 molecules in the training set used as the dependent variable for pattern matching and the pattern descriptors as the independent variables(Şener, Ekici, Gönülalan and Bodur, 2024). Regression analysis using PLS created accurate and focused models. The sp3 carbon with a charge of +1.0 was used to generate all the required fields. Initially, the cross-validated

determination coefficient q^2 and the optimal number of components (ONC) were determined using a cross-validation analysis approach with a Leave-One-Out (LOO) technique. Subsequently, the model was evaluated using a cross-validated analysis based on the determination coefficient (R^2), the standard error of estimation (SEE), and the F-value (Lipscomb, Scott and Schulman, 2010).

ADMET Prediction

The physicochemical and biological properties of small molecules are essential to determine the utility of drug candidates by integrating Lipinski's rules and ADMET predictions using the Swiss-ADMET web server (Daina, Michielin and Zoete, 2017). This resource is freely available. The six designed molecules (M1-M6) and compound 26 were submitted in silico using the five Lipinski rules (Pires, Blundell and Ascher, 2015) molecular weight (MW) ≤500, log p<5, hydrogen bond donors (HBD)≤ 5, number of hydrogen bond acceptors (HBA) ≤ 10, and rotational bonds (nrotb) ≤ 10, and additionally topological polar area (TPS)≤ 140 Water solubility, human intestinal absorption, Molar refractoriness should be between

40 and 130, metabolism, Cytochrome P450 enzymes, synthetic accessibility score and toxicity (Boutalaka et al., 2023).

Molecular docking

Prediction of binding patterns of ligands with target proteins has long been achieved through molecular docking method. Many research and commercial tools are currently available for protein docking. This study used a new molecular docking tool called CB-Dock, identifying binding sites, size, and position of protein and target molecules. The appropriate docking size is based on the query links and performs molecular docking using AutoDock (Kahn, Bosch, Levitt and Goldstein, 1975)the increment in Na ad Cl reabsorbed beyond the proximal tubule. The administration of these agents resulted in an increase in fractional sodium excretion (CNa/GFR). The server collaborates with AutoDock Vina and has undergone extensive optimization to increase the success rate of the created models. In this study, the researchers used the web server http://cao.labshare.cn/cb-dock/(Liu et al., 2020). The data entry includes ligand files in MOL2, MOL, or SDF format for compound 26 and the proposed compounds (M1, M2, M3, M4, M5, and M6.), which were selected as new candidates due to their pharmacokinetic properties (Stitou et al., 2021). In addition, the enzyme (hMAO-B) was also downloaded in PDB format from www.rcsb.org (PDB: 2V60) (Shaukat and Hussain, 2022). Crystallized water molecules, heteroatoms, etc., were automatically removed from the protein when uploaded to the CB-Dock web server. After uploading, CB-Dock uses OpenBabel to read the input files and convert them to pdbqt format (Cao and Li, 2014).

Molecular Dynamics Simulations

The CHARMM-GUI solution builder consists of five steps for setting up a simulation system. In the third step, Periodic Boundary Conditions (PBC) are established by replicating a unit cell in all directions to approximate a larger system. The simulation is then conducted solely for the atoms within the PBC box. Additionally, any unfavorable contacts between atoms are eliminated by performing a short minimization during this step. The fourth and fifth steps involve the equilibration and production phases of the simulation. Equilibration is achieved through two phases: the NVT ensemble (constant number of particles, volume, and temperature) and the NPT ensemble (constant number of particles, pressure, and temperature) (Kahn et al., 1975) the increment in Na ad Cl reabsorbed beyond the proximal tubule. The administration of these agents resulted in an increase in fractional sodium excretion (CNa/GFR). These phases ensure that the system reaches the desired temperature and pressure equilibrium. Input files for equilibration and production, along with anticipated modifications such as the molecular dynamics (MD) run duration and the frequency of energy calculations, are downloaded. GROMACS 2020. 2, a software widely used for MD simulations, was employed for both eqration and production runs in all MD calculations. The simulation setup involved the imposition of PBC considering the shape and size of the system. Non-bonded interactions were handled with a cutoff distance of 12 Å, and the neighbor searching list was buffered using the Verlet cutoff scheme. Long-range electrostatic interactions were treated using the particle mesh Ewald (PME) method. The CHARMM36 force field was applied to the protein-ligand complex. PriorBeforeproduction simulation, an energy minimization step using the steepest descent algorithm was performed with 5000 steps to reduce the system's energy. To stabilize the complex, an equilibration process was conducted (Pajzderska and Gonzalez, 2023). The complex was subjected to an NVT ensemble and an NPT ensemble for duration of 125 ps at a temperature of 300.15 K. Positional restraints of 400 kJ mol^{-1} nm^{-2} and 40 kJ mol^{-1} nm^{-2} was applied to the backbone and side chains, respectively. Following equilibration, a production simulation was conducted for 100 ns in an NPT ensemble at 300.15 K and 1 bar pressure. A

nose-hoover thermostat was employed to maintain a constant temperatured, while a Parrinello-Rahman barostat was used to control the pressure. The LINCS algorithm was utilized to constrain hydrogen bonds based on the inputs provided by CHARMM-GUI. The V-rescale thermostat at 300 K with a coupling constant of 1 ps was employed. Trajectories were stored every 2 ps. The production stage involved performing 100 ns simulations in an NPT assembly(Kidder and Montgomery, 1975).

Binding Energy Calculations

The Poisson-Boltzmann method or the Born MM/PBSA series continuous soluble surfactant is a commonly used and widely accepted method for calculating the binding free energy of a protein-ligand complex. Calculations of the binding free energy and the energy contribution of individual residues were used to estimate the inhibitory affinity of ACHE quantitatively(Fiddian-Green and Silen, 1975). The "g_mmpbsa, a GROMACS tool" was used with default parameters to calculate molecular mechanics potential energy (electrostatic van der Waals interactions) and insoluble energy (non-polar

solubility energies)(Lévêque-Simon et al., 2023).

The binding free energy can be expressed using the following equation:

$$\Delta G_{binding} = \Delta G_{complex} - (\Delta G_{protein} + \Delta G_{ligand})$$

where, $\Delta G_{complex}$ is the total free energy of the protein–ligand complex, and are the total free energies of the isolated protein and ligand in the solvent, respectively(Zwahlen, 2023).

RESULTS AND DISCUSSION

CoMFA analysis

The statistical results of the CoMFA/SE model are listed in (Table 2), where PLS analysis of CoMFA/SE model reveals that 9 was the ideal number of components. Q^2 value was 0.608 (>0.5), the correlation coefficient (R^2) was 0.933, the F value was 38.555, and the standard error (SEE) was 0.307. R^2 test value of 0.70 reflects that molecules in the test set agree with the CoMFA model. Also, it demonstrates the strong predictive ability of the CoMFA/SE model. The contribution of the steric field was 47.4%, which was slightly lower than the contribution of the electrostatic field, which was 52.6%.

Table 2. S E results.

	Q^2	N	SEE	R^2	F	R^2Test
S + E	0.608	9	0.307	0.933	38.555	0.70

CoMSIA analysis

During the CoMSIA analysis, 9 models were built based on the statistical parameter values. The results of these models, using different combinations of five variables, are presented in (Table 3). Among these models, the combined model (CoMSIA/S+E+A+H) showed the best performance with Q^2 = 0.53, R^2 = 0.88, F = 20.463, SEE = 0.41, and ONC = 4. The model

was then validated with the test set, producing an R^2test value of 0.79, indicating its effectiveness and predictive ability compared to other models. Notably, the CoMFA (S+E) model presented higher Q^2 and R^2 values than the (CoMSIA/S+E+A+H) model, making it the most appropriate choice to provide better statistical information in this research(El Bahi, Boutalaka, El Alaouy, et al., 2023).

Table 3. Possibilities of combining (COMSIA) fields.

	Q^2	N	SEE	R^2	F	R^2Test
H	0.527	9	0.417	0.87	19.64	0.673
S+H	0.53	9	0.412	0.879	20.18	0.77
S+E+A+H	**0.53**	**4**	**0.41**	**0.88**	**20.463**	**0.79**
S+E+D+A+H	0.516	5	0.408	0.881	20.637	0.79
D+A+E+H	0.52	5	0.414	0 .878	20.028	0.78
S+D+H	0.463	9	0.439	0.863	17.49	
E+H+S	0.45	7	0.43	0.868	18.28	0.47
H+D	0.40	9	0.426	0.871	18.72	0.53
E+H	0.48	7	0.434	0.866	17.941	044

The actual and predicted activity results of the CoMFA/S+E and COMSIA/S+E+A+H models for hMAO-B inhibitors are presented in (Table 4).

Table 4. Experimental and predicted pIC_{50} of the CoMFA/S+E and COMSIA/S+E+A+H models

N	pIC_{50} (M)	(CoMFA/SE)/(Predicted	residuals)	(COMSIA/SEAH)/(Predicted	Residuals)
1	5.827	5.942	-0.115	5.861	-0.034
2	6.815	7.011	-0.196	7.021	-0.206
3*	5.507	8.274	-2.767	8.079	-2.572
4	8.699	8.602	0.097	8.165	0.534
5	6.001	6.028	-0.027	6.036	-0.035
6	6.023	6.18	-0.157	6.316	-0.293
7	8.68	8.287	0.393	8.215	0.465
8	5.17	5.302	-0.132	5.689	-0.519
9*	6.36	7.059	-0.699	7.401	-1.041
10	5.958	5.849	0.109	5.935	0.023
11	6.117	6.192	-0.075	6.149	-0.032
12	6.521	6.468	0.053	6.455	0.066
13	5.445	5.541	-0.096	5.424	0.021
14	6.526	6.692	-0.166	6.5	0.026
15	6.436	6.32	0.116	6.418	0.018
16*	7.574	5.928	1.646	6.38	1.194
17*	7.882	5.807	2.075	5.162	2.72
18	6.185	6.076	0.109	5.704	0.481
19	6.495	6.356	0.139	6.871	-0.376
20	6.47	6.517	-0.047	6.725	-0.255
21	7.81	7.712	0.098	7.995	-0.185
22*	5.917	7.734	-1.817	7.698	-1.781
23	6.455	6.601	-0.146	6.335	0.12
24*	7.614	5.615	1.999	5.625	1.989
25	6.316	5.993	0.323	6.045	0.271
26	8.769	8.413	0.356	8.16	0.609
27*	6.949	4.867	2.082	5.344	1.605
28	4.892	5.328	-0.436	5.601	-0.709
29	6.238	6.324	-0.086	6.17	0.068
30	5.966	5.865	0.101	6.112	-0.146
31*	6.664	7.196	-0.532	6.865	-0.201
32	7.397	7.433	-0.036	7.52	-0.123
33	7.78	7.446	0.334	7.312	0.468
34	8.521	8.315	0.206	8.515	0.006
35	7.887	8.126	-0.239	8.53	-0.643
36	7.044	7.047	-0.003	6.928	0.116
37*	6.702	6.803	-0.101	6.526	0.176
38	7.735	8.782	-1.047	8.497	-0.762
39	6.26	6.102	0.158	5.981	0.279
40	7.777	7.701	0.076	7.698	0.079
41	6.861	6.435	0.426	6.194	0.667
42	6.276	6.34	-0.064	6.08	0.196
43	5.931	5.924	0.007	6.008	-0.077
44	5.847	5.879	-0.032	5.966	-0.119

* Test set

External validation

In order to assess the predictive capacity of the best CoMFA models developed, external validation was carried out on nine compounds. These compounds were randomly selected and excluded from the initial study.

Table 5. The results of tests carried out by Golbraikh and Tropsha

Parameter	Equation	COMFA	COMSIA	Validation Criteria
R^2 (test)	$R_{test}^2 = 1 - \dfrac{\sum (Y_{pred(test)} - Y_{obs(test)})^2}{\sum (Y_{obs(test)} - \overline{Y}_{obs(test)})^2}$	0.70	0.79	>0.60
r_0^2	$r_0^2 = 1 - \dfrac{\sum (Y_{obs(pred)} - kY_{test(pred)})^2}{\sum (Y_{test(pred)} - \overline{Y}_{test(pred)})^2}$	0.997	0.999	>0.50
r'^2_0	$r'^2_0 = 1 - \dfrac{\sum (Y_{test} - kY_{test})^2}{\sum (Y_{test} - \overline{Y}_{test})^2}$	0.736	0.703	>0.50
Δr_0^2	$\lvert r_0^2 - r'^2_0 \rvert$	0.260	0.296	< 0.30
$\dfrac{(r^2 - r_0^2)}{r^2}$	$\dfrac{(r^2 - r_0^2)}{r^2}$	-0.428	-0.257	< 0.10
$\dfrac{(r^2 - r'^2_0)}{r^2}$	$\dfrac{(r^2 - r'^2_0)}{r^2}$	-0.0547	0.115	< 0.10
K	$k = \dfrac{\sum (Y_{obs} \times Y_{pred})^2}{\sum (Y_{pred})^2}$	0.991	0.997	$0.85 \leq K \leq 1.15$
K'	$k' = \dfrac{\sum (Y_{obs} \times Y_{pred})^2}{\sum (Y_{obs})^2}$	0.943	0.939	$0.85 \leq K' \leq 1.15$

The statistical results show that the CoMFA and CoMSIA/SEHA models have a good predictive quality, corroborated by the coefficients of determination obtained in the non-cross-validation and cross-validation and the predictive ability demonstrated in the external validation. The robustness of the proposed model was assessed using Tropsha and Golbraikh's external validation criteria. The results obtained in the external validation test for the CoMFA and CoMSIA/ SEHA models are presented in (Table 5).

Y-randomization test of model

The quality of the QSAR model was tested by running ten tests with randomized methods, as shown in (Table 6). The results of the Y randomization test showed lower Q^2 and R^2 values than the model in the current study, indicating that the CoMFA/SE model was not obtained in a systematically randomized manner.

Table 6. R^2_{train} and Q^2 LOO values after the Y-randomization experiments.

Model	R	R^2	Q^2
Random 1	0.137	0.018	-0.102
Random 2	0.202	0.041	-0.106
Random 3	0.259	0.067	-0.039
Random 4	0.048	0.002	-0.095
Random 5	0.245	0.06	-0.05
Random 6	0.022	0.0004	-0.128
Random 7	0.07	0.005	-0.15
Random 8	0.0013	0.000	-0.085
Random 9	0.025	0.0006	-0.098
Random 10	0.156	0.024	-0.105
Random Models Parameters			
Average	0.116	0.022	-0.096

Interpretation of model CoMFA contour.

To provide us with clues about the change in chemical composition, a detailed study of the graphical contour maps was performed. Figure 3 shows the contour maps of the selected CoMFA/SE model. The green contours indicate regions favorable for large clustering to increase the activity of the molecule, while the yellow contours indicate regions unfavorable for large clustering to increase the activity (Figure 3A). A medium-sized green contour surrounds a region close to the variant R, indicating that the addition of a large cluster favors better activity. It explained by the fact that compound 9 (pIC$_{50}$ = 6.36), which contains a -CH$_3$ radical in R, has higher activity than compound 8 (pIC$_{50}$ = 5.17), which contains a hydrogen H in the same radical, and the same is true for compounds 21 (pIC$_{50}$ = 7.81) and 20 (pIC$_{50}$ = 6.47). The blue and red color curves, respectively, show the areas where electropositive and electronegative groups are beneficial for activity (Figure 3B). A small red spot near the R1 substituent in the para position of the molecule shows that adding attractive mesomeric groups or strongly electronegative atoms at this location makes inhibition stronger.
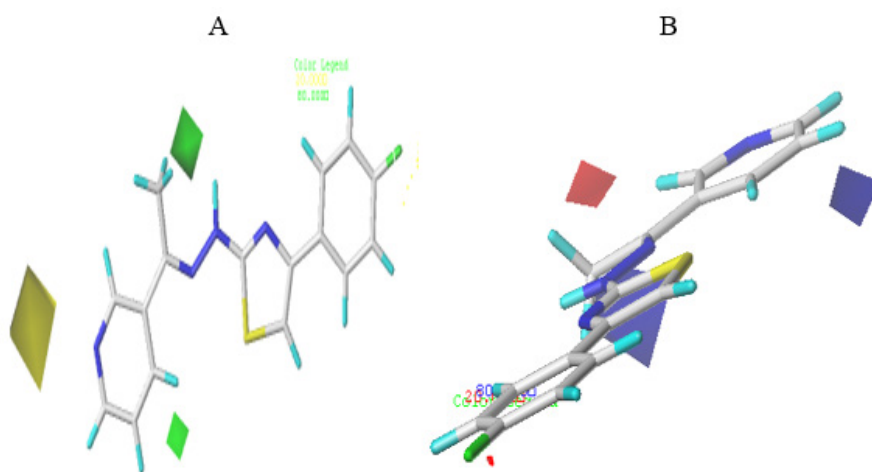
Figure 3. Contour map results of the best developed CoMFA/SE model: (A) Steric field and (B) electrostatic field.

Newly designed compounds

The initial factors affecting the inhibitory activity were identified based on the chemical structures of the proposed (4-alt-thiazole-2-yl) hydrazine derivatives, where the substitutes fitted in appropriate positions utilizing contour maps by using the best CoMFA/SE model that predicts the activity of newly designed candidates, and the data tabulated in (Table 7).

Table 7. Anticipate new designs with their activities and docking score with the CoMFA/SE model.
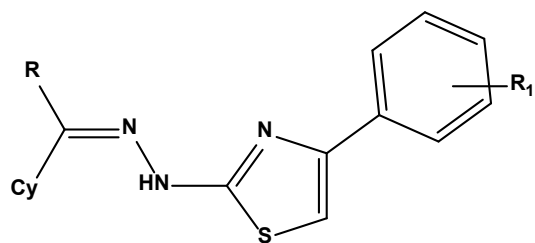
No	Structure			Predicted pIC$_{50}$	Total Score
	Cy	R	R1	CoMFA (SE)	
Comp26		CH$_3$	4-F	8.458	10.5
M1			4-	10.4	11.6
M2			4-	9.73	11.2
M3			4-	9.72	10.2

M4			4-F	9.5	09.7
M5			4-F	9.024	10.8
M6			4-	8.087	11.3
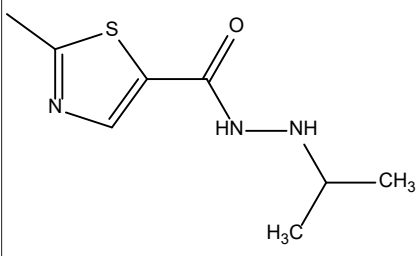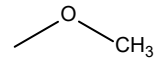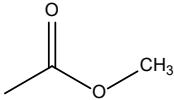
ADME-Tox prediction Drug similarity analysis

The prediction of ADMET characteristics is an essential step to reduce potential subsequent problems in clinical therapies. Therefore, pkCSM (Balerna, Fosset, Chicheportiche, Romey and Lazdunski, 1975) and SwissADME (Parr, Mulley and Rye, 1979) were adopted to predict the ADMET properties of the new (hetero)arylidene-(4-substituted-thiazol-2-yl) hydrazines. (Table 8) shows the Lipinski property profile of the proposed new molecules, while (Table 9) reveals the *in silico* ADMET properties of the new compounds M1, M2, M3, M4, M5, M6, and 26. For a given compound with logP less than 5, molecular weight (MW) (≤500Da), hydrogen bond acceptors (HBAs) less than 10, and hydrogen bond donors (HBDs) less than 5, are considered the best-adsorbed drugs (Base the Lipinski Five). (Table 8) shows that molecules M1, M2, M3, M4, M5, M6, and 26 have logP less than 5, MW less than 500 Da, HBA less than 10 and HBD less than 5, In addition, the total polar area (TPSA) is less than 140 μM, and

the ring bonds (NROTB) are less than 10, indicating that these compounds have better adsorption and bioavailability(Jain, Guin, De and Singh, 2022).

A compound with an intestinal absorption value greater than 30% is also considered resorbable. As shown in (Table 9), all compounds have a value between 50.56% and 92.30%, indicating a good level of intestinal absorption. Cytochrome P450 is an essential enzyme system for drug metabolism in the liver. CYP3A4 is a major variant of cytochrome P450. All proposed molecules are inhibitors and substrates of CYP3A4. In addition, it is important to know the toxicity of the compounds, as an effective drug does not have to be toxic. To this end, the toxicity of the compounds was examined using the Ames test. The results showed that all the newly designed particles were non-toxic, except for the reference compound 26, which remains toxic. For all predicted compounds, the synthetic accessibility score was between 2.95 and 4.36, indicating that they are easily synthesized.

Table 8. Lipinski properties of the new M1-M6 compounds and the reference compound 26.

	26	M1	M2	M3	M4	M5	M6
Lipinski	YES	YES	YES	YES	YES	YES	YES
Log kp (cm/s)	-5.49	-6.09	-5.94	-4.10	-5.25	-5.51	-6.11
Log S	-4.49	-5.04	-5.25	-7.48	-6.02	-5.51	-6.11
Log P	4.18	3.35	3.43	3.8	4.63	3.85	3.11
nHBD	1	4	3	4	3	3	3
nHBA	4	8	8	8	7	8	8
TPSA	78.41	185.08	174.08	194.31	157.01	157.01	183.31
Nrotb	4	9	10	11	9	9	11
MR	87.59	113.12	117.44	128.58	126.42	116.77	123.28
MW	312.36	448.49	462.52	488.58	476.60	448.549	340.42

Table 9. In silico ADMET properties of the proposed new compounds and reference compound 26.

Comp	Intestinal absorption (human) Numeric (% Absorbed)	CYP1A2 inhibitor	CYP2C19 inhibitor	CYP2C9 inhibitor	CYP2D6 inhibitor	CYP3A4 inhibitor	AMES toxicity	Synthetic Accessibility
26	92.304	YES	YES	YES	NO	YES	**YES**	2.95
M1	85.11	YES	NO	YES	NO	YES	NO	3.89
M2	78.66	YES	NO	YES	NO	YES	NO	4.03
M3	50 .56	NO	NO	NO	NO	YES	NO	4.32
M4	83.12	NO	YES	YES	NO	YES	NO	4.36
M5	88.18	YES	NO	YES	NO	YES	NO	4.13
M6	68.50	NO	NO	YES	NO	YES	NO	4.17

Docking results

To understand the quantitative link between structure and activity provided by the 3D-QSAR model, it is necessary to understand the method of ligand-receptor binding, which is typically studied by molecular docking. Using the online web service Atlas of Protein Communications, we identified the amino acids of interest, evaluated their chemical characteristics, and examined the important residues in the active site prior to docking (http://www.mrc-lmb.cam.ac.uk/pca/). The asteroid diagram, a new method of interaction analysis, uses a multilayer representation of non-covalent interactions. The Protein Contact Atlas was used to create asteroid diagrams of these protein structures (Figure 4A) (El Bahi, Boutalaka, Alaqarbeh, et al., 2023). For amino acids that form strong contacts with the first shell amino acids, Arg42, Glu34, Glu58, Met436, Tyr398, Tyr435, Tyr60, and Arg41, all have significant affinity for hMAO-B. The number of atomic connections is also indicated by the thickness of the blue matrices in (Figure 4B). These results provided us with the crucial data we needed to evaluate the response patterns of the chemicals studied.

A

B
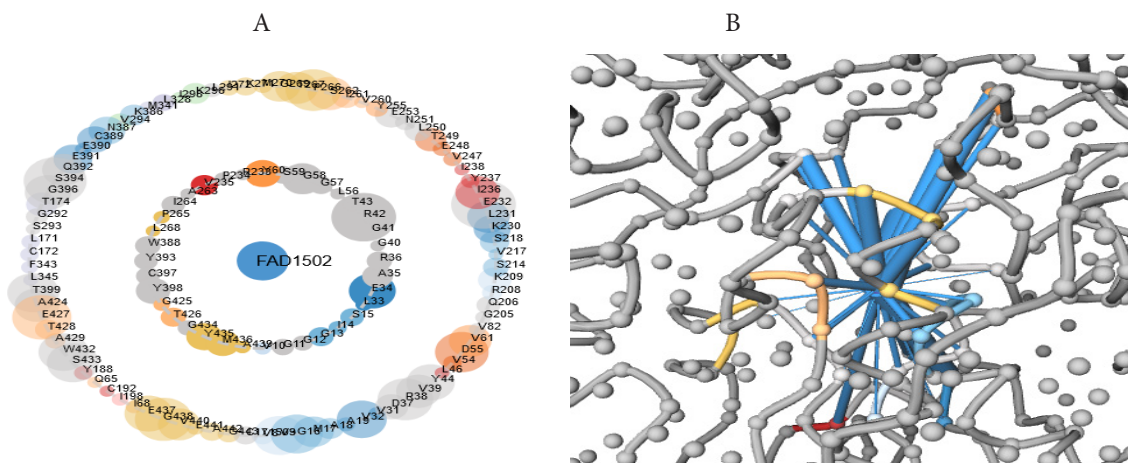
Figure 4. Asteroid graph and network view of protein-ligand interactions.

In order to validate the 3D QSAR method, this section focuses on the molecular docking methodology to obtain data on the structural basis and likely interaction between the ligand variants and the receptor. (Figure 4 and 5) illustrate the molecular docking interactions between the most active molecule 26, the recommended compound M1, and the hMAO-B receptor (PDB: 2V60). As shown in (Figure 5), compound 26 exhibits conventional hydrogen bonding interactions with residues Ile14, Ser15, and Gly434. A stacked Pi-pi interaction with residues Tyr398, Tyr435. a Pi-sulfur interaction with residue Cys397. Pi-alkyl interactions with residues Ala439, Arg42, Met436, Tyr398. and a Pi-sigma interaction with residue Tyr435. The presence of these interactions increases their biochemical efficiency as hMAO-B inhibitors. Using CB-DOCK software, the docking score was -10.5 kcal/mol. The interactions of the complex (compound M1- hMAO-B) were presented as shown in (Figure 6), which shows a Pi-pi interaction stacked with residue Tyr435. a Pi-alkyl interaction with residues Ala439, Arg42, and Met436,

In addition(Moulay Ahfid El Alaouy et al., 2021). a Pi-sulfur interaction with residues Cys397 and Tyr60. a hydrogen-carbon bond interaction with residue Gly13 and Glu58. And a stacked Pi-amide interaction with residue Tyr435. Similarly, for hydrogen bonding, classical hydrogen bonding type interactions are observed with residues Ile14, Ser15, Gln206, Met436, Tyr435, Tyr60, and Ser59. This binding plays a major role in the stability of the molecules. Due to the higher contacts of compound M1 with hMAO-B enzyme residues, the docking score was -11 kcal/mol, which is better than that of compound 26. The key residues obtained in the docking results presented above corresponded to the critical residues in the large circles of the AChE main chain. The type and number of interactions indicate that the M1 molecule has strong inhibitory activity against the hMAO-B enzyme. In addition, the results showed that the recommended chemical compound M1 has higher stability for the active site of hMAO-B enzyme. At the same time, the 3D-QSAR and docking results were consistent.
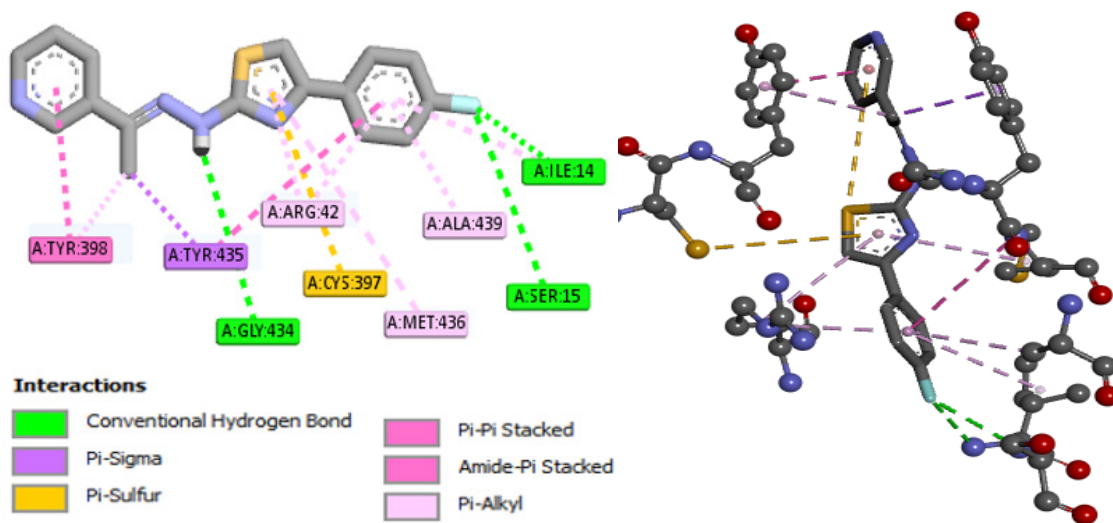
Figure 5. 2D and 3D Docking represent the interactions of the most active compounds at receptor binding sites.
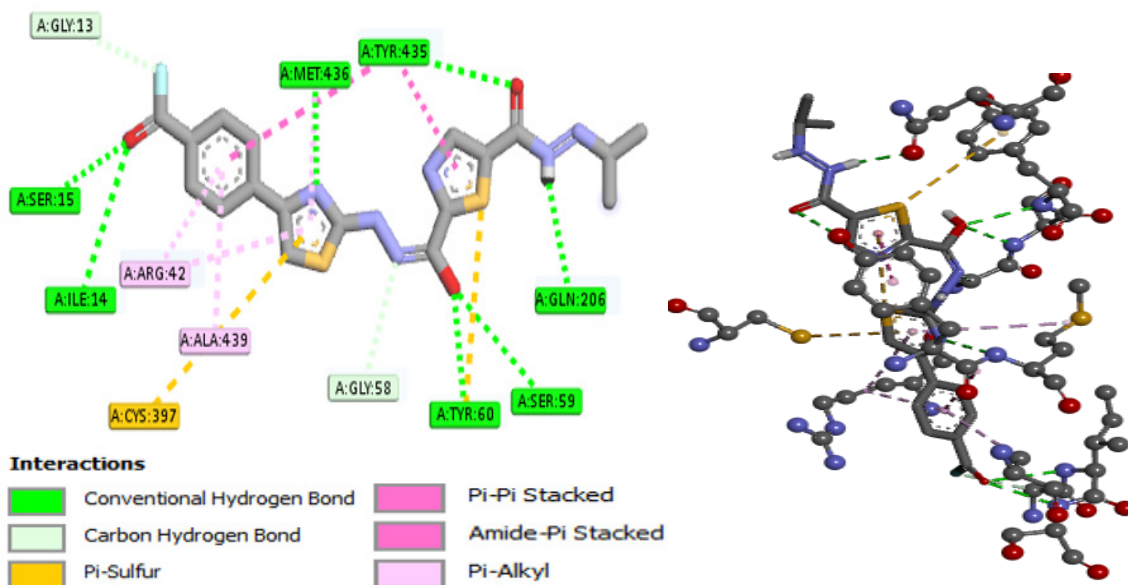
Figure 6. 2D and 3D Docking represent the interactions of the most active compound M1 at receptor binding sites.

Stability of protein-bond interactions in MD simulations

The binding stability of the two best compounds, hMAO-B-26 and hMAO-B-M1, was investigated using simulated MD calculations for 100 ns at typical room temperature settings. After simulation, visualization of the tracks indicated that all ligands remained bound to the protein pocket via the ligand-binding groove. To test the stability of each structure, RMSD, RMSF, **556**

radius of rotation, hydrogen bonding, mean center of mass (COM) between protein and linker, and binding free energy calculations (MMPBSA) were performed to assess the stability of each structure (El Alaouy et al., 2023).

RMSD graphs in (Figure 7A) show the complex, protein backbone and ligand RMSD for each structure. Complex and Backbone RMSD show an increasing and fluctuating pattern for both complexes until it

stabilizes at 70ns for Comp26 and 50ns for M1 with average values of 3.8A and 4A, respectively. The radius of gyration analysis (Figure 7C) is also consistent with RMSD results for the complexes, showing very little fluctuations for both compounds (less than 1 A) with values between 23.5 and 24. *A for Comp26 and 23.3 and 23.9 A for M1* throughout the whole simulation, which indicates the compactness and the stability of the protein-ligand system (El Alaouy et al., 2023).

Using the GROMACS software, the RMSF of the protein complex was determined based on the "C-alpha" atoms. In general, the fluctuation intensity remains below 2.0 for all compounds, except for a few residues that are loops or spins in the protein (Figure 7B).

(Figure 8A), shows the total number of hydrogen bonds created between the ligand and the protein during the 100 ns of the simulation. Both ligands maintained at least one hydrogen bond with the protein during the whole simulation time. (Figure 8B) shows the average distance of the center of mass between the ligand and the protein during 100 ns of simulation time. Both ligands maintain a stable COM distance from the protein within 2 Å or less of fluctuations. Using the contact Freq.tcl module in VMD and a threshold of 4 Å, a contact frequency (CF) study was performed to better assess the binding between the [protein] and the ligands tested. The residues with higher CF% are shown in (Figure 9). The residues with the highest contact frequency in all simulations were ILE14, ARG42, GLY58, TYR60, LEU171, CYS172, PHE343, TYR398, THR4,

GLY434, TYR435, MET436 and ALA439. Principal Component Analysis (PCA) of the complexes was performed using the Bio3D program in R, and the results are depicted in (Figure 10 A). Additionally, the program was used to calculate the dynamic cross-correlated motions (DCCM) of protein residues. The DCCM analysis assigns colors ranging from red to white to blue, indicating the intensity of correlated motion between residues. Blue colors represent negative correlation, white indicates no correlation, and red color signifies positive correlation in the motions between residues. (Figure 10 B).

MM/PBSA (Molecular Mechanics/Poisson Boltzmann Surface Area) method is a fast force field-based approach for calculating bond free energies. The G-mmpbsa software was utilized in this study to compute the MM/PBSA values. The calculated binding free energy values are presented in (Table 10). In conclusion, compounds M1 and 26 exhibited remarkable stability throughout the 100 ns MD simulation based on analyses of RMSD, Rg, RMSF, SASA, and hydrogen bonding between the protein and ligand. Additionally, the average distance between the ligand and protein complexes remained consistent. However, pathway analysis and MM/PBSA measurements of binding free energy revealed that compound 26 exhibited the highest binding free energy, while compound M1 exhibited the lowest binding free energy. Therefore, compound M1 demonstrated higher activity as an enzyme inhibitor compared to compound 26.

Table 10. Calculated binding free energies of tested compounds [kJ/mol]

Complex	ΔG	Van der Waal Energy	Electrostatic energy	Polar solvation energy	SASA energy
Comp26	- 134.288 +/- 15.082 kJ/mol	-199.514 +/- 8.970 kJ/mol	-94.064 +/- 14.525 kJ/mol	178.053 +/- 10.415 kJ/mol	-18.764 +/- 0.576 kJ/mol
M1	-150.506 +/- 12.354 kJ/mol	281.052 +/- 7.595 kJ/mol	63.585 +/- 12.016 kJ/mol	219.398 +/- 14.268 kJ/mol	-25.267 +/- 0.887 kJ/mol
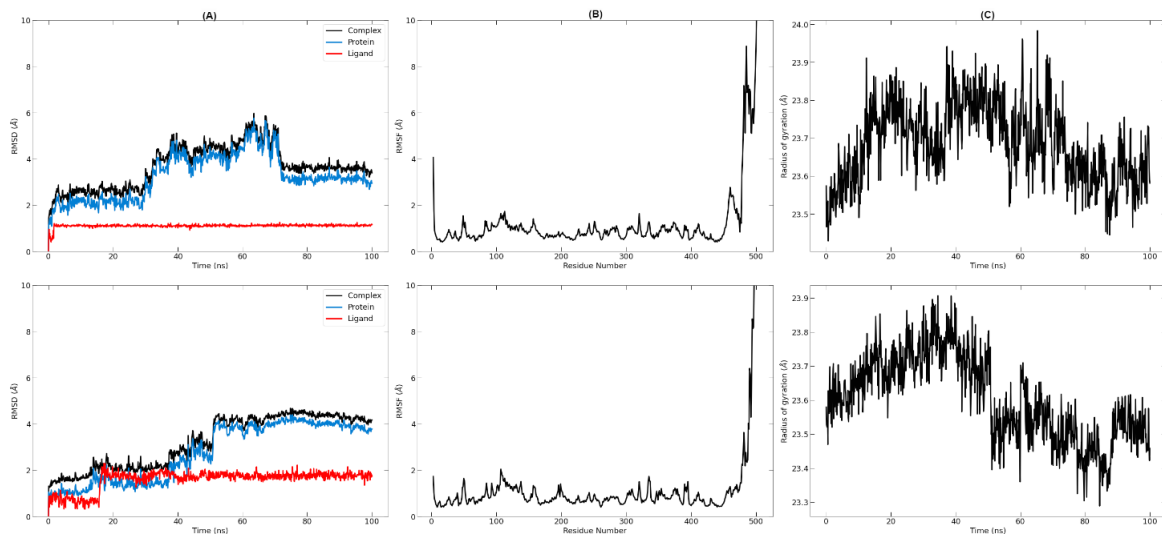
Figure 7. (A) RMSD, (B) RMSF and (C) Radius of gyration of the complexes during 100ns MD simulation. Compounds Comp26 (top) and M1 (bottom)
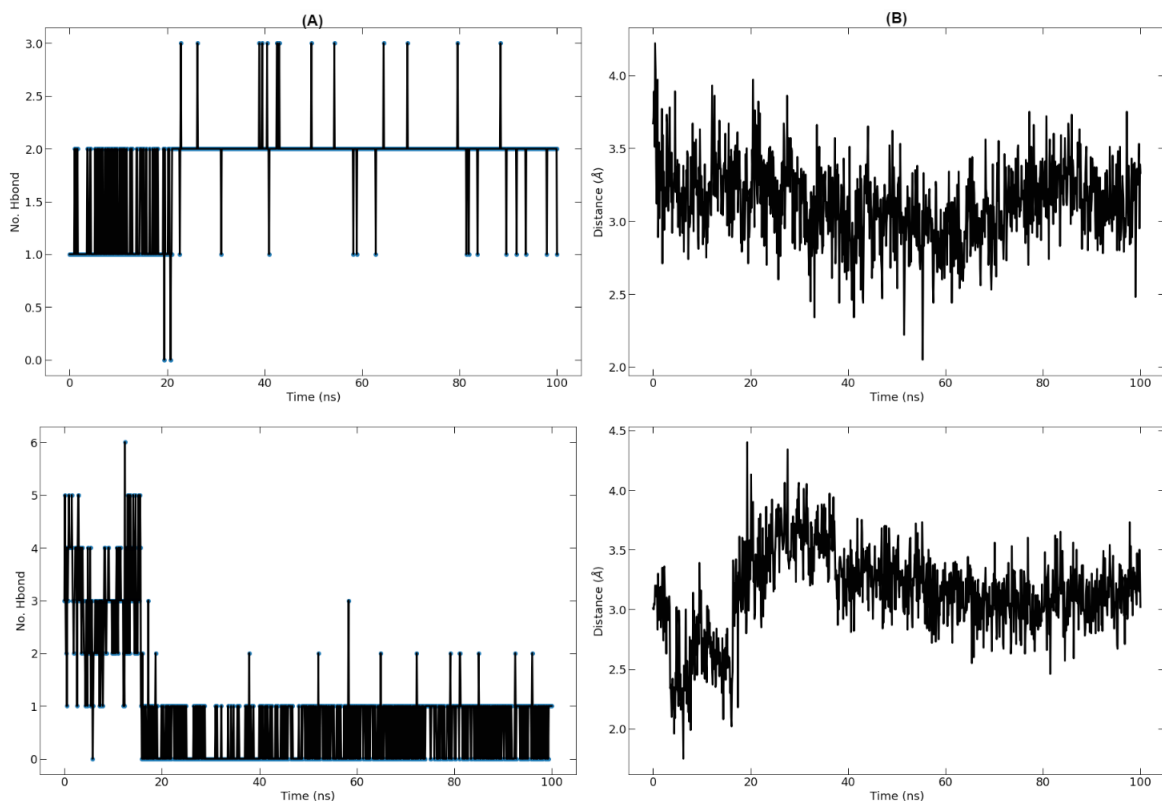
Figure 8. (A) Hydrogen Bonds (Protein-ligand) and (B) Average distance between Ligand and the Protein of the complexes during 100ns MD simulation. Compounds Comp26 (top) and M1 (bottom)
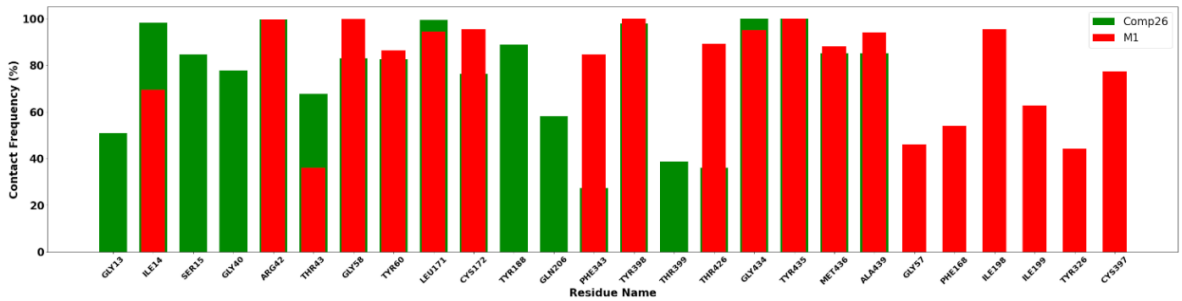
Figure 9. Contact frequency analysis
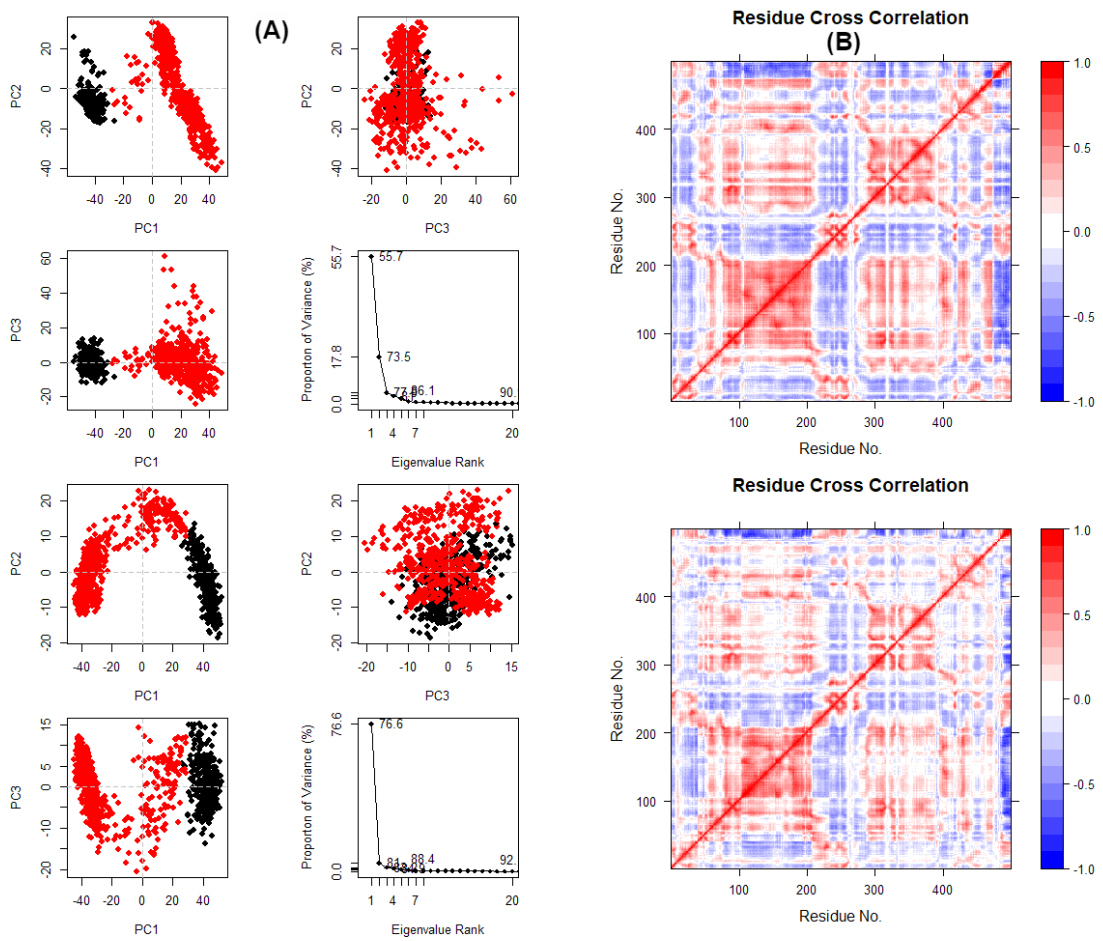
Figure 10. From left to right: **(A)** Principal Component Analysis and **(B)** Dynamic Cross-Correlation Matrix Analysis (DCCM).

CONCLUSION

Monoamine oxidase B (hMAO-B) is an attractive target for drug design because its inhibition regulates the levels of various neurotransmitters in the central nervous system. Molecules that act selectively on one of the hMAO-B isoforms have been widely studied. In this manuscript, 3D-QSAR models were developed using CoMFA/SE, and the excellent statistical results (Q^2 = 0.608; R^2 = 0.933; R^2Test = 0.7) indicate that the CoMFA/SE model has excellent predictive capabilities. Furthermore, the contour maps generated by the best CoMFA/SE model were used to develop new derivatives with increased activity. Furthermore, the docking simulations were confirmed by highlighting the potential interactions of the proposed compound M1 and the reference compound 26 with the crystal structure of hMAO-B. Molecular docking between the proposed M1 complex and the protein crystal structure (PDB: 2V60) showed that it underwent a classical hydrogen-bonding type interaction with the major and non-key residues Ile14, Ser15, Gln206, Met436, Tyr435, Tyr60, and Ser59 as well as other interactions more important than complex 26, where hydrogen bonds are responsible for the inhibitory activity(Hirenallure Maheshwarappa et al., 2022). Thus, the proposed M2 complex is more stable towards the selected protein than the reference complex 26. In addition, the MD simulation results show that both studied compounds are well stable based on the analyses of (RMSD, RMSF, RG, Contact frequency analysis, hydrogen bonding (protein-ligand) and the average distance between the bond and the protein complexes during 100 ns. Furthermore, compound 26 and the proposed compound M1 showed hMAO-B binding free energies of -134.288 kJ/mol and -150.506 kJ/mol, respectively. Thus, it can be said that compound M1 is more active than compound 26. For these newly designed molecules, prediction of Lipinski's rule and ADMET properties is essential, and similarities were observed in their pharmacokinetics. The compounds generally have good absorption, distribution and metabolism properties and are non-toxic, except for the reference compound 26 which remains toxic. The results obtained in this work clearly indicate that compound M1 has a strong potential to become promising in the treatment of several neurodegenerative diseases, such as Parkinson's diseases.

AUTHOR CONTRIBUTION STATEMENT

Moulay Ahfid El Alaouy: article writing, graph preparation, data analysis and interpretation; Marwa Alaqarbeh: paper writing, analyzed and interpreted molecular dynamic simulation data; Abdelouahid Sbai, Tahar Lakhlifi and Mohammed Bouachrine: project review, editing and supervision.

CONFLICT OF INTEREST

The authors declare that there is no conflict of interest.

REFERENCES

Aanouz, I., Belhassan, A., El-Khatabi, K., Lakhlifi, T., El-ldrissi, M. and Bouachrine, M. (2021). Moroccan Medicinal plants as inhibitors against SARS-CoV-2 main protease: Computational investigations. *Journal of Biomolecular Structure and Dynamics*, *39*(8), 2971-2979. doi:10.1080/07391102.2020.1758790

Anastassova, N., Aluani, D., Hristova-Avakumova, N., Tzankova, V., Kondeva-Burdina, M., Rangelov, M., … Yancheva, D. (2022). Study on the Neuroprotective, Radical-Scavenging and MAO-B Inhibiting Properties of New Benzimidazole Arylhydrazones as Potential Multi-Target Drugs for the Treatment of Parkinson's Disease. *Antioxidants*, *11*(5), 884. doi:10.3390/antiox11050884

Balerna, M., Fosset, M., Chicheportiche, R., Romey, G. and Lazdunski, M. (1975). Constitution and properties of axonal membranes of crustacean nerves. *Biochemistry*, *14*(25), 5500-5511. doi:10.1021/bi00696a019

Boutalaka, M., El Bahi, S., Alaqarbeh, M., El Alaouy, M. A., Koubi, Y., Khatabi, K. E., … Lakhlifi, T. (2023). Computational investigation of imidazo[2,1-b]oxazole derivatives as potential mutant BRAF kinase inhibitors: 3D-QSAR, molecular docking, molecular dynamics simulation, and ADMETox studies. *Journal of Biomolecular Structure and Dynamics*, 1-20. doi: 10.1080/07391102.2023.2233629

Bozbey, İ., Taşkor Önel, G., Türkmenoğlu, B., Gürsoy, Ş. and Dilek, E. (2022). Novel (p-tolyl)-3(2H)-pyridazinone derivatives containing substituted-1,2,3-triazole moiety as new anti-Alzheimer agents: Synthesis, in vitro and in silico assays. *Fabad Journal of Pharmaceutical Sciences*. doi:10.55262/fabadeczacilik.1128446

Cao, Y. and Li, L. (2014). Improved protein–ligand binding affinity prediction by using a curvature-dependent surface-area model. *Bioinformatics*, *30*(12), 1674-1680. doi:10.1093/bioinformatics/btu104

Chimenti, F., Maccioni, E., Secci, D., Bolasco, A., Chimenti, P., Granese, A., … Distinto, S. (2007). Selective Inhibitory Activity against MAO and Molecular Modeling Studies of 2-Thiazolylhydrazone Derivatives. *Journal of Medicinal Chemistry*, *50*(4), 707-712. doi:10.1021/jm060869d

Chimenti, F., Secci, D., Bolasco, A., Chimenti, P., Granese, A., Carradori, S., … Langer, T. (2010). Synthesis, semipreparative HPLC separation, biological evaluation, and 3D-QSAR of hydrazothiazole derivatives as human monoamine oxidase B inhibitors. *Bioorganic & Medicinal Chemistry*, *18*(14), 5063-5070. doi:10.1016/j.bmc.2010.05.070

Daina, A., Michielin, O. and Zoete, V. (2017). SwissADME: A free web tool to evaluate pharmacokinetics, drug-likeness and medicinal chemistry friendliness of small molecules. *Scientific Reports*, *7*(1), 42717. doi:10.1038/srep42717

Dhiman, P., Malik, N., Sobarzo-Sánchez, E., Uriarte, E. and Khatkar, A. (2019). Quercetin and Related Chromenone Derivatives as Monoamine Oxidase Inhibitors: Targeting Neurological and Mental Disorders. *Molecules*, *24*(3), 418. doi:10.3390/molecules24030418

El Alaouy, M. A., El Bahi, S., Boutalaka, M., Ouabane, M., Sbai, A., Maghat, H., … Lakhlifi, T. (2023). Organic compounds based on 1-(prop-2-yn-1-ylamino)-2,3-dihydro-1H-indene-4-thiol as selective human monoamine oxidase B inhibitors. Quantitative analysis of structure-activity relationships and in-silico investigations. *Moroccan Journal of Chemistry*, *Vol. 11*, Mor. J. Chem. 11 N°3 (2023) 802-817 Pages. doi:10.48317/IMIST.PRSM/MORJCHEM-V11I3.40986

El Alaouy, Moulay Ahfid, Alaqarbeh, M., Ouabane, M., Zaki, H., ElBouhi, M., Badaoui, H., … Bouachrine, M. (2023). Computational Prediction of 3,5-Diaryl-1H-Pyrazole and spiropyrazolines derivatives as potential acetylcholinesterase inhibitors for alzheimer disease treatment by 3D-QSAR, molecular docking, molecular dynamics simulation, and ADME-Tox. *Journal of Biomolecular Structure and Dynamics*, 1-14. doi:10.1080/07391102.2023.2252116

El Alaouy, Moulay Ahfid, Youness, M., Boutalaka, M., Elbouhi, M., Elmernissi, R., Sbai, A., … Bouachrine, M. (2021). The 2D-QSAR study, Drug likeness and in-silico ADMET prediction of about 3,5-diaryl-1H-pyrazole derivatives as multifunctional agents for the treatment of Alzheimer's disease. *RHAZES: Green and Applied Chemistry*, 09-28 Pages. doi:10.48419/IMIST.PRSM/RHAZES-V13.28095

El Bahi, S., Boutalaka, M., Alaqarbeh, M., El Alaouy, M. A., Koubi, Y., El Khatabi, K., … Lakhlifi, T. (2023). In-Silico Investigation of Osimertinib Based Compounds as Potential Double Mutant EGFR Kinase Inhibitors Against H1975 Cell Line: Integrating QSAR Modeling, Molecular Docking, MD Simulations, and ADME/Tox Studies. *Chemistry Africa*. doi:10.1007/s42250-023-00744-x

El Bahi, S., Boutalaka, M., El Alaouy, M. A., Bouamrane, S., Alaqarbeh, M., Choukrad, M., … Lakhlifi, T. (2023). Computational investigation of novel pyrimidine derivatives as potent FAK inhibitors *via* 3D-QSAR, molecular docking, molecular dynamics simulation and retrosynthesis. *New Journal of Chemistry*, *47*(27), 12816-12829. doi:10.1039/D3NJ02471G

Fiddian-Green, R. and Silen, W. (1975). Mechanisms of disposal of acid and alkali in rabbit duodenum. *American Journal of Physiology-Legacy Content*, *229*(6), 1641-1648. doi:10.1152/ajplegacy.1975.229.6.1641

Hirenallure Maheshwarappa, C., Kamsagara Linganna, K., Bommenahalli Revanappa, P. K., Mehdi, S., Ayachit, S., Suman, S., … Eswaran, S. (2022). Novel Glitazones Reverses Hyperglycemia In STZ Induced Hyperglycaemic Rat Model. *Fabad Journal of Pharmaceutical Sciences*, 73-82. doi:10.55262/fabadeczacilik.1078895

Jain, P., Guin, M., De, A. and Singh, M. (2022). Molecular docking, synthesis, anticancer activity, and computational investigations of thiazole-based ligands and their Cu(II) complexes. *Journal of Physical Organic Chemistry*, e4384. doi:10.1002/poc.4384

Kahn, T., Bosch, J., Levitt, M. F. and Goldstein, M. H. (1975). Effect of sodium nitrate loading on electrolyte transport by the renal tubule. *The American Journal of Physiology*, *229*(3), 746-753. doi:10.1152/ajplegacy.1975.229.3.746

Kidder, G. W. and Montgomery, C. W. (1975). Oxygenation of frog gastric mucosa in vitro. *The American Journal of Physiology*, *229*(6), 1510-1513. doi:10.1152/ajplegacy.1975.229.6.1510

Kondeva-Burdina, M., Mitkov, J., Valkova, I., Peikova, L., Georgieva, M. and Zlatkov, A. (2022). Quantitative Structure–Neurotoxicity Assessment and In Vitro Evaluation of Neuroprotective and MAO-B Inhibitory Activities of Series N-substituted 3-(1,3,7-trimethyl-xanthin-8-ylthio)propanehydrazides. *Molecules*, *27*(16), 5321. doi:10.3390/molecules27165321

Lévêque-Simon, K., Camper, A., Taïeb, R., Caillat, J., Lévêque, C. and Giner, E. (2023). Production of positronium chloride: A study of the charge exchange reaction between Ps and Cl. doi:10.48550/ARXIV.2305.17078

Lipscomb, T. P., Scott, D. P. and Schulman, F. Y. (2010). Primary site of sea lion carcinomas. *Veterinary Pathology*, *47*(1), 185; author reply 186. doi:10.1177/0300985809354348

Liu, Y., Grimm, M., Dai, W., Hou, M., Xiao, Z.-X. and Cao, Y. (2020). CB-Dock: A web server for cavity detection-guided protein–ligand blind docking. *Acta Pharmacologica Sinica*, *41*(1), 138-144. doi:10.1038/s41401-019-0228-6

Lu, Y., Gao, X., Dong, Y., Wang, T., Chen, H.-L., Maob, H., … Guo, S. (2018). Preparing bulk ultrafine-microstructure high-entropy alloys *via* direct solidification. *Nanoscale*, *10*(4), 1912-1919. doi:10.1039/C7NR07281C

Nagatsu, T. (1997). Isoquinoline neurotoxins in the brain and Parkinson's disease. *Neuroscience Research*, *29*(2), 99-111. doi:10.1016/S0168-0102(97)00083-7

Pajzderska, A. and Gonzalez, M. A. (2023). Molecular Dynamics Simulations of Selected Amorphous Stilbenoids and Their Amorphous Solid Dispersions with Poly(Vinylpyrrolidone). *Journal of Pharmaceutical Sciences*, *112*(9), 2444-2452. doi:10.1016/j.xphs.2023.03.013

Parr, G. D., Mulley, B. A. and Rye, R. M. (1979). The effect of carbonic anhydrase binding on the pharmacokinetics of chlorthalidone [proceedings]. *The Journal of Pharmacy and Pharmacology*, *31 Suppl*, 42P. doi:10.1111/j.2042-7158.1979.tb11590.x

Pires, D. E. V., Blundell, T. L. and Ascher, D. B. (2015). pkCSM: Predicting Small-Molecule Pharmacokinetic and Toxicity Properties Using Graph-Based Signatures. *Journal of Medicinal Chemistry*, *58*(9), 4066-4072. doi:10.1021/acs.jmedchem.5b00104

Secci, D., Bolasco, A., Carradori, S., D'Ascenzio, M., Nescatelli, R. and Yáñez, M. (2012). Recent advances in the development of selective human MAO-B inhibitors: (Hetero)arylidene-(4-substituted-thiazol-2-yl)hydrazines. *European Journal of Medicinal Chemistry*, *58*, 405-417. doi:10.1016/j.ejmech.2012.10.032

Shaukat, A. and Hussain, K. (2022). Quercetin Based Standardization Of Polyherbal Anti-Gout Remedy And İts Molecular Docking Study Against Anti-Gout And Anti-İnflammatory Protein Targets. *Fabad Journal of Pharmaceutical Sciences*. doi:10.55262/fabadeczacilik.1085825

Stamm, O., Latscha, U., Janecek, P. and Campana, A. (1976). Development of a special electrode for continuous subcutaneous pH measurement in the infant scalp. *American Journal of Obstetrics and Gynecology*, *124*(2), 193-195. doi:10.1016/s0002-9378(16)33297-5

Şener, K., Ekici, M., Gönülalan, E. M. and Bodur, E. (2024). Comparative Study of The Anti-Inflammatory Pathway Enzyme Activities of Selected Plant Extracts from Lamiaceae Family. *Fabad Journal of Pharmaceutical Sciences*. doi:10.55262/fabadeczacilik.1391109

Vicente-Zurdo, D., Brunetti, L., Piemontese, L., Guedes, B., Cardoso, S. M., Chavarria, D., … Santos, M. A. (2023). Rivastigmine–Benzimidazole Hybrids as Promising Multitarget Metal-Modulating Compounds for Potential Treatment of Neurodegenerative Diseases. *International Journal of Molecular Sciences*, *24*(9), 8312. doi:10.3390/ijms24098312

Yang, C., Wang, W., Liang, J.-X., Li, G., Vellaisamy, K., Wong, C.-Y., … Leung, C.-H. (2017). A Rhodium(III)-Based Inhibitor of Lysine-Specific Histone Demethylase 1 as an Epigenetic Modulator in Prostate Cancer Cells. *Journal of Medicinal Chemistry*, *60*(6), 2597-2603. doi:10.1021/acs.jmedchem.7b00133

Yücel, Y. Y. and Özdemir, E. (2023). Determination of Biological Activities of Salvia sclarea L. *Fabad Journal of Pharmaceutical Sciences*. doi:10.55262/fabadeczacilik.1293118

Zwahlen, T. A. (2023). Landscapes of DNA Mechanics and Genomes. doi:10.5075/EPFL-THESIS-8784

Innovative Approaches in Mirtazapine Delivery: Pharmacokinetic Simulations, Immediate Release to Controlled-Release Tablets, Formulation Optimization via D-optimal Mixture Design

Srk Raju SAGIRAJU*°, Pankaj Kumar SHARMA**, Jaya SHARMA***

Innovative Approaches in Mirtazapine Delivery: Pharmacokinetic Simulations, Immediate Release to Controlled-Release Tablets, Formulation Optimization via D-optimal Mixture Design

Mirtazapin Dağıtımında Yenilikçi Yaklaşımlar: Farmakokinetik Simülasyonlar, Hızlı Salımdan Kontrollü Salım Tabletlerine, D-Optimal Karışım Tasarımı Yoluyla Formülasyon Optimizasyonu

SUMMARY

This research study describes the formulation and evaluation of Mirtazapine Controlled-Release (CR) Tablets, intended to improve therapeutic efficacy and patient compliance. Utilizing pharmacokinetic data from the USFDA-approved Remeron Immediate-Release (IR) Tablets, we constructed a plasma profile curve and calculated the following pharmacokinetic parameters Cmax, T max, AUC, Vd, and Ke. The principle of superposition method was employed to simulate steady-state plasma concentrations (Css), establishing target Css max and Css min values. These targets guided the development of our controlled-release formulation, which was designed to achieve a zero-order release mechanism. The dose and release rate of the proposed controlled-release tablets were precisely adjusted to meet the targeted Css max and Css min concentrations. Our formulation strategy utilized different hydrophilic polymers such as HPMC, Carbopol, and Polyethylene oxide to create a robust ER matrix, we employed D Optimal Mixture Design to optimize the concentration of these three critical formulation variables. Dissolution studies were conducted in different media such as 0.01 N HCl, pH 4.5 Acetate buffer, and pH 6.8 Phosphate buffer for 14 hours to evaluate the rate, extent, and drug release kinetics. The successful simulation of plasma concentrations, followed by adjustments of dose, release rate, and subsequent optimization of formulation variables using the Design of experiments yielded a CR tablet that meets the pharmacokinetic endpoints set by the IR reference. This innovative approach to Mirtazapine CR tablet formulation could significantly enhance patient compliance by providing a more consistent and controlled drug delivery system.

Key Words: *Pharmacokinetic Simulations, Principle of superposition, Zero-Order release and absorption model. IR to CR conversions, Fluctuation index, Steady-state plasma concentration prediction.*

ÖZ

Bu çalışma, terapötik etkinliği ve hasta uyumunu iyileştirmeyi amaçlayan Mirtazapin Kontrollü Salım (CR) Tabletlerinin formülasyonunu ve değerlendirilmesini açıklamaktadır. USFDA onaylı Remeron Hızlı Salımlı (IR) Tabletlerden elde edilen farmakokinetik verileri kullanarak bir plazma profil eğrisi oluşturduk ve farmakokinetik parametreleri Cmax, Tmax, AUC, Vd ve Ke olarak hesapladık. Kararlı durum plazma konsantrasyonlarını (Css) simüle etmek için süperpozisyon yöntemi prensibi kullanıldı ve hedef Cssmax ve Cssmin değerleri belirlendi. Bu hedefler, sıfır-dereceli bir salım mekanizması elde etmek üzere tasarlanan kontrollü salım formülasyonunun geliştirilmesine rehberlik etmiştir. Önerilen kontrollü salım sağlayan tabletlerin dozu ve salım hızı, hedeflenen Css max ve Css min konsantrasyonlarını karşılayacak şekilde hassas bir şekilde ayarlanmıştır. Formülasyon stratejimiz doğrultusunda, sağlam bir ER matrisi oluşturmak için HPMC, Karbopol ve Polietilen oksit gibi farklı hidrofilik polimerleri kullandık; bu üç kritik formülasyon değişkeninin konsantrasyonunu optimize etmek için D Optimal Karışım Tasarımını kullandık. İlaç salım hızını, miktarını ve ilaç salım kinetiğini değerlendirmek amacıyla 0.01 N HCl, pH 4.5 Asetat tamponu ve pH 6.8 Fosfat tamponu gibi farklı ortamlarda 14 saat süreyle çözünme hızı çalışmaları yapıldı. Plazma konsantrasyonlarının başarılı bir şekilde simülasyonu, ardından doz ve salım hızının ayarlanması ve ardından deney tasarımı kullanılarak formülasyon değişkenlerinin optimizasyonu sonucunda IR referansı tarafından belirlenen farmakokinetik uç noktaları karşılayan bir CR tableti elde edilmiştir. Mirtazapin CR tablet formülasyonuna yönelik bu yenilikçi yaklaşım, daha tutarlı ve kontrollü bir ilaç iletim sistemi sağlayarak, hasta uyumunu önemli ölçüde artırabilir.

Anahtar Kelimeler: *Farmakokinetik Simülasyonlar, Süperpozisyon prensibi, Sıfır-dereceli salım ve absorpsiyon modeli, IR-CR dönüşümleri, Dalgalanma indeksi, Kararlı durum plazma konsantrasyonu tahmini.*

---

* ORCID: 0009-0003-8844-4633, Research Scholar of Pharmacy, Apex university, Jaipur, Rajasthan,302018, India
** ORCID: 0000-0001-7398-2744, Dean of Pharmacy, Apex University, Jaipur, Rajasthan,302018, India
*** ORCID:0000-0002-1406-6225, Principal School of Pharmacy, Apex University, Jaipur, Rajasthan, India

° Corresponding Author; SRK Raju Sagiraju
E-mail: raaju42@gmail.com

INTRODUCTION

Mirtazapine (Jilani et al., 2023) is an atypical antidepressant, indicated for the treatment of a major depressive disorder. Mirtazapine belongs to the group of tetracyclic antidepressants. Mirtazapine exhibits an absolute bioavailability of approximately 50% due to extensive first-pass metabolism in the gut wall. It demonstrates linear pharmacokinetics within the 15-45 mg dose range. The time to reach maximum plasma concentration (T_{max}) is around 2 hours, and its plasma protein binding is approximately 85% (Timmer et al., 2000). The conventional immediate-release (IR) formulations of Mirtazapine, showed a wider fluctuation index (FI) due to a sharp rise and drop in plasma concentrations, to address these challenges, the development of a controlled-release (CR) formulation is a logical progression in the evolution of Mirtazapine's clinical application.

The objective of this study was to formulate Mirtazapine CR tablets that could maintain steady-state plasma concentrations within therapeutic windows over a prolonged period, and potentially enhance patient compliance. This was achieved by referencing pharmacokinetic (PK) data of the IR formulation from the US FDA's chemistry and pharmacokinetic review sections (U.S. Food and Drug Administration. Drugs@ FDA: FDA-Approved Drugs).

A plasma concentration profile curve was precisely plotted from the data of Remeron IR Tablets, and PK parameters were calculated to simulate the steady-state plasma concentrations. In this study, Microsoft Excel (Microsoft Corporation) was utilized to calculate the PK parameters, including steady-state plasma concentrations, as well as to analyze the zero-order release kinetics of the drug. The software's built-in functions and data analysis tools enabled precise and efficient data processing. The principle of superposition (Ritschel et al., 1989) served as an important step in this process, enabling the determination of target C_{ss}^{max} and C_{ss}^{min} values that would guide the formulation of the CR tablets (Geraili et al., 2021).

A zero-order absorption model (Shargel L. et al., 2012) was used to simulate the plasma concentrations of the CR tablets for both the single and multiple doses to meet the targeted C_{ss}^{max}, and C_{ss}^{min} concentrations set by the IR tablets of 15 and 45 mg. The dose and zero-order release rate of the proposed CR tablets were determined and adjusted further to meet the established C_{ss}^{max}, and C_{ss}^{min} concentrations, ensuring that the final formulation would meet the desired pharmacokinetic targets.

The formulation strategy was centered around the use of HPMC, Carbopol, and Polyethylene oxide polymers (Draganoiu et al., 2005, Ganesh et al., 2008, Sunil et al., 2008) to prepare a matrix-type controlled-release system. These polymers were chosen for their proven ability to control drug release rate and maintain tablet matrix for a prolonged period. D Optimal Mixture Design (Anderson et al., 2023, Sagiraju et al., 2024) was employed to optimize the concentration of these three formulation variables to get the desired drug release. Dissolution studies were performed to determine the rate, extent, and release kinetics of the proposed CR formulation. D-Optimal Mixture Design is a statistical approach used to optimize the formulation of mixtures; this design is particularly useful for determining the ideal proportions of different components to achieve a desired outcome. In the current research study, D-Optimal Mixture Design was applied to optimize the composition of three polymers HPMC, Carbopol, and Polyethylene Oxide in the formulation of Mirtazapine-CR tablets. This design helps in efficiently exploring the combination of these components to achieve a tablet with the desired release profile, ensuring the drug is released at a controlled and sustained rate.

MATERIALS AND METHODS

1. Pharmacokinetic data collection: PK data from Remeron® 15 and 45 mg IR Tablets available on the US FDA website has been collected and used as the starting point for this study.

2. Plotting plasma concentration curve of IR tablets: Application of PK parameters to plot plasma

concentration-time curves of IR tablets of 15 and 45 mg doses.

3. Simulation of steady-state plasma concentrations: Employing the principle of superposition method to simulate the multiple dose plasma profile and determining the steady-state plasma concentrations C_{ss}^{max}, and C_{ss}^{min} for IR tablets 15, and 45 mg.

4. Simulation of Zero-Order *in vivo* absorption model: Simulation of zero-order absorption model for single dose and multiple doses. Adjusting the dose size and zero-order release rate of the proposed CR formulation to meet the desired steady-state concentrations which are finalized from the IR 15 mg and 45 mg tablets simulated profiles.

5. *In vitro* Zero-Order release rate calculation: Calculation of zero-order *in vitro* release rate as a target dissolution profile for the proposed CR formulation to meet the desired *in vivo* absorption of single dose and subsequent multiple doses for attaining the steady-state plasma concentrations.

6. Formulation optimization: The concentration of critical formulation variables a) HPMC K100 MCR, b) Carbopol 974P, and c) Polyethylene oxide WSR 303, have been optimized using D Optimal Mixture Design.

Mirtazapine (API) is supplied by Zhiyu Biotechnology, Avicel is supplied by Dow Chemicals, Polyethylene oxide WSR 303 is supplied by Dow Chemicals, Methocel K100 MCR, is supplied by Colorcon, and Carbopol 974P, is supplied by Lubrizol.

7. Dissolution testing: Conducting dissolution profile of the Mirtazapine CR tablets in 900 mL of multimedia, (0.01 N HCl, pH 4.5 acetate buffer, and pH 6.8 phosphate buffer) using USP II (paddle) apparatus at a rotation speed of 50 rpm.

Research Methodology

The research methodology involves a step-by-step approach such as simulation of the pharmacokinetic (PK) profile of Mirtazapine CR tablets with a thorough analysis of the PK data of the IR tablets for establishing the dose size and release rate for the CR formulation followed by formulation optimization using design

of experiments. PK simulations were performed to adjust the dose and release rate, ensuring that the target C_{ss}^{max} and C_{ss}^{min} concentrations were achieved. The formulation development involves the selection and optimization of suitable hydrophilic polymers to achieve the desired release profile. These experiments were planned using a D-Optimal Mixture Design to optimize these formulation variables and to achieve the desired release profile. The CR formulation was designed to reduce the FI and incidence of side effects commonly associated with peak plasma levels.

Step 1. Pharmacokinetic data of Remeron® IR Tablets available on the USFDA website has been collected from the below path.

Drugs@FDA > FDA Approved Drugs > Mirtazapine > Teva> Review

The collection of pharmacokinetic data for Remeron® IR Tablets from the USFDA website is a critical step in understanding the drug's absorption, distribution, metabolism, and excretion characteristics. This activity involves navigating through the Drugs@FDA portal to access the FDA Approved Drugs section, where Mirtazpine's approval history is available. By reviewing the drug approval package, specifically the chemistry review and clinical pharmacology and biopharmaceutical review sections, we collected this data. This data includes detailed analyses and evaluations conducted by the FDA, providing insights into the drug's behavior in the body and its interaction with biological systems. Such information is crucial for developing new formulations like the CR tablet, as it lays the groundwork for simulation studies and informs decisions regarding dosing regimens and release mechanisms. The thorough examination of this data ensures that the new formulation adheres to established safety and efficacy standards while aiming to enhance patient compliance and therapeutic outcomes.

Step 2. Construction of plasma profile curve Mirtazapine IR tablets

Utilizing the pharmacokinetic data from the US FDA Website, a detailed construction of the plasma

profiles for both 15 mg and 45 mg doses of Remeron® IR Tablets was undertaken as shown in **Figure 1**. This step is pivotal in the development of the CR formulation as it provides a clear picture of the drug's concentration in the bloodstream over time. By plotting the concentration of the drug against time, the plasma profiles for the two doses were meticulously mapped out. This allowed for the observation of the peak plasma concentrations (C_{max}), the time to reach these peaks (T_{max}), and the overall exposure to the drug (area under the curve, AUC). These profiles are instrumental in predicting the onset, duration, and intensity of the drug's therapeutic effect, as well as its safety margin. The construction of these profiles is not only a technical task requiring precision and attention to detail but also a foundational one, as it directly informs the dosing strategy and release kinetics of the new CR formulation, ensuring that it delivers the desired therapeutic effect while minimizing potential side effects.
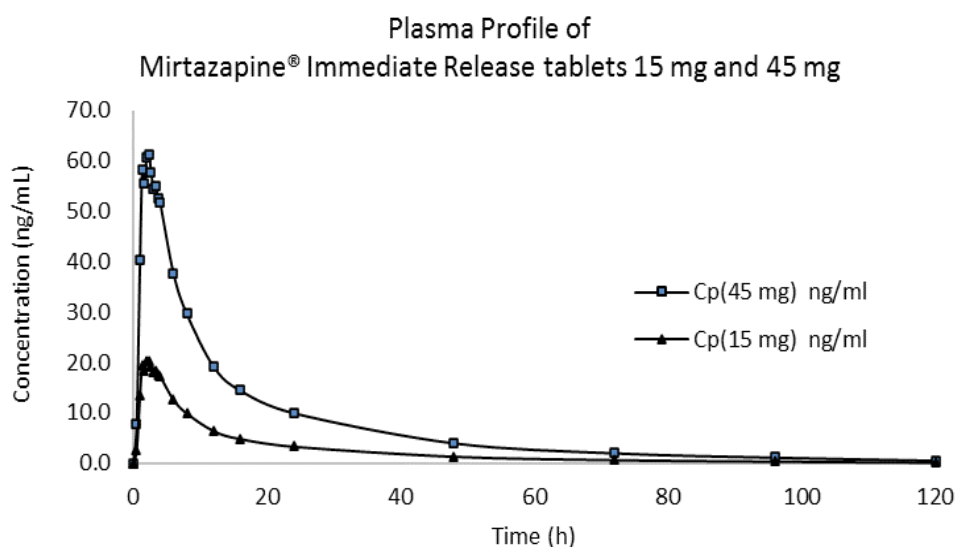
Figure 1. PK Profile of Mirtazapine 15 and 45 mg tablets plotted from the data of FDA Database

In the pharmacokinetic analysis of our study, we precisely calculated a comprehensive set of parameters from the plasma concentration profiles. These parameters are pivotal in understanding the drug's behavior within the body. The formulas used to derive each PK parameter and calculated values for each parameter were systematically presented in **Table 1** to ensure clarity and reproducibility of our methods, providing a clear and quantifiable overview of the drug's kinetics (Ducharme et al., 2022)

Table 1. The formula used for calculating the PK parameters from plasma profile (n=39)

Parameter		Formula in PK Simulations	45 mg	15 mg	units
Kel [1]	=	-slope $\{(\ln(C2{:}C1)),(t2{:}t1)\}$	0.0272	0.0272	/h
$AUC_{0\text{-}t}$ [2]	=	$\frac{1}{2}\sum_{o}^{n}[(c_1 + c_2)(t_2 - t_1)]$	899.71	299.90	ng.h/mL
$AUC_{t\text{-}\infty}$	=	c_∞/k_{el}	20.15	6.72	ng.h/mL
$AUC_{0\text{-}\infty}$	=	$AUC_{0\text{-}t}+AUC_{t\text{-}\infty}$	919.86	306.62	ng.h/mL
v_z [3]	=	$dose/(AUC_{0\text{-}\infty})(k_{el})$	1798.52	1798.52	L
C_t [4]	=	$Co.e^{-kel.t}$	*Showed in Figure 2*		
$t_{\frac{1}{2}}$ [5]	=	$0.639/K_{el}$	25.48	25.48	h
FI [6]	=	$\left(C_{max}^{ss} - C_{min}^{ss}\right)/\left(C_{Avg}^{ss}\right)$	*Refer Table 2*		
C_{Avg}^{ss} [7]	=	$F.D/Vz. Kel. \tau$ [8]	*Refer Table 2*		
C max [9]	=	Max {plasma concentration}	61.13	20.38	ng/mL
t max [10]	=	Time corresponding to C max	2.33	2.33	h

1. Elimination Rate Constant; 2. Area under the curve; 3. Volume of Distribution;

4. Concentration at time t 5. Elimination Half-life; 6. Fluctuation Index;

7. Steady-state Concentration 8. F: Fraction absorbed, D: Dose, τ: Dosing Frequency 9. Peak plasma concentration

10. Time for achieving C max

Step 3. The steady-state plasma concentrations of IR tablets with dosages of 15 mg and 45 mg were determined using the principle of superposition. This principle postulates that the concentration-time profile of multiple doses can be predicted by summing the profiles of individual doses. To achieve this, we first established the elimination curve for a single dose administered on Day -1. We employed a first-order elimination rate, which assumes that the rate of drug elimination is directly proportional to the drug concentration in the plasma.

The concentration remaining at any time (t) after administration was calculated using the formula:

$Ct= Co.e^{-kel.t}$

Where:

Ct is the plasma concentration at time (t); C_0 is the initial concentration

(e) is the base of the natural logarithm; K_{el} is the first-order elimination rate constant

(t) is the time elapsed since the drug administration

By extrapolating the elimination curve until the plasma concentration approached nearly baseline, we could determine the residual concentration after the effect of the single dose diminished. For subsequent doses, we added the calculated concentrations at corresponding times to the baseline profile as shown in **Figure 2**, thus constructing a composite curve that represents the cumulative effect of multiple doses. This approach allowed us to accurately model the pharmacokinetics of the IR tablets at steady-state, providing valuable insights into the dosing regimen and its potential therapeutic outcomes. The extrapolated elimination curve serves as a crucial component in predicting the drug's behavior over extended dosing periods and is instrumental in optimizing dosage for maximum efficacy with minimal side effects.
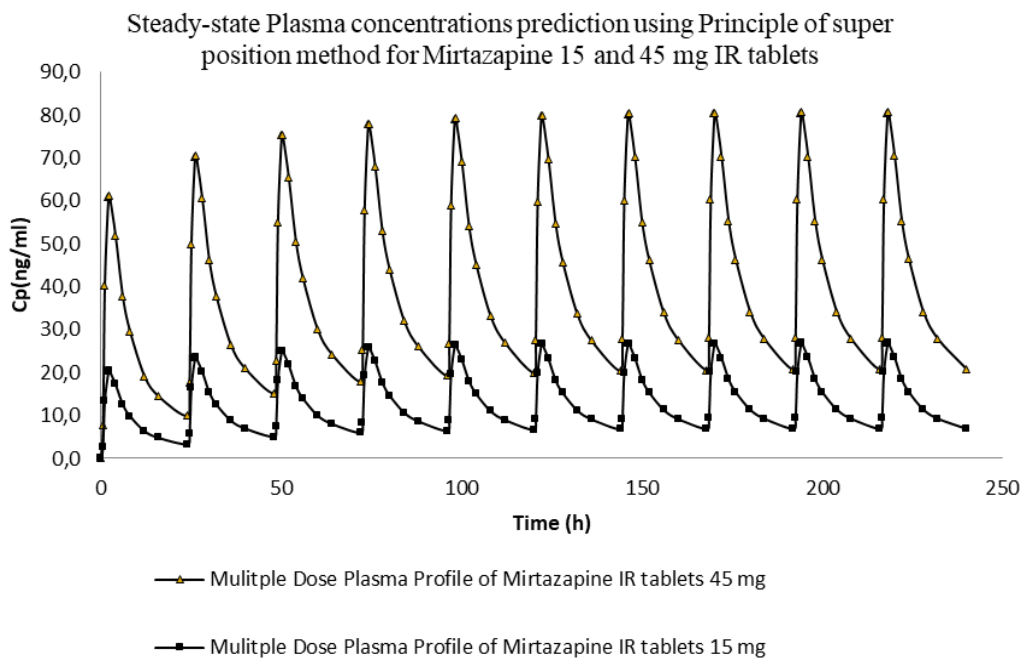
Figure 2. Simulated Steady-State Plasma Profile of Mirtazapine 15 and 45 mg IR Tablets using multiple doses with the Principle of Superposition

The FI was calculated from the steady-state plasma concentrations in **Table 2**. The FI, a measure of the extent to which plasma drug levels oscillate over a dosing interval at steady-state, was determined to be 1.56. This index is derived by dividing the range of concentration fluctuations specifically, the difference between the peak (C_{max}) and trough (C_{min}) concentrations by the mean concentration (C_{avg}) within the dosing period. The resulting value is indicative of the relative variability in drug exposure between doses. A FI of 1.56 suggests that

there is a 156% fluctuation in the mean plasma concentration, which has critical implications for both the therapeutic efficacy and safety profile of the pharmacological intervention (Wakamatsu et al., 2013). Such a substantial fluctuation could potentially lead to periods of subtherapeutic exposure, as well as peaks that may approach toxic levels. Therefore, the FI (Sheehan et al., 2012) is an essential parameter for optimizing dosage regimens to balance efficacy and minimize adverse effects, ensuring a therapeutic window that maximizes patient outcomes.

Table 2. PK parameters calculated from the steady-state plasma profile

PK Parameter	45 mg	15 mg	units
[11]$C_{ss}{}^{max}$	80.7	**26.9**	ng/mL
[12]$C_{ss}{}^{min}$	**20.8**	6.9	ng/mL
$C_{ss}{}^{avg}$	38.32	12.78	ng/mL
Fluctuation Index	1.56	1.56	--

11. steady-state maximum concentration   12. steady-state minimum concentration

Desired steady-state plasma concentrations for the proposed CR tablets of Mirtazapine tablets have been fixed based on the steady-state concentration of IR tablets as 26.9 ng/ml and 20.8 ng/ml. The $C_{ss}^{\ max}$ of 15 mg and $C_{ss}^{\ min}$ of 45 mg observed in IR tablets were selected as target plasma concentrations for the proposed CR dosage forms. These targets ensure that the plasma concentrations remain consistently within the therapeutic window, thereby delivering the desired therapeutic effect to the patient throughout the treatment duration.

Step 4. In the pharmacokinetic simulation for the CR formulation of Mirtazapine tablets, we employed a zero-order absorption model to predict the drug release and absorption kinetics. This model assumes that the drug is released at a constant rate, regardless of the concentration, which is characteristic of many CR formulations. The simulation involved calculating key PK parameters, as mentioned in **Table 4**. These parameters are crucial for designing a CR tablet that can maintain therapeutic drug levels over an extended period without the peaks and troughs associated with IR formulations. The T_{elm} and $T_{zero-order\ delivery}$ are particularly important for ensuring that the drug is released not only at a constant rate but also for a duration that aligns with the drug's elimination half-life, thereby maintaining steady-state conditions. The $D^{CR}_{Preliminary}$ and $R^0_{preliminary}$ are used to fine-tune the dosage form to ensure that the desired drug release profile is achieved, which is essential for optimizing the therapeutic efficacy and minimizing side effects. This detailed simulation approach allows for the precise tailoring of the CR tablet's pharmacokinetic profile to meet specific clinical needs.

Table 3. Formula for simulating the plasma profile of proposed Mirtazapine CR tablets (preliminary)

Parameter		Formula in PK CR Simulations	Results
[13] T_{elm}	=	$\dfrac{(ln(C_{max}^{SSDesired}) - ln(C_{Min}^{SSDesired}))}{K_{el}}$	9.45 h
[14] T_{del}	=	$\tau. - T_{elm}$	14.55 h
[15] D_{IR}	=	45 mg	
[16] $D_{CR\ Preliminary}$	=	$D_{IR} \times 0.693 \times \tau / t_{\frac{1}{2}}$	29.38 mg
[17] R^0_{prelim}	=	$D_{ER\ Prelim} \times F \times p / T_{del}$	2.02 mg/h
[18] $C_{0-tmax}^{Prelim\ Zero\ Sim}$	=	$\dfrac{(R^0_{prelim} \times (1 - (e^{-k_e \times t})))}{(V_z \times K_{el})}$	
[19] $C_{tmax-t\ inf}^{Prelim\ Zero\ Sim}$	=	$Cmax.e^{-kel.(t-t\ del)}$	

13. T for elimination T_{elm}: The time required for the drug to be eliminated from the body after it has been completely absorbed.

14. T for delivery of dose in zero-order T_{del}: The duration over which the drug is released from the CR tablet at a constant rate.

15. Immediate - release tablets dose

16. CR preliminary dose ($D_{CR\ Preliminary}$): The initial dose of the CR formulation to achieve the desired plasma concentration profile.

17. CR preliminary release rate ($R^0_{preliminary}$): The rate at which the drug is released from the CR tablet into the systemic circulation.

18. Simulated plasma concentrations for the CR tablets from 0-t_{max}

19. Simulated plasma concentrations for the CR tablets from t_{max}-t_{inf}

Using the above formulae the calculations have been done for the determination of essential parameters needed for the simulations i.e. T elm, T delivery of the dose (for determining the dissolution time point for the CR dosage form), Dose for the proposed CR dosage form (preliminary dose) $D_{CR\,Prelim}$ and Preliminary release rate $R_{0\,Prelim}$ of the proposed CR dosage form , and presented in Table 3. Plasma concentrations for a single dose have been calculated using the above formula of $C^{prelim\,zero-order}_{0-t\,max}$ until t max and the elimination curve is constructed post tmax by calculating the decay concentrations using the formula $C^{prelim\,zero-order}_{t\,max-t\,inf}$. Plasma concentrations of multiple dosing of the proposed CR formulation have been calculated using the principle of superposition which is similar to the one used for IR formulations.

In the graphical representation of PK data shown below, the delineation of plasma concentration profiles following both single and multiple dosing regimens provides critical insights into the drug's absorption, distribution, metabolism, and excretion characteristics. The multiple dose profile, in particular, elucidates the time course to reach steady-state concentrations, a pivotal milestone in therapeutic drug monitoring.

The graph shown in Figure 3, indicates that steady-state conditions are attained after approximately 10 days of repeated dosing. This temporal aspect is reflective of the drug's PK properties, such as its half-life and accumulation factor. Achieving steady-state concentrations depends on both the drug's elimination rate constant and the dosing interval. At this point the input (dose rate) and output (clearance rate) of the drug reach an equilibrium, resulting in consistent plasma levels that are conducive to sustained therapeutic effect.
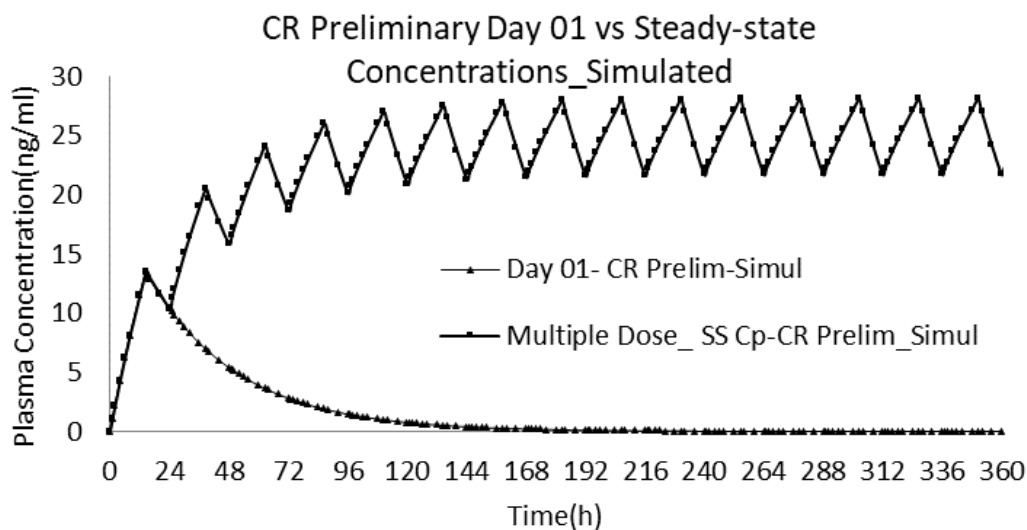
Figure 3. Simulated Steady-State plasma profile of Mirtazapine 29.38 mg CR tablets with R_0 - 2.02 mg/h (preliminary) using multiple doses with the principle of superposition

According to the simulated plasma profile provided, it is determined that the maximum steady-state plasma concentration (C_{ss}^{max}) is 28.15 ng/ml, while the minimum steady-state plasma concentration (C_{ss}^{min}) is 21.77 ng/ml. However, the steady-state plasma concentrations indicated in Table 4 are slightly lower than the observed values, indicating the need for further reduction in both dose and release rate to meet the desired targets for the proposed CR dosage form.

Table 4. Steady-State plasma concentrations of CR preliminary dose and release rate - Mirtazapine CR tablets (Preliminary)

Parameter	value	units
C_{ss}^{max} desired	26.9	ng/ml
C_{ss}^{min} desired	20.8	ng/ml
C_{ss}^{max} achieved	28.15	ng/ml
C_{ss}^{min} achieved	21.77	ng/ml
Fluctuation Index	0.255	--

The proposed adjustment needs a precise approach for reducing the dose, based on the difference between the existing and targeted plasma concentrations. Additionally, a careful modulation of the release rate is advocated as shown in **Table 5** to reduce the peak plasma levels and improve consistency between doses.

This strategic optimization is anticipated to improve the therapeutic index of the CR formulation, ensuring efficacious drug delivery within the optimal therapeutic window, while avoiding the potential for adverse drug reactions.

Table 5. Formula for simulating the plasma profile of proposed Mirtazapine CR tablets (Final)

Parameter		Formula in PK CR Simulations	Results
$^{20}D_{CR\,final}$	=	$\dfrac{c_{max\ desired}^{ss}\,(ng/ml)}{c_{max\ achievend}^{ss}\,(ng/ml)} \times D_{CR\ Preliminanary}$	28 mg
$^{21}R_{final}^{0}$	=	$D_{CR\,final}\,/\,t_{del}$	1.93 mg/hr

20. CR Final dose ($D_{CR\,final}$): The final dose of the CR formulation to achieve the desired plasma concentration profile.

21. CR preliminary release rate (R^0_{final}): The final rate at which the drug is released from the CR tablet into the systemic circulation.

The initial dose was set at 29.38 mg with a zero-order release rate of 2.02 mg/h. Subsequent adjustments entailed a reduction in both the dose and the release rate to achieve correspondence with the desired steady-state concentrations. The revised dosing parameters presented in **Table 5**, now set at 28 mg for the dose and 1.93 mg/h for the release rate,

have successfully yielded steady-state concentrations that align precisely with the target values of 26.9 ng/ml C_{ss}^{max} and 20.8 ng/ml C_{ss}^{min}.

These findings underscore the significance of dose optimization in CR formulations to ensure therapeutic efficacy and minimize the potential for adverse effects.
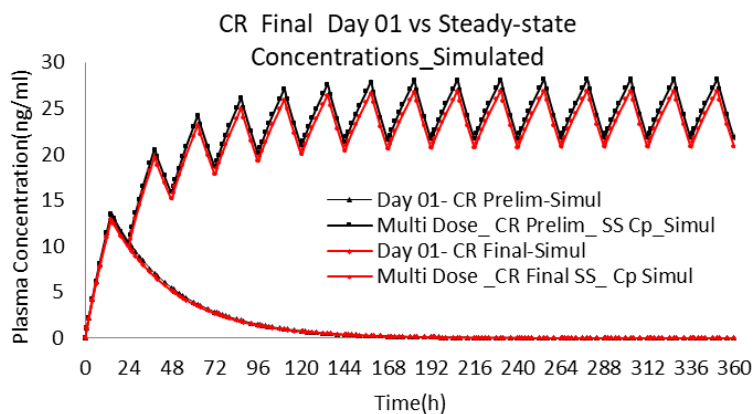
Figure 4. Simulated Steady-State plasma profile of Mirtazapine 28 mg CR tablets with R_0 - 1.93 mg/h (Final) using multiple doses with the principle of superposition

In **Figure 4**, the anticipated steady-state plasma concentrations, C_{ss}^{max}, and C_{ss}^{min} resulting from the simulations mentioned above were determined to be 26.9 and 20.8 ng/mL, respectively, aligning with the desired concentrations for the suggested CR dosage forms. As a result, the dosage for the proposed CR formulation and the *in-vivo* absorption rate constant in zero-order have been finalized at 28 mg and 1.93 mg/h, respectively, and are detailed in **Table 6**.

Table 6. Steady-State plasma concentrations of CR final dose and release rate - Mirtazapine CR tablets (final)

Parameter	value	units
Css max desired	26.9	ng/ml
Css min desired	20.8	ng/ml
Css max achieved	26.9	ng/ml
Css min achieved	20.8	ng/ml
Fluctuation Index	0.255	--

Step 5. Based on the above two parameters, the in-vitro release rate was determined using the below formula

$$\%drug\,relase = \frac{t \times 100 \times R^0_{final}}{dose} = 6.88 \%/h$$

RESULTS AND DISCUSSION

Step 6. In this study, D-optimal Mixture Design (Bodea et al., 1997, Jin et al., 2008, Habib et al., 2022) **Table 7** was employed to optimize the formulation variables of Hydroxypropyl Methylcellulose (HPMC) K100 MCR, Polyethylene Oxide (Polyox) WSR 303, and Carbopol 974P for achieving Zero-Order Controlled-Release. Dissolution at 6 hours (h) and 12 hours (h) in pH 6.8 buffer were selected as responses to assess the rate and extent of formulations and 14 h is the last time point as per the T Del determined in **Table 3**. Design-Expert software (version 13) from State Ease® was employed to design the experiments, analyze the data, and optimize the formulation components. This software facilitated the systematic exploration and identification of optimal conditions, ensuring efficient and reliable formulation development.

Factor A, B, and C are selected as HPMC K100 MCR at 0-60 mg/tablet, PEO WSR 303 at 0-60 mg/tablet, and Carbopol 974 P at 0-60 mg/tablet respectively, the mixture total (A+B+C) was fixed as 80 mg/tablet.

Two models, namely the linear model and the Special cubic model, were evaluated for their suitability in predicting dissolution profiles at 6 hours and 12 hours. While both models demonstrated alias-free behavior and statistically significant p-values (< 0.05), the Special cubic model exhibited a negative Predicted R square. Consequently, the linear model was chosen for its superior predictive performance, offering valuable insights into optimizing formulation variables for controlled-release applications.

Table 7. D-optimal Mixture Design for composition optimization of formulation variables of Mirtazapine CR tablets (n=10 runs)

Run	Components			Response: % Drug Release	
	A: HPMC K100 MCR (mg)	B: PEO WSR 303 (mg)	C: Carbopol 974P (mg)	6 h	12 h
1	25.2	29.8	25.0	12	25
2	60.0	10.8	9.2	25	49
3	0.0	60.0	20.0	15	36
4	43.8	6.4	29.8	30	58
5	0.0	20.0	60.0	42	87
6	28.9	0.0	51.1	38	78
7	60.0	10.8	9.2	23	45
8	20.0	60.0	0.0	15	37
9	20.0	60.0	0.0	12	28
10	2.5	38.5	39.0	37	68

The above experimental design layout consisted of a systematic arrangement to investigate the effects of three formulation factors on two responses, dissolution at 6 hours and 12 hours. With a total of 10 experiments conducted, the design aimed to comprehensively explore the influence of Hydroxypropyl Methylcellulose (HPMC) K100 MCR, Polyethylene Oxide (Polyox) WSR 303, and Carbopol 974P on the controlled-release kinetics of the formulation. Each experiment represented a unique combination of factor levels, facilitating the assessment of their individual and combined effects on the desired dissolution profiles.

In the Design of Experiments (DoE) for tablet formulation, the above three critical factors were selected for investigation. The formulation process utilized a wet granulation method, with the following excipients kept constant across all DoE runs, 2% PVP K30 as a binder, dissolved in ethanol, Avicel PH101 as a diluent to ensure the proper tablet weight and consistency, 1% colloidal silicon dioxide as an anti-adherent to prevent sticking during processing, 1% magnesium stearate as a lubricant to facilitate tablet ejection from the dies.

The total weight of each tablet was maintained at 300 mg. The process began with the precise weighing of all excipients, followed by sifting through a screen to ensure uniform particle size. Subsequently, the PVP ethanol solution was added to the mix. After thorough blending, the wet mass was dried and milled to achieve the desired granule size. The granules were then blended with colloidal silicon dioxide to enhance flow properties. Finally, magnesium stearate was incorporated as a lubricant. The resulting blend was compressed into tablets using 9.5 mm standard punches to ensure uniformity in size and weight.

Table 8. ANOVA Table for Response 1-dissolution at 6 h time point in pH 6.8 phosphate buffer

Source	Sum of Squares	df	Mean Square	F Value	p-value Prob > F	Remarks
Model	888.71	2	444.36	11.10	0.0067	significant
Linear Mixture	888.71	2	444.36	11.10	0.0067	
Residual	280.19	7	40.03			
Lack of Fit	273.69	5	54.74	16.84	0.0570	not significant
Pure Error	6.5	2	3.25			
Cor Total	1168.9	9				

The ANOVA **Table 8** for the first response reveals the significance of the model, with an F value of 11.10 and a corresponding p-value of 0.0067, indicating statistical significance. There is only a 0.67% chance that a "Model F Value" this large could occur due to noise. Values of "Prob > F" less than 0.05 indicate model terms are significant. Moreover, the lack of fit is

not deemed significant, affirming the adequacy of the suggested model. The "Lack of Fit F-value" of 16.84 implies there is a 5.70% chance that a "Lack of Fit F-value" this large could occur due to noise.

In this case, Linear Mixture Components are significant model terms. Values greater than 0.1000 indicate the model terms are not significant.
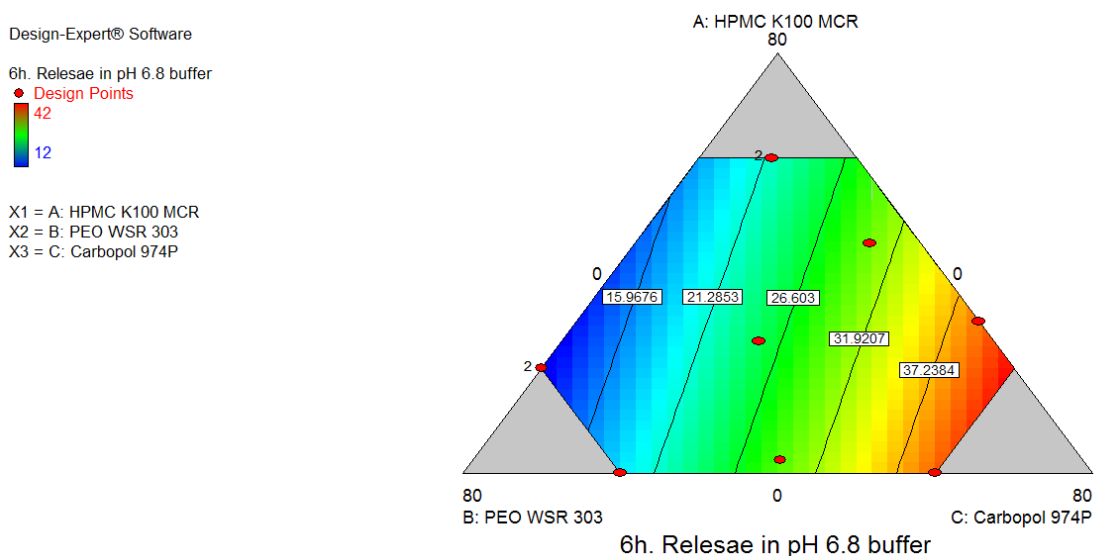
Figure 5. Model graph of dissolution in pH 6.8 phosphate buffer at 6 hours

Table 9. ANOVA Table for Response 2-dissolution at 12 h time point in pH 6.8 phosphate buffer

Source	Sum of Squares	df	Mean Square	F Value	p-value Prob > F	Remarks
Model	3036.04	2	1518.02	10.70	0.0074	Significant
Linear Mixture	3036.04	2	1518.02	10.70	0.0074	
Residual	992.86	7	141.84			
Lack of Fit	944.36	5	188.87	7.79	0.1177	Not significant
Pure Error	48.50	2	24.25			
Cor Total	4028.90	9				

The ANOVA **Table 9** for the second response reveals the significance of the model, with an F value of 10.70 and a corresponding p-value of 0.0074, indicating statistical significance. There is only a 0.74% chance that a "Model F Value" this large could occur due to noise. Values of "Prob > F" less than 0.05 indicate model terms are significant. Moreover, the lack of fit is not deemed significant, affirming the

adequacy of the suggested model. The "Lack of Fit F-value" of 7.79 implies there is a 11.77% chance that a "Lack of Fit F- value" this large could occur due to noise.

In this case, Linear Mixture Components are significant model terms. Values greater than 0.1000 indicate the model terms are not significant.
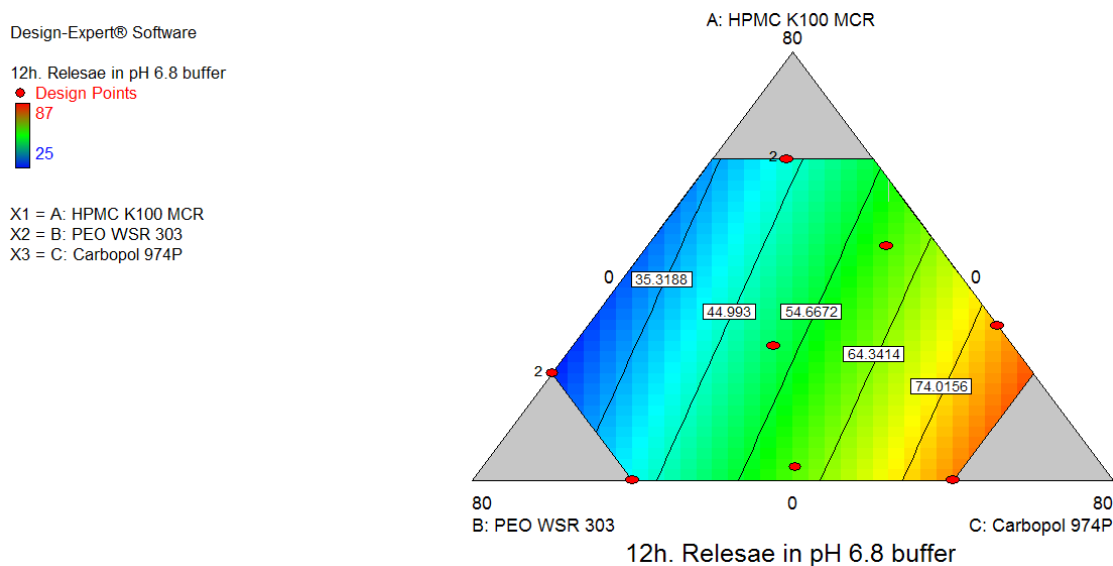
Figure 6. Model graph of dissolution in pH 6.8 phosphate buffer at 12 hours

Based on the findings of ANOVA and model graphs **Figure 5**, and **Figure 6** the recommended model for the first and second responses is the linear mixture model, which effectively captures the relationship between the formulation factors and the dissolution profiles at 6 and 12 hours. This analysis underscores the robustness of the experimental design and the reliability of the statistical model in elucidating the factors influencing the controlled-release kinetics of the formulation.

Table 10. Regression table for response 1, 2-dissolution at 6h, 12h time point in pH 6.8 phosphate buffer

Regression Analysis	Response 1- Dissolution at 6 h	Response 2- Dissolution at 12 h
R-Squared	0.7536	0.7603
Adj R-Squared	0.6832	0.6918
Pred R-Squared	0.6198	0.6361
Adeq Precision	8.128	8.183

The regression **Table 10** indicates a strong relationship between the independent variables and the dependent variable, as evidenced by an R-squared (R^2) value of about 0.75-0.76 This suggests that 75%-76% of the variability in the dependent variable can be explained by the model. The Adjusted R-squared, which is 0.68-0.69, adjusts for the number of predictors in the model and indicates a good fit as well. The Predicted R-squared of 0.62-0.63 is in reasonable agreement with the Adjusted R-squared, which implies that the model should predict future observations with a similar level of accuracy.

Furthermore, an Adequate Precision ratio of around 8 indicates that the model has a desirable signal-to-noise ratio and that the model's predictions can be considered reliable. Overall, these metrics suggest that the regression model is statistically significant and can be used for making predictions with confidence.

The results indicated that a linear mixture model significantly influenced both dissolution responses. Among the formulation variables, Carbopol 974P emerged as the most significant factor, followed by HPMC and Polyox. Diagnostic plots revealed satisfactory results with no outliers detected.

Table 11. Numerical optimization- constraints

Name	Goal	Lower limit	Upper limit
HPMC K100 MCR	Minimize	0	60
PEO WSR 303	Minimize	0	60
Carbopol 974P	in range	0	60
6 h. Release in pH 6.8 buffer	Maximize	12	42
12 h. Release in pH 6.8 buffer	Maximize	25	87

Constraints were given for factors and responses using numerical optimization **Table 11**. Five solutions with desirability values greater than 0.8 were found based on the provided constraints in **Table 12**. The Design of Experiment (DoE) suggested specific factor combinations to achieve desired dissolution targets, specifically, Factor A (HPMC) and Factor B (Polyox) were recommended within the range of 0-20 mg, while Factor C (Carbopol) at 50-60 mg per tablet was identified as optimal for achieving the desired controlled-release profile as shown in **Figure 7**.

Table 12. Solutions of numerical optimization with desirability

Solutions	HPMC K100 MCR	PEO WSR 303	Carbopol 974P	6h. Release	12h. Release	Desirability
1	15.96	4.03	60	42.0	82.9	0.894
2	20	0	60	42.6	83.7	0.891
3	0	20	60	39.8	80.0	0.860
4	13.3	13.3	53.3	38.2	76.2	0.812
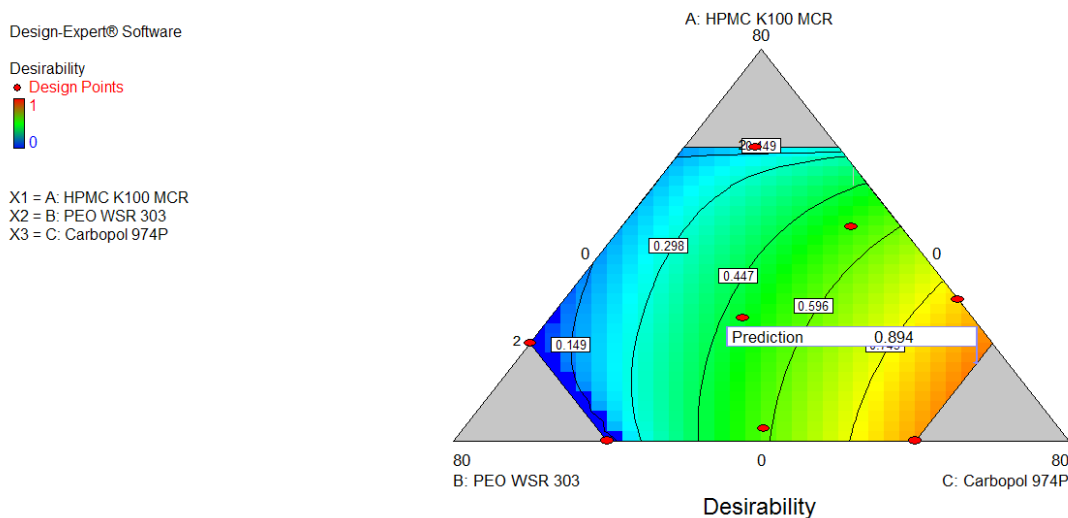
Figure 7. Desirability plot of overlay plot

Step 7. The conclusion of the design of experiments (DoE) was the execution of a final trial, which was selected based on a desirability index exceeding 0.8. This trial underwent dissolution testing in various media, including 0.01 N HCl, pH 4.5 acetate buffer, and pH 6.8 phosphate buffer, The dissolution profile obtained as presented in **Table 13**, was compared against a predetermined zero-order target dissolution profile in **Figure 8**. The results were promising, demonstrating a dissolution behavior that was comparable to the target profile. This indicates a successful optimization of the formulation parameters, aligning with the desired release characteristics of the tablets.

Typically, formulation development begins with *in vitro* evaluations to predict the *in vivo* performance of the dosage form. However, in this study, to design controlled-release (CR) dosage forms based on immediate-release (IR) formulations, we initiated the process with pharmacokinetic (PK) simulations. This involved conducting simulations of IR multiple dosing to establish steady-state plasma concentration targets. Using these targets, CR dosing plasma concentrations were simulated for both single and multiple dosing regimens, which allowed us to set precise *in vitro* release targets before commencing the dosage form design.

As part of the CR formulation development, the Design of Experiments (DoE) was implemented to systematically optimize the formulation components. The optimized formulation was subsequently evaluated through multi-media dissolution studies to ensure that the dissolution profiles aligned with the predefined *in vitro* release targets. This step was critical in verifying that the *in vitro* release behavior would match the desired zero-order release profile, thereby providing confidence in the anticipated *in vivo* performance.

Table 13. *In vitro* dissolution conditions and dissolution profile in multi-media

In vitro Evaluation conditions	
Apparatus	Lab India Dissolution apparatus with autosampler
The volume of the medium	900 ml.
Temperature	$37^0 \pm 0.5^0$ C
Apparatus	USP Type II (paddle)
RPM	50
Sample collection intervals	1, 2 4, 6, 8, 10, 12 and 14 h.

Dissolution Profile in Multi-media				
Time	0.01 M HCl	pH 4.5 Acetate buffer	pH 6.8 phosphate buffer	Target Zero-Order
0	0	0	0	**0**
1	15	4.49	7.86	**6.88**
2	25.4	12.12	12.9	**13.76**
4	42.2	22.37	26.24	**27.52**
6	60.7	37	42.36	**41.28**
8	75.9	52.44	58.12	**55.04**
10	85.4	67	72.12	**68.8**
12	91.9	77.38	87.43	**82.56**
14	96.4	90	99.02	**96.32**
Slope				
Zero-order release rate	*6.95*	*6.60*	*7.21*	***6.88***
Slope (Actual/Target)	*101.07*	*95.93*	*104.80*	*--*
F2 Similarity factor	*43*	*70*	*76*	*--*
R^2				
Regression coefficient	*0.95*	*1.00*	*1.00*	***1.00***
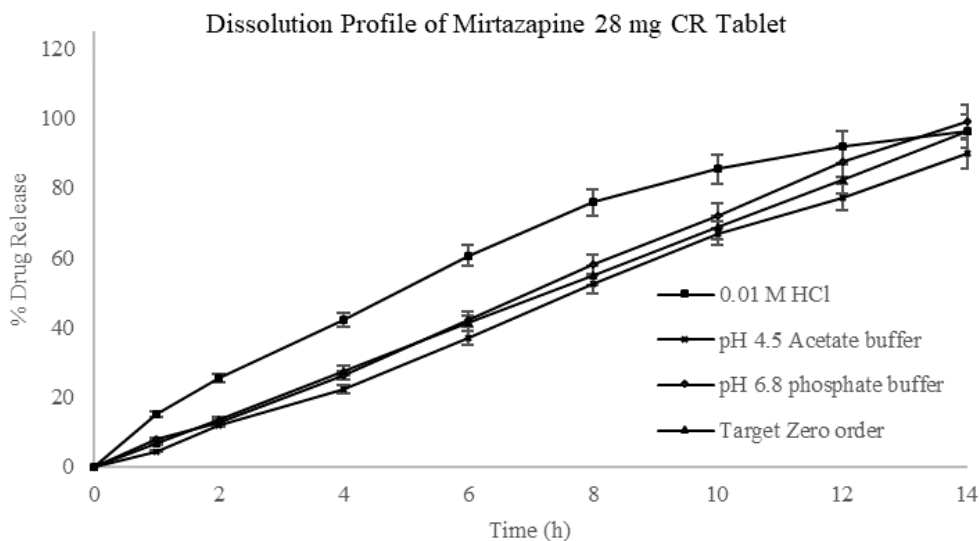
Figure 8. Dissolution profile of Mirtazapine 28 mg CR tablets in multi-media

The similarity factor (F_2) was calculated for the target zero-order release profile compared to *in vitro* dissolution in 0.01 N HCl (pH 2), pH 4.5 acetate buffer, and pH 6.8 phosphate buffer, yielding values of 43, 70, and 76, respectively. Although the F_2 value at pH 2.0 was lower than the generally accepted threshold of 50, this is not considered problematic due to the total dissolution time and the anticipated T_max exceeding 12 hours. The lower F_2 at acidic pH is not relevant to the overall performance of the CR formulation, as the release behavior in the higher pH media (pH 4.5 and pH 6.8), with F_2 values of 70 and 76, respectively, is more pertinent to the intended therapeutic effect. These values indicate satisfactory release profiles at these pH levels, which are more reflective of the physiological conditions post-gastric transit.

Although the formulation was designed for pH-independent drug release due to the high solubility of Mirtazapine at lower pH, a slightly faster release rate was observed in acidic conditions compared to the target zero-order release. However, the overall release slope across all pH conditions remained close to the target zero-order kinetics, nearly 100% in all three media. This suggests that the proposed CR formulation is adequate for achieving the desired *in vivo* targets, even with slight variations in release at lower pH.

(Ranjan et al., 2011) developed CR chitosan microspheres of Mirtazapine, demonstrating improved bioavailability and altered PK parameters, with increased AUC, prolonged half-life, and reduced clearance. The CR formulation achieved sustained drug release up to 48 hours (Ranjan et al., 2011). *In vivo* studies conducted in rats further confirmed the enhanced pharmacokinetic profile, highlighting the potential of CR microspheres in optimizing Mirtazapine's therapeutic effect.

(Koradia et al., 2018) developed unidirectional buccoadhesive CR tablets of Mirtazapine using Carbopol 934P and HPMC K4M, achieving controlled drug release over 6 hours with enhanced permeability through the buccal mucosa (Koradia et al., 2018). The formulation showed optimal swelling, good bioadhesive strength, and stability, offering a potential alternative delivery system for Mirtazapine.

A study by Vysloužil et al. developed PLGA microparticles for the CR of Mirtazapine using the o/w solvent evaporation method (Vysloužil et al., 2014). The microparticles, prepared with dichloromethane and stabilized with PVA, showed high encapsulation efficiency (64.2%) and released the drug over 5 days. The release followed near zero-order kinetics (R^2 0.95–0.98), with drug release driven by a combination of diffusion and surface erosion, enhanced by polymer swelling and chain relaxation.

CONCLUSION

The study successfully formulated Mirtazapine controlled-release (CR) tablets that met the pharmacokinetic targets derived from the IR reference product. The optimized formulation, achieved through a D-optimal mixture design, demonstrated a CR profile consistent with the zero-order kinetics model. Dissolution studies further confirmed the formulation's consistency and robustness, ensuring a reliable and predictable release of the drug. "The obtained *in vitro* dissolution results demonstrated an almost zero-order release profile, with an R-squared value close to one, across pH conditions ranging from 2.0 to 6.8. The release rate, observed was between 6.6%/h to 7.2%/h, which approximates the target zero-order release rate of 6.8%/h, suggesting zero-order absorption of Mirtazapine in vivo conditions. However, a bioavailability study may be necessary to confirm these findings."

This research provides a novel methodology for the development of CR tablets aligning with zero-order kinetics, potentially improving patient adherence and therapeutic outcomes for Mirtazapine, underscoring the application of the D-optimal mixture design in achieving a consistent and robust formulation. This approach has potential applications for other medications requiring controlled-release mechanisms, representing a significant advancement in pharmaceutical formulation.

AUTHOR CONTRIBUTIONS

SRK Raju Sagiraju was responsible for conducting developing the hypothesis, literature research, performing pharmacokinetic simulations, conducting experiments using DoE, statistical analysis, interpretation of the data, preparing and reviewing the study text. Pankaj Kumar Sharma and Jaya Sharma reviewed the data, manuscript, and approved the final version.

CONFLICT OF INTEREST

The authors declare that there is no conflict of interest.

REFERENCES

Anderson, M. J., Whitcomb, P. J., & Bezener, M. A. (2023). *A primer on mixture design: What's in it for formulators.* Statease

Bodea, A., & Leucuta, S. E. (1997). Optimization of hydrophilic matrix tablets using a D-optimal design. *International Journal of Pharmaceutics, 153*(2), 247-255. https://doi.org/10.1016/S0378-5173(97)00117-8

Draganoiu, E., Muça, B., Stansbrey, A., Guo, H., et al. (2005). Effect of carbomer and hydroxypropyl methylcellulose combination on drug release from matrix tablets. *European Journal of Pharmaceutical Sciences, 25, S222-S223.*

Ducharme, M. P., & Shargel, L. (Eds.). (2022). *Shargel and Yu's applied biopharmaceutics and pharmacokinetics* (8th ed.). McGraw-Hill Education. Retrieved from https://accesspharmacy.mhmedical.com/content.aspx?bookid=3127&sectionid=264437548

Ganesh, S., Radhakrishnan, M., Ravi, M., Prasanna kumar, B., & Kalyani, J. (2008). *In vitro* evaluation of the effect of combination of hydrophilic and hydrophobic polymers on controlled-release zidovudine matrix tablets. *Indian Journal of Pharmaceutical Sciences, 70*(4), 461-465. https://doi.org/10.4103/0250-474X.44594. PMID: 20046771; PMCID: PMC2792557

Geraili, A., Xing, M., & Mequanint, K. (2021). Design and fabrication of drug-delivery systems toward adjustable release profiles for personalized treatment. *WIREs Nanomedicine and Nanobiotechnology.* https://doi.org/10.1002/VIW.20200126

Habib, B. A., Abdeltawab, N. F., & Salah Ad-Din, I. (2022). D-optimal mixture design for optimization of topical dapsone niosomes: in vitro characterization and in vivo activity against *Cutibacterium acnes. Drug Delivery, 29*(1), 821–836. https://doi.org/10.1080/10717544.2022.2048131

Jilani, T. N., Gibbons, J. R., Faizy, R. M., et al. (2023). Mirtazapine. *In StatPearls [Internet]. Treasure Island (FL): StatPearls Publishing.* Retrieved from https://www.ncbi.nlm.nih.gov/books/NBK519059/

Jin, X., Zhang, Y., Xiao, L., & Zhao, Z. (2008). Optimization of extended zero-order release gliclazide tablets using D-optimal mixture design. *Yakugaaku Zasshi, 128*(10), 1475-1483. The Pharmaceutical Society of Japan.

Koradia, H., & Chaudhari, K. (2018). Formulation of unidirectional buccal tablet of Mirtazapine: An *in vitro* and *ex vivo* evaluation. *Journal of Drug Delivery Science and Technology, 43*, 233-242. https://doi.org/10.1016/j.jddst.2017.10.012

Ranjan, O. P., Shavi, G. V., Nayak, U. Y., Arumugam, K., Averineni, R. K., Meka, S. R., & Sureshwar, P. (2011). controlled-release chitosan microspheres of mirtazapine: *In vitro* and in vivo evaluation. *Archives of Pharmacal Research, 34*(11), 1919-1929. https://doi.org/10.1007/s12272-011-1112-1

Ritschel, W. A. (1989). Biopharmaceutic and pharmacokinetic aspects in the design of controlled-release peroral drug delivery systems. *Drug Development and Industrial Pharmacy*, *15*(6–7), 1073–1103. https://doi.org/10.3109/03639048909043666

Sagiraju, S. R. K. Raju, Ekmekçi, E., Aldeniz, E. E., & Dude, U. (2024). Statistical applications in pharmaceutical product development: A comprehensive review. *International Journal for Multidisciplinary Research, 6*(1). https://doi.org/10.36948/ijfmr.2024.v06i01.13216

Shargel, L., Wu-Pong, S., & Yu, A. C. (Eds.). (2012). Chapter 7. Pharmacokinetics of oral absorption. *In Applied Biopharmaceutics & Pharmacokinetics (6th ed.).* The McGraw-Hill Companies.

Sheehan, J. J., Reilly, K. R., Fu, D. J., & Alphs, L. (2012). Comparison of the peak-to-trough fluctuation in plasma concentration of long-acting injectable antipsychotics and their oral equivalents. *Innovations in Clinical Neuroscience, 9*(7-8), 17-23. PMID: 22984648; PMCID: PMC3442749.

Sunil Prabhu, Naveen Kanthamneni & Chan Ma (2008) Novel Combinations of Rate-Controlling Polymers for the Release of Leuprolide Acetate in the Colon*, Drug Delivery*, 15:2, 119-125, DOI: 10.1080/10717540801905157

Timmer, C.J., Sitsen, J.M.A. & Delbressine, L.P. (2000) Clinical Pharmacokinetics of Mirtazapine. *Clin Pharmacokinetics* 38, 461–474. https://doi.org/10.2165/00003088-200038060-00001

U.S. Food and Drug Administration. (n.d.). *Approval history: Remeron (Mirtazapine) tablets.* Drugs@ FDA: FDA-Approved Drugs. Retrieved February 05, 2024, from

Vysloužil, J., Doležel, P., Kejdušová, M., Košťál, V., Beneš, L., & Dvořáčková, K. (2014). Long-term controlled-release of PLGA microparticles containing antidepressant mirtazapine. *Pharmaceutical Development and Technology, 21*(2), 214–221. https://doi.org/10.3109/10837450.2014.991874

Wakamatsu, A., Aoki, K., Sakiyama, Y., Ohnishi, T., & Sugita, M. (2013). Predicting pharmacokinetic stability by multiple oral administration of atypical antipsychotics. *Innovations in Clinical Neuroscience, 10*(3), 23-30. PMID: 23630647; PMCID: PMC3638848.

The Rise of Artificial Intelligence in Pharma: Shaping the Future of Drug Discovery

Ayca DEDEOGLU-ERDOGAN*°, Armanc MAT**, Enise Ece GURDAL***, Meric KOKSAL****

The Rise of Artificial Intelligence in Pharma: Shaping the Future of Drug Discovery

Yapay Zekanın Eczacılıkta Yükselişi: İlaç Keşfinin Geleceğini Şekillendirmek

SUMMARY

Drug discovery as an important scientific area that serves human health, requires continuous advancement for improved quality of life and survival rates. However, drug discovery is a long and expensive process. The studies aimed at dealing with these problems have enabled to combination of artificial intelligence (AI) with drug development stages. For every step of the R&D process, AI plays a vital role in facilitating and accelerating the work. Firstly, AI methods (deep learning and convolutional neural networks) help predict the 3D structure of protein making it easier for the rational design of compounds to target a specific protein among other potential outcomes. After estimation of the protein structure of interest, it is also possible to determine the protein-ligand interactions by utilizing AI technologies like random forest. The other stage, namely finding the hit compounds is also possible through AI-assisted QSAR models such as deep neural networks. Besides, there are many AI methods (k-nearest neighbor and support vector machines) for ADMET prediction to optimize lead compounds. Finally, AI techniques also aid in choosing the most suitable synthesis plan. In the light of the latest advances, AI has become the focus of the pharmaceutical industry. However, despite the potential benefits of AI in drug discovery, several challenges must be considered including the availability of suitable data and bioethical issues. This article provides a comprehensive review of the benefits and applications of AI in various stages of drug discovery.

Key Words: *Artificial intelligence, drug discovery, machine learning, deep learning*

ÖZ

İnsan sağlığına ve refahına hizmet eden önemli bir bilimsel alan olan ilaç keşfi, yaşam kalitesinin ve hayatta kalma oranlarının iyileştirilmesi için sürekli ilerlemeyi gerektirmektedir. Ancak ilaç keşfi uzun ve pahalı bir süreçtir. Bu sorunların üstesinden gelmeye yönelik çalışmalar, yapay zekanın ilaç geliştirme süreciyle birleştirilmesini sağlamıştır. Ar-Ge sürecinin her adımında yapay zeka, işi kolaylaştırma ve hızlandırma konusunda hayati bir rol oynar. Öncelikle, bazı yapay zeka yöntemleri (derin öğrenme ve evrişimsel sinir ağları), ilaç molekülünün belirli bir proteini hedeflemesini kolaylaştırmak için proteinin 3 boyutlu yapısını tahmin etmeye yardımcı olmaktadır. Protein yapısının modellenmesiyle beraber, rastgele orman gibi yapay zeka algoritmalarından yararlanılarak protein-ligand etkileşimlerinin belirlenmesi de mümkün olmaktadır. Takip eden aşamada, öncü bileşiklerin keşfi de derin sinir ağları gibi yapay zeka destekli QSAR modellerinin kullanılmasıyla sağlanmaktadır. Ayrıca, öncü bileşiği optimize etmek amacıyla ADMET tahminine yardımcı birçok yapay zeka yöntemi de (k-en yakın komşuluk, and destek vektör makineleri) bulunmaktadır. Bunun yanı sıra yapay zeka teknikleri en uygun sentez planının seçilmesinde de yol göstericidir. Güncel gelişmelerin ışığında yapay zeka, ilaç sektörünün odak noktası haline gelmiştir. Ancak, ilaç keşfinde yapay zekanın potansiyel faydalarına rağmen, uygun verilerin mevcudiyeti ve biyoetik konular da dahil olmak üzere dikkate alınması gereken çeşitli zorluklar da vardır. Bu makale, yapay zekanın ilaç keşfinin çeşitli aşamalarındaki yararları ve uygulamalarını kapsamlı bir şekilde incelemektedir.

Anahtar Kelimeler: *Yapay zeka, ilaç keşfi, makine öğrenmesi, derin öğrenme*

* ORCID: 0000-0001-5936-5328, Department of Pharmaceutical Chemistry, Faculty of Pharmacy, Yeditepe University, Atasehir, 34755 Istanbul, Turkey
** ORCID: 0009-0001-8379-3987, Faculty of Pharmacy, Yeditepe University, Atasehir, 34755 Istanbul, Turkey
*** ORCID: 0000-0003-1064-8639, Department of Organic Chemistry, Faculty of Chemistry, Martin-Luther-University Halle-Wittenberg, Halle (Saale), Germany
          Department of Nano-optics, Max Planck Institute for the Science of Light, 91058, Erlangen, Germany
**** ORCID: 0000-0001-7662-9364, Department of Pharmaceutical Chemistry, Faculty of Pharmacy, Yeditepe University, Atasehir, 34755 Istanbul, Turkey

° Corresponding Author; Ayca DEDEOGLU-ERDOGAN,
E-mail: elifaycadedeoglu@gmail.com

INTRODUCTION

The Pioneering Steps of Artificial Intelligence in Healthcare

The notion of incorporating machine-based intelligence into human daily life has been a longstanding concept, with roots in ancient myths and the creation of automatons in Chinese and Egyptian cultures (Lewis, 2014). Intelligent behavior, in this context, is generally defined as making decisions according to the information collected by the system. This concept eventually paved the way for the development of Artificial Intelligence (AI) in 1955, marking a significant milestone in the intersection of machines and intelligent decision-making. Subsequently, the integration of AI into various parts of the developing world gained momentum and its entrance into the pharmaceutical field occurred in the 70s with the introduction of Dendral at Stanford University (Lindsay *et al.* 1993). Regarded as one of the earliest applications of AI in the healthcare system, Dendral played a crucial role in identifying unknown organic molecules. It achieved this by analyzing mass spectra and using the information from chemical databases available at the time. Since then, AI has been applied in numerous areas of healthcare systems including personalized medicine, assisted diagnostics, health economics, drug discovery, and development. It is important to note that AI encompasses a spectrum of definitions and approaches, leading to a diverse range of solutions addressing industry challenges today.

Machine Learning And Deep Learning Models

In an AI concept, it is essential to cover key subfields such as solution searching, reasoning, and knowledge representation, with particular emphasis on the primary paradigm of machine learning (ML). ML is an evolving field of computational algorithms which are designed to imitate human intelligence by learning through the surrounding environment and experiences (Naqa and Murphy, 2015). k-nearest neighborneighbor (k-NN), support vector machines (SVM) and random forest (RF) are the main types of ML (Cortes and Vapnik, 1995, Lavecchia *et al.*, 2013, Melville *et al.*, 2009). The k-NN algorithm, a form of instance-based learning or lazy learning, is a simple and intuitive method to predict the class, property, or rank of a molecule based on the nearest training examples in the feature space. It has been used for envisaging activities of various compounds such as anti-convulsants, dopamine D1 antagonists, protein kinase inhibitors, psychoactive cannabinoids, steroids, anti-inflammatory and anticancer drugs, and estrogen receptor agonists (Lavecchia, 2015). Support vector machines (SVMs), as supervised machine learning algorithms, have gained popularity in drug discovery applications for tasks like compound classification and property predictions for novel active compounds. In a study applying SVM to pharmacokinetic (PK) modeling, Doniger *et al.* worked on 179 central nervous system (CNS) active compounds and 145 inactive molecules for predicting blood-brain barrier (BBB)penetration. Using 30 tests, the AI model was performed with 81.5% success (Heikamp and Bajorath, 2014, Doniger *et al.*, 2002). Random Forest (RF) is a supervised learning method to be applied to classification and some problems. The method involves tree predictors that each tree depends on the values of a random vector independently and with the same layout for each of the generated vectors (Breiman, 2001). The optimal selection of chemical features (molecular descriptors) is an important act to take before the research for the efficient application of AI techniques in virtual screening for identification of bioactive molecules in drug discovery. This selection plays a role in the accuracy of affinity prediction. RF-based approaches automatically select molecular descriptors of training data for ligands of kinases, nuclear hormone receptors, and other enzymes (Cano *et al.*, 2017).

Deep learning (DL), a subfield of ML, involves artificial neural networks (ANNs), and provides advantages compared to statistical modeling. One

notable advantage of DL is that it does not require rigidly structured experimental designs, instead, it can map functions using historical or incomplete data. ANNs are good recognizers of patterns and robust classifiers, with the ability to generate when making decisions based on imprecise input data (Cheng and Sutariya, 2012). ANNs have many application areas in drug design such as pharmacokinetics, neurodegenerative diseases, cardiovascular diseases, infectious and microbial diseases, immunology and virology, medical diagnosis, cosmetics and dermatology, proteomics-genomics etc. (Dobchev and Karelson, 2016). The computational model inspired in the natural neurons, ANN, covers the interconnected and sophisticated computing factors to process information and solve problems. ANNs comprise different types, such as multilayer perceptron (MLP) networks, recurrent neural networks (RNNs), and convolutional neural networks (CNNs). The MLP network is used for pattern recognition, optimization aids, process identification, and controls. RNNs can memorize and store information. CNNs have used in biological system modeling, processing complex brain functions, pattern recognition, and sophisticated signal processing (Paul *et al.* 2021). Examples of method domains of AI are summarized in Figure 1.
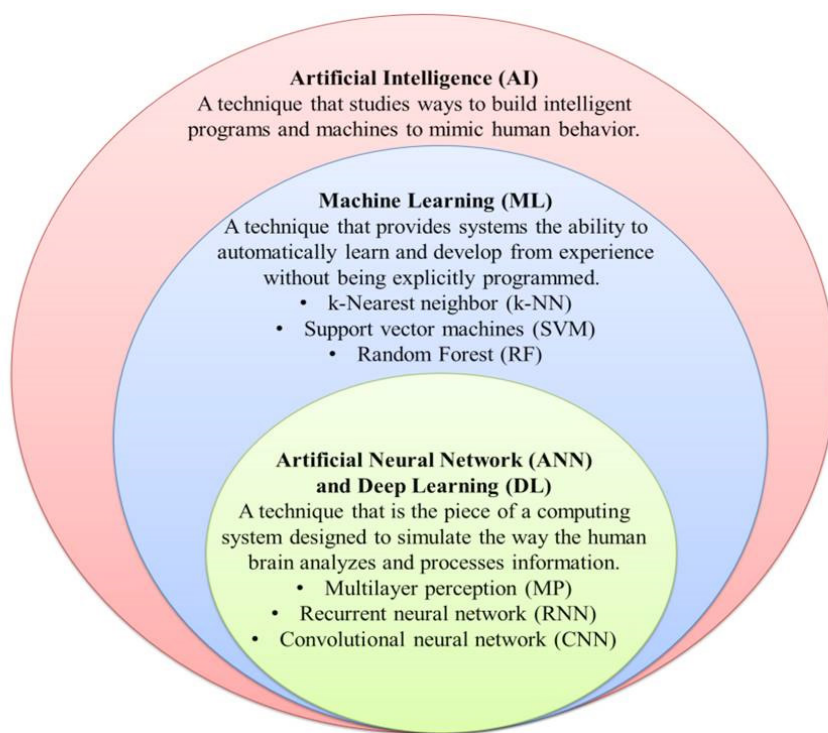
Figure 1. Method domains of AI

Drug Discovery Process

The drug discovery process is a complex and long pathway that consists of considerable steps. The initial phase involves evaluating of three-dimensional (3D) structure of the target protein and examining protein-protein/drug interactions. Following target identification, potential hit compounds targeted on selected protein are chosen by using computer-aided drug design systems such as molecular docking, virtual screening, and drug repurposing (Rao and Srinivas, 2011). Once identified, the selected compounds are synthesized and then the compounds undergo *in vitro* and *in vivo* assays to determine their activities, toxicities, and pharmacokinetic properties. Moreover, quantitative structure–activity relationship (QSAR) and *de novo* studies are utilized in combination with the

activity data for lead identification and optimization steps. After these steps, the drug candidates are selected for preclinical and clinical studies for more in-depth analysis (Schneider and Fechner, 2005). The

drugs that successfully pass all the clinical phases are reviewed by FDA or any other autority to be ready for the market (Chan *et al.*, 2019). The drug development process is visually summarized in Figure 2.
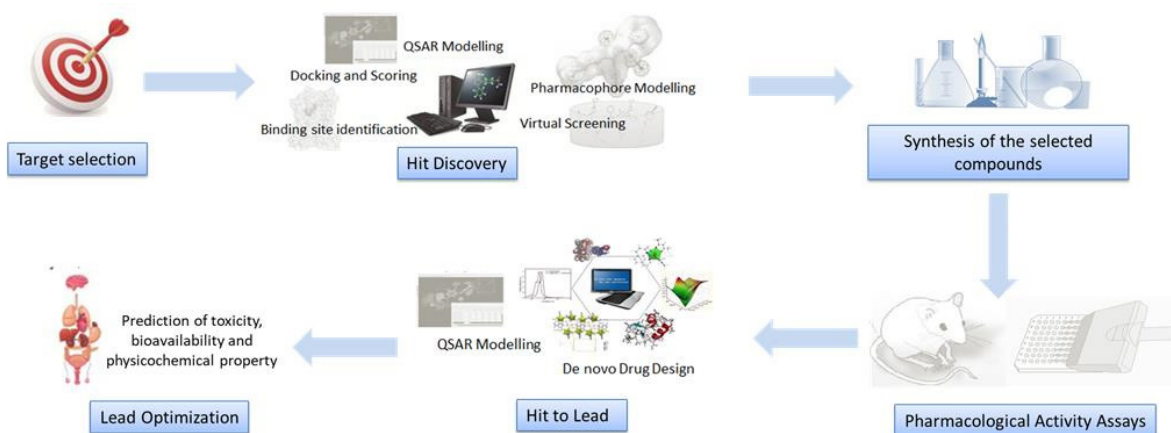
Figure 2. AI-aided drug development process

Drug development is an extended, complex, and costly process, marked by a considerable degree of uncertainty regarding the success of a drug (Fuloria *et al.*, 2013). The research and development (R&D) process requires analyzing a large amount of data for hypothesis and compound identification. It necessitates the integration of datasets with the targeted pathophysiology, extraction of pertinent data aligning with specific research goals, and establishing correlations between subjects for improvement. For every step of the R&D process, AI plays a pivotal role in streamlining and expediting the work.

To discover an effective agent, conducting error-free lab tests or clinical trials is imperative, as every error poses an obstacle and hinders the progress of the process. Therefore, developing an agent that can efficiently treat individuals with highly accurate results is paramount. The integration of advanced techniques, such as AI models, into the drug discovery process, holds the potential to mitigate human-based errors and save valuable time. Major biopharmaceutical companies are increasingly turning to artificial intelligence as a solution to the challenges in drug design. Pfizer, for instance, employs

a machine learning system called IBM Watson to enhance the search for immuno-oncology drugs. Sanofi has agreed to utilize the artificial intelligence platform developed by the UK-based Exscientia to research the treatment of metabolic disorders. Numerous other biopharmaceutical companies have similar collaborations or internal AI programs, reflecting a growing consensus within the industry that AI can offer solutions to critical challenges in drug development (Fleming, 2018).

Target Identification

The overexpression of numerous proteins is the fundamental reason for the progress of many diseases. The successful therapeutic approach for these diseases is design and development of drug molecules that target the overexpressed proteins. Therefore, it is essential to predict the structure of the protein to design the drug molecule that selectively interacts with it (Madhukar *et al.*, 2017). Structure-based drug design, which involves examining the three-dimensional (3D) structures of proteins, is a valuable strategy for identifying active small molecules targeting protein of interest. However, measuring the

3D structure of proteins is a time-consuming and expensive process, prompting the development of algorithms to predict protein structures to overcome these problems. Although the sequence knowledge of most proteins is currently available, achieving precise *de novo* prediction of their 3D structures remains a significant challenge. Recently, the powerful capability of feature extraction has enabled the utilization of deep learning technologies in predicting the secondary structure, backbone torsion angle, and residue contacts of proteins (Spencer *et al.*, 2014, Li *et al.*, 2017). The use of deep learning modules, particularly convolutional neural networks (CNN), is advantageous in addressing the overfitting problem in protein structure prediction (Wang and Zhang, 2017). Notably, the AlphaFold2 model has emerged as a highly accurate tool for predicting protein folding, as evidenced by the impressive results in the CASP14 assessment. This model is based on the neural network algorithm that incorporates multi-sequence alignments and pairwise features, refining predictions iteratively (Jumper *et al.*, 2021). The landscape of AI-based computational tools for target identification is further detailed in Table 1.

In research, Jumper and colleagues presented a computational method that could predict protein structures with near-experimental accuracy. Their created neural network AlphaFold was submitted to CASP14. AlphaFold structures outperformed rival approaches in CASP14 by a significant margin. The next best performing method had a median backbone accuracy of 2.8 Å r.m.s.d.95, while AlphaFold structures had a median backbone accuracy of 0.96 Å r.m.s.d.95 (Figure 3a). A carbon atom's width is around 1.4 Å, which can be used as a benchmark for precision. When the backbone is highly precise, in addition to extremely accurate domain structures (Figure 3b). AlphaFold may generate highly accurate side chains (Figure 3c) . This significantly outperforms template-based approaches, even in the presence of strong templates. AlphaFold's all-atom accuracy was 1.5 Å r.m.s.d.95, while the best alternative method's all-atom accuracy was 3.5 Å r.m.s.d.95. With precise domains and domain-packing, our approaches scale to exceedingly long proteins (Figure 3d). Lastly, the model's ability to produce accurate, per-residue dependability estimations should allow users to utilize these predictions with confidence (Jumper *et al.*, 2021).
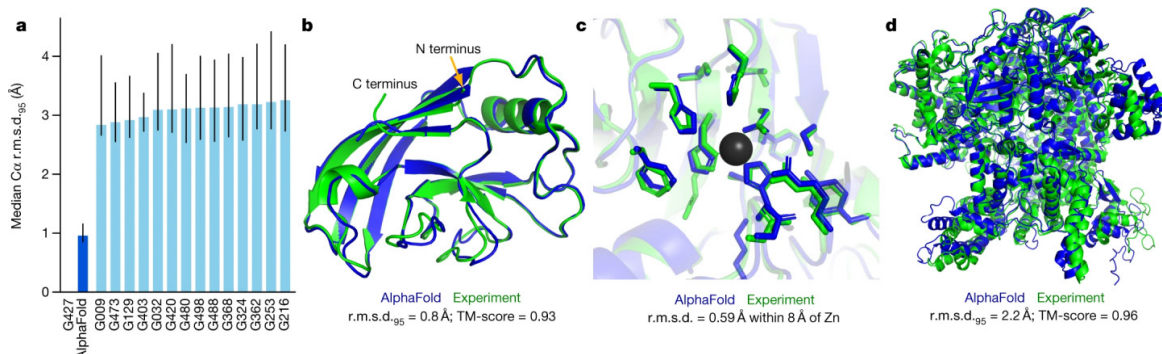
Figure 3. High prediction accuracy of AlphaFold structure. **a**, AlphaFold's performance on the CASP14 dataset (*n* = **87 protein domains**) in comparison to the top-15 entries (out of 146 entries), group numbers match the numbers given to participants by CASP. The information is provided by the median and its 95% confidence interval, which are calculated using 10,000 bootstrap samples. **b**, the real (experimental) structure (green) and the AlphaFold prediction of CASP14 target T1049 (PDB 6Y4F, blue) are comparisons. Four residues in the crystal structure's C terminus are not shown because they are B-factor outliers. **c**, CASP14 target T1056 (PDB 6YJ1). An illustration of a zinc-binding site that is accurately predicted (while AlphaFold does not specifically predict the zinc ion, it does have correct side chains). **d**, CASP target T1044, a 2,180-residue single (PDB 6VR4) chain was predicted with correct domain packing. The figure is reproduced from Jumper, J., Evans, R., Pritzel, A. *et al.* Highly accurate protein structure prediction with AlphaFold. Nature 596, 583–589 (2021). https://doi.org/10.1038/s41586-021-03819-2. Copyright © 2021, The Author(s). The figure was cropped from the original one retaining the data provided by authors.

A study used AI-generative models to create a series of hinge cores based on the binding posture of a reported chemical (GLPG-3970, 3) with the AlphaFold protein structure (Chemistry42). A hit molecule targeting SIK2 was produced using a new scaffold following molecular docking, manufacturing, and biological assessment. Compound **8g** was found through additional SAR investigation to have better efficacy against SIK2 than the previously reported inhibitors (Figure 4). *In vitro* studies also confirmed the *in silico* studies, proving that this compound has high activity, good ADMET profiles, and great selectivity over other AMPK kinases. As a result, an artificial intelligence method for finding new and selective kinase inhibitors is offered by this work (*Zhu et al.*, 2023).
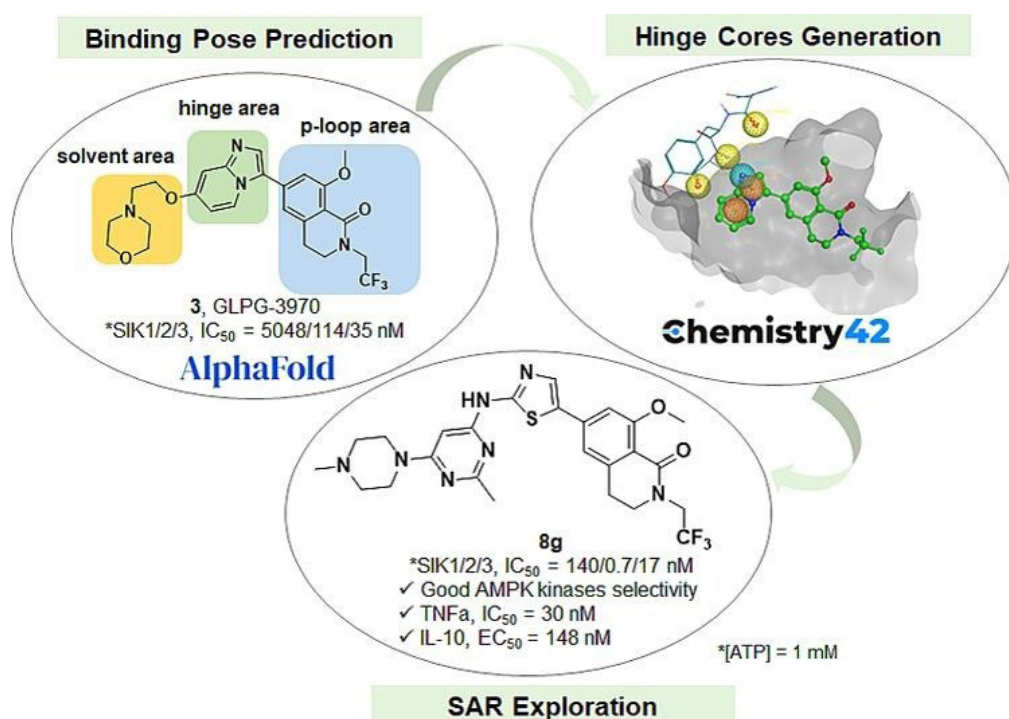
Figure 4. Design of compound 8g as AMPK kinase inhibitor (Zhu *et al.,* 2023)

Table 1. AI-Based computational tools for target identification

Tools	Description (available websites)	References
AlphaFold2	An AI system developed by DeepMind to predict a protein's 3D structure from its amino acid sequence. (https://colab.research.google.com/github/sokrypton/ColabFold/blob/main/AlphaFold2.ipynb)	Jumper *et al.*, 2021
RosettaFold	A three tract neural network, learning the patterns in sequences, and protein's amino acid interactions with one another, and predicts a protein's three-dimensional structure.	Baek *et al.*, 2021
DeepFragLib	Protein-specific fragment library built using deep neural networks.	Wang *et al.*, 2019
ProteinNet	A standardized data set for machine learning of protein structure to provide protein sequences, structures, MSAs, PSSMs, and standardized training/validation/test splits.	Cao *et al.*, 2012b

MSA: multiple sequence alignments, PSSM: position-specific scoring matrices

Hit Discovery

Virtual screening (VS) is one of the primary computational methods in drug discovery to identify bioactive molecules capable of binding target proteins. It is an efficient method that is used in early drug development to eliminate compounds that cannot target the protein of interest and to identify new hits (Lavecchia and Giovanni, 2013). As a result, virtual screening has become an indispensable tool in overcoming challenges associated with high costs and low success rates in drug discovery. Virtual screening methods are broadly categorized into two groups: structure-based drug design (SBDD) and ligand-based drug design (LBDD). SBDD relies on understanding the possible interactions between ligands and the structurally resolved target protein. On the other hand, LBDD focuses on assessing the similarity of a designed compound to known bioactive agents. SBDD needs 3D structural knowledge of the target protein (Dror *et al.*, 2004). The most used technique for SBDD, molecular docking, provides the prediction of the binding pose of the ligand in the target protein and determines its binding affinity (Blundell, 2019). In molecular docking techniques, many possible ligand poses have relied on the target protein, and the ligands are ordered by a scoring function (SF). Molecular docking programs implement a search algorithm in which the conformation of the ligand

is determined recursively up to the convergence to the minimum energy is achieved. Finally, as the sum of the electrostatic and Van der Waals energies, an affinity scoring function, ΔG U total i kcal/mol, is used to rank the candidate postures. The forces that propel these particular interactions in biological systems are directed at complementarities between the ligand or substrate and the binding site surfaces in terms of electrostatics and shape (Pagadala *et al.*, 2017). Consequently, an increase in protein-ligand binding and structural data makes it possible to identify the protein-ligand interactions by using AI technology, which provides progress in SBVS (Table 2).

Recently, many researchers have utilized molecular docking techniques to identify the possible interactions between compounds and target proteins. For example, in a study, to combat viruses a new class of compounds was introduced and to assess their antiviral efficacy against the major protease M pro of SARS-CoV-2 (2019-nCoV) the Auto Dock Vina program was used. As a result, when compared to lopinavir as a reference drug, three compounds had the most promising antiviral efficacy against SARS-CoV-2. The findings highlight the consistency of the in vitro and in silico studies (Alamshany *et al.*, 2023).

Table 2. AI-Based computational tools for hit discovery

Tools	Description (available websites)	Reference
RepCOOL	A novel network-based method for drug repositioning.	Fahimian *et al.*,2020
DeepConv-DTI	A deep learning method to predict drug-target interaction. (https://github.com/GIST-CSBL/DeepConv-DTI)	Lee *et al.*, 2019
DeepH-DTA	A deep learning method to predict drug-target interaction. (https://github.com/Hawash-AI/deepH-DT)	Abdel-Basset *et al.*, 2020
DeepPurpose	Provides the library for drug-target prediction based on deep learning.	Huang *et al.,* 2020
AutoDock	Provides the prediction of how small molecules, such as substrates or drug candidates, bind to a receptor of known 3D structure. (https://autodock.scripps.edu/)	Österberg *et al.*, 2002
MOE	A drug discovery software platform that integrates visualization, modeling, and simulations, as well as methodology development, in one package. (https://www.chemcomp.com)	Reynolds et al., 2010
GLIDE	A molecular modeling software developed by Schrödinger, for docking of small molecules into proteins and other biopolymers.	Pagadala *et al.*, 2017

Recently, new categories of machine and deep learning-based scoring functions (SFs) have been introduced to discern the relationship between interaction terms for predicting binding affinity. ML methods such as RF and SVM are leveraged to enhance the efficacy of SFs (Ballester, 2019; Ain *et al.,* 2015; Shen *et al.,* 2019; Coley *et al.,* 2020; Li *et al.,* 2020). These approaches introduce non-linear relationships between individual energy terms and binding affinity, notably improving screening and scoring capabilities. For instance, Wang and Zhang incorporated a ΔvinaRF parameterization correction technique, integrating RF with AutoDock scoring function, demonstrating excellent performance compared to GlideScore XP (Repasky *et al.*, 2012).

Traditional ML methods face limitations in manual recognition and feature extraction, hindering large-scale applications. The emergence of deep learning (DL) methods addresses this challenge. Capitalizing on the success of CNN in image processing, this technique is employed to extract features from protein-ligand interaction maps for predicting protein-ligand affinity. Jimenez *et al* utilized a 3D graph CNN model that provides a good relationship with experimental data in the datasets to show predictive binding affinities (Jimenez *et al.*, 2018). Pereira *et al.* established a deep convolutional neural networks method called DeepVS that gets the outcomes of MD as the input of DCNN, and can automatically learn and extract relevant features from the basic data (Pereira *et al.*, 2016, Jiang *et al.*, 2018).

Hit To Lead Optimization

In the process of lead optimization, potent lead compounds can be found by analyzing and predicting the activity of a series of drug analogs. The quantitative structure-activity relationship (QSAR) models for virtual screening are derived by the standard ligand-based drug design to find the potent candidates from a series of hits compounds by prediction of pharmacological activity. QSAR mainly refers to the use of mathematical methods for examining the quantitative mapping relationship of the structural or physicochemical properties of compounds with their pharmacological activities. By screening the molecular database, QSAR method automatically chooses the most promising compounds for synthesis and analysis. It saves time and money by reducing the blindness of the experiment and accelerating the drug development process with the desired pharmacological activity. The process of QSAR method consists of data collection, data selection, generating molecular descriptors, the establishment of a mathematical model, interpretation, and application of models. With the development of ML techniques, AI models are used in QSAR research to construct mathematical models of the relationship between chemical structure and pharmacological activity (Zhong *et al.*, 2018, Dobchev *et al.*, 2014, Dudek *et al.*, 2006, Ning and Karypis, 2011). Neural networks (NNs) method was introduced to QSAR analysis by Aoyama *et al.* in 1990. Various traditional ML methods, such as RF and SVM, have also been widely utilized to construct QSAR models (Aoyama *et al.*, 1990). In recent years, DL methods have been implemented to QSAR modeling due to the ability of dealing with various chemical characters and the merit of extracting features automatically (Ghasemi *et al.*, 2018) (Table 3).

Numerous research on the use of AI-assisted QSAR models, such as RF and DNN, to identify the hit compounds have been published in recent years. To show that RF and DNN were better in hit prediction efficiency, Tsou LK and colleagues conducted comparison tests between DNN and other ligand-based virtual screening (LBVS) techniques. Several triple-negative breast cancer (TNBC) inhibitors were identified as strong hits by DNN screening of the 165,000-compound database. Their findings demonstrate the potential of DNN as an effective hit prediction module and offer experimental proof that machine learning is capable of identifying strong hits *in silico* from a small training set (Figure 5) (Tsou *et al.*, 2020).
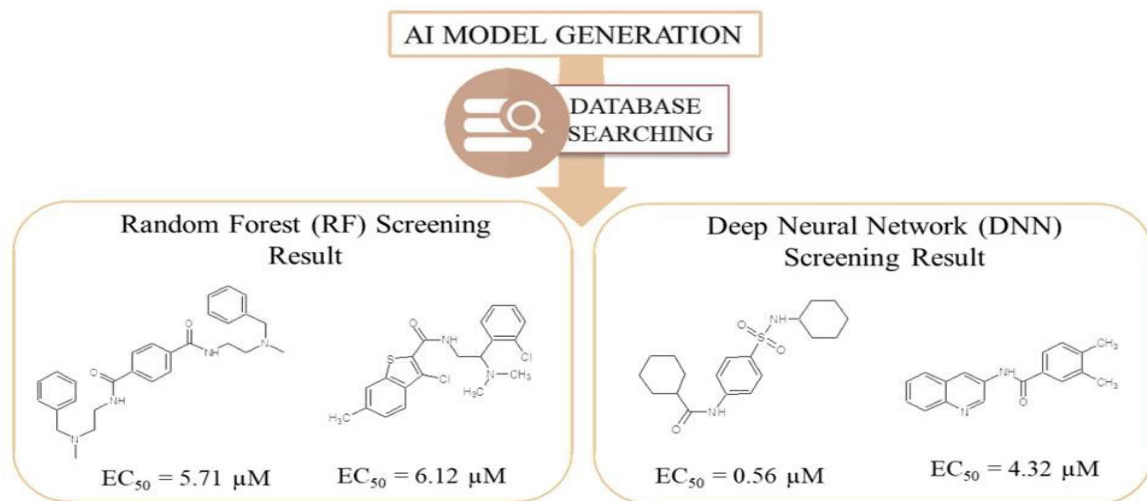
Figure 5. Tsou LK and coworkers' studies compounds (Tsou *et al.*, 2020)

In a different research, Koksal and Tugcu used QSARINS software to create QSAR models that predicted the analgesic and anti-inflammatory properties of several 2-benzoxazolinone derivatives. These models work based on the rule that the drug candidates' hydrophobicity, halogen count, and molecular structure shape are important indicators of their analgesic and anti-inflammatory properties.

Seventy-seven novel compounds were introduced as possible analgesic and anti-inflammatory medications based on the previously investigated compounds and the models that were built. As a result, the majority of the recently developed compounds showed encouraging analgesic and anti-inflammatory effects (Tugcu and Koksal, 2018).

Table 3. AI-Based computational tools for hit-tolerated optimization

Tools	Description	Reference
DeepVS	Firstly, used deep learning to improve the performance of SBVS and used the DCNNs model. This method takes the result of molecular docking as the input of DCNN, and can automatically learn and extract relevant features.	Pereira *et al.*, 2016
BindScope	CNN-based protein-ligand docking and binding predictor	Skalic *et al.*, 2019
DeepConv-DTI	Provides prediction of drug-target interactions via deep learning with convolution on protein sequences.	Lee *et al.*, 2019
OntoQSAR	A machine learning model that interprets chemical and biological data in quantitative structure-activity relationship studies.	Angelo *et al.*, 2020
QSARINS	A software for the development and validation of multiple linear regression Quantitative Structure-Activity Relationship (QSAR) models by Ordinary Least Squares method and Genetic Algorithm for variable selection.	Gramatica *et al.*, 2013

SBVS: structure-based drug design,

DCNN: deep convolutional neural networks,

CNN: convolutional neural networks

Lead Optimization

Prediction of pharmacokinetic properties is not only crucial for decreasing the risks of late-stage drug development but also aids researchers in optimizing screening by prioritizing the testing of the most promising compounds. Absorption, distribution, metabolism, elimination, and toxicity (ADMET) prediction is an efficient method during hit-to-lead and lead optimization steps. It is documented that success rate and production efficiency in the drug development process mainly depend on the early estimation and optimization of the ADMET properties of the lead compounds. However, relying on *in vivo* experiments for estimating the ADMET of a compound comes with high costs, prolonged time requirements, and the need for substantial material and animal resources (Caldwell *et al.*, 2009). The utilization of AI-assisted ADMET prediction has proven to be a cost-effective strategy, reducing drug development costs by up to 50%, making it a popular method in early drug discovery (Wang *et al.*, 2019; Tan *et al.,* 2010). In addition, the success of AI-assisted ADMET prediction has been notably enhanced with the availability of high-quality data and more accurate statistical analysis methods. There are many approaches to ADMET modeling in drug discovery. Among ML methods, k-NN, SVM, RF and ANNs are used in the ADMET property investigation (Obrezanova *et al.*, 2007, Kortagere *et al.*, 2008, Cao *et al.*, 2010, Cao *et al.*, 2012, Klon *et al.*, 2006, Lombardo *et al.*, 2006, Wang *et al.*, 2016). For example, DeepTox is a useful ML method that not only identifies static and dynamic properties within the chemical descriptors of the compounds but also predicts the toxicity of a molecule based on predefined 2500 toxicophore features (Mayr *et al.*, 2016). A variety of AI tools used in ADMET prediction are detailed in Table 4.

Computer-aided AI methods are used for early and accurate prediction of adverse reaction of the drug compounds. For example, using in silico methods, Oner et al. analyzed the anticancer characteristics of Tetrahydrocannabinol (THC), Tetrahydrocannabivarin (THCV), and Cannabidiol (CBD). The ADMET properties of these compounds was evaluated using Protox-II. According to result, CBD has the lowest risk for immunotoxicity, carcinogenicity, and hepatotoxicity. On the other hand, the possibility of being inert in terms of mutagenicity and cytotoxicity is highest. Furthermore, CBD has the highest potential for preventing lung cancer (Gallerdo *et al.*, 2024).

Günes and colleagues developed a model to predict 329 known antidepressant medications (ADRs) of which 27 were approved. They then looked at three ML algorithms (SVM, k-NN, and multilayer perception) to see which is more suitable for this task. To predict ADRs with AI model, they combined the chemical structures and biological properties (target protein, enzymes, and transporters) of compounds with the known ADRs of those drugs. The model they created using MLP with BestFirst and CfsSubsetEval, based on the chemical features of the approved antidepressants, correctly predicted the ADRs associated with the withdrawal of indalpine, zimelidine, pheniprazine, amineptine, and medifoxamine. The outcomes demonstrated the approach's external validity by correctly predicting a respectable number of previously identified ADRs from the literature (Günes *et al.*, 2021).

Table 4. AI-Based computational tools for lead optimization

Tools	Description (available website)	Reference
ProTox-II	A webserver for the prediction of toxicity of chemicals. (http://tox.charite.de/protox_II)	Banerjee *et al.*, 2018
ADMETlab	A platform for systematic ADMET evaluation based on a comprehensively collected ADMET database. (http://admet.scbd.com)	Dong *et al.*, 2018
COSMOfrag	Provides its broad applicability for the accurate prediction of thermodynamic, environmental, or physiological properties.	Hornig and Klamt, 2005

ADMET: absorption, distribution, metabolism, excretion, and toxicity

The integration of AI in four essential stages, namely target identification, hit discovery, hit-to-lead optimization, and lead optimization, significantly reduces time and costs compared to traditional methods. Notably, some drugs designed through AI-driven approaches have received approval from the FDA for clinical trials (Liu *et al.*, 2019, Mak *et al.*, 2022, Soni *et al.*, 2022, Pun *et al.*, 2023). Since 2023, four prominent drugs that were FDA-approved for clinical trials are listed in Table 5.

Table 5. FDA-approved drugs for clinical trials

Drug	Clinical phase	Years when began the clinical trials	Therapeutical target	Pharmacological activity	Organization
DSP-1181	Phase 1	2020	5-HT1A receptor agonist	Obsessive-compulsive disorder	Exscientia and Sumitomo Dainippon Pharma
EXS21546	Phase 1	2020	Adenosine A2a receptor antagonist	Autoimmune oncology treatment	Exscientia and Evotec
DSP-0038	Phase 1	2021	Dual target on 5-HT1A receptor and 5HT2A receptor antagonist	Alzheimer's diseases	Exscientia and Sumitoto Dainippan Pharma
INSO18-055	Phase 2	2023	Anti-fibrotic small molecule inhibitor	Idiopathic Pulmonary Fibrosis	In silico Medicine

AI-Assisted Synthesis Planning

In drug discovery, the design of drug molecules must align with synthesizability to advance through the optimization process and yield compounds with improved properties. For this reason, organic synthesis is an essential part of drug discovery. Choosing the most suitable synthesis plan provides many advantages in terms of cost and time. Therefore, numerous computational approaches have been built to promote synthesis planning. There are three main tasks for AI-assisted synthesis: predicting retrosynthetic strategy, forecasting reaction conditions, and predicting side products of the selected reaction (Struble *et al.*, 2020, Segler *et al.*, 2018) (Figure 6).
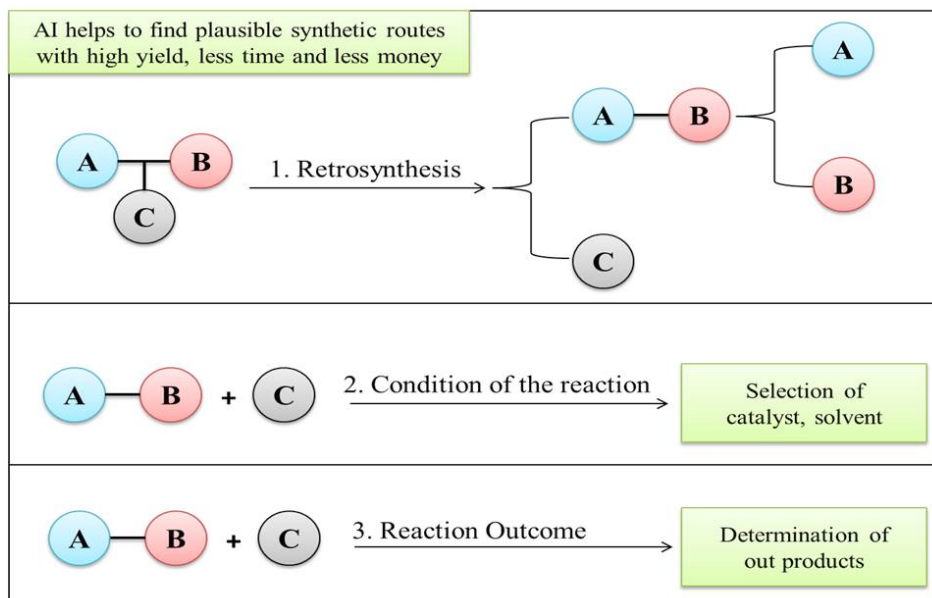
Figure 6. AI-assisted synthesis prediction

Retrosynthetic analysis is defined as transforming a target molecule into intermediates or precursors regardless of the reactivity reagents. Retrosynthesis pathway predictions cover the sequential cutting of the target compounds at different positions. Monte Carlo tree search (MCTS) is a method that was used in retrosynthesis prediction to perform branch decisions (Browne *et al.*, 2012). In recent years, various ML-based techniques have been introduced for retrosynthetic reaction prediction. For example, Liu *et al.* used a sequence-to-sequence-based model for retrosynthetic reaction prediction (Liu *et al.*, 2017). In 2017, Segler *et al.* utilized the first deep learning to find plausible synthetic routes with high yield and less time. Instead of manually encoding, a database of known reactions is provided to convert into reaction templates, considering the core of the reaction and the nearest neighbor atoms. The prediction of templates related to the targeted product in retrosynthetic analysis has been tackled using ANN. This approach enables the direct learning of retrosynthetic strategies through data. Furthermore, ANNs can select an efficient tree-search for a logical pathway among numerous reaction templates by filtering out results from implausible chemical reactions (Segler *et al.*, 2017). The work by Segler *et al.* demonstrated the feasibility of utilizing data-driven approaches, and this methodology has since been further enhanced with the availability of multiple open-sources as well as commercial tools (Table 6).

Table 6. AI-Based computational tools for synthesis planning

Tools	Description (available website)	Reference
Chemical.AI	A professional website to predict retrosynthesis routes.	https://chemical.ai
AiZynthFinder	A fast, robust, and flexible open-source software for retrosynthetic planning. (http://www.github.com/MolecularAI/aizynthfinder)	Genheden *et al.*, 2020
SciFinder	Make a whole retrosynthetic analysis powered by the renowned CAS collection of reactions, reducing the synthetic planning time.	Gabrielson., 2018
Reaxys	Provides prediction retrosynthesis combines high-quality reaction data with AI technology.	Goodman., 2009

According to CAS data, the SciFinder retrosynthesis planner builds pathways to desired compounds using experimental and predicted reaction steps from 121 million reactions in the CAS collection, which is compiled over 110 years of chemistry research. As an example, using SciFinder, the retrosynthesis of compound **A** is illustrated in Figure 7 (https://www.cas.org/resources/press-releases/scifinder-n-predictive-retrosynthesis).
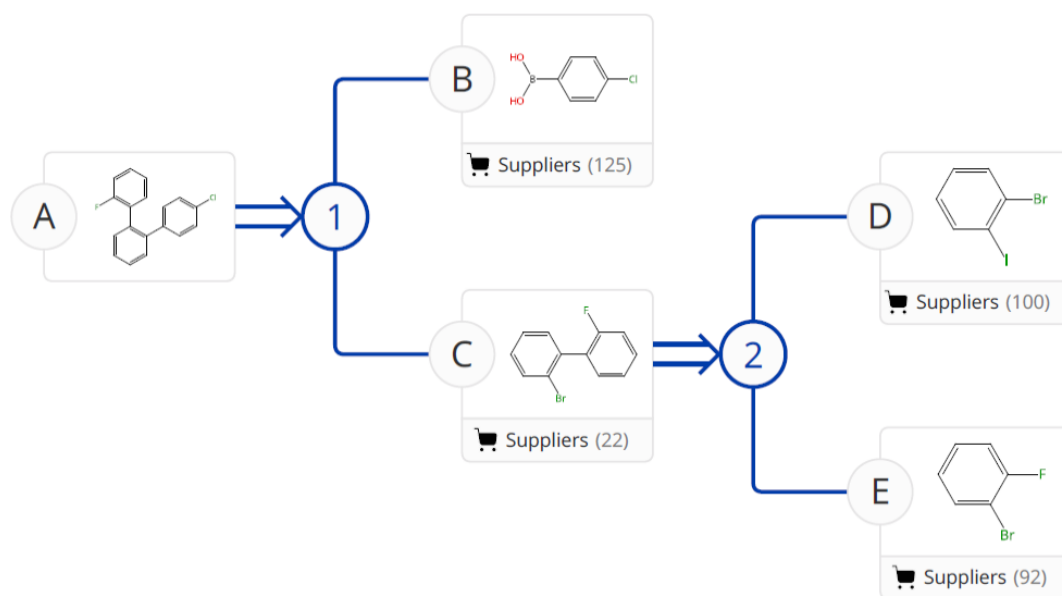
Figure 7. An example of a retrosynthesis tool of SciFinder produced at *https://scifinder-n.cas.org*

AI techniques are also effective in the prediction of the products and yields of organic reactions based on the molecular properties of the reactants. Recently, several studies on AI algorithms to generalize yield prediction have been documented (Hessler and Baringhaus, 2018, Struble *et al.*, 2020). Recurrent neural networks (RNNs) can be used to form *de novo* chemical discovery by using simplified molecular input line entry systems (SMILES) string representations of the structure. In chemical synthesis, starting materials and resulting compounds are encoded by SMILES strings and linked in an encoder-decoder architecture. The overall performance of this technology has demonstrated comparability to rule-based expert systems, although significant variations have been observed across different reaction classes (Savage *et al.*, 2017). An alternative approach involves the use of recommender systems to identify reactants yielding a desired product in combination with a chemical reaction graph. Differently, the recommender systems have been employed for identifying reactants yielding a targeted product with a chemical reaction graph. The utilization of deep neural networks combined with a Monte Carlo tree search provides an excellent performance for retrosynthetic prediction (Segler *et al.*, 2018).

Challenges of Using AI in Healthcare

Despite many advantages of bringing AI to drug discovery, it also has several challenges that must be considered (Blanco-Gonzalez *et al.*, 2023, Vamathevan *et al.*, 2019). The first challenge is suitable data availability. ML and DL approaches require a large volume of data for analyzing different tasks (Tsuji *et al.*, 2021). However, the accessible data can be restricted, or data can be low quality or inconsistent, leading to low accuracy and reliability of the results (Gomez *et al.,* 2018). Another difficulty arises from the fact that the data obtained in healthcare services are unclear,

noisy, and incomplete. This prevents AI from having clean and structured data and makes it difficult to apply AI in drug development (Manne and Kantheti, 2021). Finally, privacy and confidentiality are the most controversial topics of using AI in the drug discovery process. Providing personal information to any database and reusing this information without permission causes ethical problems (Aung *et al.,* 2021). To overcome this problem, measures protecting the confidentiality of patient information are necessary to be addressed within certain policies.

CONCLUSION

In summary, AI has attracted a lot of attention recently and has been successfully integrated into many steps of drug discovery. AI makes the drug discovery process shorter, cheaper, more advanced, and more reliable when compared to traditional drug discovery methods. In addition to assistance in quick and seamless identification of the hit compound, AI also contributes to the prediction of the potentially active drug candidate, understanding of drug-target interactions, ADMET properties, as well as suggestions of synthesis routes of active molecules. AI can also contribute to establishing the safety and efficacy of the product in clinical trials, as well as ensuring proper positioning and costing in the market through comprehensive market analysis and prediction. However, there are a limited number of AI-designed drugs that recived approval from FDA for clinical trials. Although specific challenges remain about the implementation of this technology, AI has gained a role as an invaluable tool in the pharmaceutical industry. All in all, AI serves as a golden key that has the potential to save lives by addressing critical segments of the drug discovery process, offering hope for numerous diseases that currently lack effective treatments or preventive measures.

CONFLICT OF INTEREST

The authors declare that there is no conflict of interest.

AUTHOR CONTRIBUTION STATEMENT

REFERENCES

Abdel-Basset, M., Hawash, H., Elhoseny, M., Chakrabortty, R. K., & Ryan, M. (2020). DeepH-DTA: deep learning for predicting drug-target interactions: a case study of COVID-19 drug repurposing. *Ieee Access, 8,* 170433-170451.

Ain, Q. U., Aleksandrova, A., Roessler, F. D., & Ballester, P. J. (2015). Machine-learning scoring functions to improve structure-based binding affinity prediction and virtual screening. *Wiley Interdisciplinary Reviews: Computational Molecular Science, 5(6),* 405-424. doi: 10.1002/wcms.1225.

Angelo, R. M., Io, A. K., Almeida, M. P., Silveira, R. G., Oliveira, P. R., Alcazar, J. J. OntoQSAR: An ontology for interpreting chemical and biological data in quantitative structure-activity relationship studies. *International Computer Science Conference, 203-206*, 2020, San Diego, CA, USA

Aoyama, T., Suzuki, Y., & Ichikawa, H. (1990). Neural networks applied to pharmaceutical problems. III. Neural networks applied to quantitative structure-activity relationship (QSAR) analysis. *Journal of Medicinal Chemistry, 33(9),* 2583-2590. doi: 10.1021/jm00171a037

Aung, Y. Y., Wong, D. C., & Ting, D. S. (2021). The promise of artificial intelligence: a review of the opportunities and challenges of artificial intelligence in healthcare*. British Medical Bulletin, 139(1),* 4-15. doi: 10.1093/bmb/ldab016.

Alamshany, Z. M., Khattab, R. R., Hassan, N. A., El-Sayed, A. A., Tantawy, M. A., Mostafa, A., & Hassan, A. A. (2023). Synthesis and molecular docking study of novel pyrimidine derivatives against COVID-19. *Molecules, 28(2),* 739. doi: 10.3390/molecules28020739.

Baek, M., DiMaio, F., Anishchenko, I., Dauparas, J., Ovchinnikov, S., Lee, G. R., ... & Baker, D. (2021). Accurate prediction of protein structures and interactions using a three-track neural network. *Science, 373(6557),* 871-876. doi: 10.1126/science.abj8754

Ballester, P. J. (2019). Selecting machine-learning scoring functions for structure-based virtual screening. *Drug Discovery Today: Technologies, 32,* 81-87. doi: 10.1016/j.ddtec.2020.09.001

Banerjee, P., Eckert, A. O., Schrey, A. K., & Preissner, R. (2018). ProTox-II: a webserver for the prediction of toxicity of chemicals. *Nucleic Acids Research, 46(1),* 257-263. doi: 10.1093/nar/gky318

Blanco-Gonzalez, A., Cabezon, A., Seco-Gonzalez, A., Conde-Torres, D., Antelo-Riveiro, P., Pineiro, A., & Garcia-Fandino, R. (2023). The role of ai in drug discovery: challenges, opportunities, and strategies. *Pharmaceuticals, 16(6),* 891.doi: 10.3390/ph16060891

Blundell, T. L. (1996). Structure-based drug design. *Nature, 384(6604),* 23. doi: 10.1038/384023a0

Bernard, S., Adam, S., & Heutte, L. (2012). Dynamic random forests. *Pattern Recognition Letters, 33(12),* 1580-1586. doi: 10.1016/j.patrec.2012.04.003

Browne, C. B., Powley, E., Whitehouse, D., Lucas, S. M., Cowling, P. I., Rohlfshagen, P., ... & Colton, S. (2012). A survey of monte carlo tree search methods. *IEEE Transactions on Computational Intelligence and AI in games, 4(1),* 1-43. doi: 10.1109/TCIAIG.2012.2186810

Caldwell, G. W., Yan, Z., Tang, W., Dasgupta, M., & Hasting, B. (2009). ADME optimization and toxicity assessment in early-and late-phase drug discovery. *Current Topics in Medicinal Chemistry, 9(11),* 965-980. doi: 10.2174/156802609789630929

Cano, G., Garcia-Rodriguez, J., Garcia-Garcia, A., Perez-Sanchez, H., Benediktsson, J. A., Thapa, A., & Barr, A. (2017). Automatic selection of molecular descriptors using random forest: Application to drug discovery. *Expert Systems with Applications, 72,* 151-159. doi: 10.1016/j.eswa.2016.12.008

Cao, D. S., Xu, Q. S., Liang, Y. Z., Chen, X., & Li, H. D. (2010). Prediction of aqueous solubility of druglike organic compounds using partial least squares, back-propagation network and support vector machine. *Journal of Chemometrics, 24(9),* 584-595.doi: 10.1002/cem.1321

Cao, D. S., Zhao, J. C., Yang, Y. N., Zhao, C. X., Yan, J., Liu, S., ... & Liang, Y. Z. (2012). In silico toxicity prediction by support vector machine and SMILES representation-based string kernel. *SAR and QSAR in Environmental Research, 23(1-2),* 141-153. doi: 10.1080/1062936X.2011.645874.

Cao, T., Wu, X., & Hu, X.. ProteinNET: A Protein Interaction Network Integration System. In Modern Advances in Intelligent Systems and Tool, 71-76, 2012, Berlin, Heidelberg.

Chan, H. S., Shan, H., Dahoun, T., Vogel, H., & Yuan, S. (2019). Advancing drug discovery via artificial intelligence. *Trends in Pharmacological Sciences*, *40*(8), doi: 592-604. 10.1016/j.tips.2019.06.004

Cheng, F., & Sutariya, V. (2012). Applications of artificial neural network modeling in drug discovery. *Clinical and Experimental Pharmacology, 2(3),* 1-2. doi: 10.4172/2161-1459.1000e113

Coley, C. W., Eyke, N. S., & Jensen, K. F. (2020). Autonomous discovery in the chemical sciences part I: Progress. *Angewandte Chemie International Edition, 59*(51*),* 22858-22893. doi: 10.1002/anie.201909987

Cortes, C., & Vapnik, V. (1995). Support-vector networks. *Machine Learning, 20,* 273-297. Retrieved from https://link.springer.com/article/10.1007/BF00994018.

Dobchev, D., & Karelson, M. (2016). Have artificial neural networks met expectations in drug discovery as implemented in QSAR framework. *Expert Opinion on Drug Discovery, 11*(7)*,* 627-639. doi: 10.1080/17460441.2016.1186876

Dobchev, D., G Pillai, G., & Karelson, M. (2014). In silico machine learning methods in drug development. *Current Topics in Medicinal Chemistry, 14*(16)*,* 1913-1922. doi: 10.2174/1568026614666140929124203

Dong, J., Wang, N. N., Yao, Z. J., Zhang, L., Cheng, Y., Ouyang, D., ... & Cao, D. S. (2018). ADMETlab: a platform for systematic ADMET evaluation based on a comprehensively collected ADMET database. *Journal of Cheminformatics, 10,* 1-11. doi: 10.1186/s13321-018-0283-x

Doniger, S., Hofmann, T., & Yeh, J. (2002). Predicting CNS permeability of drug molecules: comparison of neural network and support vector machine algorithms. *Journal of Computational Biology, 9(6),* 849-864. doi: 10.1089/10665270260518317.

Dror, O., Shulman-Peleg, A., Nussinov, R., & Wolfson, H. J. (2004). Predicting molecular interactions in silico: I. A guide to pharmacophore identification and its applications to drug design. *Current Medicinal Chemistry, 11(1),* 71-90. doi: 10.2174/0929867043456287.

Dudek, A. Z., Arodz, T., & Gálvez, J. (2006). Computational methods in developing quantitative structure-activity relationships (QSAR): a review. *Combinatorial Chemistry & High Throughput Screening, 9(3),* 213-228. doi: 10.2174/138620706776055539.

El Naqa, I., & Murphy, M. J. (2015). What is machine learning? *Springer International Publishing. 3-11,* 2015, Berlin, Germany.

Fahimian, G., Zahiri, J., Arab, S. S., & Sajedi, R. H. (2020). RepCOOL: computational drug repositioning via integrating heterogeneous biological networks. *Journal of Translational Medicine, 18*(1)*,* 1-10. Retrieved from https://translational-medicine.biomedcentral.com/articles/10.1186/s12967-020-02541-3

Fleming, N. (2018). How artificial intelligence is changing drug discovery. *Nature, 557*(7706)*,* 55-55. Retrieved from http://www.nature.com/nature/index.html

Fuloria, N. K., Fuloria, S., & Vakiloddin, S. (2013). Phase zero trials: a novel approach in drug development process. *Renal Failure, 35(7),* 1044-1053. doi: 10.3109/0886022X.2013.810543

Gabrielson, S. W. (2018). *SciFinder. Journal of the Medical Library Association: JMLA, 106*(4)*,* 588. doi: 10.5195/jmla.2018.515

Gallardo, A. A., Gutierrez, M. R., Gomez, L. A. J., Dumbrique, H. E. L., Liquido, M. I. H., Margaret, M., ... & Labrador, A. M. (2024). A Comparative Analysis on the Potential Anticancer Properties of Tetrahydrocannabinol, Cannabidiol, and Tetrahydrocannabivarin Compounds Through In Silico Approach. *Asian Pacific Journal of Cancer Prevention, 25*(3)*,* 839-856. doi: 10.31557/APJCP.2024.25.3.839.

Genheden, S., Thakkar, A., Chadimová, V., Reymond, J. L., Engkvist, O., & Bjerrum, E. (2020). AiZynthFinder: a fast, robust and flexible open-source software for retrosynthetic planning. *Journal of Cheminformatics, 12*(1)*,* 70. doi: 10.1186/s13321-020-00472-1

Ghasemi, F., Mehridehnavi, A., Pérez-Garrido, A., & Pérez-Sánchez, H. (2018). Neural network and deep-learning algorithms used in QSAR studies: merits and drawbacks. *Drug Discovery Today, 23*(10)*,* 1784-1790. doi: 10.1016/j.drudis.2018.06.016

Goodman, J. (2009). Computer Software Review, *Journal of Chemical Information and Modeling, 49,* 2897-2898. doi: 10.1021/ci900437n

Gómez-Bombarelli, R., Wei, J. N., Duvenaud, D., Hernández-Lobato, J. M., Sánchez-Lengeling, B., Sheberla, D., ... & Aspuru-Guzik, A. (2018). Automatic chemical design using a data-driven continuous representation of molecules. *ACS Central Science, 4(2),* 268-276. doi: 10.1021/acscentsci.7b00572

Güneş, S. S., Yeşil, Ç., Gurdal, E. E., Korkmaz, E. E., Yarım, M., Aydın, A., & Sipahi, H. (2021). Primum non nocere: In silico prediction of adverse drug reactions of antidepressant drugs. *Computational Toxicology, 18,* 100165. doi: 10.1016/j.comtox.2021.100165

Gramatica, P., Chirico, N., Papa, E., Cassani, S., & Kovarich, S. (2013). QSARINS: A new software for the development, analysis, and validation of QSAR MLR models. *Journal of Computational Chemistry, 34(24),* 2121-2132. doi: 10.1002/jcc.23361

Heikamp, K., & Bajorath, J. (2014). Support vector machines for drug discovery. *Expert Opinion on Drug Discovery, 9(1),* 93-104. doi: 10.1517/17460441.2014.866943

Hessler, G., & Baringhaus, K. H. (2018). Artificial intelligence in drug design. *Molecules, 23(10),* 2520. doi: 10.3390/molecules23102520

Hornig, M., & Klamt, A. (2005). COSMO f rag: a novel tool for high-throughput ADME property prediction and similarity screening based on quantum chemistry. *Journal of Chemical Information and Modeling, 45(5),* 1169-1177. doi: 10.1021/ci0501948

Huang, K., Fu, T., Xiao, C., Glass, L., & Sun, J. (2020). Deep purpose: a deep learning based drug repurposing toolkit. *ArXiv Preprint ArXiv*:2004.08919. doi: 10.48550/arXiv.2004.08919

Jiang, L., Xu, M., Liu, T., Qiao, M., & Wang, Z. Deepvs: A deep learning based video saliency prediction approach. *In Proceedings of the European Conference on Computer Vision (eccv),* 602-617, 2018, Munich, Germany.

Jiménez, J., Skalic, M., Martinez-Rosell, G., & De Fabritiis, G. (2018). K deep: protein–ligand absolute binding affinity prediction via 3d-convolutional neural networks. *Journal of Chemical Information and Modeling, 58(2),* 287-296. doi: 10.1021/acs.jcim.7b00650

Jumper, J., Evans, R., Pritzel, A., Green, T., Figurnov, M., Ronneberger, O., ... & Hassabis, D. (2021). Highly accurate protein structure prediction with AlphaFold. *Nature, 596(7873),* 583-589. Retrieved from https://www.nature.com/articles/s41586-021-03819-2

Klon, A. E., Lowrie, J. F., & Diller, D. J. (2006). Improved naive Bayesian modeling of numerical data for absorption, distribution, metabolism and excretion (ADME) property prediction. *Journal of Chemical Information and Modeling, 46(5),* 1945-1956. doi: 10.1021/ci0601315

Kortagere, S., Chekmarev, D., Welsh, W. J., & Ekins, S. (2008). New predictive models for blood–brain barrier permeability of drug-like molecules. *Pharmaceutical Research, 25,* 1836-1845. doi: 10.1007/s11095-008-9584-5

Lavecchia, A. (2015). Machine-learning approaches in drug discovery: methods and applications. *Drug Discovery Today, 20(3),* 318-331. doi: 10.1016/j.drudis.2014.10.012

Lavecchia, A., & Di Giovanni, C. (2013). Virtual screening strategies in drug discovery: a critical review. *Current Medicinal Chemistry, 20(23),* 2839-2860. doi: 10.2174/09298673113209990001

Lee, I., Keum, J., & Nam, H. (2019). DeepConv-DTI: Prediction of drug-target interactions via deep learning with convolution on protein sequences. PLoS *Computational Biology, 15(6),* e1007129. doi: 10.1371/journal.pcbi.1007129

Lewis, T., & Writer, S. (2014). A brief history of artificial intelligence. *Live Science, 61(4),* 000812561986492 doi: 10.1177/0008125619864925

Li, H., Hou, J., Adhikari, B., Lyu, Q., & Cheng, J. (2017). Deep learning methods for protein torsion angle prediction. *BMC Bioinformatics, 18(1),* 1-13. Retrieved from https://bmcbioinformatics.biomedcentral.com/articles/10.1186/s12859-017-1834-2

Li, H., Sze, K. H., Lu, G., & Ballester, P. J. (2020). Machine-learning scoring functions for structure-based drug lead optimization. *Wiley Interdisciplinary Reviews: Computational Molecular Science, 10(5),* e1465. doi: 10.1002/wcms.1465

Lindsay, R. K., Buchanan, B. G., Feigenbaum, E. A., & Lederberg, J. (1993). DENDRAL: a case study of the first expert system for scientific hypothesis formation. *Artificial intelligence, 61(2),* 209-261. doi: 10.1016/0004-3702(93)90068-M

Liu, B., He, H., Luo, H., Zhang, T., & Jiang, J. (2019). Artificial intelligence and big data facilitated targeted drug discovery. *Stroke and Vascular Neurology, 4(4),* 206-213. doi: 10.1136/svn-2019-000290.

Liu, B., Ramsundar, B., Kawthekar, P., Shi, J., Gomes, J., Luu Nguyen, Q., ... & Pande, V. (2017). Retrosynthetic reaction prediction using neural sequence-to-sequence models. *ACS Central Science, 3(10),* 1103-1113. doi: 10.1021/acscentsci.7b00303

Lombardo, F., Obach, R. S., DiCapua, F. M., Bakken, G. A., Lu, J., Potter, D. M., ... & Zhang, Y. (2006). A hybrid mixture discriminant analysis–random forest computational model for the prediction of volume of distribution of drugs in human. *Journal of Medicinal Chemistry, 49(7),* 2262-2267. doi: 10.1021/jm050200r

Madhukar, N. S., Khade, P. K., Huang, L., Gayvert, K., Galletti, G., Stogniew, M., ... & Elemento, O. (2017). A new big-data paradigm for target identification and drug discovery. *Biorxiv,* 134973. doi: 10.1101/134973

Mak, K. K., Balijepalli, M. K., & Pichika, M. R. (2022). Success stories of AI in drug discovery-where do things stand?. *Expert Opinion on Drug Discovery, 17(1),* 79-92. doi: 10.1080/17460441.2022.1985108

Manne, R., & Kantheti, S. C. (2021). Application of artificial intelligence in healthcare: chances and challenges. *Current Journal of Applied Science and Technology, 40(6),* 78-89. Retrieved from https://papers.ssrn.com/sol3/papers.cfm?abstract_id=4393347

Mayr, A., Klambauer, G., Unterthiner, T., & Hochreiter, S. (2016). DeepTox: toxicity prediction using deep learning. *Frontiers in Environmental Science, 3,* 80. Retrieved from https://www.frontiersin.org/journals/environmental-science/articles/10.3389/fenvs.2015.00080/full

Melville, J. L., Burke, E. K., & Hirst, J. D. (2009). Machine learning in virtual screening. *Combinatorial Chemistry & High Throughput Screening, 12(4),* 332-343. doi: 10.2174/138620709788167980

Ning, X., & Karypis, G. (2011). In silico structure-activity-relationship (SAR) models from machine learning: a review. *Drug Development Research, 72(2),* 138-146. doi: 10.1002/ddr.20410

Obrezanova, O., Csányi, G., Gola, J. M., & Segall, M. D. (2007). Gaussian processes: a method for automatic QSAR modeling of ADME properties. *Journal of Chemical Information and Modeling, 47(5),* 1847-1857. doi: 10.1021/ci7000633

Österberg F, Morris GM, Sanner MF, Olson AJ, Goodsell DS (2002). Automated docking to multiple target structures: incorporation of protein mobility and structural water heterogeneity in AutoDock. *Proteins, 46,* 34-40. doi: 10.1002/prot.10028

Pagadala, N. S., Syed, K., & Tuszynski, J. (2017). Software for molecular docking: a review. *Biophysical Reviews, 9,* 91-102. doi: 10.1007/s12551-016-0247-1

Paul, D., Sanap, G., Shenoy, S., Kalyane, D., Kalia, K., & Tekade, R. K. (2021). Artificial intelligence in drug discovery and development. *Drug Discovery Today, 26(1),* 80. doi: 10.1016/j.drudis.2020.10.010

Pereira, J. C., Caffarena, E. R., & Dos Santos, C. N. (2016). Boosting docking-based virtual screening with deep learning. *Journal of Chemical Information and Modeling, 56(12),* 2495-2506. doi: 10.1021/acs.jcim.6b00355

Pun, F. W., Ozerov, I. V., & Zhavoronkov, A. (2023). AI-powered therapeutic target discovery. *Trends in Pharmacological Sciences, 44(9),* 561-572. doi: 10.1016/j.tips.2023.06.010

Rao, V. S., & Srinivas, K. (2011). Modern drug discovery process: An in silico approach. *Journal of Bioinformatics and Sequence Analysis, 2(5),* 89-94. Retrieved from http://www.academicjournals.org/JBSA

Repasky, M. P., Murphy, R. B., Banks, J. L., Greenwood, J. R., Tubert-Brohman, I., Bhat, S., & Friesner, R. A. (2012). Docking performance of the glide program as evaluated on the Astex and DUD datasets: a complete set of glide SP results and selected results for a new scoring function integrating WaterMap and glide. *Journal of Computer-aided Molecular Design, 26,* 787-799. doi: 10.1007/s10822-012-9575-9.

Reynolds CH, Merz KM, Ringe D, eds. (2010). Drug Design: Structure- and Ligand-Based Approaches (1 ed.). *Cambridge, UK: Cambridge University Press.* ISBN 978-0521887236.

Savage, J., Kishimoto, A., Buesser, B., Diaz-Aviles, E., & Alzate, C. Chemical reactant recommendation using a network of organic chemistry. I*n Proceedings of the Eleventh ACM Conference on Recommender Systems,* 210-214, 2017, Como, Italy.

Schneider, G., & Fechner, U. (2005). Computer-based de novo design of drug-like molecules. *Nature Reviews Drug Discovery, 4(8),* 649-663. Retrieved from https://www.nature.com/articles/nrd1799

Segler, M. H., Preuss, M., & Waller, M. P. (2018). Planning chemical syntheses with deep neural networks and symbolic AI. *Nature, 555(7698),* 604-610. Retrieved from https://www.nature.com/articles/nature25978

Segler, M., Preuß, M., & Waller, M. P. (2017). Towards" alphachem": Chemical synthesis planning with tree search and deep neural network policies. *ArXiv Preprint ArXiv:*1702.00020. doi: 10.48550/arXiv.1702.00020

Shen, C., Ding, J., Wang, Z., Cao, D., Ding, X., & Hou, T. (2020). From machine learning to deep learning: Advances in scoring functions for protein–ligand docking. *Wiley Interdisciplinary Reviews: Computational Molecular Science, 10(1),* e1429. doi: 10.1002/wcms.1429

Skalic, M., Martínez-Rosell, G., Jiménez, J., & De Fabritiis, G. (2019). PlayMolecule BindScope: large scale CNN-based virtual screening on the web. *Bioinformatics, 35(7),* doi: 1237-1238. 10.1093/bioinformatics/bty758

Soni, K., & Hasija, Y. Artificial Intelligence Assisted Drug Research and Development. In 2022 IEEE Delhi Section Conference (DELCON), pp. 1-10, 2022, New Delhi, India.

Spencer, M., Eickholt, J., & Cheng, J. (2014). A deep learning network approach to ab initio protein secondary structure prediction. IEEE/ACM Transactions on Computational Biology and *Bioinformatics, 12(1),* 103-112. doi: 10.1109/TCBB.2014.2343960

Struble, T. J., Alvarez, J. C., Brown, S. P., Chytil, M., Cisar, J., DesJarlais, R. L., ... & Jensen, K. F. (2020). Current and future roles of artificial intelligence in medicinal chemistry synthesis. *Journal of Medicinal Chemistry, 63(16),* 8667-8682. doi: 10.1021/acs.jmedchem.9b02120

Tan, J. J., Cong, X. J., Hu, L. M., Wang, C. X., Jia, L., & Liang, X. J. (2010). Therapeutic strategies underpinning the development of novel techniques for the treatment of HIV infection. *Drug Discovery Today, 15(*5-6*),* 186-197. doi: 10.1016/j.drudis.2010.01.004

Tsou, L. K., Yeh, S. H., Ueng, S. H., Chang, C. P., Song, J. S., Wu, M. H., ... & Ke, Y. Y. (2020). Comparative study between deep learning and QSAR classifications for TNBC inhibitors and novel GPCR agonist discovery. *Scientific Reports, 10(*1*),* 16771. Retrieved from https://www.nature.com/articles/s41598-020-73681-1

Tsuji, S., Hase, T., Yachie-Kinoshita, A., Nishino, T., Ghosh, S., Kikuchi, M., ... & Tanaka, H. (2021). Artificial intelligence-based computational framework for drug-target prioritization and inference of novel repositionable drugs for Alzheimer's disease. *Alzheimer's Research & Therapy, 13(*1*),* 1-15. Retrieved from https://alzres.biomedcentral.com/articles/10.1186/s13195-021-00826-3

Tugcu, G., & Koksal, M. (2019). A QSAR Study for Analgesic and Anti-inflammatory Activities of 5-/6-Acyl-3-alkyl-2-Benzoxazolinone Derivatives. *Molecular Informatics, 38(*8-9*),* 1800090. doi: 10.1002/minf.201800090

Vamathevan, J., Clark, D., Czodrowski, P., Dunham, I., Ferran, E., Lee, G., ... & Zhao, S. (2019). Applications of machine learning in drug discovery and development. *Nature Reviews Drug Discovery, 18(*6*),* 463-477.

Wang, C., & Zhang, Y. (2017). Improving scoring-docking-screening powers of protein–ligand scoring functions using random forest. *Journal of Computational Chemistry, 38(*3*),* 169-177. doi: 10.1002/jcc.24667

Wang, L., Ding, J., Pan, L., Cao, D., Jiang, H., & Ding, X. (2019). Artificial intelligence facilitates drug design in the big data era. *Chemometrics and Intelligent Laboratory Systems, 194,* 103850. doi: 10.1016/j.chemolab.2019.103850

Wang, N. N., Dong, J., Deng, Y. H., Zhu, M. F., Wen, M., Yao, Z. J., ... & Cao, D. S. (2016). ADME properties evaluation in drug discovery: prediction of Caco-2 cell permeability using a combination of NSGA-II and boosting. *Journal of chemical information and modeling, 56(*4*),* 763-773. doi: 10.1021/acs.jcim.5b00642

Wang, T., Qiao, Y., Ding, W., Mao, W., Zhou, Y., & Gong, H. (2019). Improved fragment sampling for ab initio protein structure prediction using deep neural networks. *Nature Machine Intelligence, 1(*8*),* 347-355. doi: 10.1038/s42256-019-0075-7

Zhong, F., Xing, J., Li, X., Liu, X., Fu, Z., Xiong, Z., ... & Jiang, H. (2018). Artificial intelligence in drug design. *Science China Life Sciences, 61,* 1191-1204. doi: 10.1007/s11427-018-9342-2

Zhu, W., Liu, X., Li, Q., Gao, F., Liu, T., Chen, X., ... & Zhavoronkov, A. (2023). Discovery of novel and selective SIK2 inhibitors by the application of AlphaFold structures and generative models. *Bioorganic & Medicinal Chemistry, 91*, 117414. doi: 10.1016/j.bmc.2023.117414

An Overview of Synthetic Derivatives of Thiazole and Their Role in Therapeutics

Manoj KASHYAP*, Muslek Uddin MAZUMDER**°, Pooja PATOWARY***,
Apurba TALUKDAR****, Bhargab Jyoti SAHARIAH*****, Manish MAJUMDER******

An Overview of Synthetic Derivatives of Thiazole and Their Role in Therapeutics

SUMMARY

Thiazole derivatives have attracted much attention in medicinal chemistry due to their diverse pharmacological activities. This study provides an overview of the latest synthetic derivatives of thiazole and their therapeutic applications. Innovative methodologies have been adopted to enhance the structural diversity and optimize the pharmacological properties of thiazole-based compounds. These synthetic derivatives exhibit a broad spectrum of therapeutic activities, and understanding the essential features responsible for the observed pharmacological effects has been pivotal in structure-activity relationship studies. Drug development efforts have focused on modulating thiazole derivatives for improved bioavailability, selectivity, and reduced toxicity. This abstract highlights the potential of thiazole derivatives in targeting specific biological activity, paving the way for developing innovative therapeutic agents. Thiazole moiety as a heterocyclic compound was studied for its different pharmacological actions. The derivatives obtained from thiazole have diverse therapeutic actions along with antimicrobial activity, antitubercular activity, antidiabetic activity, anticonvulsant, anti-inflammatory actions, and antitumor activities. The mechanism of actions of all these activities is also studied by the researcher to provide scientific evidence and validation of their actions. Utilization of synthetic chemistry for exploration of various pharmacological potential of thiazole derivatives will lead the future pharmacologists to a newer dimension for new drug discovery and also these derivatives can be further optimized for the development of alternative options for the treatment of various diseases. The versatility of thiazole scaffolds presents promising opportunities for discovering new drugs with enhanced efficacy and improved pharmacokinetic profiles. As researchers continue to delve into the synthesis and pharmacological evaluation of thiazole derivatives, their significance in modern drug design and therapy becomes increasingly evident.

Key Words: *Thiazole, heterocyclic, antitubercular, antimicrobial, anti-inflammatory.*

Tiyazolün Sentetik Türevlerine ve Tedavideki Rollerine Genel Bir Bakış

ÖZ

Tiyazol türevleri, çeşitli farmakolojik aktivitelerinden dolayı medisinal kimyada büyük ilgi görmüştür. Bu çalışma, tiyazolün en yeni sentetik türevlerine ve bunların terapötik uygulamalarına genel bir bakış sunmaktadır. Tiyazol bazlı bileşiklerin yapısal çeşitliliğini artırmak ve farmakolojik özelliklerini optimize etmek için yenilikçi metodolojiler benimsenmiştir. Bu sentetik türevler geniş bir yelpazede terapötik aktivite göstermektedir ve gözlemlenen farmakolojik etkilerden sorumlu olan temel özelliklerin anlaşılması, yapı-aktivite ilişkisi çalışmalarında önemli bir rol oynamıştır. İlaç geliştirme çalışmaları, iyileştirilmiş biyoyararlanım, seçicilik ve azaltılmış toksisite için tiyazol türevlerinin modülasyonuna odaklanmıştır. Bu özet tiyazol türevlerinin spesifik biyolojik aktiviteyi hedeflemedeki potansiyelini vurgulayarak, yenilikçi terapötik ajanların geliştirilmesinin önünü açmaktadır. Heterosiklik bir bileşik olarak tiyazol, farklı farmakolojik etkileri açısından incelenmiştir. Tiyazolden elde edilen türevler, antimikrobiyal, antitüberküloz, antidiyabetik, antikonvülsan, antiinflamatuvar ve antitümör aktiviteler dahil olmak üzere çeşitli terapötik etkilere sahiptir. Tüm bu aktivitelerin etki mekanizmaları, aktivitelerin bilimsel kanıtlarını ve geçerliliğini sağlamak için araştırmacılar tarafından da incelenmiştir. Tiyazol türevlerinin çeşitli farmakolojik potansiyellerinin araştırılması için sentetik kimyanın kullanılması, geleceğin farmakologlarını yeni ilaç keşfinde daha yeni bir boyuta taşıyacak ve ayrıca bu türevler, çeşitli hastalıkların tedavisi için alternatif seçeneklerin geliştirilmesi amacıyla daha da optimize edilebilecektir. Tiyazol halkasının çok yönlülüğü, etkinliği artırılmış ve farmakokinetik profilleri iyileştirilmiş yeni ilaçların keşfedilmesi için umut verici fırsatlar sunmaktadır. Araştırmacılar tiyazol türevlerinin sentezi ve farmakolojik değerlendirmesi üzerinde çalışmaya devam ettikçe, bunların modern ilaç tasarımı ve tedavisindeki önemi giderek daha belirgin hale gelmektedir.

Anahtar Kelimeler: *Tiyazol, heterosiklik, antitüberküloz, antimikrobiyal, antiinflamatuvar.*

---

* ORCID: 0000-0002-9675-8646, Department of Pharmaceutical Chemistry, NETES Institute of Pharmaceutical Science (NEMCARE Group of Institutions), Kamrup, Assam, India.
** ORCID: 0000-0002-1540-3086, Research Scholar, Assam Science and Technology University, Guwahati, Assam, India.
*** ORCID: 0000-0002-0476-2868, Department of Pharmaceutical Chemistry, NETES Institute of Pharmaceutical Science (NEMCARE Group of Institutions), Kamrup, Assam, India.
**** ORCID: 0000-0001-9538-2512, Department of Pharmaceutics, NETES Institute of Pharmaceutical Science (NEMCARE Group of Institutions), Kamrup, Assam, India.
***** ORCID: 0000-0003-0440-6983, Department of Pharmaceutics, NETES Institute of Pharmaceutical Science (NEMCARE Group of Institutions), Kamrup, Assam, India.
****** ORCID: 0000-0001-8035-7429, Department of Pharmaceutical Chemistry, NETES Institute of Pharmaceutical Science (NEMCARE Group of Institutions), Kamrup, Assam, India.

° Corresponding Author; Muslek Uddin MAZUMDER
E-mail: muslekm@gmail.com

INTRODUCTION

Thiazoles are a class of heterocyclic compounds that contain a unique aromatic pentagonal ring structure and are identified by the molecular formula C_3H_3NS. At room temperature, the unbound form of thiazoles appears as a pale yellow liquid. The thiazole nucleus serves as a fundamental structural component of vitamin B, highlighting the biological importance of this heterocyclic moiety. In synthetic chemistry, thiazoles are vital in the controlled generation of carbene entities. This is achieved by conjugating them with transition metals to form metal-thiazole complexes, which serve as catalysts in catalytic processes of considerable significance, such as the Stetter reaction and benzoin condensation. The strategic integration of thiazoles with transition metals permits the precise generation of free carbene species and imparts catalytic prowess to the resulting complexes, thus driving progress in synthetic methodologies in organic chemistry (Ali & Sayed, 2021; Alrazzak, 2018).

Compounds containing thiazole moieties, commonly referred to as thiazole derivatives, exhibit a broad range of biological activities encompassing antipsychotic, analgesic, anticancer, antiallergic, antihypertensive, antibacterial, anti-inflammatory, antimalarial, and antifungal properties. Thiazole-based scaffolds are essential due to their incorporation into the structural frameworks of FDA-approved drugs, highlighting their clinical relevance. Moreover, these thiazole-containing scaffolds are pivotal constituents in over 70 experimental drugs, indicating the ongoing exploration and potential therapeutic applications of thiazole-derived compounds in pharmaceutical research and development. Most naturally occurring thiazole rings are found in microbial and marine sources. Therefore, thiazoles or compounds containing them have several uses as pharmacological agents, making thiazole an effective nucleus (Rajiani & Ismail, 2019; Singh et al., 2020) analgesic, antibacterial, anticancer, antiallergic,

antihypertensive, antiinflammatory, antimalarial, antifungal and antipsychotic. The scaffold is present in more than 18 FDA approved drugs and also in more than 70 experimental drugs. Only a few reviews are available in the literature despite its great medicinal importance. During the course of time, this scaffold has been studied extensively for its antiviral activities and provided compounds with activity in the nM range. However, no focused review is available on the compilation of antiviral activities shown by this scaffold. Objective: In the present review, we have made an effort to compile antiviral literature of thiazoles reported from the year 2011 to till date. Methods: We searched the SciFinder database (excluding patent literature).

Thiazole, a unique heterocyclic ring of nitrogen and sulfur atoms, holds significant importance in chemistry. It is found in many heterocyclic compounds with antibacterial, anticancer, anti-inflammatory, anticonvulsant, and antibiotic properties. Thiazoles display diverse activities and are essential heterocyclic rings with five members. The thiazole derivative compounds in this category are classified as natural, semisynthetic, or synthetic. According to molecular orbital techniques, thiazole molecules are aromatic and contain some dienic character, as evidenced by the pi-bond ordering. The widespread presence of thiazole and its derivatives in various chemical, biological, and medicinal applications makes it an attractive area of research for scientists and chemists (Gartel & Kandel, 2008; Knott-Hunziker et al., 1979).

The boiling points of free thiazole lie between the range of 116°C to 118°C. Thiazole is characterized by its flammability and pale-yellow liquid form, emitting a fragrance similar to pyridine. Its aromatic properties are attributed to a single pair of electrons from the Sulphur atom that has delocalized and formed a 6π-electron system. Additionally, proton nuclear magnetic resonance demonstrates the strong aromaticity of the thiazole protons, where the chemical shift value of each thiazole ring proton falls between

7.27 and 8.77 ppm. The thiazole resonance structures are depicted in Figure 1. Electrophilic substitution occurs preferentially at the C_5 position, followed by the C_4 position, as indicated by the computed π-electron density. On the other hand, nucleophilic substitution takes place at the C_2 position (Abdu-Rahem et al., 2021; Borcea et al., 2021).
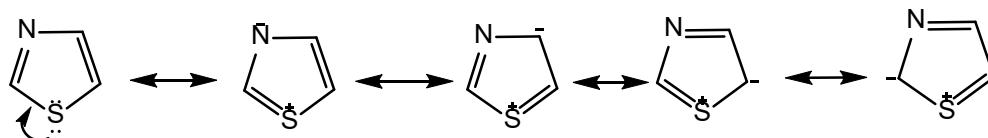
Figure 1. Resonance structures of thiazole

Biological Activities of Thiazole Derivatives

Antimicrobial Activity

Thiazole derivatives have been synthesized systematically as antimicrobial agents to combat the increasing challenge of multidrug-resistant bacterial strains. These derivatives have been specifically developed to target various highly resilient strains, including *E. species, A. baumannii, P. aeruginosa, E. cloacae, S. aureus, and Candida* species. These strains have demonstrated acquired resistance to fluconazole and are critical in the pathogenesis of numerous human diseases, such as pulmonary and urinary tract infections (Berkow & Lockhart, 2017). The absence of effective medications to combat resistant gram-negative bacteria is primarily attributed to several decades of inadequate innovative antimicrobial drug development. Consequently, novel medicines with distinct and relatively unique mechanisms of action are urgently required to target both susceptible and resistant strains. This calls for a concerted effort in the field of antimicrobial drug development to identify and develop new drugs with the potential to address the growing challenge of antibiotic resistance (Holmes et al., 2016).

A new set of chemical compounds known as 2-(4-arylpiperazine-1-yl)-N-[4-(2-(4-substituted phenyl)thiazol-4-yl)phenyl] acetamide derivatives were prepared and tested for their effectiveness in fighting against microorganisms (specifically 2a-2f) Figure 2. The reference medications ketoconazole and chloramphenicol were employed in the tests of the compounds against both gram-positive and gram-negative bacteria and fungus, respectively. However, the compound's antibacterial activity was generally weaker than the reference drugs, with most compounds having a minimum inhibitory concentration (MIC) of between 100-400 μg/ml, while the reference drugs had a MIC of 25–50 μg/ml. For gram-positive *E. faecalis*, only two compounds (2b and 2c) in Figure 2. demonstrated marginally increased efficacy, with a MIC of 100 μg/ml (Yurttaş et al., 2015).

A newly developed compound called 2,4-disubstituted thiazole has promising potential as an antimicrobial agent against a gram-positive bacterial strain. The tube dilution technique was used to prepare this compound, and compounds 3a-c (Figure 3) were found equally effective against *S. aureus*. This result highlights the effectiveness of these particular derivatives as antimicrobial agents. The systematic analysis of the antimicrobial profiles of these newly developed thiazole derivatives provides valuable insights into their pharmacological attributes and paves the way for further investigations into their method of action and potential therapeutic applications (Arora et al., 2015; Testing, 2000).

New imidazolyl thiazole derivatives were synthesized, and two compounds (4a and 4b) were found to have the notable antibacterial activity when compared against standard drugs like fluconazole and ciprofloxacin. Their minimum inhibitory concentrations (MICs) were observed to range from 1.95 to 3.91 μg/ml and 3.91 to 15.62 μg/ml for 4a

and 4b (Figure 4), respectively, signifying significant efficacy, particularly against *Bacillus* species and *M. luteus* (Łaczkowski et al., 2015; Testing, 2000).

Karale et al. synthesized a total of 24 molecules with antibacterial activity, among which compounds 5a and 5b (Figure 5) demonstrated moderate to low activity against *E. coli, S. typhi, B. subtilis, and S. aureus* and were found to be structurally similar to ciprofloxacin. However, compounds 5c to 5e (Figure 5) displayed the highest activity against *B. subtilis* (16-18 mm) and *S. aureus* (17 mm), highlighting their potential as effective antimicrobial agents. These findings provide valuable insights into developing novel antibacterial compounds with improved efficacy against commonly encountered bacterial pathogens (Karale et al., 2015).

Assessment of synthetic compounds (6a and 6b) Figure 6 that contain thiazoles and thiazolidinediones were conducted to determine their antibacterial efficacy against a variety of gram-negative and gram-positive bacteria, including *B. subtilis, S. aureus*, and *S. epidermidis P. aeruginosa*, *Proteus vulgaris*, and *Klebsiella pneumonia*. Fungal strains were also included in the assessment. Compounds with electron-withdrawing groups demonstrated inhibition zones against *S. aureus, S. epidermidis, and B. subtilis*. Minimum inhibitory concentrations (MICs) for these gram-positive bacteria ranged from 0.98 to 3.9 μg/ml, while ampicillin displayed an MIC of 0.24 μg/ml. The antibacterial activity of the compounds varied,

indicating the importance of structural characteristics and microbial targets when assessing efficacy across different species (Salem, 2017).

The antibacterial activity of 6-[(1/4-methyl imidazole/triazole/tetrazole-2/3/5-yl) thiol] derivatives was evaluated by Cankilic et al. against a diverse range of filamentous fungi, yeast, and bacteria. The N-(4-substituted thiazol-2-yl) acetamide analogs of compound 7 (Figure 7) exhibited antibacterial efficacies ranging from mild to moderate. Only compound 7 achieved 50% inhibition of *Listeria monocytogenes* among the tested compounds (Cankılıç & Yurttaş, 2017).

Elsebaei et al. examined a novel series of phenylthiazoles featuring alkynyl linkages, with compound 8 (Table 1) emerging as a promising candidate due to its efficacy in inhibiting the growth of antibiotic-resistant bacteria. The most potent compound exhibited exceptional activity against clinically relevant MRSA strains, with a minimal inhibitory concentration below 0.5 μg/ml. In terms of hepatic metabolism, compound 8 (Figure 8) demonstrated favorable stability, with a half-life ($t_{1/2}$) of 4.5 hours. Further, in a neutropenic mouse thigh infection model, this compound demonstrated comparable efficacy at low doses compared to vancomycin. These results indicate that phenylthiazoles have promise as a class of antibiotics with potent activity against drug-resistant bacteria (Elsebaei et al., 2018).

Table 1. Thiazole derivatives showing antimicrobial activity.

Activity	Compounds	Structures	
Antimicrobial agents	**Compounds (2a-2f):** aryl piperazine-1-yl)-N-[4-(2-(4-substituted phenyl) thiazol-4-yl)phenyl] acetamides derivatives	**2a**: R=H, R₁=Ph-CH₂ **2b**:R=H, R₁=C₅H₅N **2c**:R=H, R₁=Pyrimidine **2d**: R=4-OMe-Ph R₁=C₅H₅N **2e**: R=4-Cl-Ph R₁=Ph-CH₂ **2f**: R=4-F-Ph R₁=Ph-CH₂ **Figure 2.** 2-(4-methyl piperazine-1-yl)-N-(4-(2-phenylthiazol-4-yl)phenyl)acetamide	
	Compounds (3a-c): Structure of 2,4-disubstituted (E)-1-(3,4-methoxyphenyl)-N-(4-phenylthiazol-2-yl) methaniminederivatives	**3a**: R=4-NO₂ R=H **3c**: R=H R₁=4-OMe **Figure 3(a,c).** 4-methyl-N-(4-(p-tolyl) thiazol-2-yl)benzamide	**3b** **Figure 3b.** (E)-N-(3,4-dimethoxybenzylidene) -4-phenylthiazol-2-amine
	Compounds (4a-b): structures of (E)-2-(2-((1H-imidazol-2-yl)methylene) hydrazineyl)-4-argiothiazole	**4a**: Ar= 4-Br-C₆H₄ **4b**: Ar= aamantyl **Figure 4.** (E)-2-(2-((1H-imidazole-2-yl)methylene) hydrazinyl)-4-argiothiazole	
	Compounds (5a-e): structures of different (E)-3-(3-(2,4-dimethylthiazol-5-yl)-1-(4-fluorophenyl)-1H-pyrazol-4-yl)-1-(2-hydroxyphenyl)prop-2-en-1-one thiazole derivatives	**Figure 5a.** (E)-3-(3-(2,4-dimethylthiazol-5-yl)-1-(4-fluorophenyl)-1H-pyrazol-4-yl)-1-(2-hydroxyphenyl)prop-2-en-1-one	**Figure 5b.** 2-(3-(2,4-dimethylthiazol-5-yl)-1-(4-fluorophenyl)-1H-pyrazol-4-yl)-4H-chromen-4-one
		Figure 5c. 2,4-dichloro-6-(3'-(2,4-dimethylthiazol-5-yl)-1'-(4-fluorophenyl)-3,4-dihydro-1'H,2H-[3,4'-bipyrazol]-5-yl) phenol	**Figure 5d**. 4-bromo-2-(3'-(2,4-dimethylthiazol-5-yl)-1'-(4-fluorophenyl)-3,4-dihydro-1'H, 2H-[3,4'-bipyrazol]-5-yl)phenol
		Figure 5e. (Z)-5-chloro-2-((3-(2,4-dimethylthiazol-5-yl)-1H-pyrazol-4-yl)(4-fluorophenyl)methylene) -6-methylbenzofuran-3(2H)-one	
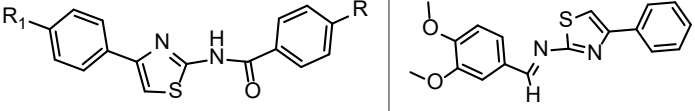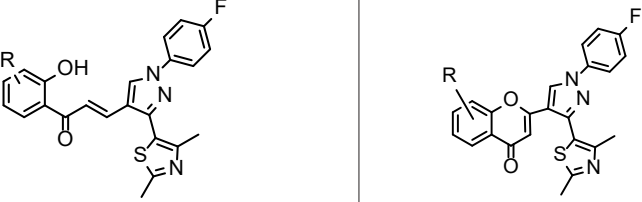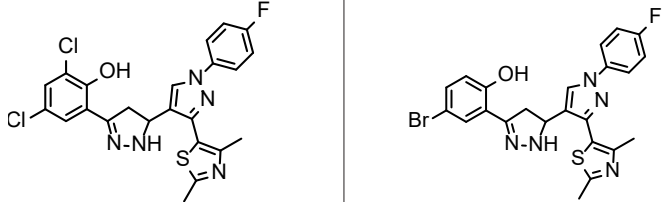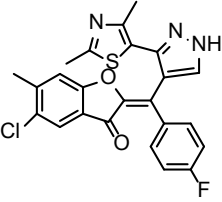
Antimicrobial agents	**Compounds (6a-b):** E-2-cyano-2-(4,5-dialkyl-3-phenylthiazol-2(3H)-ylidene)-N-(furan-2-ylmethyl) acetamide	**6a**: R = COMe **6b**: R= 4-Ph-NO$_2$ **Figure 6**. (E)-2-cyano-2-(4,5-dimethyl-3-phenylthiazol-2(3H)-ylidene)-N-(furan-2-ylmethyl)acetamide
	Compound 7: 2-(argiothio)-N-(thiazol-2-yl)acetamide	**7** **Figure7**. 2-(argiothio)-N-(thiazol-2-yl)acetamide
	Compound 8: New (E)-2-(1-(2-(4-(cyclopropylethynyl) phenyl)-4-methylthiazol-5-yl) ethylidene)hydrazine-1-carboximidamide compounds	**Figure 8**. (E)-2-(1-(2-(4-(cyclopropyl ethynyl)phenyl)-4-Methyl thiazole-5-yl)ethylidene)hydrazinecarboximidamide
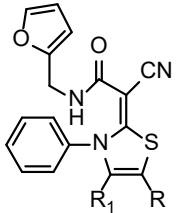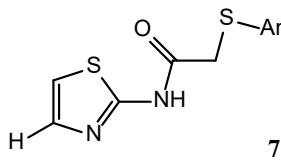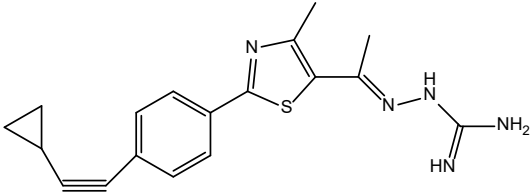
Antitubercular activity

Tuberculosis (TB) is a persistent global health concern, resulting in the loss of millions of lives annually. The severity of TB is amplified when drug-resistant strains of the pathogen *Mycobacterium tuberculosis* arise. In 2019, TB was responsible for the death of 1.4 million individuals, making it the leading fatal infectious health problem and one of the top ten causes of death globally. Although established treatments like pyrazinamide, rifampicin, ethambutol, and isoniazid have proved effective in treating the disease, TB's global incidence experiences a marginal annual decline of approximately 2%, according to the World Health Organization (WHO) data. However, the persistent challenge of drug-resistant tuberculosis, particularly the severe healthcare threat posed by multiple-drug-resistant tuberculosis (MDR-TB), requires rapid attention and innovative antitubercular agents to counteract the escalating prevalence of resistant strains. This imperative underscores the need to strengthen the therapeutic arsenal against this

608

formidable infectious disease (Fogel, 2015; Ran et al., 2016).

Bekker et al. conducted an *in vitro* investigation to assess a novel usnic acid derivative's capacity to suppress the development of *M. smegmatis* and *M. tuberculosis*. According to the study, for best results, specific configurations of amino acids inside the thiazole ring were required. The findings revealed notable protein kinase activity, especially against the strains of *S. lividans* and *M. smegmatis*. The kanamycin-resistant *M. smegmatis* strain exhibited enhanced susceptibility to (-) usnic acid thiazole compared to the (+) isomer, with 9a and 9b (Figure 9) demonstrating potent inhibitory activity. Both isomers exhibited a similar effect on *M. tuberculosis* H37Rv, with isomer 9b exhibiting greater efficacy than 9a (Bekker et al., 2015).

Researchers led by Guzeldemirci evaluated the antimycobacterial efficacy of a brand-new class of substances against *M. tuberculosis* H37Rv in culture. Derivatives of 2-[6-(4-bromophenyl) imidazo

N-(arylidene) thiazol-3-yl acetohydrazides were produced. With an IC$_{50}$ greater than 1.6 mg/mL and 99% inhibition, compound 10a showed the greatest potency of all the compounds tested. Compound 10b, in contrast, had a comparatively lower inhibition rate (91%) and an IC$_{50}$ of 1.05 µg/mL than its counterparts. These results demonstrate these synthetic chemical's potential, especially compound 10b(Figure 10), as candidates with significant antimycobacterial activity (Ulusoy Güzeldemirci & Gürsoy, 2017).

The antitubercular efficacy of arylidenehydrazide derivatives with an imidazo[2,1-b] thiazole moiety (compound 11) was studied by Guzeldemirci et al. against *M. tuberculosis* H37Rv. Using a broth microdilution assay in BACTEC 12B medium, the researchers evaluated the compound's antitubercular potential. The results showed that the compound had modest activity, with IC$_{50}$ values between 6.16 and 100 mg/ml. In contrast, rifampicin, the reference medication, exhibited an IC$_{50}$ value of 50 µg/ml. Compound 11(Figure 11) demonstrated the highest potency, equal to rifampicin, with an IC$_{50}$ value of 0.125 µg/ml. These findings suggest that compound 11 has the potential to be an effective antitubercular agent, warranting further investigation (Ulusoy Güzeldemirci et al., 2017).

Karale et al. conducted research utilizing the 2,4,5-trisubstituted thiazoles to assess their efficacy against *M. tuberculosis* H37Rv with the Microplate Alamar Blue Assay (MABA) test. The results showed that these thiazoles exhibited significant inhibitory effects against the bacterium, with compound 12a showing notable antitubercular activity (MIC values of 2.1 µg/mL and 1.8 µg/mL). The researchers further optimized the compounds by incorporating a third substituent, which resulted in promising outcomes. In particular, substances 12b-c (Figure 12) demonstrated the potential to reduce inactive *M. tuberculosis* H37Ra by over 90% at 10 µM, highlighting their potential as effective antitubercular agents. These findings suggest that 2,4,5-trisubstituted thiazoles, precisely compound 12b-c, may be promising candidates for developing new antitubercular agents (Karale et al., 2019.

Table 2. Thiazole derivatives showing antitubercular activity.

Activity	Compounds	Structures	
Antituberculosis agents	**Compounds (9a-b):** structures of new (R)-2-acetyl-6-(2-aminothiazol-4-yl)-3,7,9-trihydroxy-8,9b-dimethyldibenzo[b,d]furan-1(9bH)-one derivatives	**Figure 9a**. (R)-2-acetyl-6-(2-aminothiazol-4-yl)-3,7,9-trihydroxy-8,9b-dimethyldibenzo[b,d]furan-1(9bH)-one	**Figure 9b**. (S)-2-acetyl-6-(2-aminothiazol-4-yl)-3,7,9-trihydroxy-8,9b-dimethyldibenzo [b,d]furan-1(9bH)-one
	Compounds (10a-b): structures of (E)-N'-(argiomethylene)-2-(6-phenylimidazo[2,1-b]thiazol-3-yl)acetohydrazide derivatives	**10a**: Ar=2-NO$_2$-Ph **10b**: Ar=2,4-di-NO$_2$-Ph **10b**:IC50 of 1.05 µg/mL **Figure 10**. (E)-N'-(argiomethylene)-2-(6-phenylimidazo[2,1-b]thiazol-3-yl)acetohydrazide	
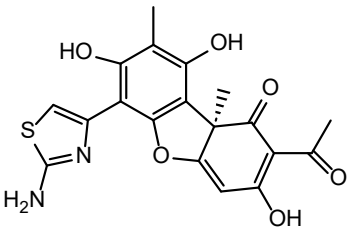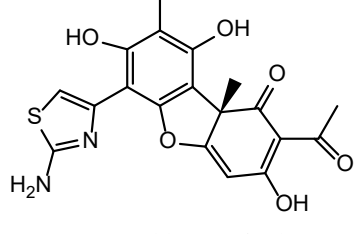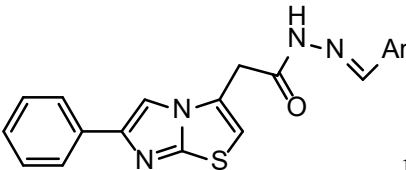
Antituberculosis agents	**Compound 11**: structure of (E)-2-(6-(4-chlorophenyl) imidazo[2,1-b]thiazol-3-yl)-N'-((5-nitrofuran-2-yl) methylene)acetohydrazide	11:IC50 of 0.125 µg/mL **Figure 11**. (E)-2-(6-(4-chlorophenyl)imidazo[2,1-b] thiazol-3-yl)-N'-((5-nitrofuran-2-yl) methylene)acetohydrazide
	Compounds (12a-c): Structures of 2,4,5-trisubstituted 1-(2,5-dimethylthiazol-4-yl)ethan-1-one thiazole derivatives.	**12 a**:R$_1$=isopropyl, R$_2$=benzonitrile **Figure 12a**. 1-(2,5-dimethylthiazol-4-yl)ethan-1-one **12b**:R$_1$=isopropyl,R$_2$=5methylbenzo[1,3]dioxole R$_3$=(S)N-methyl-1-phenylethamine **12c**:R$_1$=isopropyl,R$_2$=5methylbenzo[1,3]dioxole R$_3$=(R)N-methyl-1-phenylethamine **Figure12(b,c).** 1-(2,5-dimethylthiazol-4-yl)ethan-1-one
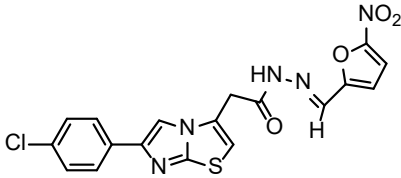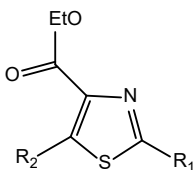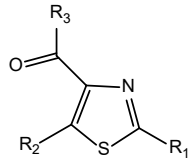
Anticancer Activity

Cancer is a complex illness that develops when some cells accumulate genetic and epigenetic changes, with cells migrating to other tissues (Ch et al., 2021). A plethora of commercially available anticancer drugs exist, but the majority of them are quite hazardous and can become resistant, which means that the treatment would not work. As a result, there is a significant drive to develop novel, potential anticancer medication prototypes (Ghorab & Al-Said, 2012).

Braga et al. conducted a study to evaluate the potential cytotoxicity of a diverse range of thiazole molecules on cancer cell lines. The researchers identified that compound 13 showed potent efficacy against HL-60 promyelocytic leukemia cells with an IC$_{50}$ of 43 µM while exhibiting minimal toxicity towards normal Vero cells. However, MCF-7 breast cancer cells resisted most of the tested compounds. The selective cytotoxicity of compound 13 with its promising potential suggests that it could be further explored as an anticancer agent, especially in the treatment of breast cancer and promyelocytic leukemia (Braga et al., 2016; Küster et al., 2012)

to investigate their cytotoxic activity against three human cancers and normal (Vero) cells.

Gomha et al. conducted a study on the synthesis of arylazothiazoles and their efficacy against colorectal (HCT-116) and hepatic (HepG2) cancer cell lines using the MTT assay. The results were promising, with compounds such as 14b displaying potent anti-hepatocellular carcinoma effects (IC$_{50}$ = 4.9 ± 0.5 µM), surpassing cisplatin's effectiveness. In gastrointestinal cancer cell lines, 14a and 14b outperformed cisplatin (IC$_{50}$ = 3.1 ± 0.6 µM). As a result, compound 14b has shown promise as a subject for more research in anticancer drug development. Moreover, a novel class of pyridine thiazole hybrid compounds demonstrated potent cytotoxicity against stomach carcinoma MGC803 and colon cancer HCT-116. These results imply that these substances provide effective treatment options for these types of cancer (Islam et al., 2019).

Kantevari et al. examined the cytotoxicity of imidazole thiazole-linked compounds against four cancer cell lines: MCF-7, DU-145, MIAPaCa-2, and SK-N-SH. Among the substances examined, substance 15a (Figure 15) demonstrated the highest

potency, with an IC_{50} value of 4.2±0.6 µM. These findings suggest that certain derivatives, particularly compound 15a, show promise as potential cytotoxic agents against cancer cells and warrant further investigation (Nagireddy et al., 2019).

Güzeldemirci et al. conducted a study to evaluate the efficacy of arylidenehydrazide compounds containing imidazo[2,1-b] thiazole compound (16a and 16b) against various viruses such as HSV-1, influenza, coxsackie B4, feline coronavirus, parainfluenza-3, and Punta toro. The study revealed that compounds 16a and 16b (Figure 16) demonstrated notable antiviral activity. Moreover, compound 16a demonstrated effective antiviral activity against feline coronavirus (IC_{50} 9 µM) and HSV-1 (KOS) (IC_{50} 7.5 µM), indicating its potential for further development as diverse antiviral agents. These findings could be significant in advancing the development of novel antiviral agents and contribute to managing viral infections (Ulusoy Güzeldemirci et al., 2017).

Galochkina et al. synthesized a few compounds based on investigated imidazo[2,1-b] thiazole as possible influenza virus inhibitors. They found that three derivatives (17a-c) Figure 17 with thiophene substitution were effective against the H1N1 influenza virus in MDCK cells. The IC_{50} values of these compounds ranged from 13 ± 3 to 49 ± 6 µM. Compound 17b had the highest activity with an IC_{50} of 13 ± 3 µM and a selecting index (SI) of 77, better than the standard drug rimantadine. More research is needed to explore the antiviral potential of thiophene-substituted derivatives, especially compound 17b (Equine et al., 2009; Galochkina et al., 2019).

Table 3. Thiazole derivatives showing anticancer activity.

Activity	Compounds	Structures
Anticancer agents	**Compound 13**: Structure of (E)-2-(2-ethylidenehydrazineyl)-4-(p-tolyl)thiazole derivatives	13: IC50 of 43 µM, R$_1$=4-quinoline, R$_2$=OMe **Figure 13**. (E)-2-(2-ethylidenehydrazinyl)-4-(p-tolyl)thiazole
	Compounds (14a-b): Structures of 4-((1Z,2E)-1-(2-methylhydrazineylidene)-2-(2-(4-methylthiazol-2-yl)hydrazineylidene)propyl)morpholine derivatives	**14a**: Ar= C$_6$H$_5$ **14a**:IC50 = 4.9 ± 0.5 µM **Figure 14a.** 4-((1Z,2E)-1-(2argiohydrazono)-2-(2-(4-methylthiazol-2-yl)hydrazono)propyl)morpholine **14b**: Ar= 4-Cl-C$_6$H$_4$ **14b**:IC50 = 3.1 ± 0.6 µM **Figure 14b.** 2-((E)-2-((Z)-1-(2-argiohydrazono)-1-morpholinopropan-2-ylidene)hydrazinyl)thiazol-4(5H)-one
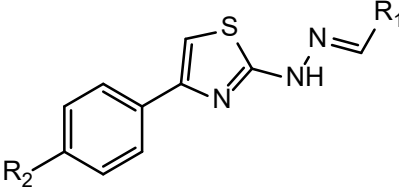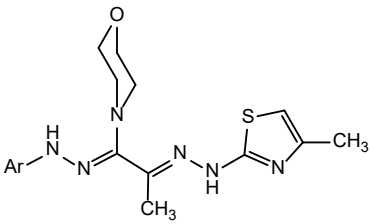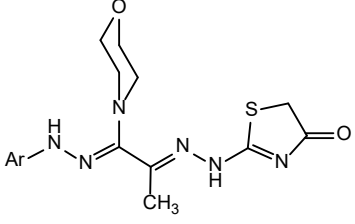
Anticancer agents	**Compound 15a**: Structure of imidazo[2,1-b]thiazole-coupled noscapine derivatives.	15a: IC50 of 4.2±0.6 μM **Figure15a**. (3S)-3-((5R)-6-(((6-(3-(4-fluorophenyl)-3-oxopropyl)imidazo[2,1-b]thiazol-3-yl)methyl)-4-methoxy-3a,5,6,7,8,9a-hexahydro-[1,3]dioxolo[4,5-g]isoquinolin-5-yl)-6,7-dimethoxy-3,3a-dihydroisobenzofuran-1(7aH)-one
	Compounds (16a-b): Structures of imidazo[2,1-b]thiazole-coupled noscapine derivatives.	**16a**:R=4-OH-C_6H_4 **16 b**: R=$2,4$-Cl_2-C_6H_3 16a: IC50 of 9 μM 16b: IC50 of 7.5 μM **Figure 16(a,b)**. 2-(6-(4-chlorophenyl)imidazo[2,1-b]thiazol-3-yl)-N'-(propan-2-ylidene)acetohydrazide
	Compounds (17a-c): Structures of imidazol[2,1-b]thiazole-based 2,7,7-trimethyl-7,8-dihydrobenzo[4,5]thiazolo[3,2-b][1,2,4]triazol-5(6H)-one derivatives	17a: IC50 of 31 ± 3 μM 17b: IC50 of 13 ± 3 μM 17c: IC50 of 49 ± 6 μM **17a**: R_1=H, R_2=2- bromothiophene **17 b**: R_1=H, R_2=2- chlorothiophene **17c**: R_1=Me, R_2=2- bromothiophene **Figure 17(a-c)**. 2,7,7-trimethyl-7,8-dihydrobenzo[4,5]thiazolo[3,2-b][1,2,4]triazol-5(6H)-one
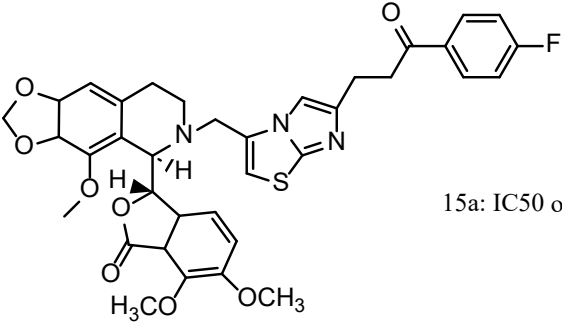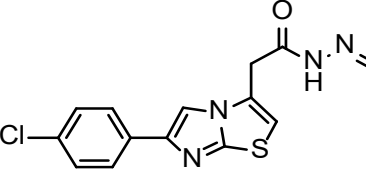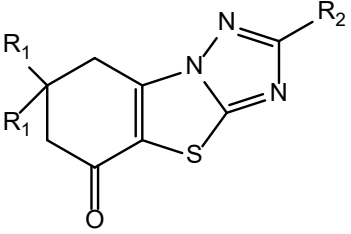
Antidiabetic activity

Insulin-dependent diabetes mellitus, or diabetes, is a complicated metabolic disease identified by hyperglycemia. Hyperglycemia mainly results from abnormalities in either secretion or insulin actions. Diabetes shows a definite pattern of pathogenesis and diverse presentation of disease progression(Banday et al., 2021). About 10% of the world's population suffers from diabetes, a metabolic disease that is becoming more and more common (Karale et al., 2019).

Meng et al. synthesized a series of 2-imino-3-substituted-5-heterarylidene-1,3-thiazolidine-4-ones

and conducted a study to assess their efficacy as PTP1B inhibitors. The results of this study indicate that pyrrole substitutions at position 5, particularly exemplified by compound 18, exhibit superior inhibitory activity. Compound 18, in particular, demonstrated a significant PTP1B inhibitory activity with an IC_{50} of 6.37 μM. Compound 18 presents itself as a promising candidate for further structural optimization, which could lead to the development of potent PTP1B inhibitors (Meng et al., 2016).

Ganou et al. synthesized a series of 4-thiazolinone derivatives and identified compound 19 as a potent

inhibitor of PTP1B, with an IC_{50} value of 0.92 µM. Molecular docking studies revealed that compound 19 can form hydrogen bonds and establish non-covalent interactions with crucial catalytic residues, indicating its potential therapeutic efficacy in treating PTP1B-related conditions. These findings suggest that compound 19 holds promise as a candidate for developing novel PTP1B inhibitors (Ganou et al., 2018).

Wu et al. synthesized thiazole-5-carboxylates containing ethyl 4-(substituted phenoxymethyl) motifs, which were potent inhibitors of PTP1B. Among these, compound 20 showed an IC_{50} value of 4.46 µM, making it the most potent inhibitor. The biological activity of these compounds was significantly influenced by structural modifications made to the benzene ring. These findings underscore the importance of such alterations in optimizing thiazole-5-carboxylates as inhibitors of PTP1B (Wu et al., 2020).

Patel et al. developed a series of thiazolidine-4-one derivatives, among which compound 21e demonstrated noteworthy inhibitory activity against PTP1B, with an IC_{50} of 5.88 ± 0.06 µM. Molecular docking studies elucidated the mechanism of its action, revealing that it interacts with catalytic residues, Cys215, Ser216, and Gln262, acting as a potent antagonist. Moreover, compounds 21a–f also exhibited significant inhibitory efficacy, showcasing the potential for designing enhanced PTP1B inhibitors for therapeutic development. These findings suggest that the development of PTP1B inhibitors may hold promise for future therapeutic interventions (Patel et al., 2020).

Maezaki et al. have synthesized a diverse range of quinoline salts in combination with thiazole bases, including Substance 22, which exhibits potent Dipeptidyl peptidase-4 (DPP-4) inhibitory activity (IC_{50} = 0.38 µM). The molecular docking study revealed a crucial salt bridge and hydrophobic contact with Tyr547, indicating that compound 22 and its

analogs hold great potential as therapeutic agents for DPP-4 inhibition in metabolic disorders. The findings of this study may contribute to the development of effective treatments for metabolic disorders (Maezaki et al., 2017).

Celestina and her colleagues have successfully synthesized two compounds, 23a and 23b (Figure 23), with a diverse range of substitutions such as nitro, fluorine, methyl, chlorine, and bromine. These compounds have displayed robust Aldose reductase (ALR2) inhibitory activity, as evidenced by their IC_{50} values of 40 and 60 µM. Furthermore, docking studies have revealed that the hippuric acid chain present in the compounds has strong interactions with the crucial catalytic residues located in the ALR2 enzyme's anionic interaction zone. This finding highlights the potential of these compounds as a promising source of inhibitors for therapeutic applications (Celestina et al., 2020).

Sever et al. have synthesized N-(thiazolbenzothiazole-2-yl) acetamides, which demonstrate potent inhibitory activity against aldose reductase (AR), surpassing that of quercetin. The low K values of these compounds (0.04 ± 0.01 µM and 0.08 ± 0.02 µM) indicate superior AR inhibition with competitive behavior. Furthermore, cellular experiments have confirmed the safety of these compounds, and molecular docking studies have shown their potential as selective AR inhibitors, suggesting therapeutic promise. These findings demonstrate the potential of N-(thiazolbenzothiazole-2-yl) acetamides as a class of compounds(Figure 24) to be explored further for their therapeutic potential as AR inhibitors (Sever et al., 2020).

Sahu et al. created a library of twenty chemicals called thiazole-1,3,5-triazine and analyzed them using ADME. Viral antimalarial screening was carried out along with docking experiments on both natural and mutant Pf-DHFR (Dihydrofolate reductase) complexes. The findings indicated that compounds 26a-b were potent against trophozoites,

dead rings, and schizonts. These compounds exhibited noteworthy efficacy against chloroquine-resistant strains, with IC_{50} values of 12.48, 10.03, and 11.34 µg/ml. Chloroquine's reference compound had IC_{50} values of 0.7 and 1.2 µg/ml. Further investigation of 25a-b is recommended due to their promising antimalarial efficacy (Sahu et al., 2019).

Filho et al. conducted a study to evaluate the efficacy of a novel series of 1,3-thiazoles against *T. cruzi.* While several compounds demonstrated

toxicity in macrophages and rat cardiomyoblast cells at doses below 50 µM, molecule 26 exhibited the highest potency against *T. cruzi,* surpassing benznidazole and gentian violet. The compound showed an IC_{50} value of 0.37 µM, indicating its potential for developing anti-*T. Cruzi* agents. Therefore, compound 26 and other compounds in the series have displayed promising results that could be explored to create effective and safe anti-*T. cruzi* agents (de Oliveira Filho et al., 2017).

Table 4. Thiazole derivatives showing antidiabetic activity

Activity	Compounds	Structures
Antidiabetic agents	**Compound 18:** Structure of 2-imino-3-substituted 5-heteroarylidene-1,3-thiazolidine-4-one derivatives.	18:IC_{50} of 6.37 µM **Figure 18**. Ethyl 5-((Z)-((Z)-3-(4-fluorophenyl)-2-((4-fluorophenyl) imino)-4-oxothiazolidin-5-ylidene)methyl) -2,4-dimethyl-1H-pyrrole-3-carboxylate
	Compound 19: Structure of ethyl (Z)-4-((5-(3-methylbenzylidene)-4-oxo-2-phenylthiazolidin-3-yl) methyl)benzoate	19:IC_{50} of 0.92 µM **Figure 19.** (Z)-ethyl 4-((5-(3-methylbenzylidene)-4-oxo-2-phenyl thiazolidine-3-yl)methyl)benzoate
	Compound 20: structure of ethyl 4-(substituted phenoxy methyl) thiazole-5-carboxylate derivatives	20:IC_{50} of 4.46 µM **Figure 20**. Ethyl 2-(2-bromo-4-hydroxyphenyl)-4-((4-methoxyphenyl)methyl)thiazole-5-carboxylate
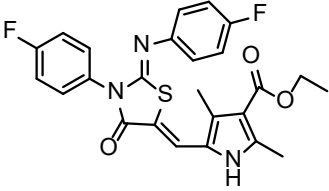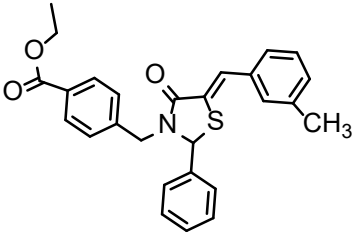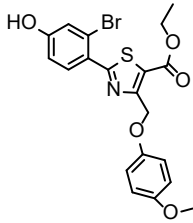
Compounds (21a-f): structures of thiazolidin-4-one 4-one derivatives	**21 a**: x=S, R=CH₃ **21b**: x=S, R=NO₂ **21c**: x=S, R=Cl **21d**: x=O, R=CH₃ **21e**: x=S, R=NO₂ **21f**: x=NH, R=NO₂ 21e:IC₅₀ of 5.88 ± 0.06 μM **Figure 21.** (2E,5Z)-5-(cyclopenta-1,3-dien-1-ylmethylene) -2-(p-tolylimino)thiazolidin-4-one	

Compounds (21a-f): structures of thiazolidin-4-one 4-one derivatives

21 a: x=S, R=CH₃
21b: x=S, R=NO₂
21c: x=S, R=Cl
21d: x=O, R=CH₃
21e: x=S, R=NO₂
21f: x=NH, R=NO₂

21e:IC$_{50}$ of 5.88 ± 0.06 μM

Figure 21. (2E,5Z)-5-(cyclopenta-1,3-dien-1-ylmethylene)-2-(p-tolylimino)thiazolidin-4-one

---

Compound 22: structures of thiazole based 2-(3-(aminomethyl)-2-isobutyl-4-(p-tolyl)quinolin-6-yl)thiazole-4-carboxylic acid

2HCl
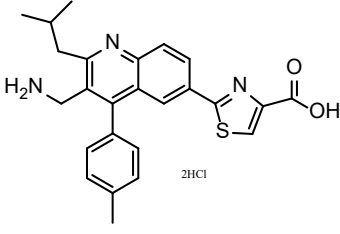
22:IC$_{50}$ of 0.38 μM

Figure 22. 2-(3-(aminomethyl)-2-isobutyl-4-(p-tolyl)quinoline-6-yl)thiazole-4-carboxylic acid

---

Compounds (23a-b): structures of 1,3-diarylpyrazol-rhodanine-3-hippuric acid derivatives
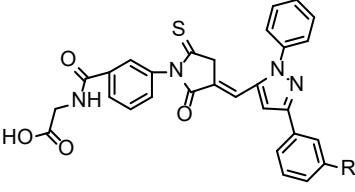
23a: R=F
23b: R=CH₃

23a:IC$_{50}$ of 40 μM
23b:IC$_{50}$ of 60 μM
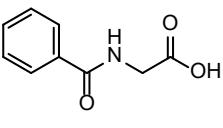
hippuric acid

Figure 23. (E)-2-(3-(2-oxo-3-((1-phenyl-3-(m-tolyl)-1H-pyrazole-5-yl)methylene)-5-thioxopyrrolidin-1-yl)benzamido)acetic acid

---

Compounds (24a-b): structures of 2-[(4-amino-5-aryl-4H-1,2,4-triazol-3-yl)thio]-N-(thiazolbenzothiazol-2-yl)acetamides
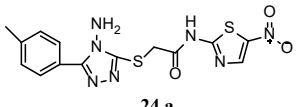
24 a

Figure 24a. 2-((4-amino-5-(p-tolyl)-4H-1,2,4-triazol-3-yl)thio)-N-(5-nitrothiazol-2-yl)acetamide
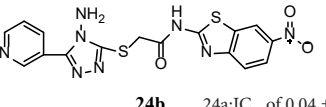
24b

24a:IC$_{50}$ of 0.04 ± 0.01 μM
24b:IC$_{50}$ of 0.08 ± 0.02 μM

Figure 24b. 2-((4-amino-5-(pyridin-3-yl)-4H-1,2,4-triazol-3-yl)thio)-N-(6-nitrobenzo[d]thiazol-2-yl)acetamide

---

Compounds (25a-b): structures of 5-isopropyl-2-(4-methylpiperazin-1-yl)-N-phenylthiazole-4-carboxamides and thiazole-1,3,5-triazines
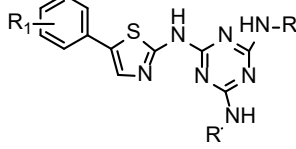
25a:IC$_{50}$ of 12.48 μM
25b:IC$_{50}$ of 11.34 μM

25a: R₁=2,4-di-Cl, R=propyl
25b: R₁=2,4-di-Cl, R=Me

Figure 25(a,b). N2,N4-dimethyl-N6-(5-phenylthiazol-2-yl)-1,3,5-triazine-2,4,6-triamine

---

Compound 26: structure of (E)-2-(2-(1-(3,4-dichlorophenyl)ethylidene)hydrazineyl)-4,5-dimethylthiazole
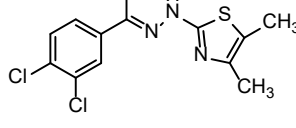
26:IC$_{50}$ of 0.37 μM

Figure26. (E)-2-(2-(1-(3,4-chlorophenyl)ethylidene)hydrazine)-4,5-dimethyl thiazole

Anti-inflammatory activity

The response of the human body to various stimuli is characterized by inflammation. It is crucial to administer chronic or recurrent treatment for several inflammatory conditions, such as psoriasis, asthma, and arthritis. Nonsteroidal anti-inflammatory drugs (NSAIDs) are the primary treatment modalities to address symptoms such as fever, pain, and acute and chronic inflammation. However, their prolonged therapeutic usage is linked to severe adverse consequences, such as renal disease, unfavorable cardiovascular events, and gastrointestinal (GI) issues, as well as complications, such as bleeding and nephrotoxicity. These potential risks mandate meticulous consideration in the prolonged administration of NSAIDs for the management of inflammatory conditions (Bally et al., 2017; Cao et al., 2014; Goldstein & Cryer, 2014; Lucas et al., 2019; Rostom et al., 2002).

Khloya et al., have developed a novel class of pyrazolyl thiazole carboxylates and investigated the anti-inflammatory properties of their acid analogs through carrageenan-induced rat paw edema. The synthesized ester compounds have demonstrated superior potency to their acid counterparts, with compounds 27a-c (Figure 27) exhibiting significant efficacy in the 93.66% to 89.59% range. The results indicate that the recently developed substances may be efficacious treatments that reduce inflammation. The study's findings may open the door to more investigation and advancement of anti-inflammatory drugs (Khloya et al., 2015).

Jakob et al. have reported the development of a green and efficient multi-component one-pot synthesis method for the preparation of 4-(substituted)-4-(4-(substituted phenyl) 2-carboxamide and 2-(substituted) thiazol-2(3H)-ylidene) thiophene-2thiazol-5-yl-4-(4-(substituted phenyl)) (diphenyl-2-yl) methanone. The synthesized 28 compounds (Figure 28) were evaluated for their inhibitory potential against lipoxygenase (LOX) and COX-1/COX-2 enzymes. The findings of this study are of significant value in developing new and potent drugs (Jacob & Manju, 2020).

Table 5. Thiazole derivatives with anti-inflammatory activity.

Activity	Compounds	Structures	
Anti-inflammatory agents	**Compounds (27a-c)**: structure of ethyl 4-(4-chlorophenyl)-2-(3-(4-chlorophenyl)-1-phenyl-1H-pyrazol-4-yl)thiazole-5-carboxylate	 **Figure27a**. Ethyl 4-(4-chlorophenyl)-2-(3-(4-chlorophenyl)-1-phenyl-1H-pyrazol-4-yl)thiazole-5-carboxylate	 **27b**: R₁=F, R₂=H **27c**: R₁=FOMe, R₂=Cl **Figure 27(b,c)**. 2-(1-phenyl-3-(p-tolyl)-1H-pyrazol-4-yl)-4-(p-tolyl)thiazole-5-carboxylic acid
	Compound 28: structure of N-(3-phenyl-4-(4-(substituted phenyl) thiazol- 2(3H)-ylidene) thiophene-2-carbox-amide	 **Figure 28** - (2-(diphenylamino)-4-(*p*-tolyl)thiazol-5-yl)(thiophen-2-yl)methanone	
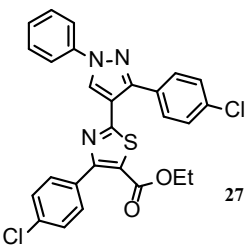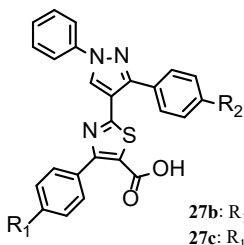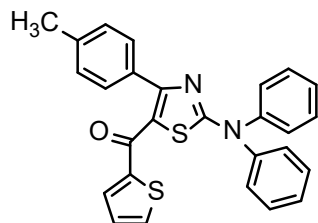
Antioxidant activity

Antioxidants are increasingly recognized for their potential as preventive and curative agents for various ailments. Reactive oxygen species (ROS) are continually produced due to extreme oxidative stress and routine organ activities. High concentrations of free radicals in the body can damage various biological macromolecules within cells and tissues, including DNA, lipids, proteins, and enzymes. Such damage poses a risk of mutations, which may lead to cancer. Additionally, heightened levels of free radicals are implicated in numerous inflammatory, autoimmune, cardiovascular, neurodegenerative, and metabolic disorders, as well as cellular aging. Given these associations, mitigating oxidative damage is an essential preventive and therapeutic strategy for various illnesses. Notably, recent years have witnessed significant advancements in developing novel antioxidant agents, particularly emphasizing the thiazole moiety within newly synthesized molecules. These developments hold great promise for the future of antioxidant therapy (Khan & Wang, 2018)including trichloroethylene (TCE).

Thota et al. have recently synthesized a novel class of molecules featuring thiazole- and indole-substituted coumarin moieties. These molecules have been found to possess potent antioxidant properties. Among them, compounds 29a-c(Figure 29) have demonstrated the highest efficacy, surpassing ascorbic acid in DPPH (2,2-diphenyl-1,1-picrylhydrazyl) scavenging. The IC_{50} values of the compounds 29a, 29b, and 29c were found to be 11.04 ± 0.18, 11.28 ± 0.06, and 12.16 ± 0.28 μg/ml, respectively. The compounds have shown commendable antioxidant activity, indicating their potential for therapeutic applications. Further investigation into their free radical scavenging properties is required (Thota et al., 2015).

Djukic et al. have synthesized a new class of 1,3-thiazole compounds, specifically 30a and 30c, demonstrating significant antioxidant activity in DPPH, FRAP (Ferric reducing antioxidant power), and TBARS (Thiobarbituric acid reactive substances) assays. Compound 30b exhibited robust FRAP activity but lower efficacy in DPPH and TBARS tests. 30a and 30c showed potent antioxidant effects comparable to vitamin C in TBARS. These findings highlight the potential for diverse antioxidant capabilities among thiazolidinedione derivatives, underscoring the therapeutic promise of 30a and 30c (Figure 30). Further investigation is needed to explore these compounds' full potential (Djukic et al., 2018).

The antioxidant capacity of 2-alkylamino-4-(1-methylbenzimidazol-2-yl) thiazoles was assessed using the DPPH assay, which revealed exceptional scavenging abilities with a descending order of 31b > 31d >31e > 31a > 31c(Figure 31). All synthesized compounds surpassed BHA (butylated hydroxyanisole) in antioxidant activity, as evidenced by HOMO (highest occupied molecular orbital) and LUMO (lowest unoccupied molecular orbital) energy levels. These results underscore the potential of the synthesized thiazole derivatives as promising antioxidants, suggesting their suitability for therapeutic interventions or industrial applications (Afifi et al., 2019).

The findings of Mert et al. have revealed a novel class of sulfonamide derivatives that exhibit potent inhibition of cytosolic isoforms I and II of carbonic anhydrase (CA). These derivatives have a modified chalcone core, and compound 32 has shown the most promising performance among all compounds. Compound 32(Figure 32) has a Ki value of 9.88 nm against hCA I, which is superior to the reference drug AZA. While all compounds have demonstrated action against hCA II (Ki range: 18.25 to 55.43 nm), compound 32 has emerged as a potent CA inhibitor, warranting further research to enhance its therapeutic selectivity (Mert et al., 2016).

Jaidi et al. produced many 2,4,5-trisubstituted thiazole compounds and assessed their effectiveness in inhibiting the cytosolic carbonic anhydrase (CA) III isoform using size exclusion high-performance dynamic light scattering chromatography. The results

indicated that Substance 33(Figure 33) without any substituent was the most potent among the substituted compounds, showing an inhibitory constant (Ki) of 0.5 μM. These observations suggest that a structural relationship exists between the compounds and their activity, highlighting the potential of these substances as inhibitors of the CA III isoform (Al-Jaidi et al., 2020).

Table 6. Thiazole derivatives showing antioxidant activity.

Activity	Compounds	Structures	
Antioxidant agents	**Compounds (29a-c)**: structures of (Z)-3-(2-(2-(1-(2-oxo-2H-chromen-3-yl)ethylidene)hydrazineyl)thiazol-4-yl)-2H-chromen-2-one derivatives	**29 a**:R=H, R₁=F **29 b**:R=H, R₁=I **Figure 29 (a,b).** (Z)-1,5-dimethyl 3-(2-(4-(2-oxo-2H-chromen-3-yl)thiazol-2-yl)hydrazono)indolin-2-one	**29 c** 29a: IC50 of 11.04 ± 0.18μM 29b: IC50 of 11.28 ± 0.06 μM 29c: IC50 of 12.16 ± 0.28 μM **Figure29c.** (Z)-3-(2-(2-(1-(2-oxo 2H-chromen-3-yl)ethylidene) hydrazinyl)thiazol-4-yl)-2H chromen-2-one
	Compounds (30a-c): structures of 2-(2-((1H-indol-5yl)methylene)-hydrazinyl)–thiazoles derivatives	**30 a**:R=2-OCH₃ **30 b**:R=3-OCH₃ **Figure 30(a,b).** (E)-ethyl 2-(2-((5-benzylidene-4-oxo-4,5-dihydrothiazol-2-yl)amino)thiazol-4-yl)acetate	**30c** **Figure30c.** (E)-3-(2,6-dimethoxyphenyl)-1-(2-(ethylamino)-4-methylthiazol-5-yl)prop-2-en-1-one
	Compounds (31a-e): structures of 2-alkylamino-4-(1-methylbenzimidazol-2-yl)thiazole	**31a**:R=CH₃ **31 b**:R=CH₂CH₃ **31 c**:R=CH₃C₂CH₃ **31 d**:R=CH(CH₃)₂ **31 e**:R=(CH₂)₃CHe **Figure 31(a-e).** N-methyl-4-(1-methyl-1H-benzo [d]imidazol-2-yl)thiazol-2-amine	
	Compound 32: structures of (E)-1-(4-hydroxy-3-((E)-phenyldiazenyl)phenyl)-3-phenylprop-2-en-1-one derivatives	**32** R=1,3-dimethoxybenzene **Figure 32.** (E)-1-(4-hydroxy-3-((E)-phenyldiazenyl) phenyl)-3-phenyl prop-2-en-1-one	
	Compound 33: structure of 2-amino-5-phenyl thiazole-4-carboxylic acid derivatives	**Figure 33.** 2-amino-5-phenyl thiazole-4-carboxylic acid	
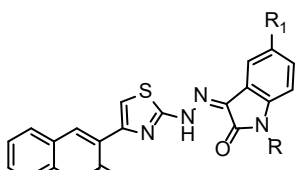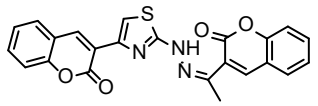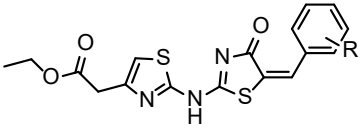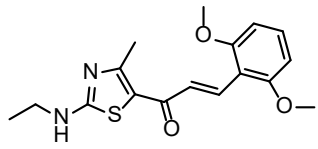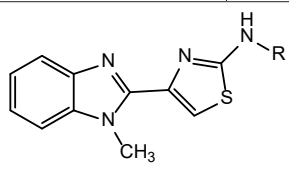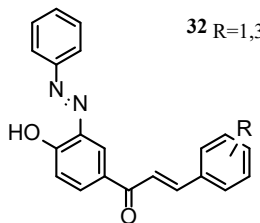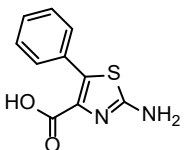
Anticonvulsant activity

Epilepsy, also known as convulsion, is a neurological disorder that affects approximately 67 million individuals worldwide, representing around 2-5% of the global population. The underlying cause of epilepsy is primarily attributed to the imbalance between inhibitory (GABAergic) and excitatory (glutamatergic) neurotransmitters at the synaptic level. This condition results in unpredictable seizures that can have varying intensities and durations. The impact of epilepsy on individuals and society at large is significant, as it can lead to disability, social stigma, and increased healthcare costs. Therefore, understanding the mechanisms underlying epilepsy and identifying effective treatment strategies is paramount (Chiroma et al., 2022).

Epilepsy, a neurological disorder, is characterized by unexpected changes in behavior accompanied by rhythmic and synchronous firing of brain neurons. This condition is noteworthy for the abnormal synchronous activity of neurons in the brain that leads to seizures, which are often unpredictable and can vary in intensity and duration. Understanding the complex interplay of factors involved in epilepsy is critical for the development of effective treatments and interventions that can improve the quality of life for those affected by this disorder (Surineni et al., 2019).

Łączkowski and his team have synthesized ten new hydrazinylthiazole compounds, designated as 34a-j(Figure 34), which incorporate cyclopropyl moieties inspired by the growing use of such compounds in clinical trials. The compounds underwent rigorous evaluations to assess their anticonvulsant properties and demonstrated significant efficacy. In the maximal electroshock test, the trifluoromethyl and chloromethyl groups showed the most promise, while in the pentylenetetrazole (PTZ) test, the methoxy- and azido groups exhibited high efficacy. Significantly, none of the compounds adversely impacted motor coordination, as demonstrated by the rotarod test, suggesting their safety. These results underscore the potential of these cyclopropyl-containing thiazole derivatives as versatile agents with promising therapeutic applications, warranting further clinical investigation (Łączkowski et al., 2018).

Siddiqui and colleagues synthesized compound 35a-c (Figure 35.), a hybrid thiazole-pyridazine structure containing an amide linkage. The compound demonstrated potent anticonvulsant properties, with median effective doses of 88.23 mg/kg and 24.38 mg/kg in PTZ and Maximum electroshock (MES) tests, respectively. The GABA (γ-amino butyric acid) estimate test also revealed a significant increase in GABA levels, confirming compound 35a-c GABA modulatory action. Molecular docking studies that targeted the active site of the GABA receptor supported this mechanism. These results suggest that compound 35a-c has potential as an anticonvulsant intervention, warranting further exploration for clinical applications (Siddiqui et al., 2020).

Table 7. Thiazole derivatives showing anticonvulsant activity.

Activity	Compounds	Structures
Anticonvulsants	**Compounds (34a-j):** structures of (E)-2-(2-(cyclopropylmethylene) hydrazineyl)-4-(p-tolyl) thiazole derivatives	**34a**:R=F **34f**:R=OCH$_3$ **34b**:R=Br **34g**:R=2,4-diF **34c**:R=Cl **34h**:R=CN **34d**:R=CH$_3$ **34i**:R=N$_3$ **34e**:R=CF$_3$ **34j**:R=NO$_2$ **Figure 34**. (E)-2-(2-(cyclopropyl methylene) hydrazinyl)-4-(p-tolyl)thiazole
	Compounds (35a-c): structures of (E)-5-((Z)-3-nitrobenzylidene)-2-(thiazol-2-ylimino) thiazolidin-4-one derivatives	**Figure 35a**. (2E,5Z)-5 (3nitrobenzylidene)-2-(thiazol-2-ylimino)thiazolidin-4-one **Figure 35b**. 2-(3-methyl-2,4-dioxothiazolidin-5-yl)-N-(thiazol-2-yl)acetamide	**Figure 35c**. (Z)-ethyl 2-(2,4-dioxo-5-(2-oxo-2-(thiazol-2-ylamino) ethylidene)thiazolidin-3-yl)acetate
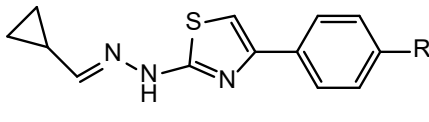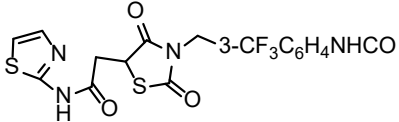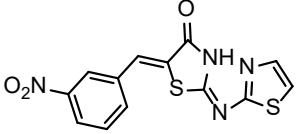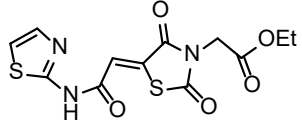
CONCLUSION

A fascinating class of chemical molecules, thiazole derivatives have attracted a lot of interest in the drug research community because of their remarkable pharmacological variety and adaptability. These compounds have demonstrated various therapeutic properties, including anti-inflammatory, antimicrobial, anticancer, antidiabetic, anticonvulsant, antioxidant, and antituberculosis effects. Researchers have conducted extensive studies to understand the precise molecular features that impact the pharmacological outcomes of thiazole derivatives. This has allowed for the rational design of novel compounds with low toxicity and higher potency. The ability of thiazole derivatives to modulate multiple biological pathways and molecular targets is a beacon of hope to develop the effective and safe therapeutic agents. A series of compounds can be synthesized and characterized to evaluate their biological actions, and studies have demonstrated that thiazole derivatives hold great promise for targeting a range of diseases and conditions. These findings are not just exciting but also inspire us with the potential to develop novel drugs that can address unmet medical needs.

FUTURE PERSPECTIVES

Recent advancements in synthetic methodologies have allowed for modifying various thiazole derivatives addressing the challenges of bioavailability, selectivity, and toxicity. Thiazole-based compounds have shown immense potential to interfere with cellular processes involved in inflammation, microbial infections, cancer progression, and diabetes, paving the way for targeted therapeutic interventions. The broadening knowledge in this field contributes to a deeper understanding of the diverse pharmacological actions of thiazole derivatives, offering insights for future medicinal chemists. Given that the thiazole structure provides several sites for substitution with functional groups, many other compounds of biological interest are expected to be synthesized. Developing

new compounds with unique physicochemical, pharmacodynamic, and pharmacokinetic properties could be instrumental in future drug development. The remarkable therapeutic diversity demonstrated by synthetic thiazole derivatives underscores their significance as valuable contributors to the ongoing search for safe and effective pharmaceutical agents.

AUTHOR CONTRIBUTION STATEMENT

Concept: M.K., M.U.M., Design: M.K., M.U.M., Software: M.K., Literature Search: M.K., M.U.M., Writing: M.K., M.U.M., P.P., A.T., Review & Editing: M.M., B.J.S.

CONFLICT OF INTEREST

The authors declare that there is no conflict of interest

REFERENCES

Abdu-Rahem, L. R., Ahmad, A. K., & Abachi., F. T. (2021). Synthesis And Medicinal Attributes Of Thiazole Derivatives: A Review. *Systematic Reviews in Pharmacy*, *12*(1), 290–295.

Afifi, O. S., Shaaban, O. G., Abd El Razik, H. A., Shams El-Dine, S. E. D. A., Ashour, F. A., El-Tombary, A. A., & Abu-Serie, M. M. (2019). Synthesis and biological evaluation of purine-pyrazole hybrids incorporating thiazole, thiazolidinone, or rhodanine moiety as 15-LOX inhibitors endowed with anticancer and antioxidant potential. *Bioorganic Chemistry*, *87*(April), 821–837. https://doi.org/10.1016/j.bioorg.2019.03.076

Al-Jaidi, B. A., Deb, P. K., Telfah, S. T., Dakkah, A. N., Bataineh, Y. A., Khames Aga, Q. A. Al, Al-dhoun, M. A., Ahmad Al-Subeihi, A. A., Odetallah, H. M., Bardaweel, S. K., Mailavaram, R., Venugopala, K. N., & Nair, A. B. (2020). Synthesis and evaluation of 2,4,5-trisubstituted thiazoles as carbonic anhydrase-III inhibitors. *Journal of Enzyme Inhibition and Medicinal Chemistry*, *35*(1), 1483–1490. https://doi.org/10.1080/14756366.2020.1786820

Ali, S. H., & Sayed, A. R. (2021). Review of the synthesis and biological activity of thiazoles. *Synthetic Communications*, *51*(5), 670–700. https://doi.org/10.1080/00397911.2020.1854787

Alrazzak, N. A. (2018). Synthesis, characterization, and study of some of the physical properties of novel 1,3,4-oxadiazole derivatives. *IOP Conference Series: Materials Science and Engineering*, *454*(1). https://doi.org/10.1088/1757-899X/454/1/012096

Arora, P., Narang, R., Bhatia, S., Nayak, S. K., Singh, S. K., & Narasimhan, B. (2015). Synthesis, molecular docking, and QSAR studies of 2, 4-disubstituted thiazoles as antimicrobial agents. *Journal of Applied Pharmaceutical Science*, *5*(2), 028–042. https://doi.org/10.7324/JAPS.2015.50206

Bally, M., Dendukuri, N., Rich, B., Nadeau, L., Helin-Salmivaara, A., Garbe, E., & Brophy, J. M. (2017). Risk of acute myocardial infarction with NSAIDs in real-world use: Bayesian meta-analysis of individual patient data. *BMJ (Online)*, *357*(Cox 2). https://doi.org/10.1136/bmj.j1909

Banday, M. Z., Sameer, A. S., & Nissar, S. (2021). *Pathophysiology of diabetes : An overview*. https://doi.org/10.4103/ajm.ajm

Bekker, O. B., Sokolov, D. N., Luzina, O. A., Komarova, N. I., Gatilov, Y. V., Andreevskaya, S. N., Smirnova, T. G., Maslov, D. A., Chernousova, L. N., Salakhutdinov, N. F., & Danilenko, V. N. (2015). Synthesis and activity of (+)-usnic acid and (-)-usnic acid derivatives containing 1,3-thiazole cycle against Mycobacterium tuberculosis. *Medicinal Chemistry Research*, *24*(7), 2926–2938. https://doi.org/10.1007/s00044-015-1348-2

Berkow, E. L., & Lockhart, S. R. (2017). Fluconazole resistance in Candida species: A current perspective. *Infection and Drug Resistance*, *10*, 237–245. https://doi.org/10.2147/IDR.S118892

Borcea, A. M., Ionuț, I., Crişan, O., & Oniga, O. (2021). An overview of the synthesis and antimicrobial, antiprotozoal, and antitumor activity of thiazole and bisthiazole derivatives. *Molecules*, *26*(3). https://doi.org/10.3390/molecules26030624

Braga, S. F. P., Fonseca, N. C., Ramos, J. P., de Souza-Fagundes, E. M., & de Oliveira, R. B. (2016). Synthesis and cytotoxicity evaluation of thiosemicarbazones and their thiazole derivatives. *Brazilian Journal of Pharmaceutical Sciences*, *52*(2), 299–307. https://doi.org/10.1590/S1984-82502016000200008

Cao, Y. L., Tian, Z. G., Wang, F., Li, W. G., Cheng, D. Y., Yang, Y. F., & Gao, H. M. (2014). Characteristics and clinical outcome of nonsteroidal anti-inflammatory drug-induced acute hepato-nephrotoxicity among Chinese patients. *World Journal of Gastroenterology*, *20*(38), 13956–13965. https://doi.org/10.3748/wjg.v20.i38.13956

Celestina, S. K., Sundaram, K., & Ravi, S. (2020). In vitro studies of potent aldose reductase inhibitors: Synthesis, characterization, biological evaluation and docking analysis of rhodanine-3-hippuric acid derivatives. *Bioorganic Chemistry*, *97*(January), 103640. https://doi.org/10.1016/j.bioorg.2020.103640

Ch, A., Piña-s, P., Ruiz-tachiqu, M., Vadillo, E., Monroy-garc, A., Guti, M., Barrera, D., & Mayani, H. (2021). *Cancer Biology, Epidemiology, and Treatment in the 21st Century : Current Status and Future Challenges From a Biomedical Perspective*. *28*, 1–21. https://doi.org/10.1177/10732748211038735

Chiroma, S. S., Nazifi, A. B., Jamilu, Y., Musa, A., Bichi, L. A., & Chiroma, S. M. (2022). Anticonvulsant activity and mechanism of actions of fractions of Ipomoea asarifolia (Desr) (Convolvulaceae) ethanol leaf extract. *Bulletin of the National Research Centre*. https://doi.org/10.1186/s42269-022-00839-4

de Oliveira Filho, G. B., Cardoso, M. V. de O., Espíndola, J. W. P., Oliveira e Silva, D. A., Ferreira, R. S., Coelho, P. L., Anjos, P. S. dos, Santos, E. de S., Meira, C. S., Moreira, D. R. M., Soares, M. B. P., & Leite, A. C. L. (2017). Structural design, synthesis and pharmacological evaluation of thiazoles against Trypanosoma cruzi. *European Journal of Medicinal Chemistry*, *141*, 346–361. https://doi.org/10.1016/j.ejmech.2017.09.047

Djukic, M., Fesatidou, M., Xenikakis, I., Geronikaki, A., Angelova, V. T., Savic, V., Pasic, M., Krilovic, B., Djukic, D., Gobeljic, B., Pavlica, M., Djuric, A., Stanojevic, I., Vojvodic, D., & Saso, L. (2018). In vitro antioxidant activity of thiazolidinone derivatives of 1,3-thiazole and 1,3,4-thiadiazole. *Chemico-Biological Interactions*, *286*(February 2017), 119–131. https://doi.org/10.1016/j.cbi.2018.03.013

Elsebaei, M. M., Mohammad, H., Abouf, M., Abutaleb, N. S., Hegazy, Y. A., Ghiaty, A., Chen, L., Zhang, J., Malwal, S. R., Oldfield, E., Seleem, M. N., & Mayhoub, A. S. (2018). Alkynyl-containing phenylthiazoles: Systemically active antibacterial agents effective against methicillin-resistant Staphylococcus aureus (MRSA). *European Journal of Medicinal Chemistry*, *148*, 195–209. https://doi.org/https://doi.org/10.1016/j.ejmech.2018.02.031

Equine, V., Virus, E., Virus, R. S., Valley, R., Virus, F., & Virus, T. (2009). *New thiopyrano[2,3-. 2*, 105–112.

Fogel, N. (2015). Tuberculosis: A disease without boundaries. *Tuberculosis*, *95*(5), 527–531. https://doi.org/10.1016/j.tube.2015.05.017

Galochkina, A. V., Bollikanda, R. K., Zarubaev, V. V., Tentler, D. G., Lavrenteva, I. N., Slita, A. V., Chirra, N., & Kantevari, S. (2019). Synthesis of novel derivatives of 7,8-dihydro-6H-imidazo[2,1-b][1,3]benzothiazol-5-one and their virus-inhibiting activity against influenza A virus. *Archiv Der Pharmazie*, *352*(2), 1–8. https://doi.org/10.1002/ardp.201800225

Ganou, C. A., Eleftheriou, P. T., Theodosis-Nobelos, P., Fesatidou, M., Geronikaki, A. A., Lialiaris, T., & Rekka, E. A. (2018). Docking analysis targeted to the whole enzyme: an application to the prediction of inhibition of PTP1B by thiomorpholine and thiazolyl derivatives. *SAR and QSAR in Environmental Research*, *29*(2), 133–149. https://doi.org/10.1080/1062936X.2017.1414874

Gartel, A. L., & Kandel, E. S. (2008). miRNAs: Little known mediators of oncogenesis. *Seminars in Cancer Biology*, *18*(2), 103–110. https://doi.org/10.1016/j.semcancer.2008.01.008

Ghorab, M. M., & Al-Said, M. S. (2012). Antitumor activity of novel pyridine, thiophene, and thiazole derivatives. *Archives of Pharmacal Research*, *35*(6), 965–973. https://doi.org/10.1007/s12272-012-0603-z

Goldstein, J. L., & Cryer, B. (2014). Gastrointestinal injury associated with NSAID use: A case study and review of risk factors and preventative strategies. *Drug, Healthcare and Patient Safety*, *7*, 31–41. https://doi.org/10.2147/DHPS.S71976

Holmes, A. H., Moore, L. S. P., Sundsfjord, A., Steinbakk, M., Regmi, S., Karkey, A., Guerin, P. J., & Piddock, L. J. V. (2016). Understanding the mechanisms and drivers of antimicrobial resistance. *The Lancet*, *387*(10014), 176–187. https://doi.org/10.1016/S0140-6736(15)00473-0

Islam, M. S., Ghawas, H. M., El-Senduny, F. F., Al-Majid, A. M., Elshaier, Y. A. M. M., Badria, F. A., & Barakat, A. (2019). Synthesis of new thiazole-pyrrolidine–(spiro oxindole) tethered to 3-acyl indole as anticancer agents. *Bioorganic Chemistry*, *82*, 423–430. https://doi.org/10.1016/j.bioorg.2018.10.036

Jacob P, J., & Manju, S. L. (2020). Identification and development of thiazole lead as COX-2/5-LOX inhibitors through in-vitro and in-vivo biological evaluation for anti-inflammatory activity. *Bioorganic Chemistry*, *100*(January), 103882. https://doi.org/10.1016/j.bioorg.2020.103882

Karale, B. K., Takate, S. J., Salve, S. P., Zaware, B. H., & Jadhav, S. S. (2015). Synthesis and antibacterial screening of novel fluorine-containing heterocycles. *Oriental Journal of Chemistry*, *31*(1), 307–315. https://doi.org/10.13005/ojc/310135

Karale, U. B., Krishna, V. S., Krishna, E. V., Choudhari, A. S., Shukla, M., Gaikwad, V. R., Mahizhaveni, B., Chopra, S., Misra, S., Sarkar, D., Sriram, D., Dusthackeer, V. N. A., & Rode, H. B. (2019). Synthesis and biological evaluation of 2,4,5-trisubstituted thiazoles as antituberculosis agents effective against drug-resistant tuberculosis. *European Journal of Medicinal Chemistry*, *178*, 315–328. https://doi.org/10.1016/j.ejmech.2019.05.082

Khan, M. F., & Wang, G. (2018). Environmental Agents, Oxidative Stress and Autoimmunity. *Current Opinion in Toxicology*, *7*, 22–27. https://doi.org/10.1016/j.cotox.2017.10.012

Khloya, P., Kumar, S., Kaushik, P., Surain, P., Kaushik, D., & Sharma, P. K. (2015). Synthesis and biological evaluation of pyrazolylthiazole carboxylic acids as potent anti-inflammatory-antimicrobial agents. *Bioorganic and Medicinal Chemistry Letters*, *25*(6), 1177–1181. https://doi.org/10.1016/j.bmcl.2015.02.004

Knott-Hunziker, V., Waley, S. G., Orlek, B. S., & Sammes, P. G. (1979). Penicillinase active sites: Labelling of serine-44 in β-lactamase I by 6β-bromopenicillanic acid. *FEBS Letters*, *99*(1), 59–61. https://doi.org/10.1016/0014-5793(79)80248-3

Küster, T., Lense, N., Barna, F., Hemphill, A., Kindermann, M. K., Heinicke, J. W., & Vock, C. A. (2012). A New promising application for highly cytotoxic metal compounds: η 6-arene ruthenium (II) phosphite complexes for the treatment of alveolar echinococcosis. *Journal of Medicinal Chemistry*, *55*(9), 4178–4188. https://doi.org/10.1021/jm300291a

Ła̧czkowski, K. Z., Jachowicz, K., Misiura, K., Biernasiuk, A., & Malm, A. (2015). Synthesis and biological evaluation of novel 2-(1H-imidazol-2-ylmethylidene)hydrazinyl- 1,3-thiazoles as potential antimicrobial agents. *Heterocyclic Communications*, *21*(2), 109–114. https://doi.org/10.1515/hc-2014-0194

Łączkowski, K. Z., Konklewska, N., Biernasiuk, A., Malm, A., Sałat, K., Furgała, A., Dzitko, K., Bekier, A., Baranowska-Łączkowska, A., & Paneth, A. (2018). Thiazoles with cyclopropyl fragment as antifungal, anticonvulsant, and anti-*Toxoplasma gondii* agents: synthesis, toxicity evaluation, and molecular docking study. *Medicinal Chemistry Research*, *27*(9), 2125–2140. https://doi.org/10.1007/s00044-018-2221-x

Lee, A., Mg, C., Jc, C., Jf, K., & Jp, K. (2007). *renal function in adults with normal renal function (Review)*. https://doi.org/10.1002/14651858.CD002765.pub3.www.cochranelibrary.com

Lucas, G. N. C., Leitão, A. C. C., Alencar, R. L., Xavier, R. M. F., Daher, E. D. F., & Silva Junior, G. B. da. (2019). Pathophysiological aspects of nephropathy caused by nonsteroidal anti-inflammatory drugs. *Jornal Brasileiro de Nefrologia : ʾorgao Oficial de Sociedades Brasileira e Latino-Americana de Nefrologia*, *41*(1), 124–130. https://doi.org/10.1590/2175-8239-JBN-2018-0107

Maezaki, H., Tawada, M., Yamashita, T., Banno, Y., Miyamoto, Y., Yamamoto, Y., Ikedo, K., Kosaka, T., Tsubotani, S., Tani, A., Asakawa, T., Suzuki, N., & Oi, S. (2017). Design of potent dipeptidyl peptidase IV (DPP-4) inhibitors by employing a strategy to form a salt bridge with Lys554. *Bioorganic and Medicinal Chemistry Letters*, *27*(15), 3565–3571. https://doi.org/10.1016/j.bmcl.2017.05.048

Meng, G., Zheng, M., Wang, M., Tong, J., Ge, W., Zhang, J., Zheng, A., Li, J., Gao, L., & Li, J. (2016). Design and synthesis of new potent PTP1B inhibitors with the skeleton of 2-substituted imino-3-substituted-5-heteroarylidene-1,3-thiazolidine-4-one: Part I. *European Journal of Medicinal Chemistry*, *122*, 756–769. https://doi.org/10.1016/j.ejmech.2016.05.060

Mert, S., Alım, Z., İşgör, M. M., Beydemir, Ş., & Kasımoğulları, R. (2016). The synthesis of novel pyrazole-3,4-dicarboxamides bearing 5-amino-1,3,4-thiadiazole-2-sulfonamide moiety with effective inhibitory activity against the isoforms of human cytosolic carbonic anhydrase I and II. *Bioorganic Chemistry*, *68*, 64–71. https://doi.org/10.1016/j.bioorg.2016.07.006

Nagireddy, P. K. R., Kommalapati, V. K., Siva Krishna, V., Sriram, D., Tangutur, A. D., & Kantevari, S. (2019). Imidazo[2,1-b]thiazole-Coupled Natural Noscapine Derivatives as Anticancer Agents. *ACS Omega*, *4*(21), 19382–19398. https://doi.org/10.1021/acsomega.9b02789

Patel, A. D., Pasha, T. Y., Lunagariya, P., Shah, U., Bhambharoliya, T., & Tripathi, R. K. P. (2020). A Library of Thiazolidin-4-one Derivatives as Protein Tyrosine Phosphatase 1B (PTP1B) Inhibitors: An Attempt To Discover Novel Antidiabetic Agents. *ChemMedChem*, *15*(13), 1229–1242. https://doi.org/10.1002/cmdc.202000055

Rajiani, I., & Ismail, N. (2019). Management innovation in balancing technology innovation to harness universities performance in the era of community 4.0. *Polish Journal of Management Studies*, *19*(1), 309–321. https://doi.org/10.17512/pjms.2019.19.1.24

Ran, K., Gao, C., Deng, H., Lei, Q., You, X., Wang, N., Shi, Y., Liu, Z., Wei, W., Peng, C., Xiong, L., Xiao, K., & Yu, L. (2016). Identification of novel 2-aminothiazole conjugated nitrofuran as antitubercular and antibacterial agents. *Bioorganic and Medicinal Chemistry Letters*, *26*(15), 3669–3674. https://doi.org/10.1016/j.bmcl.2016.05.088

Rostom, A., Wells, G., Tugwell, P., Welch, V., Dube, C., & McGowan, J. (2002). Prevention of NSAID-induced gastroduodenal ulcers | Prävention NSAR-induzierter Gastroduodenalulzera. *Praxis*, *91*(14), 617. https://doi.org/10.1024/0369-8394.91.14.617

Sahu, S., Ghosh, S. K., Gahtori, P., Pratap Singh, U., Bhattacharyya, D. R., & Bhat, H. R. (2019). *In silico* ADMET study, docking, synthesis, and antimalarial evaluation of thiazole-1,3,5-triazine derivatives as Pf-DHFR inhibitor. *Pharmacological Reports*, *71*(5), 762–767. https://doi.org/10.1016/j.pharep.2019.04.006

Salem, M. A. (2017). Synthesis of new thiazole, bithiazolidinone, and pyrano [2,3-d] thiazole derivatives as potential antimicrobial agents. *Croatica Chemica Acta*, *90*(1), 1–9. https://doi.org/10.5562/cca2955

Sever, B., Altıntop, M. D., Demir, Y., Akalın Çiftçi, G., Beydemir, Ş., & Özdemir, A. (2020). Design, synthesis, *in vitro*, and *in silico* investigation of aldose reductase inhibitory effects of new thiazole-based compounds. *Bioorganic Chemistry*, *102*(April), 104110. https://doi.org/10.1016/j.bioorg.2020.104110

Siddiqui, A. A., Partap, S., Khosla, S., Yar, M. S., & Mishra, R. (2020). Synthesis anti-convulsant activity, and molecular docking study of novel thiazole pyridazine hybrid analogues. *Bioorganic Chemistry*, *99*(January), 103584. https://doi.org/10.1016/j.bioorg.2020.103584

Singh, I. P., Gupta, S., & Kumar, S. (2020). Thiazole Compounds as Antiviral Agents: An Update. *Medicinal Chemistry*, *16*(1), 4–23. https://doi.org/10.2174/1573406415666190614101253

Surineni, G., Gao, Y., Hussain, M., Liu, Z., Lu, Z., Chhotaray, C., Islam, M. M., Hameed, H. M. A., & Zhang, T. (2019). Design, synthesis, and in vitro biological evaluation of novel benzimidazole tethered allylidenehydrazinylmethylthiazole derivatives as potent inhibitors of Mycobacterium tuberculosis. *MedChemComm*, *10*(1), 49–60. https://doi.org/10.1039/c8md00389k

Testing, E. C. for A. S. (2000). EUCAST Definitive Document E.DEF 3.1, June 2000: Determination of minimum inhibitory concentrations (MICs) of antibacterial agents by agar dilution. *Clinical Microbiology and Infection : The Official Publication of the European Society of Clinical Microbiology and Infectious Diseases*, *6*(9), 509–515.

Thota, S., Nadipelly, K., Shenkesi, A., & Yerra, R. (2015). Design, synthesis, characterization, antioxidant and in vitro cytotoxic activities of novel coumarin thiazole derivatives. *Medicinal Chemistry Research*, *24*(3), 1162–1169. https://doi.org/10.1007/s00044-014-1184-9

Ulusoy Güzeldemirci, N., & Gürsoy, E. (2017). Yeni imidaz o[2,1-b]tiyazol türevlerinin sentezi ve antitüberküler etkilerinin değerlendirilmesi. *Marmara Pharmaceutical Journal*, *21*(1), 102–109. https://doi.org/10.12991/marupj.259887

Ulusoy Güzeldemirci, N., Karaman, B., & Küçükbasmaci, Ö. (2017). İmidazo[2,1-B] Tiyazol Çekirdeği Taşıyan Bazı Arilidenhidrazit Türevlerinin Antibakteriyel, Antitüberküler Ve Antiviral Aktivite Tayinleri. *Turkish Journal of Pharmaceutical Sciences*, *14*(2), 157–163. https://doi.org/10.4274/tjps.25743

Wu, J., Ma, Y., Zhou, H., Zhou, L., Du, S., Sun, Y., Li, W., Dong, W., & Wang, R. (2020). Identification of protein tyrosine phosphatase 1B (PTP1B) inhibitors through De Novo Evolution, synthesis, biological evaluation, and molecular dynamics simulation. *Biochemical and Biophysical Research Communications*, *526*(1), 273–280. https://doi.org/10.1016/j.bbrc.2020.03.075

Yılmaz Cankılıç, M., & Yurttaş, L. (2017). Study on the Antimicrobial Effects of Novel Thiazole Derivatives. *Marmara Pharmaceutical Journal*, *21*(3), 654–654. https://doi.org/10.12991/marupj.323584

Yurttaş, L., Özkay, Y., Karaca Gençer, H., & Acar, U. (2015). Synthesis of Some New Thiazole Derivatives and Their Biological Activity Evaluation. *Journal of Chemistry*, *2015*. https://doi.org/10.1155/2015/464379

Ocular Drug Delivery Routes: Diseases Overview and Advanced Administration Methods

Ceren YETGIN*, Fatma Nur TUĞCU-DEMİRÖZ**, Sevgi TAKKA****°

Ocular Drug Delivery Routes: Diseases Overview and Advanced Administration Methods

SUMMARY

The eye, which is essential for vision, is susceptible to diseases such as diabetic retinopathy, age-related macular degeneration, glaucoma, and dry eye syndrome. These conditions can significantly impair quality of life and lead to blindness. Traditional treatments for eye diseases, especially eye drops, have low bioavailability and short retention times on the ocular surface. To overcome these problems, new drug delivery systems such as hydrogels, contact lenses, microneedles, and nanosystems have been developed to increase drug penetration and maintain therapeutic effects.

Drug delivery to the eye can occur via systemic, topical, intravitreal, intracorneal, subconjunctival, and suprachoroidal routes, each with different advantages and limitations. Systemic administration often results in low ocular drug concentrations and systemic side effects. Topical eye drops are easy to apply and localized, but face difficulties in absorption and retention. Intravitreal and suprachoroidal injections provide targeted delivery to the posterior segment but are invasive and carry infection risks. Subconjunctival and intracorneal routes offer less invasive alternatives with improved targeting capabilities. Nanosystems and controlled-release technologies hold promise for overcoming current barriers and aim to increase drug bioavailability, extend release times, and improve patient compliance. Overall, advancing drug delivery methods is important for effective treatment of both anterior and posterior segment eye diseases.

Key Words: *Ocular, intravitreal, nanosystems, hydrogel.*

Oküler İlaç İletim Yolları: Hastalıklara Genel Bakış ve İleri Uygulama Yöntemleri

ÖZ

Görmeyi sağlayan göz, diyabetik retinopati, yaşa bağlı makula dejenerasyonu, glokom ve kuru göz sendromu gibi hastalıklara karşı hassastır. Bu durumlar yaşam kalitesini önemli ölçüde bozabilir ve körlüğe yol açabilir. Göz hastalıkları için geleneksel tedaviler, özellikle göz damlaları, düşük biyoyararlanım ve göz yüzeyinde kısa tutulma sürelerine sahiptir. Bu durumların üstesinden gelmek için ilaç penetrasyonunu artırmak ve terapötik etkileri sürdürmek için hidrojeller, kontakt lensler, mikroiğneler ve nanosistemler gibi yeni ilaç taşıyıcı sistemleri geliştirilmiştir.

Göze ilaç iletilmesi, her biri farklı avantajlara ve sınırlamalara sahip olan sistemik, topikal, intravitreal, intrakorneal, subkonjonktival ve suprakoroidal yollarla gerçekleşebilir. Sistemik uygulama genellikle düşük oküler ilaç konsantrasyonlarına ve sistemik yan etkilere neden olur. Topikal göz damlaları uygulaması kolay ve lokalizedir ancak emilim ve tutulmada zorluklarla karşı karşıyadır. İntravitreal ve suprakoroidal enjeksiyonlar, arka segmente hedefli uygulama sağlar ancak invazivdir ve enfeksiyon riskleri taşır. Subkonjonktival ve intrakorneal yollar, iyileştirilmiş hedefleme yetenekleriyle daha az invaziv alternatifler sunar. Nanosistemler ve kontrollü salım teknolojileri, mevcut engellerin üstesinden gelmede umut vadediyor ve ilaç biyoyararlanımını artırmayı, salım sürelerini uzatmayı ve hasta uyumunu iyileştirmeyi amaçlıyor. Genel olarak, ilaç iletme yöntemlerini ilerletmek, hem ön segment hem de arka segment göz hastalıklarının etkili tedavisi için öneme sahiptir.

Anahtar Kelimeler: *Göz, intravitreal, nanosistem, hidrojel*

---

* ORCID: 0000-0001-6451-0497, Gazi University Faculty of Pharmacy, Department of Pharmaceutical Technology, Ankara, Turkey.
** ORCID: 0000-0002-9468-3329, Gazi University Faculty of Pharmacy, Department of Pharmaceutical Technology, Ankara, Turkey.
*** ORCID: 0000-0003-4429-9836, Gazi University Faculty of Pharmacy, Department of Pharmaceutical Technology, Ankara, Turkey.

° Corresponding Author; Sevgi TAKKA
 E-mail: takka@gazi.edu.tr

INTRODUCTION

The eye, a remarkably sensitive organ crucial for vision, comprises a complex system of interconnected structures housed within a spherical shape. Numerous diseases may occur in this sensitive structure due to internal and external factors. While diseases that occur in the eye reduce the quality of life of the patient with symptoms, such as itching, burning sensation, redness, blurred vision, or visual defects, some diseases may cause vision loss in later cases. The eye is basically divided into two: the anterior segment and the posterior segment. These segments contain specialized tissues, such as sclera, choroid, retina, cornea, lens, iris, and pupil (Kearns & Williams, 2009). The most common diseases in these specialized tissues can be listed as diabetic retinopathy (DR), age-related macular degeneration (AMD), glaucoma, dry eye syndrome (DES), retinitis, and various infections. DR and AMD are the leading causes of blindness in older people. According to estimates by the National Eye Institute, the prevalence of conditions like glaucoma, DR, and AMD is expected to double by 2050 (Cabrera, Wang, Reddy, Acharya, & Shin, 2019). Among the oldest and most widely used dosage forms for ocular administration are topically applied eye drops. Conventional eye drops are usually dosage forms, such as solutions, suspensions, and emulsions. However, these topically applied eye drops have a short retention time on the eye's surface (they move away from the eye surface within a few seconds after application) and their ability to penetrate the eye surface is limited (Janagam, Wu, & Lowe, 2017). For this reason, researchers turned to new research on the application of drugs to the eye. Different administration routes such as the subconjunctival route, intracorneal route, suprachoroidal route and different formulation strategies such as gel, lens, microneedle, nanosystems have been developed.

In this review common eye diseases are mentioned and drug administration methods to the eye will be evaluated with the drug delivery systems used.

Diseases of The Eye

Eye diseases are examined according to whether they are effective in the anterior or posterior segment, and a treatment strategy is developed. In general, similar drug application methods can be used for diseases with the same segment of effect. DES, glaucoma, and infections like uveitis, blepharitis, and conjunctivitis are diseases in the anterior segment of the eye. As an example of anterior segment disease, DES is mentioned in detail as a subtitle. Diseases in the posterior segment can be listed as AMD, DR, DME, vitreoretinopathy, endophthalmitis, and cytomegalovirus retinitis (CMVR). Posterior segment diseases are bleeding, tears, or inflammation that occur in the retina, usually due to bacteria, viruses, or various tissue anomalies. It can also be caused by bacteria that cause inflammation in the vitreous, such as endophthalmitis. As subheadings, AMD, DR, and CMVR, as examples of posterior segment diseases, are explained in detail and current treatments are mentioned.

Anterior Segment Diseases

Dry eye syndrome (DES)

Although the causes of DES are not fully elucidated, it can be defined as one of the most common eye disorders affecting the lacrimal glands in general, resulting in insufficient or poor-quality tear production (Dartt, 2004). DES symptoms are often observed in the form of dryness, stinging, burning sensation in the eye, redness, vision problems, and itching (Shoari, Kanavi, & Rasaee, 2021). Additionally, the causes of DES include disruption of the structure of the tear film due to abnormalities in the mucin, lipid, and protein profiles of tears, as well as inflammation of the ocular surface and tear-producing glands (Yelleppeddi et al., 2015). Restasis®, Systane®, and Refresh® are commercial drugs that moisturize the eye's surface, while Hylo-Comod® and TheraTears® are commercial drugs that mimic and are used for the symptomatic treatment of DES. While these treatments may provide a short-term solution to symptomatic disorders, they will not treat the pathophysiological problem

of DES. Anti-inflammatory therapies, such as cyclosporines and corticosteroids, are used to permanently treat the disease (Thacker, Singh, Basu, & Singh, 2023). Commercially available Restasis® and Ikervis® are cyclosporine A emulsions for DES. Cequa®, approved by the FDA (Food and Drug Administration), is the first nanomicellar-based system containing cyclosporine A.

Glaucoma

Glaucoma, one of the leading causes of irreversible blindness worldwide, occurs when damage and loss occur in the retinal cells and optic nerves over time. Intraocular fluid is constantly present inside the eye and plays a role in the nutrition of the eye. Intraocular fluid is constantly renewed by being thrown out of the eye through some channels (Feng, Wang, Zhang, Zhang, & Song, 2023). Causes such as blockage in these channels cause intraocular fluid to not drain away and intraocular pressure to rise. As a result, the nutrition of the optic nerve cells is prevented and over time, the optic nerve cells are damaged and die (Weiwei Wang & Wang, 2023). As nerve cells die, vision loss occurs from the periphery to the center. When all the cells die, permanent vision loss occurs. Treatment is aimed at lowering intraocular pressure. Some of the drugs indicated for its treatment are timolol, dorzolamide, brimonidine, latanoprost, and bimatoprost. The current treatment for glaucoma is eye drops applied several times a day.

Posterior Segment Diseases

Age-related macular degeneration (AMD)

AMD affects people over the age of 50-55 and is one of the most common causes of irreversible blindness in humans (Choi, Nawash, Du, Ong, & Chhablani, 2023). The disease is divided into wet and dry AMD. Wet AMD is characterized by choroidal neovascularization, resulting from the accumulation of vascular leaks in the subretinal space caused by anomalies in the blood vessels (Grimes, Aloney, Skondra, & Chhablani, 2023). Wet AMD accounts for approximately 15% of all AMD and is the primary

type of AMD that causes blindness. Pharmacological treatment of the disease is performed with anti-vascular endothelial growth factor (anti-VEGF) antibodies. Lucentic® (Ranibizumab), Avastin® (Bevacizumab), Macugen® (Pegaptanib), and Eylea® (Aflibercept) are the current treatment methods for the disease, which are administered Intravitreal at intervals of 4-6 weeks. In the dry form of AMD, drusen formation and atrophies are seen in RPE (Abidi, Karrer, Csaky, & Handa, 2022). Although scarring can cause vision loss, it progresses more slowly than the wet form and is much less likely to cause blindness. Cardiovascular disease, advancing age, and a history of smoking are thought to be factors that influence the disease (Pennington & DeAngelis, 2016; Seddon, Willett, Speizer, & Hankinson, 1996). Although there is no complete cure for dry AMD so far, various treatment strategies (vitamins, carotenoids, antioxidants) can be applied to slow the progression of the disease and relieve symptoms (Chiou, 2011).

Diabetic retinopathy (DR)

DR is one of the leading causes of blindness in the 20-74 age group and the incidence of the disease is reported to be 35% in diabetic patients (Georgiou & Prokopiou, 2023). Proliferative or non-proliferative disease may progress. Non-proliferative DR is the initial stage of DR and the most common form of the disease. It is characterized by several microvascular changes, such as increased permeability of retinal vessels, capillary occlusion, and loss of endothelial intercellular connections (Wei Wang & Lo, 2018). Proliferative DR involves the abnormal formation of new blood vessels on the surface of the retina or optic disc, followed by fibrosis (Osaadon, Fagan, Lifshitz, & Levy, 2014). Macular edema occurs because of the accumulation of subretinal fluid caused by neovascularization and the breakdown of the BRB (Im, Jin, Chow, & Yan, 2022). DME can surface at any stage of DR progression, causing blindness in later stages. Pharmacological treatment of the disease is anti-VEGF agents, as in AMD.

Cytomegalovirus retinitis (CMVR)

Human cytomegalovirus (CMV) is a common virus that is usually asymptomatic in healthy individuals. However, it can cause severe disease in immunocompromised individuals, such as patients receiving immunosuppressive therapy or infected with human immunodeficiency virus (HIV) (Landolfo, Gariglio, Gribaudo, & Lembo, 2003). More than half of adults worldwide are infected with this virus by the age of 40. If CMVR is not diagnosed early and adequately treated, it usually causes a decrease in visual acuity and may cause blindness in advanced cases (Port et al., 2017). In patients with mild CMVR, the infection begins in the retina periphery, and patients may see images, such as flies flying (Eid, Bakri, Kijpittayarit, & Razonable, 2008). In more severe cases, retinal hemorrhages, retinal tears, retinal edema, and vascular leaks are observed (Faber, Wiley, Lynn, Gross, & Freeman, 1992). Current treatment of CMV retinitis is administered by intravenous infusion or intravitreal injection. The intravenous infusion treatment procedure is the administration of ganciclovir, cidofovir, or foscarnet for at least one hour 1-3 times a day for 2-3 weeks (Teoh, Ou, & Lim, 2012). Intravitreal injection treatments on the market are the injection of ganciclovir; or foscarnet 2-3 times a week. The ganciclovir implant (Vitrasert®), developed by Bausch & Lomb, is the first intraocular sustained-release device approved for treating CMV retinitis. Intraocular administration of ganciclovir minimized systemic side effects. The ganciclovir implant consists of a non-biodegradable polymer that releases approximately 1 μg/h of ganciclovir over 5-8 months. Application of the device through an invasive procedure causes complications, such as endophthalmitis, retinal detachment, and vitreous hemorrhage (Wang, Jiang, Joshi, & Christoforidis, 2013). Additionally, since it is not biodegradable, it must be surgically removed after treatment. Considering all these difficulties in the treatment of the disease, Yetgin et al. developed ganciclovir-loaded transfersomes for topical application to provide a controlled release and increase permeability (Yetgin, Tuğcu-Demiröz, & Takka, 2022).

Novel Drug Delivery Systems Applied to The Eye

Hydrogels

Hydrogels are three-dimensional, polymeric networks with physical properties for a variety of biomedical applications, especially controlled release at a specific site (Xu, Wang, Liu, & Gong, 2023). They are formed by physical or chemical cross-linking of amphiphilic and hydrophilic polymers and have swelling properties. One of the most important characteristics of hydrogels is their physicochemical similarity with natural tissues; They are generally very soft and have an elastic texture with a high water content (Duvvuri, Janoria, Pal, & Mitra, 2007). Hydrogels can deliver drugs as microneedles to the cornea and suprachoroidal region (Than et al., 2018). Environmentally sensitive hydrogels gel upon response to a physical (temperature, growing area, etc.) or chemical (pH, ionic strength, enzyme, etc.) stimulus (Rafael et al., 2019). Thermosensitive *in situ* hydrogels can be administered by injection into the vitreous or subconjunctiva, delivered to the suprachoroidal or intracorneal region with hollow microneedles, or applied topically to the surface of the eye. The biggest advantage of *in situ* hydrogels is that they can be injected in liquid form at room temperature and become a gel inside the eye, serving as a reservoir containing the drug.

Contact Lens

The drug-loaded contact lens placed on the cornea acts as a controlled-release reservoir(Ross et al., 2019; Xu et al., 2018). Hydrophobic polymers such as silicone are added to hydrogel-based lenses, which are generally obtained by polymerization of a monomer such as hydroxyethyl methacrylate (HEMA), to increase oxygen permeability (Fan et al., 2020). Contact lenses aim to increase the transfer of the drug from the cornea by prolonging the time the drug stays on the cornea, thus increasing the possibility of the drug spreading to the intraocular tissues (Kim et al., 2023). The ability to wear drug-loaded contact lenses for a long time without the need for daily replacement provides ease of application for the patient.

Microneedle

Ocular microneedles are micrometer-sized needles designed to deliver drugs to ocular surfaces (Glover et al., 2023). There are different types of microneedles, and they can act through different mechanisms after penetrating the ocular surface. Hollow microneedles can inject drugs through these holes. With this method, liquid doses are applied (Jung, Kim, Chung, Hejri, & Prausnitz, 2022). Microneedles can be designed as a drug-loaded nonbiodegradable polymeric matrix and released throughout the ocular surface (Roy, Galigama, Thorat, Garg, & Venuganti, 2020; Suriyaamporn et al., 2023). Dissolving microneedles can dissolve at the application site and release drugs (Datta, Roy, Garg, & Venuganti, 2022; Than et al., 2018). Solid microneedles by coating the outer surface with the drug, the coating material can penetrate the ocular surface after application (Kim, Grossniklaus, Edelhauser, & Prausnitz, 2014).
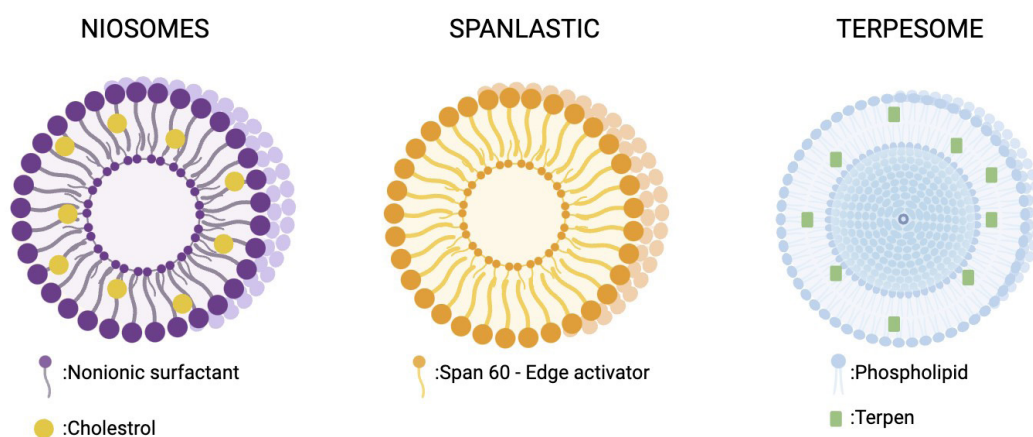
Figure 1. Representation of niosome, spanlastic, and terpesome. Created with BioRender.com.

Nanosystems

The term nanosystems include nano-sized drug carriers systems such as nanoparticles, nanoemulsions, nanosuspensions, liposomes, niosomes, dendrimers, transfersomes, and polymeric micelles (Aminu et al., 2020). These systems generally provide controlled drug release and targeted drug delivery. They are also biocompatible and biodegradable. Nanosystems release drugs to the eye in a controlled manner, allowing dosing intervals to be extended. Additionally, when flexible systems such as liposomes are applied topically, they can more easily penetrate the eye and distribute into intraocular tissues (Agarwal et al., 2016). In Table 1, studies on nanoemulsion, micelle, nanosuspension, solid lipid particle, nanofiber, transfersome, liposome, and dendrimer nanosystems observed through different application routes are presented and briefly explained. It is seen that there are many studies in the literature regarding the application of niosomes to the eyes (Abdelkader et al., 2012; Alyami, Abdelaziz, Dahmash, & Iyire, 2020; Durak et al., 2020; Zeng et al., 2016). Besides these, spanlastics and terpesomes are novel developed systems for applying drugs to the eye topically, with their flexible structure and high penetration properties (Figure 1.).

Niosomes, unlike liposomes, are vesicle-shaped drug carrier systems that contain nonionic surfactants instead of phospholipids in their structure (Villate-Beitia et al., 2018). Since nonionic surfactant provides flexibility to the structure, they are considered more flexible systems than liposomes (Rajera, Nagpal, Singh, & Mishra, 2011; Sankhyan & Pawar, 2012); In addition, nonionic surfactants do not pose a risk to the eye as they are nontoxic, biocompatible and non-immunogenic (Kazi et al., 2010). An essential feature of non-ionic surfactants is that they inhibit p-glyco-

protein, thus increasing intracellular uptake and targeting (Bhardwaj, Tripathi, Gupta, & Pandey, 2020). In the literature, generally, sorbitan esters (Span 60®, span 80®), polyoxyethylene sorbitan esters (Polysorbates (Tween 20®, tween 40®)), macrogol ethers (Brij 30®, brij 35®) are used as nonionic surfactants. Yetgin et al. developed niosomes containing ganciclovir for intravitreal injection to provide a controlled release and increase permeability (Yetgin, Çoban, Tuğcu-Demiröz, Sağır, & Takka, 2022).

Spanlastics are ultra-deformable vesicles based on nonionic surfactant and edge activator, which were introduced to the literature by Kaur and Kakkar (Kakkar & Kaur, 2011). Unlike niosomes, they do not contain cholesterol in their composition, but instead contain an edge activator that helps to form a more flexible double-layered membrane. In the study, a surfactant-based, elastic, vesicular drug delivery system (spanlastics) was developed to target the posterior segment of the eye via a topical route. The system consists of span 60® and tween 80® used as edge activators. As a result of the ex vivo permeation study, spanlastics showed two times better corneal permeability than the niosome. Two hours after topical application to rabbit eyes, fluorescent vesicles were intact in the vitreous and intraocular tissues. The results showed that spanlastics could be used as drug carriers to the posterior segment of the eye.

Terpesomes contain terpenes instead of cholesterol unlike liposome. Terpenes are natural compounds consisting of multiple isoprene (C_5H_8) units, and they accumulate in the lipophilic hydrocarbon molecules of the lipid bilayer of cells, facilitating their passage into the cell. Terpenes are used in the pharmaceutical field, and there are also eye drops on the market called Ectodol® (4-terpene-ol, limonene, eugenol), which contain terpenes to increase ocular permeability (Reyes-Batlle et al., 2021).

There are older and new studies in which terpenes, such as terpene-4-ol, eugenol, limonene, and cineole are used as penetration enhancers in ocular systems (Afouna, Khedr, Abdel-Naim, & Al-Marzoqi, 2010; Anand, Anbukkarasi, Thomas, & Geraldine, 2021; El-Gendy, Mansour, El-Assal, & Ishakb, 2020).

Younes et al. developed cubosome containing sertaconazole nitrate (STZ) targeted to the cornea and added monoterpene (limonene) into the formulation as a penetration enhancer (Younes, Abdel-Halim, & Elassasy, 2018). The ex vivo corneal permeability study indicated that the formulation increased the corneal permeability of STZ. Additionally, studies in rabbits reported good in vivo corneal tolerability and superior in vivo corneal uptake compared to STZ suspension.

Table 1. The administration routes of the drugs to the eye and the drug delivery systems

Administration Route	Drug Delivery System	Active Pharmaceutical Ingredient	Targeted Area	In Vivo/Ex Vivo Studies	References
Topical	Self-nanoemulsifying system	Brimonidine tartrate	Anterior segment	The formulation showed an increase in permeation of about 2.35 times that of the marketed formulation.	(Vikash et al., 2023)
Topical	Micelle	Flurbiprofen	Anterior segment	3D corneal spheroids showed an increase in transcorneal penetration efficiency. A study with corneal epithelial cells indicated prolonged retention of the drug on the ocular surface. According to in vivo study, showed a better ocular anti-inflammation effect.	(Weng et al., 2018)
Topical	Gel containing niosome	Flurbiprofen	Anterior segment	According to an in vivo rabbit study, the formulation showed higher C_{max} and AUC_{0-12} values than those of the solution. The formulation showed rapid anti-inflammatory effects in the inflamed.	(El-Sayed, Hussein, Sarhan, & Mansour, 2017)
Topical	Insert containing nanofiber	Besifloxacin	Anterior segment	Ex vivo transport studies reported that the insert possessed a drug delivery level close to that of the marketed drug. Single-dose application of inserts was effectively reduced bacterial keratitis in rabbit eyes compared to multiple dosing with the marketed drug.	(Polat et al., 2020)
Topical	Electrolyte-sensitive in situ gel containing transfersome	Natamycin	Anterior segment	Transcorneal permeability was significantly higher than the drug suspension. The ocular disposition studies in rabbits demonstrated the superiority of the formulation in terms of drug delivery compared to plain transfersome.	(Janga et al., 2019)
Topical	Contact lens	Betaxolol hydrochloride	Anterior segment	The *in vivo* conjunctivitis treatment of rabbits for 72 h showed that the lens presented a better therapeutic effect than one dose administration of drug solution per day.	(Wei et al., 2020)
Topical	Chitosan film	Brimonidine tartrate	Anterior segment	The permeability of *ex vivo* rabbit corneas was determined to be 1.62×10^{-5} cm/s. They reported that this is much higher than the permeation coefficient from many previous systems.	(Li, Wang, Gui, & Yang, 2020)
Topical	Hydroxypropyl methylcellulose (HPMC)-Eudragit film	Chloramphenicol	Anterior segment	Only *in vitro* studies.	(Boateng & Popescu, 2016)
Topical	Electrospun nanofiber insert Solvent-cast polymeric insert	Dexamethasone	Anterior segment	Only *in vitro* studies.	(Bhattarai et al., 2017)
Topical	Chitosan insert	Bimatoprost	Anterior segment	*In vivo* studies in rabbits showed have sustained reduction of intraocular pressure (IOP) for six days with IOP of 15.9 mmHg and 14.6 mmHg for different inserts at 120 h.	(Jadhav & Yadav, 2022)
Topical	Hyaluronic acid-poly vinyl alcohol (PVA) film	Dexamethasone Levofloxacin	Anterior segment	*Ex vivo* study with porcine eyes demonstrated capability to deliver drugs to the cornea and across the sclera, to potentially target the posterior eye segment.	(Ghezzi et al., 2023)
Topical	Nanofibers-based thermo-responsive gel	Fenofibrate	Posterior segment	According to an *ex vivo* drug permeation study across goat cornea, confocal microscopy showed better penetration efficiency of formulation compared to plain rhodamine B solution.	(Pandit et al., 2023)
Intravitreal injection	Liposome	Sunitinib	Posterior segment	According to a fundus fluorescein angiography study, liposomes revealed an inhibitory effect on neovascularization in a mouse model while the intravitreal injection of sunitinib solubilized with cyclodextrin was inefficient.	(Tavakoli et al., 2022)

Intravitreal injection	Microparticles	Sunitinib	Posterior segment	MPs suppressed choroidal neovascularization in mice for six months in rabbits.	(Tsujinaka et al., 2020)
Intrascleral	Nanosuspension-loaded dissolving microneedle	Triamcinolone acetonide	Posterior segment	*Ex vivo* transscleral deposition studies with porcine sclera showed that deposited into the sclera formulation was 4.5-fold higher than drug-loaded microneedle.	(Wu et al., 2022)
Intracorneal	Dissolving microneedles	Model drug	Anterior segment	Microneedles were applied to mice with keratitis where they were observed to be successfully delivered to the inside of the cornea. Study results showed that the therapeutic efficacy of the microneedles persisted for 7 days.	(K. Lee et al., 2018)
Intracorneal	Hyaluronic acid-based microneedle	DC-101	Posterior segment	*In vivo* studies in mice showed a reduction in neovascularization.	(Than et al., 2018)
Subconjunctival injection	Injectable gel-based dendrimer	Dexamethasone	Anterior segment	*In vivo* study in rats showed favorable clinically relevant outcomes, with reduced central corneal thickness and improved corneal clarity compared to controls treated with the free drug and placebo gel.	(Soiberman et al., 2017)
Subconjunctival injection	Dendrimer	Dexamethasone	Anterior segment	In an *in vivo* study using a rabbit model, the formulation was reported to suppress lacrimal gland inflammation.	(Lin et al., 2018)
Subconjunctival injection	Chitosan coated nanoparticle	Bevacizumab	Posterior segment	A pharmacokinetic study in rats, along with confocal microscopy, showed a higher concentration of the drug and better penetration of the formulation compared to the drug solution. In a retinopathy model, it demonstrated a greater reduction in VEGF levels compared to both topical and intravitreal administration of the formulation.	(Pandit, Sultana, & Aqil, 2021)
Suprachoroidal injection	Poly (lactic-co-glycolic acid) (PLGA) microparticle	Acriflavine	Posterior segment	Intravitreal injection of microparticles in mice suppressed choroidal neovascularization for at least 9 weeks, while suprachoroidal injection in rats suppressed it for at least 18 weeks.	(Hackett et al., 2020)
Suprachoroidal injection	*In situ* hyaluronic acid-polyethylene glycol (PEG) hydrogel	Bevacizumab	Posterior segment	The release time of the formulation was evaluated through *in vivo* studies in rabbits.	(Jung et al., 2022)
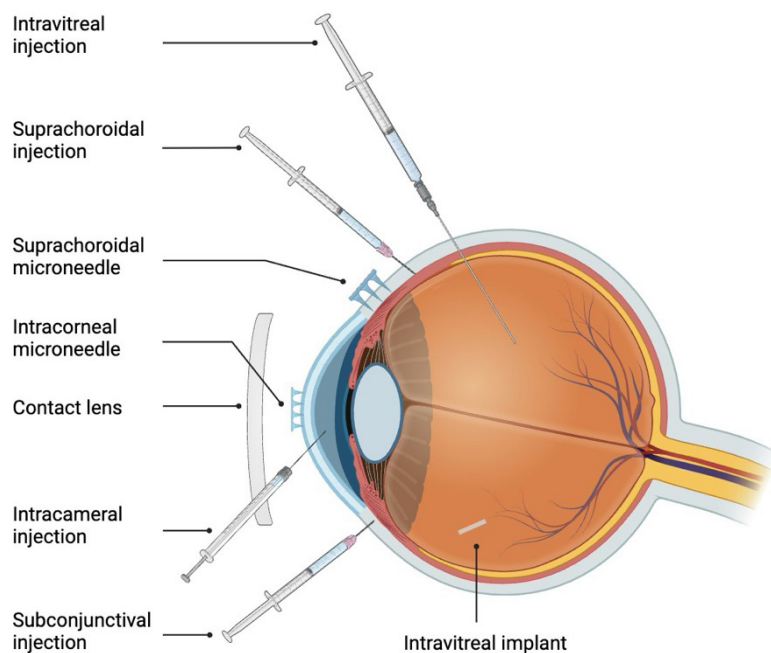
Figure 2. Routes of drug administration to the eye and drug delivery systems. Created with BioRender.com.

Route of Drug Administration to the Eye

Considering the literature studies, drugs can be administered to the eye through systemic, topical, intravitreal, intracorneal, subconjunctival, and suprachoroidal routes. The methods of drug administration approved by the FDA or supported by the literature for ocular delivery are depicted in Figure 2., along with the sites of application. In Table 1, literature studies are presented with dosage forms and the routes of drug administration to the eye. Furthermore, in subtenon, retrobulbar, and peribulbar injection methods, the drug is administered to the tissues around the eye or intramuscularly. These methods are generally preferred to provide regional anesthesia in eye surgeries (Agban, Thakur, Mugisho, & Rupenthal, 2019). In the posterior juxtascleral route, the drug is administered adjacent to the sclera, targeting the posterior segment of the eye. This route enhances application by delivering medication specifically to the posterior segment (Kaiser, Goldberg, Davis, & Group, 2007). The advantages and disadvantages of ocular drug administration methods are presented in Table 2. This section evaluates the routes of drug administration to the eye concerning drug forms, and literature examples are provided.

Table 2. Advantages and disadvantages of ocular drug delivery method.

Administration Route	Advantages	Disadvantages
Systemic	Provides widespread distribution; effective on the entire body. (Especially in cases where the condition, such as a viral infection, spreads systemically.)	May affect non-target organs; low drug concentration in the eye.
Topical	Easy to apply; localized effects; widely used.	Limited absorption due to tear drainage and corneal barrier.
Intravitreal	Direct delivery into the eye; effective for posterior segment diseases.	Requires an injection; risk of infection.
Intracorneal	Direct effect on corneal diseases.	Invasive method; may cause discomfort during application.
Subconjunctival	Direct drug delivery to tissues around the eye; broad distribution.	May require local anesthesia; irritation can occur after application.
Suprachoroidal	Targeted drug delivery for posterior segment diseases.	Difficult to apply; invasive with a risk of infection.
Subtenon/ Retrobulbar	Administered around the eye, often used for local anesthesia during surgery.	Risk of anesthesia complications; discomfort and infection risk in intramuscular applications.
Posterior Juxtascleral	Allows direct drug delivery to the posterior segment; specific targeting.	Only used for posterior segment treatments; the technique can be difficult and invasive.

Systemic Application

When drugs are administered systemically, they distribute throughout the body via the bloodstream. Consequently, systemic drug administration often requires high doses to achieve therapeutic effects in the target area. However, this approach carries a high risk of side effects and toxicity due to the need for elevated drug concentrations throughout the body. Moreover, the eye's lower vascularity compared to other organs poses a challenge, and the blood-retinal barrier (BRB) restricts the transfer of drugs to the retina. Only a small fraction of the drug administered systemically permeates through the inner BRB and reaches the vitreous, where it exerts its effects (29). Visudyne® (Verteporfin), indicated for neovascularization due to age-related macular degeneration (AMD), represents the first clinically validated liposomal photosensitizer system (Thrimawithana, Young, Bunt, Green, & Alany, 2011). It is administered via intravenous infusion over 10 minutes. Approximately 15 minutes after drug application, verteporfin is activated by a non-thermal red laser (50 J/cm2, 83 sec) aimed at the relevant area in the posterior segment of the eye. If necessary, treatment can be repeated every 3 months. Verteporfin has hydrophobic properties, leading to its tendency to aggregate in hydrophilic environments. Therefore, it is loaded into the lipophilic double-layered membrane of liposomes (Ghosh, Carter, & Lovell, 2019). Cymevene®; indicated for cytomegalovirus retinitis (CMVR), is administered via intravenous infusion over at least one hour, 1-3 times daily for 2-3 weeks. High doses of antiviral agents are required to achieve therapeutic levels in the posterior segment through intravenous infusion. Consequently, severe systemic side effects such as neutropenia, anemia, and thrombocytopenia may occur (Hughes, Olejnik, Chang-Lin, & Wilson, 2005). Additionally, long-term treatment may increase the risk of bone marrow toxicity and the development of viral drug resistance (Gilbert & Boivin, 2005).

Local Application

Topical Application

Applying medication to the eye's surface in the form of eye drops is the most common and traditional method. While eye drops are widely used for ocular treatment, they have limitations such as low bioavailability and short retention time on the ocular surface due to factors like tearing and reflexive blinking. Typically, liquid medications applied as eye drops are washed away from the eye's surface within about 5 minutes after application. Consequently, less than 3% of the administered dose manages to penetrate through the eye's surface and reach the intraocular

tissues. (Kearns & Williams, 2009). Although topical application is effective for treating diseases in the anterior segment of the eye, it poses challenges in reaching the posterior segment with traditional eye drops.

In cases where a disease primarily affects the anterior segment of the eye, enhancing the effectiveness of topically applied drugs can be crucial. Here are some strategies to achieve this:

1. The time the formulation remains on the eye surface can be increased. For this purpose, formulations can be designed to increase viscosity (e.g. gel, ointment) (El-Sayed et al., 2017; Fang et al., 2021; Gupta et al., 2007; Shi et al., 2019; Srividya, Cardoza, & Amin, 2001) or increase mucoadhesive properties (Swain et al., 2023; Verma et al., 2019; Zeng et al., 2016).

2. Strategies to increase penetration can be developed by adding penetration enhancing substances to the formulation (Afouna et al., 2010; Afouna, Khedr, & Al-Marzoqi, 2009; Asim et al., 2021; El-Gendy et al., 2020) or by choosing high elasticity nanocarriers.

When commercial drugs are evaluated, eye drops in the form of solution, suspension, or emulsion are the usual preparations. Besides, dosage forms in the form of ointment or gel and applied topically are also available in the market. Through drug forms that can be applied topically to the eye, such as drug-loaded contact lenses, film, insert, or in situ gel, retention time on the eye's surface can be extended, and as a result, its transfer rate can be increased (Gade, Nirmal, Garg, & Venuganti, 2020; R. C. Li et al., 2020; Maulvi et al., 2017; Pollard et al., 2023; Sarmout, Xiao, Hu, Rakhmetova, & Koole, 2023).

In recently study, it was reported that spanlastic containing levofloxacin increased the penetration of the drug through the rabbit cornea by approximately 1.5 times compared to the drug solution (Agha, Girgis, El-Sokkary, & Soliman, 2023).

In a different recent study, terpesomes containing fenticonazole nitrate were developed as an ocular carrier system. In formulations containing a single terpene species, fenchone, eugenol, or limonene were used as terpenes. As a result of the *in vivo* study, it was reported that terpesomes loaded with fenticonazole nitrate optimized for drug suspension remained on the eye surface significantly longer than the drug suspension (Albash, Al-Mahallawi, Hassan, & Alaa-Eldin, 2021).

Subconjunctival Route

In this method, the drug solution is administered under the conjunctiva by implant or liquid injection. Since the application area is close to the surface, a smaller needle is used compared to intravitreal injection, and applying a form of drug, such as an implant, is much easier. In general, there is no damage to the tissues, and it is a less invasive and painless method (Soiberman et al., 2017). Administration via the subconjunctival route eliminates the conjunctival epithelial barrier, which is rate-limiting for the permeation of water-soluble drugs. There are studies on hydrogel, in situ hydrogel, solution or implant placement under the conjunctiva (Lin et al., 2018; Misra et al., 2009; Pandit et al., 2021; Voss et al., 2015).

Rong et al. developed a hydrogel system containing insulin-loaded chitosan nanoparticles and applied it to rats with DR by subconjunctival injection (Rong et al., 2019). After subconjunctival injection, it was observed that structural damage in the retina, retinal cell apoptosis, and VEGF protein expression decreased significantly. There was no apparent damage to retinal function, structure, or neurons after injection. As a result, they reported that subconjunctival injection is safe.

Intravitreal Route

The intravitreal route is the administration of the drugs directly into the vitreous. This method provides the highest amount of drug reaching the vitreous with minimal systemic absorption and has been used in clinical practice for a long time. However, since it is an invasive method, it may cause some ocular complications. Inserting a needle through the sclera or making an incision here may cause bacterial inflammation. In

these patients, cataract formation, increased intraocular pressure and glaucoma, choroidal hemorrhage, endophthalmitis, vitreous hemorrhage, retinal breaks, and retinal detachment (separation of the retinal nerve layer from the underlying pigment epithelial layer) may develop over time (Thrimawithana et al., 2011). When the literature is examined, studies are on developing intravitreal implants that are biodegradable and have an extended release period (Bendicho-Lavilla et al., 2023; Guerra et al., 2023). Intravitreal injections on the market are in solution form and dose intervals are short. Examples of these are presented in the diseases of the eye section. To extend the release time of a formulation administered by intravitreal injection, in situ gels can be used or the drug can be loaded into a nanocarrier (Famili, Kahook, & Park, 2014; S. Lee et al., 2023; López-Cano et al., 2021).

Tsujinaka et al. self-aggregating microparticles containing the VEGF receptor inhibitor sunitinib have been developed (Tsujinaka et al., 2020). *In vivo* experiment results indicated that the effect persists for 6 months after a single dose of microparticles injection containing sunitinib. Factors influential in the sustained release were the sustained release of sunitinib from microparticles and the formation of a solid depot by microparticles containing sunitinib.

Intracorneal Route

Drugs can be applied into the cornea via microneedles. Than et al. developed a tape carrying microneedles containing a series of drugs, which is applied to the cornea by the patient (Than et al., 2018). In the study, a controlled-release hyaluronic acid-based microneedle containing DC101, an anti-angiogenic monoclonal antibody, was designed. The *in vivo* study results reported approximately 90% reduction in neovascular area in eyes treated with the microneedle they developed. An eye patch applied over the cornea is an easy and non-invasive method to increase patient compliance. Such intracorneal drug delivery strategies promise the ability to easily treat many eye diseases at home.

Suprachoroidal Route

Suprachoroidal space (SCS) is the space between the sclera and choroid surrounding the posterior segment of the eye. Drug delivery to the SCS is a new and exciting way to deliver medication to the posterior segment. It does not involve risks related to penetration into the eye and can accommodate up to 1 mL of fluid. While BRB is not omitted in this method, it may be the preferred method for administration of drugs targeting the RPE. Drug delivery from SCS to the vitreous has been shown to decrease as drug lipophilicity and molecular weight increase. SCS can be injected with small-sized microneedles, an implant can be applied or a catheter can be placed (Bhattacharyya et al., 2022; Hackett et al., 2020; Jung et al., 2022; Patel et al., 2012; Sher, Goldberg, Bubis, Barak, & Rotenstreich, 2021). In 2004, microcannulated sclerotomy for SCS was approved by the FDA (iScience catheter, Ellex Medical, Adelaide, Australia) (FDA, 2004). Clinical trials testing the safety and effectiveness of microneedle injections into the SCS are ongoing. Studies to date reported the safety and effectiveness of this procedure and that it can be performed under local anesthesia (Chiang, Jung, & Prausnitz, 2018). Ongoing clinical trials testing the safety and effectiveness of microneedle injections into the SCS have shown that this procedure is safe and efficient and can be performed under local anesthesia.

Jung et al. developed a hyaluronic acid cross-linked with poly(ethylene glycol) diacrylate hydrogel containing bevacizumab (Bev-HA) and applied it to SCS in rabbit eyes with microneedle (Jung et al., 2022). They reported that Bev solution cleared from SCS within 5 days, even if formulated with high viscosity. To extend the release time, they synthesized in situ Bev-HA hydrogel. *In vivo* studies in rabbits reported Bev release from the Bev-HA to be >6 months. The Bev-HA hydrogel was well tolerated as assessed by clinical, histological analysis, fundus imaging, intraocular pressure measurement, and examination.

CONCLUSION

Drug delivery to the eye can be administrated via topical, periocular, intravitreal, and other intraocular routes, depending on the disease area. Although the intravitreal route is the most effective method for diseases affecting the posterior segment, it has many side effects and being invasive is a great difficulty. Studies are being carried out to extend the release time of the formulation applied intravitreally and to reduce the side effects caused by drug administration into the vitreous. Nanosystems are promising in this regard. Drug administration via the subconjunctival and suprachoroidal route can be considered a less invasive and safer method. Effective and safe drug carrier systems can be developed by applying a controlled release system with an extended dose range via subconjunctival route, suprachoroidal route, and intracorneal route.

Considering the topical method, it is a method that is easy to apply because the patient can apply it herself without the need for a healthcare institution and has a low probability of side effects since it is not an invasive method. It is aimed at developing topically applied drug carrier systems that have an extended stay on the eye surface and can pass through the eye surface for anterior and posterior segment diseases. The primary issue in topical application is the low ocular residence time, leading to a significant part of the drug being removed before exerting its effect. In connection with this matter, with penetrating and flexible nano drug carrier systems, the bioavailability of the topically applied drug can be increased by extending its release time and increasing its permeability.

AUTHOR CONTRIBUTION STATEMENT

Determination of the subject (CY, FNT, ST). Literature research and writing (CY). Reviewing the text (FNT, ST). Supervision (ST).

CONFLICT OF INTEREST

The authors declare that there is no conflict of interest.

REFERENCES

Abdelkader, H., Ismail, S., Hussein, A., Wu, Z. M., Al-Kassas, R., & Alany, R. G. (2012). Conjunctival and corneal tolerability assessment of ocular naltrexone niosomes and their ingredients on the hen's egg chorioallantoic membrane and excised bovine cornea models. *International Journal of Pharmaceutics, 432*(1-2), 1-10. doi:https://doi.org/10.1016/j.ijpharm.2012.04.063

Abidi, M., Karrer, E., Csaky, K., & Handa, J. T. (2022). A Clinical and Preclinical Assessment of Clinical Trials for Dry Age-Related Macular Degeneration. *Ophthalmology Science, 2*(4), 100213. doi:https://doi.org/10.1016/j.xops.2022.100213

Afouna, M. I., Khedr, A., Abdel-Naim, A. B., & Al-Marzoqi, A. (2010). Influence of Various Concentrations of Terpene-4-ol Enhancer and Carbopol-934 Mucoadhesive upon the Ocular Transport and the Intraocular Pressure Lowering Effects of Dorzolamide Ophthalmic Formulations Using Albino Rabbits. *Journal of pharmaceutical sciences, 99*(1), 119-127. doi:https://doi.org/10.1002/jps.21803

Afouna, M. I., Khedr, A., & Al-Marzoqi, A. (2009). Effects of (-)-Carveol and HPMC on the In Vitro Ocular Transport and the In Vivo Intraocular Pressure Lowering Effects of Dorzolamide Formulations in Normotensive New Zealand Rabbits. *Drug Development Research, 70*(3), 191-198. doi:https://doi.org/10.1002/ddr.20294

Agarwal, R., Iezhitsa, I., Agarwal, P., Abdul Nasir, N. A., Razali, N., Alyautdin, R., & Ismail, N. M. (2016). Liposomes in topical ophthalmic drug delivery: an update. *Drug delivery, 23*(4), 1075-1091.

Agban, Y., Thakur, S. S., Mugisho, O. O., & Rupenthal, I. D. (2019). Depot formulations to sustain periocular drug delivery to the posterior eye segment. *Drug discovery today, 24*(8), 1458-1469.

Agha, O. A., Girgis, G. N., El-Sokkary, M. M., & Soliman, O. A. E.-A. (2023). Spanlastic-laden in situ gel as a promising approach for ocular delivery of Levofloxacin: In-vitro characterization, microbiological assessment, corneal permeability and in-vivo study. *International Journal of Pharmaceutics: X, 6*, 100201. https://doi.org/100210.101016/j.ijpx.102023.100201.

Albash, R., Al-Mahallawi, A. M., Hassan, M., & Alaa-Eldin, A. A. (2021). Development and Optimization of Terpene-Enriched Vesicles (Terpesomes) for Effective Ocular Delivery of Fenticonazole Nitrate: In vitro Characterization and in vivo Assessment. *Int J Nanomedicine, 16*, 609-621. doi:https://doi.org/10.2147/IJN.S274290

Alyami, H., Abdelaziz, K., Dahmash, E. Z., & Iyire, A. (2020). Nonionic surfactant vesicles (niosomes) for ocular drug delivery: Development, evaluation and toxicological profiling. *Journal of Drug Delivery Science and Technology, 60*, 102069. doi:https://doi.org/10.1016/j.jddst.2020.102069

Aminu, N., Bello, I., Umar, N. M., Tanko, N., Aminu, A., & Audu, M. M. (2020). The influence of nanoparticulate drug delivery systems in drug therapy. *Journal of Drug Delivery Science and Technology, 60*. doi:https://doi.org/10.1016/j.jddst.2020.101961.

Anand, T., Anbukkarasi, M., Thomas, P. A., & Geraldine, P. (2021). A comparison between plain eugenol and eugenol-loaded chitosan nanoparticles for prevention of selenite-induced cataractogenesis. *Journal of Drug Delivery Science and Technology, 65*, 102696. doi:https://doi.org/10.1016/j.jddst.2021.102696

Asim, M. H., Ijaz, M., Mahmood, A., Knoll, P., Jalil, A., Arshad, S., & Bernkop-Schnurch, A. (2021). Thiolated cyclodextrins: Mucoadhesive and permeation enhancing excipients for ocular drug delivery. *Int J Pharm, 599*, 120451. doi:https://doi.org/10.1016/j.ijpharm.2021.120451

Bendicho-Lavilla, C., Seoane-Viano, I., Santos-Rosales, V., Diaz-Tome, V., Carracedo-Perez, M., Luzardo-Alvarez, A. M., . . . Otero-Espinar, F. J. (2023). Intravitreal implants manufactured by supercritical foaming for treating retinal diseases. *J Control Release, 362*, 342-355. doi:https://doi.org/10.1016/j.jconrel.2023.08.047

Bhardwaj, P., Tripathi, P., Gupta, R., & Pandey, S. (2020). Niosomes: A review on niosomal research in the last decade. *Journal of Drug Delivery Science and Technology, 56*, 101581. doi:https://doi.org/10.1016/j.jddst.2020.101581

Bhattacharyya, S., Hariprasad, S. M., Albini, T. A., Dutta, S. K., John, D., Padula, W. V., . . . Joseph, G. (2022). Suprachoroidal Injection of Triamcinolone Acetonide Injectable Suspension for the Treatment of Macular Edema Associated With Uveitis in the United States: A Cost-Effectiveness Analysis. *Value Health, 25*(10), 1705-1716. doi:https://doi.org/10.1016/j.jval.2022.07.008

Bhattarai, R. S., Das, A., Alzhrani, R. M., Kang, D., Bhaduri, S. B., & Boddu, S. H. (2017). Comparison of electrospun and solvent cast polylactic acid (PLA)/poly (vinyl alcohol)(PVA) inserts as potential ocular drug delivery vehicles. *Materials Science and Engineering: C, 77*, 895-903. https://doi.org/810.1016/j.msec.2017.1003.1305.

Boateng, J. S., & Popescu, A. M. (2016). Composite bi-layered erodible films for potential ocular drug delivery. *Colloids Surf B Biointerfaces, 145*, 353-361. doi:https://doi.org/10.1016/j.colsurfb.2016.05.014

Cabrera, F. J., Wang, D. C., Reddy, K., Acharya, G., & Shin, C. S. (2019). Challenges and opportunities for drug delivery to the posterior of the eye. *Drug Discov Today, 24*(8), 1679-1684. doi:https://doi.org/10.1016/j.drudis.2019.05.035

Chiang, B., Jung, J. H., & Prausnitz, M. R. (2018). The suprachoroidal space as a route of administration to the posterior segment of the eye. *Advanced drug delivery reviews, 126*, 58-66.

Chiou, G. C. (2011). Pharmacological treatment of dry age-related macular degeneration (AMD). *Taiwan Journal of Ophthalmology, 1*(1), 2-5.

Choi, A., Nawash, B. S., Du, K., Ong, J., & Chhablani, J. (2023). Barriers to care in neovascular age-related macular degeneration: Current understanding, developments, and future directions. *Surv Ophthalmol*. doi:https://doi.org/10.1016/j.survophthal.2023.09.001

Dartt, D. A. (2004). Dysfunctional neural regulation of lacrimal gland secretion and its role in the pathogenesis of dry eye syndromes. *The ocular surface, 2*(2), 76-91. doi:https://doi.org/10.1016/s1542-0124(12)70146-5

Datta, D., Roy, G., Garg, P., & Venuganti, V. V. K. (2022). Ocular delivery of cyclosporine A using dissolvable microneedle contact lens. *Journal of Drug Delivery Science and Technology, 70*, 103211.

Durak, S., Esmaeili Rad, M., Alp Yetisgin, A., Eda Sutova, H., Kutlu, O., Cetinel, S., & Zarrabi, A. (2020). Niosomal Drug Delivery Systems for Ocular Disease-Recent Advances and Future Prospects. *Nanomaterials (Basel), 10*(6), 1191. doi:https://doi.org/10.3390/nano10061191

Duvvuri, S., Janoria, K. G., Pal, D., & Mitra, A. K. (2007). Controlled delivery of ganciclovir to the retina with drug-loaded Poly (d, L-lactide-co-glycolide)(PLGA) microspheres dispersed in PLGA-PEG-PLGA Gel: a novel intravitreal delivery system for the treatment of cytomegalovirus retinitis. *Journal of Ocular Pharmacology and Therapeutics, 23*(3), 264-274.

Eid, A., Bakri, S., Kijpittayarit, S., & Razonable, R. (2008). Clinical features and outcomes of cytomegalovirus retinitis after transplantation. *Transplant Infectious Disease, 10*(1), 13-18. doi:https://doi.org/10.1111/j.1399-3062.2007.00241.x

El-Gendy, M. A., Mansour, M., El-Assal, M. I. A., & Ishakb, R. A. H. (2020). Delineating penetration enhancer-enriched liquid crystalline nanostructures as novel platforms for improved ophthalmic delivery. *International Journal of Pharmaceutics, 582*, 119313. doi:https://doi.org/10.1016/j.ijpharm.2020.119313

El-Sayed, M. M., Hussein, A. K., Sarhan, H. A., & Mansour, H. F. (2017). Flurbiprofen-loaded niosomes-in-gel system improves the ocular bioavailability of flurbiprofen in the aqueous humor. *Drug development and industrial pharmacy, 43*(6), 902-910. doi:https://doi.org/10.1080/03639045.2016.1272120

Faber, D. W., Wiley, C. A., Lynn, G. B., Gross, J. G., & Freeman, W. R. (1992). Role of HIV and CMV in the pathogenesis of retinitis and retinal vasculopathy in AIDS patients. *Invest Ophthalmol Vis Sci, 33*(8), 2345-2353. Retrieved from https://www.ncbi.nlm.nih.gov/pubmed/1321796

Famili, A., Kahook, M. Y., & Park, D. (2014). A combined micelle and poly (serinol hexamethylene urea)-co-poly (N-isopropylacrylamide) reverse thermal gel as an injectable ocular drug delivery system. *Macromolecular Bioscience, 14*(12), 1719-1729. doi:https://doi.org/10.1002/mabi.201400250

Fan, X., Torres-Luna, C., Azadi, M., Domszy, R., Hu, N., Yang, A., & David, A. E. (2020). Evaluation of commercial soft contact lenses for ocular drug delivery: A review. *Acta biomaterialia, 115*, 60-74.

Fang, G. H., Wang, Q. X., Yang, X. W., Qian, Y., Zhang, G. W., Zhu, Q., & Tang, B. (2021). Vesicular phospholipid gels as topical ocular delivery system for treatment of anterior uveitis. *Colloids and Surfaces a-Physicochemical and Engineering Aspects, 627*, 127187. doi:https://doi.org/10.1016/j.colsurfa.2021.127187

FDA, U. S. F. A. D. A. (2004). iScience Surgical Ophthalmic Microcannula.

Feng, L., Wang, C., Zhang, C., Zhang, W., & Song, W. (2023). Role of epigenetic regulation in glaucoma. *Biomedicine & Pharmacotherapy, 168*, 115633.

Gade, S. K., Nirmal, J., Garg, P., & Venuganti, V. V. K. (2020). Corneal delivery of moxifloxacin and dexamethasone combination using drug-eluting mucoadhesive contact lens to treat ocular infections. *Int J Pharm, 591*, 120023. doi:https://doi.org/10.1016/j.ijpharm.2020.120023

Georgiou, M., & Prokopiou, E. (2023). Diabetic retinopathy and the role of Omega-3 PUFAs: A narrative review. *Experimental Eye Research*, 109494. doi:https://doi.org/10.1016/j.exer.2023.109494

Ghezzi, M., Ferraboschi, I., Fantini, A., Pescina, S., Padula, C., Santi, P., . . . Nicoli, S. (2023). Hyaluronic acid–PVA films for the simultaneous delivery of dexamethasone and levofloxacin to ocular tissues. *International Journal of Pharmaceutics, 638*, 122911. doi:https://doi.org/10.1016/j.ijpharm.2023.122911

Ghosh, S., Carter, K. A., & Lovell, J. F. (2019). Liposomal formulations of photosensitizers. *Biomaterials, 218*, 119341. doi:https://doi.org/10.1016/j.biomaterials.2019.119341

Gilbert, C., & Boivin, G. (2005). Human cytomegalovirus resistance to antiviral drugs. *Antimicrobial Agents and Chemotherapy, 49*(3), 873-883. doi:https://doi.org/10.1128/AAC.49.3.873-883.2005

Glover, K., Mishra, D., Gade, S., Lalitkumar, K., Wu, Y., Paredes, A. J., . . . Singh, T. R. R. (2023). Microneedles for advanced ocular drug delivery. *Advanced drug delivery reviews*, 115082.

Grimes, K. R., Aloney, A., Skondra, D., & Chhablani, J. (2023). Effects of systemic drugs on the development and progression of age-related macular degeneration. *Survey of Ophthalmology*. doi:https://doi.org/10.1016/j.survophthal.2023.01.007

Guerra, M. C. A., Neto, J. T., Gomes, M. G., Dourado, L. F. N., Orefice, R. L., Heneine, L. G. D., . . . Fialho, S. L. (2023). Nanofiber-coated implants: Development and safety after intravitreal application in rabbits. *Int J Pharm, 636*, 122809. doi:https://doi.org/10.1016/j.ijpharm.2023.122809

Gupta, H., Jain, S., Mathur, R., Mishra, P., Mishra, A. K., & Velpandian, T. (2007). Sustained ocular drug delivery from a temperature and pH triggered novel in situ gel system. *Drug Deliv, 14*(8), 507-515. doi:https://doi.org/10.1080/10717540701606426

Hackett, S. F., Fu, J., Kim, Y. C., Tsujinaka, H., Shen, J., Lima, E. S. R., . . . Campochiaro, P. A. (2020). Sustained delivery of acriflavine from the suprachoroidal space provides long term suppression of choroidal neovascularization. *Biomaterials, 243*, 119935. doi:https://doi.org/10.1016/j.biomaterials.2020.119935

Hughes, P. M., Olejnik, O., Chang-Lin, J. E., & Wilson, C. G. (2005). Topical and systemic drug delivery to the posterior segments. *Adv Drug Deliv Rev, 57*(14), 2010-2032. doi:https://doi.org/10.1016/j.addr.2005.09.004

Im, J. H. B., Jin, Y. P., Chow, R., & Yan, P. (2022). Prevalence of diabetic macular edema based on optical coherence tomography in people with diabetes: A systematic review and meta-analysis. *Surv Ophthalmol, 67*(4), 1244-1251. doi:https://doi.org/10.1016/j.survophthal.2022.01.009

Jadhav, C., & Yadav, K. S. (2022). Formulation and evaluation of polymer-coated bimatoprost-chitosan matrix ocular inserts for sustained lowering of IOP in rabbits. *Journal of Drug Delivery Science and Technology, 77*, 103885. doi:https://doi.org/10.1016/j.jddst.2022.103885

Janagam, D. R., Wu, L., & Lowe, T. L. (2017). Nanoparticles for drug delivery to the anterior segment of the eye. *Adv Drug Deliv Rev, 122*, 31-64. doi:https://doi.org/10.1016/j.addr.2017.04.001

Janga, K. Y., Tatke, A., Dudhipala, N., Balguri, S. P., Ibrahim, M. M., Maria, D. N., . . . Majumdar, S. (2019). Gellan Gum Based Sol-to-Gel Transforming System of Natamycin Transfersomes Improves Topical Ocular Delivery. *J Pharmacol Exp Ther, 370*(3), 814-822. doi:https://doi.org/10.1124/jpet.119.256446

Jung, J. H., Kim, S. S., Chung, H., Hejri, A., & Prausnitz, M. R. (2022). Six-month sustained delivery of anti-VEGF from in-situ forming hydrogel in the suprachoroidal space. *J Control Release, 352*, 472-484. doi:https://doi.org/10.1016/j.jconrel.2022.10.036

Kaiser, P. K., Goldberg, M. F., Davis, A. A., & Group, A. A. C. S. (2007). Posterior juxtascleral depot administration of anecortave acetate. *Survey of Ophthalmology, 52*(1), S62-S69.

Kakkar, S., & Kaur, I. P. (2011). Spanlastics--a novel nanovesicular carrier system for ocular delivery. *Int J Pharm, 413*(1-2), 202-210. doi:https://doi.org/10.1016/j.ijpharm.2011.04.027

Kazi, K. M., Mandal, A. S., Biswas, N., Guha, A., Chatterjee, S., Behera, M., & Kuotsu, K. (2010). Niosome: A future of targeted drug delivery systems. *J Adv Pharm Technol Res, 1*(4), 374-380. doi:https://doi.org/10.4103/0110-5558.76435

Kearns, V. R., & Williams, R. L. (2009). Drug delivery systems for the eye. *Expert Rev Med Devices, 6*(3), 277-290. doi:https://doi.org/10.1586/erd.09.4

Kim, T. Y., Lee, G.-H., Mun, J., Cheong, S., Choi, I., Kim, H., & Hahn, S. K. (2023). Smart Contact Lens Systems for Ocular Drug Delivery and Therapy. *Advanced drug delivery reviews*, 114817. https://doi.org/114810.111016/j.addr.112023.114817.

Kim, Y. C., Grossniklaus, H. E., Edelhauser, H. F., & Prausnitz, M. R. (2014). Intrastromal delivery of bevacizumab using microneedles to treat corneal neovascularization. *Investigative ophthalmology & visual science, 55*(11), 7376-7386.

Landolfo, S., Gariglio, M., Gribaudo, G., & Lembo, D. (2003). The human cytomegalovirus. *Pharmacol Ther, 98*(3), 269-297. doi:https://doi.org/10.1016/s0163-7258(03)00034-2

Lee, K., Song, H. B., Cho, W., Kim, J. H., Kim, J. H., & Ryu, W. (2018). Intracorneal injection of a detachable hybrid microneedle for sustained drug delivery. *Acta Biomater, 80*, 48-57. doi:https://doi.org/10.1016/j.actbio.2018.09.039

Lee, S., Hong, H. K., Song, J. S., Jeong, S. I., Chung, J. Y., Woo, S. J., & Park, K. D. (2023). Intravitreal injectable hydrogel rods with long-acting bevacizumab delivery to the retina. *Acta Biomater, 171*, 273-288. doi:https://doi.org/10.1016/j.actbio.2023.09.025

Li, B., Wang, J., Gui, Q., & Yang, H. (2020). Drug-loaded chitosan film prepared via facile solution casting and air-drying of plain water-based chitosan solution for ocular drug delivery. *Bioactive materials, 5*(3), 577-583. doi:https://doi.org/10.1016/j.bioactmat.2020.04.013

Li, R. C., Guan, X. P., Lin, X. L., Guan, P. Y., Zhang, X., Rao, Z. Q., . . . Zhao, J. H. (2020). Poly(2-hydroxyethyl methacrylate)/β-cyclodextrin-hyaluronan contact lens with tear protein adsorption resistance and sustained drug delivery for ophthalmic diseases. *Acta biomaterialia, 110*, 105-118. doi:https://doi.org/10.1016/j.actbio.2020.04.002

Lin, H., Liu, Y., Kambhampati, S. P., Hsu, C. C., Kannan, R. M., & Yiu, S. C. (2018). Subconjunctival dendrimer-drug therapy for the treatment of dry eye in a rabbit model of induced autoimmune dacryoadenitis. *Ocul Surf, 16*(4), 415-423. doi:https://doi.org/10.1016/j.jtos.2018.05.004

López-Cano, J. J., Sigen, A., Andrés-Guerrero, V., Tai, H., Bravo-Osuna, I., Molina-Martínez, I. T., . . . Herrero-Vanrell, R. (2021). Thermo-Responsive PLGA-PEG-PLGA Hydrogels as Novel Injectable Platforms for Neuroprotective Combined Therapies in the Treatment of Retinal Degenerative Diseases. *Pharmaceutics, 13*(2), 234. https://doi.org/210.3390/pharmaceutics13020234.

Maulvi, F. A., Choksi, H. H., Desai, A. R., Patel, A. S., Ranch, K. M., Vyas, B. A., & Shah, D. O. (2017). pH triggered controlled drug delivery from contact lenses: Addressing the challenges of drug leaching during sterilization and storage. *Colloids Surf B Biointerfaces, 157*, 72-82. doi:https://doi.org/10.1016/j.colsurfb.2017.05.064

Misra, G. P., Singh, R. S., Aleman, T. S., Jacobson, S. G., Gardner, T. W., & Lowe, T. L. (2009). Subconjunctivally implantable hydrogels with degradable and thermoresponsive properties for sustained release of insulin to the retina. *Biomaterials, 30*(33), 6541-6547. doi:https://doi.org/10.1016/j.biomaterials.2009.08.025

Osaadon, P., Fagan, X. J., Lifshitz, T., & Levy, J. (2014). A review of anti-VEGF agents for proliferative diabetic retinopathy. *Eye (Lond), 28*(5), 510-520. doi:https://doi.org/10.1038/eye.2014.13

Pandit, J., Chaudhary, N., Emad, N. A., Ahmad, S., Solanki, P., Aqil, M., . . . Solanki, P. (2023). Fenofibrate loaded nanofibers based thermo-responsive gel for ocular delivery: Formulation development, characterization and in vitro toxicity study. *Journal of Drug Delivery Science and Technology*, 104935. https://doi.org/104910.101016/j.jddst.102023.104935.

Pandit, J., Sultana, Y., & Aqil, M. (2021). Chitosan coated nanoparticles for efficient delivery of bevacizumab in the posterior ocular tissues via subconjunctival administration. *Carbohydrate Polymers, 267*, 118217. doi:https://doi.org/10.1016/j.carbpol.2021.118217

Patel, S. R., Berezovsky, D. E., McCarey, B. E., Zarnitsyn, V., Edelhauser, H. F., & Prausnitz, M. R. (2012). Targeted Administration into the Suprachoroidal Space Using a Microneedle for Drug Delivery to the Posterior Segment of the Eye. *Investigative ophthalmology & visual science, 53*(8), 4433-4441. doi:https://doi.org/10.1167/iovs.12-9872

Pennington, K. L., & DeAngelis, M. M. (2016). Epidemiology of age-related macular degeneration (AMD): associations with cardiovascular disease phenotypes and lipid factors. *Eye and vision, 3*(1), 1-20. doi:https://doi.org/10.1186/s40662-016-0063-5

Polat, H. K., Bozdag Pehlivan, S., Ozkul, C., Calamak, S., Ozturk, N., Aytekin, E., . . . Calis, S. (2020). Development of besifloxacin HCl loaded nanofibrous ocular inserts for the treatment of bacterial keratitis: In vitro, ex vivo and in vivo evaluation. *Int J Pharm, 585*, 119552. doi:https://doi.org/10.1016/j.ijpharm.2020.119552

Pollard, T. D., Seoane-Viaño, I., Ong, J. J., Januskaite, P., Awwad, S., Orlu, M., . . . Goyanes, A. (2023). Inkjet drug printing onto contact lenses: deposition optimisation and non-destructive dose verification. *International Journal of Pharmaceutics: X, 5*, 100150. https://doi.org/100110.101016/j.ijpx.102022.100150.

Port, A. D., Orlin, A., Kiss, S., Patel, S., D'Amico, D. J., & Gupta, M. P. (2017). Cytomegalovirus Retinitis: A Review. *J Ocul Pharmacol Ther, 33*(4), 224-234. doi:https://doi.org/10.1089/jop.2016.0140

Rafael, D., Andrade, F., Martinez-Trucharte, F., Basas, J., Seras-Franzoso, J., Palau, M., . . . Schwartz, S., Jr. (2019). Sterilization Procedure for Temperature-Sensitive Hydrogels Loaded with Silver Nanoparticles for Clinical Applications. *Nanomaterials (Basel), 9*(3), 380. doi:https://doi.org/10.3390/nano9030380

Rajera, R., Nagpal, K., Singh, S. K., & Mishra, D. N. (2011). Niosomes: a controlled and novel drug delivery system. *Biol Pharm Bull, 34*(7), 945-953. doi:https://doi.org/10.1248/bpb.34.945

Reyes-Batlle, M., Rodriguez-Talavera, I., Sifaoui, I., Rodriguez-Exposito, R. L., Rocha-Cabrera, P., Pinero, J. E., & Lorenzo-Morales, J. (2021). In vitro amoebicidal effects of arabinogalactan-based ophthalmic solution. *Int J Parasitol Drugs Drug Resist, 16*, 9-16. doi:https://doi.org/10.1016/j.ijpddr.2021.04.005

Rong, X., Ji, Y., Zhu, X., Yang, J., Qian, D., Mo, X., & Lu, Y. (2019). Neuroprotective effect of insulin-loaded chitosan nanoparticles/PLGA-PEG-PLGA hydrogel on diabetic retinopathy in rats. *Int. J. Nanomedicine, 14*, 45-55. doi:https://doi.org/10.2147/IJN.S184574

Ross, A. E., Bengani, L. C., Tulsan, R., Maidana, D. E., Salvador-Culla, B., Kobashi, H., . . . Ciolino, J. B. (2019). Topical sustained drug delivery to the retina with a drug-eluting contact lens. *Biomaterials, 217*, 119285. doi:https://doi.org/10.1016/j.biomaterials.2019.119285

Roy, G., Galigama, R. D., Thorat, V. S., Garg, P., & Venuganti, V. V. K. (2020). Microneedle ocular patch: Fabrication, characterization, and ex-vivo evaluation using pilocarpine as model drug. *Drug development and industrial pharmacy, 46*(7), 1114-1122.

Sankhyan, A., & Pawar, P. (2012). Recent Trends in Niosome as Vesicular DrugDelivery System. *Journal of Applied Pharmaceutical Science*(Issue), 20-32. https://doi.org/10.7324/JAPS.2012.2625.

Sarmout, M., Xiao, Y. T., Hu, X., Rakhmetova, A., & Koole, L. H. (2023). A novel approach to achieve semi-sustained drug delivery to the eye through asymmetric loading of soft contact lenses. *Heliyon, 9*(6). doi:https://doi.org/10.1016/j.heliyon.2023.e16916

Seddon, J. M., Willett, W. C., Speizer, F. E., & Hankinson, S. E. (1996). A prospective study of cigarette smoking and age-related macular degeneration in women. *Jama, 276*(14), 1141-1146. https://doi.org/doi:1110.1001/jama.1996.03540140029022 Retrieved from https://www.ncbi.nlm.nih.gov/pubmed/8827966

Sher, I., Goldberg, Z., Bubis, E., Barak, Y., & Rotenstreich, Y. (2021). Suprachoroidal delivery of bevacizumab in rabbit in vivo eyes: Rapid distribution throughout the posterior segment. *Eur J Pharm Biopharm, 169*, 200-210. doi:https://doi.org/10.1016/j.ejpb.2021.10.003

Shi, H., Wang, Y., Bao, Z. S., Lin, D. Q., Liu, H., Yu, A. L., . . . Xu, X. (2019). Thermosensitive glycol chitosan-based hydrogel as a topical ocular drug delivery system for enhanced ocular bioavailability. *International Journal of Pharmaceutics, 570*, 118688. doi:https://doi.org/10.1016/j.ijpharm.2019.118688

Shoari, A., Kanavi, M. R., & Rasaee, M. J. (2021). Inhibition of matrix metalloproteinase-9 for the treatment of dry eye syndrome; a review study. *Exp Eye Res, 205*, 108523. doi:https://doi.org/10.1016/j.exer.2021.108523

Soiberman, U., Kambhampati, S. P., Wu, T., Mishra, M. K., Oh, Y., Sharma, R., . . . Kannan, R. M. (2017). Subconjunctival injectable dendrimer-dexamethasone gel for the treatment of corneal inflammation. *Biomaterials, 125*, 38-53. doi:https://doi.org/10.1016/j.biomaterials.2017.02.016

Srividya, B., Cardoza, R. M., & Amin, P. D. (2001). Sustained ophthalmic delivery of ofloxacin from a pH triggered in situ gelling system. *J Control Release, 73*(2-3), 205-211. doi:https://doi.org/10.1016/s0168-3659(01)00279-6

Suriyaamporn, P., Pornpitchanarong, C., Pamornpathomkul, B., Patrojanasophon, P., Rojanarata, T., Opanasopit, P., & Ngawhirunpat, T. (2023). Ganciclovir nanosuspension-loaded detachable microneedles patch for enhanced drug delivery to posterior eye segment. *Journal of Drug Delivery Science and Technology, 88*, 104975.

Swain, R., Moharana, A., Habibullah, S., Nandi, S., Bose, A., Mohapatra, S., & Mallick, S. (2023). Ocular delivery of felodipine for the management of intraocular pressure and inflammation: Effect of film plasticizer and in vitro in vivo evaluation. *Int J Pharm, 642*, 123153. doi:https://doi.org/10.1016/j.ijpharm.2023.123153

Tavakoli, S., Puranen, J., Bahrpeyma, S., Lautala, V. E., Karumo, S., Lajunen, T., . . . Urtti, A. (2022). Liposomal sunitinib for ocular drug delivery: A potential treatment for choroidal neovascularization. *Int J Pharm, 620*, 121725. doi:https://doi.org/10.1016/j.ijpharm.2022.121725

Teoh, S. C., Ou, X., & Lim, T. H. (2012). Intravitreal ganciclovir maintenance injection for cytomegalovirus retinitis: efficacy of a low-volume, intermediate-dose regimen. *Ophthalmology, 119*(3), 588-595. doi:https://doi.org/10.1016/j.ophtha.2011.09.004

Thacker, M., Singh, V., Basu, S., & Singh, S. (2023). Biomaterials for dry eye disease treatment: Current overview and future perspectives. *Exp Eye Res, 226*, 109339. doi:https://doi.org/10.1016/j.exer.2022.109339

Than, A., Liu, C., Chang, H., Duong, P. K., Cheung, C. M. G., Xu, C., . . . Chen, P. (2018). Self-implantable double-layered micro-drug-reservoirs for efficient and controlled ocular drug delivery. *Nat Commun, 9*(1), 4433. doi:https://doi.org/10.1038/s41467-018-06981-w

Thrimawithana, T. R., Young, S., Bunt, C. R., Green, C., & Alany, R. G. (2011). Drug delivery to the posterior segment of the eye. *Drug discovery today, 16*(5-6), 270-277. doi:https://doi.org/10.1016/j.drudis.2010.12.004

Tsujinaka, H., Fu, J., Shen, J., Yu, Y., Hafiz, Z., Kays, J., . . . Campochiaro, P. A. (2020). Sustained treatment of retinal vascular diseases with self-aggregating sunitinib microparticles. *Nat Commun, 11*(1), 694. doi:https://doi.org/10.1038/s41467-020-14340-x

Verma, A., Sharma, G., Jain, A., Tiwari, A., Saraf, S., Panda, P. K., . . . Jain, S. K. (2019). Systematic optimization of cationic surface engineered mucoadhesive vesicles employing Design of Experiment (DoE): A preclinical investigation. *Int J Biol Macromol, 133*, 1142-1155. doi:https://doi.org/10.1016/j.ijbiomac.2019.04.118

Vikash, B., Pandey, N. K., Kumar, B., Wadhwa, S., Goutam, U., Alam, A., . . . Gupta, G. (2023). Formulation and evaluation of ocular self-nanoemulsifying drug delivery system of brimonidine tartrate. *Journal of Drug Delivery Science and Technology, 81*, 104226. doi:https://doi.org/10.1016/j.jddst.2023.104226

Villate-Beitia, I., Gallego, I., Martinez-Navarrete, G., Zarate, J., Lopez-Mendez, T., Soto-Sanchez, C., . . . Pedraz, J. L. (2018). Polysorbate 20 non-ionic surfactant enhances retinal gene delivery efficiency of cationic niosomes after intravitreal and subretinal administration. *Int J Pharm, 550*(1-2), 388-397. doi:https://doi.org/10.1016/j.ijpharm.2018.07.035

Voss, K., Falke, K., Bernsdorf, A., Grabow, N., Kastner, C., Sternberg, K., . . . Hovakimyan, M. (2015). Development of a novel injectable drug delivery system for subconjunctival glaucoma treatment. *J Control Release, 214*, 1-11. doi:https://doi.org/10.1016/j.jconrel.2015.06.035

Wang, J., Jiang, A., Joshi, M., & Christoforidis, J. (2013). Drug delivery implants in the treatment of vitreous inflammation. *Mediators of inflammation, 2013*. doi:https://doi.org/10.1155/2013/780634

Wang, W., & Lo, A. C. (2018). Diabetic retinopathy: pathophysiology and treatments. *International Journal of Molecular Sciences, 19*(6), 1816. doi:https://doi.org/10.3390/ijms19061816

Wang, W., & Wang, H. (2023). Understanding the complex genetics and molecular mechanisms underlying glaucoma. *Molecular Aspects of Medicine, 94*, 101220.

Wei, Y., Hu, Y., Shen, X., Zhang, X., Guan, J., & Mao, S. (2020). Design of circular-ring film embedded contact lens for improved compatibility and sustained ocular drug delivery. *Eur J Pharm Biopharm, 157*, 28-37. doi:https://doi.org/10.1016/j.ejpb.2020.09.010

Weng, Y. H., Ma, X. W., Che, J., Li, C., Liu, J., Chen, S. Z., . . . Liang, X. J. (2018). Nanomicelle-Assisted Targeted Ocular Delivery with Enhanced Anti-inflammatory Efficacy In Vivo. *Adv Sci (Weinh), 5*(1), 1700455. doi:https://doi.org/10.1002/advs.201700455

Wu, Y., Vora, L. K., Mishra, D., Adrianto, M. F., Gade, S., Paredes, A. J., . . . Singh, T. R. R. (2022). Nanosuspension-loaded dissolving bilayer microneedles for hydrophobic drug delivery to the posterior segment of the eye. *Biomater Adv, 137*, 212767. doi:https://doi.org/10.1016/j.bioadv.2022.212767

Xu, J., Xue, Y., Hu, G., Lin, T., Gou, J., Yin, T., . . . Tang, X. (2018). A comprehensive review on contact lens for ophthalmic drug delivery. *Journal of controlled release, 281*, 97-118.

Xu, N., Wang, J., Liu, L., & Gong, C. (2023). Injectable hydrogel-based drug delivery systems for enhancing the efficacy of radiation therapy: A review of recent advances. *Chinese Chemical Letters*, 109225.

Yellepeddi, V. K., Sheshala, R., McMillan, H., Gujral, C., Jones, D., & Raghu Raj Singh, T. (2015). Punctal plug: a medical device to treat dry eye syndrome and for sustained drug delivery to the eye. *Drug Discov Today, 20*(7), 884-889. doi:https://doi.org/10.1016/j.drudis.2015.01.013

Yetgin, C., Çoban, Ö., Tuğcu-Demiröz, F. N., Sağır, B., & Takka, S. (2022). Development and Evaluation of Ganciclovir Loaded Niosomes for The Treatment of Cytomegalovirus Retinitis. *FIGON DMD & EUFEPS European Medicines Days, Book of Abstracts*(Netherlands), 45.

Yetgin, C., Tuğcu-Demiröz, F. N., & Takka, S. (2022). *Transfersomes For Topical Ocular Administration: Development And In Vitro Characterization* (Vol. Abstract and Full-Text Papers).

Younes, N. F., Abdel-Halim, S. A., & Elassasy, A. I. (2018). Corneal targeted Sertaconazole nitrate loaded cubosomes: Preparation, statistical optimization, in vitro characterization, ex vivo permeation and in vivo studies. *Int J Pharm, 553*(1-2), 386-397. doi:https://doi.org/10.1016/j.ijpharm.2018.10.057

Zeng, W., Li, Q., Wan, T., Liu, C., Pan, W., Wu, Z., . . . Lin, Y. (2016). Hyaluronic acid-coated niosomes facilitate tacrolimus ocular delivery: Mucoadhesion, precorneal retention, aqueous humor pharmacokinetics, and transcorneal permeability. *Colloids and Surfaces B: Biointerfaces, 141*, 28-35. doi:https://doi.org/10.1016/j.colsurfb.2016.01.014

Nanomaterials Marvels: Transformative Advancements in Biomedicine, Drug Delivery, and Pharmaceutical Analysis

Amaresh PRUSTY[*°], Sasmita Kumari PADHİ[**]

Nanomaterials Marvels: Transformative Advancements in Biomedicine, Drug Delivery, and Pharmaceutical Analysis

SUMMARY

Nanoparticles are solid colloidal particles ranging in size from 10 to 1000 nm having high surface area-to-volume ratio which allows them for efficient interaction with biological systems. Nanoparticles offer many benefits in comparison to larger particles such as increased surface-to-volume ratio and increased magnetic properties. Nanomaterials hold the potential to revolutionize critical domains like Biomedicine, Drug Delivery, and Pharmaceutical Analysis. These particles can be functionalized with specific molecules to target diseased cells or tissues, enhancing the efficacy of drugs while minimizing side effects. For instance, gold nanoparticles conjugated with antibodies can be used for targeted cancer therapy, delivering therapeutic agents directly to tumor cells. Similarly, drugs encapsulated within nanoparticles can be protected from premature degradation and released in a controlled manner at the target site improving their drug solubility, and enhance cellular uptake, leading to better therapeutic effect in treatment strategies. Polymeric nanoparticles, liposomes, and micelles are some examples of commonly used nanocarriers for drug delivery. Nanomaterials are finding increasing applications in pharmaceutical analysis and can be employed as highly sensitive detection probes for drugs, metabolites, and biomarkers. Additionally, nanomaterials can be used for the separation and purification of biomolecules, facilitating accurate and efficient analysis. This review explores different types of nano material's used exploring their new advances and applications in biomedicine, drug delivery, and pharmaceutical analysis. As research continues to overcome current challenges, nanomaterials unique properties hold immense promise for revolutionizing healthcare and improving patient outcomes.

Key Words: Biomedicine, Nanoparticles, Carbon nanotubes, Drug Delivery.

Nanomalzemeler Harikalar Yaratıyor: Biyomedikal, İlaç Taşınması ve Farmasötik Analizde Dönüştürücü Gelişmeler

ÖZ

Nanoparçacıklar, 10 ila 1000 nm boyutlarında, biyolojik sistemlerle etkin etkileşime olanak tanıyan büyük yüzey alanı-hacim oranına sahip olan katı kolloidal parçacıklardır. Nanoparçacıklar, daha büyük partiküllerle karşılaştırıldığında, artan yüzey-hacim oranının artması ve manyetik özelliklerin artması gibi bir çok avantaj sunmaktadır. Nanomalzemeler, Biyomedikal, İlaç Taşınması ve Farmasötik Analiz gibi kritik alanlarda devrim yaratma potansiyeline sahiptir. Bu parçacıklar, hastalıklı hücreleri veya dokuları hedeflemek için belirli moleküllerle işlevselleştirilebilir, böylece ilaçların etkinliği artırılırken yan etkiler en aza indirilebilir. Örneğin, antikorlarla konjuge edilmiş altın nanoparçacıklar, hedefli kanser tedavisi için kullanılabilir ve terapötik ajanları doğrudan tümör hücrelerine iletebilir. Benzer şekilde, nanoparçacıkların içine kapsüllenmiş ilaçlar, erken bozunmaya karşı korunabilir ve hedef bölgeye kontrollü bir şekilde salınabilir, böylece ilaç çözünürlükleri iyileştirilebilir ve hücresel tutulum artırılabilir, bu da tedavi stratejilerinde daha iyi terapötik etkiye yol açabilir. Polimerik nanoparçacıklar, lipozomlar ve miseller, ilaç taşınması için yaygın olarak kullanılan nano taşıyıcıların bazı örnekleridir. Nanomalzemeler, farmasötik analizlerde giderek daha fazla uygulama alanı bulmakta olup ilaçlar, metabolitler ve biyobelirteçler için son derece hassas tespit probları olarak kullanılabilmektedir. Ayrıca nanomalzemeler biyomoleküllerin ayrıştırılması ve saflaştırılmasında da kullanılabilir, bu da doğru ve etkili analizlerin yapılmasını kolaylaştırır. Bu derlemede biyomedikal, ilaç taşınması ve farmasötik analiz alanlarındaki yeni gelişmeleri ve uygulamaları keşfederek farklı tipteki nano malzemelerin kullanımı ele alınmaktadır.

Anahtar Kelimeler: Biyomedikal, Nanopartiküller, Karbon nanotüpler, İlaç Taşınması.

---

[*] ORCID: 0000-0002-2978-8044, Department of Pharmaceutics, Royal College of Pharmacy and Health Sciences, Berhampur. Odisha. India.
[**] ORCID: 0009-0009-7989-1021, College of Nursing. MKCG College. Berhampur. Odisha. India.

[°] Corresponding Author; Dr. Amaresh Prusty
E-mail: amareshprusty@gmail.com

INTRODUCTION

In 21st century where research and innovation are increasing the life span of human beings, the science of nanotechnology has offering unprecedented opportunities in the field of biomedicine, drug delivery, and pharmaceutical analysis.Nanoparticles have garnered significant attention for their potential in enhancing drug delivery (Wilczewska et al., 2012; Din et al., 2017; Etheridge et al., 2013; Fay et al., 2017), where they used for precise release of therapeutic agents in controlled manner reducing both the dosage and frequency. These materials show distinctive chemical, physical, and biological characteristics possessing larger surface-area-to-volume ratio, tenable geometry, and interactive potential with biomolecules which makes them an ideal candidate for targeted drug delivery. This transformative approach aims to minimize side effects, reduce dosages, and enhance therapeutic outcomes. The application of nanomaterials in drug delivery represents a paradigm shift in pharmaceutical sciences. Their ability to interact with biomolecules facilitates efficient uptake across cell membranes, maximizing drug efficacy. Nanomaterials' capacity to regulate the rate of drug release is a crucial feature in the biomedicine, which is the branch of medicine concerned with the practical application of principles from biology and physiology. One of the most critical areas of study for creating new nanomaterials for use in biomedicine is the hunt for better diagnostic agents.

The vast family of nanomaterials, both organic and inorganic, allows for selective design tailored to specific applications. Their distinct properties like interactions with ligands, smaller drug molecules, or antibodies make them invaluable tools for advancing analytical techniques. Despite the numerous advantages, nanoparticles pose challenges such as non-toxicity, bio-distribution, accumulation, and clearance from the human body. Nanoparticles are effective in drug delivery due to increased ligand binding, increased binding efficiency, and thereby achieve great-

er therapeutic efficiency (Hainfeld et al., 2014). Nanomaterials have revolutionized drug delivery by enhancing the pharmacokinetics and therapeutic efficacy of drugs (Egwu et al., 2024). Liposomes, polymeric nanoparticles, and dendrimers are some examples of nanocarriers used to encapsulate drugs and improve their bioavailability. This review gives brief insights the vivid role of nanomaterials, emphasizing their significance into the biomedicine, drug delivery, and pharmaceutical analysis. Exploring of these marvels opens new frontiers, paving the way for groundbreaking advancements with far-reaching implications for healthcare and pharmaceuticals.

Recent advancements in nanomaterials

Nanomaterials encompass a diverse range of materials, including nanoparticles, nanotubes, nanofibers, nanogels, and more. Researchers are developing new nanomaterials with tailored properties to meet specific biomedical needs. For instance, graphene oxide, a two-dimensional nanomaterial, has gained attention for its exceptional mechanical strength, electrical conductivity, and significant role in tissue engineering and drug delivery. Different types of nano materials are discussed below,

1. Carbon nanotubes(CNTs)

These nanoparticles have nanometer diameter and a length of micrometres and they are made up of enrolled cylindrical graphitic sheets (named graphene) wrapped up into a seamless cylinder with a nanometer sized diameter. Due to their nano size they can easily make their way to inside cells, delivering drugs directly to the cytoplasm or nucleus that improve the pharmacological and therapeutic efficacy of the drug. CNTs possess some unique properties in their structure which, makes them suitable for drug delivery for the treatment of various diseases (Rozhin et al., 2022; Bolshakova et al., 2022; Alberto et al., 2005). The electron transport within carbon nanotubes (CNTs) occurs through quantum effects due to their nanoscale dimensions, propagating exclusively along the tube's axis. Owing to their small size in the nanometer scale,

CNTs offer the advantage of delivering smaller drug doses to specific diseased cells, minimizing side effects on healthy cells a significant improvement over conventional drug. These results in enhanced efficiency in targeting disease cells (Harris 2009). The ideal property of CNTs for easy movement in the human body is due to their enhanced solubility when combined with lipids by reducing the risk of blockage of vital body organ pathways. Regarding optical properties, CNTs exhibit robust absorbance in specific spectral windows, such as near-infrared (NIR) light. Functionalizing them with binding entities specific to tumor cells enables the selective destruction of disease cells, particularly in cancer, in drug delivery applications using NIR light. Due to better cell penetration qualities and high drug loading capacities in comparison to dendrimers, polymers, and liposomes, carbon nanotubes have wide spread applications in drug delivery for cancer treatment. These nanotubes have lager inner volume, making them suitable as drug containers and ease of cell uptake (Mishra & Sahu 2020). Still, the particles have some problems in drug delivery due to their lack of solubility, clumping occurrences, and half-life (Gupta & Nayak 2019). CNTs prove advantageous as nanovectors for drug delivery, as evidenced by efficient cell uptake and prominent effects, demonstrating their potential as less harmful drug nanovehicles (Ashwin et al., 2009). Also, encapsulation of drugs in CNTs helps to enhance water dispersibility, better bioavailability, and reduced toxicity resulting, in controlled release of loaded molecules (Zhu et al., 2005). In recent developments, Yinghuai Zhu, & Narayan S Hosmane introduced a novel method for cancer treatment and the technique is called Boron Neutron Capture Therapy. They successfully attached substituted C2B10 carborane cages to single-wall carbon nanotubes (SWCNTs) via nitrene cycloaddition. The resulting water-soluble SWCNTs, functionalized with carborane units and ethoxide moieties, demonstrated concentrated boron atoms in tumor cells compared to blood and other organs. This highlights their potential as effective nano vehicles for boron neutron capture therapy in cancer treatment (Zhu et al., 2017). Their strong optical absorbance in the 700 to 1,100 nm near-infrared window, combined with suitable functionalization chemistry, allows for optical stimulation inside living cells.

2. Nanofibres

Nanofibers encapsulate drug molecules and release them through different mechanisms, such as burst release, sustainable release, or tunable release. Most conventional drug delivery systems are administered through enteral routes, like tablets, capsules, and granules, or parenteral routes, including intravenous, intra-arterial, intramuscular, or subcutaneous. However, the main drawbacks through these routes are first-pass metabolism, discomfort, and pain. So, direct administration of drugs into the buccal cavity offers a solution to these issues. Incorporating active substances into nanofibers facilitates drug delivery in the buccal cavity. Nanofibers, particularly those prepared by electro spinning, are designed to quickly interact with saliva, dissolving or disintegrating in the mouth of patient. This results in the rapid release of drugs into the buccal mucosa for immediate absorption. In controlled-release scenarios, the drug delivery system must dissolve or disintegrate within a defined timeframe. Both oral and transcutaneous controlled-release methods enable pharmaceutical drug administration once or twice a day, enhancing patient compliance and reducing toxic plasma peak concentrations associated with multiple administrations of immediate-release formulations (Sarma et al., 2024; Contreras-Cáceres et al., 2019; Thakur & Sankar, 2023).

3. Nanogels

Nanogels are single or multiple types of nanoparticles surrounded by a cross-linked hydrophilic polymer network. In the biomedical and pharmaceutical fields, nanogels find applications in regeneration of body tissues, wound healing, surgical devices, implantation, and various drug delivery methods such as peroral, rectal, vaginal, ocular, and transdermal

routes. While still in the early stages of development, the utilization of 3D printing has gained attention in nano gel production, but still this technique is considered one of the most convenient methods for nano gel manufacturing, especially as the demand for precise nanogels production increases for personalized medicine, biomedical applications, and specialized drug delivery. Nanogels are use in drug delivery system due to their high drug encapsulation capacity, uniformity, tunable size, ease of preparation, minimal toxicity, stability in the presence of serum, and stimuli responsiveness property. Nanogels utilize active targeting moieties for the delivery of drugs by altering their stability in an environment (temperature, pH, and concentration of glutathione) sensitive manner (Liu et al., 2022; Li et al., 2024; Liwei et al., 2019 ; Murphy et al., 2011; Wu et al., 2016).

The research work published by Wang et al. suggests formulation of nano gel taking chitosan-poly (N-isopropylacrylamide-co-acrylamide) for paclitaxel delivery taking acryl amide at 5.5% w/w and to increase the volume phase transition temperature from 32 °C to 38 °C and thereby decrease the critical aggregation concentration from 5 μg/mL to 1.1 μg/mL that shows effective cellular uptake of payloads through electrostatic absorptive endocytosis which exhibits outstanding anticancer efficacy in HT-29 human colon cancer (Wang et al., 2014). Similarly various other researchers like Oh et al. develop a self-organized 3-diethylaminopropyl bearing glycol chitosan nanogel containing drug doxorubicin and *In vitro* evaluation report shows release was significantly accelerated when placed in the acidic medium of pH 6.8 (Oh et al., 2010). Other notable work like by Chen et al. prepared dual thermo- and pH-sensitive micellar nanogels composed of m PEG-iso propylidene glycerol containing drug paclitaxel for tumor treatment (Chen et al., 2014). So, these research outcomes suggest the potential of nanogels in targeted drug delivery and their role in enhancing therapeutic outcomes.

4. Polymeric nanoparticles

Polymeric nanoparticles (NPs) fall within the size range of 1 to 1000 nm and can be loaded with active compounds entrapped within or surface-adsorbed onto the polymeric core. These particles due to their small size have gained significant attention in recent years for drug carriers in controlling drug release by protecting drugs and other bioactive molecules against the environment, and there by improves the bioavailability and therapeutic index (Soppimath et al., 2001; Cano et al., 2019).

The production of polymeric NPs depends on the type of drug to be loaded and its specific requirements for administration. The methods are based on two main strategies: the dispersion of preformed polymers or the polymerization of monomers (Jawahar et al., 2012). During preparation process, organic solvents must have to be dissolve in polymer, as these solvents may possess toxicity problems. Similarly, removing solvent residues from the final product becomes necessary. Polymeric nanoparticles possess a wide range of different physical properties, such as composition, concentration, size, shape, surface properties, crystallinity, and dispersion state, which are assessed by near-infrared spectroscopy, electrophoresis, electron microscopy, dynamic light scattering (DLS) or photon correlation spectroscopy (PCS), and chromatography (Doktorovova et al., 2014). The comprehensive characterization of polymeric NPs is crucial not only for their applicability but also to address concerns related to nanotoxicology and exposure assessment in workplaces. This is essential for evaluating health and safety hazards and controlling manufacturing processes.

5. Inorganic nanoparticles

The drug delivery system containing inorganic nanoparticles is often achieved through surface functionalization with specific ligands. Gold nanoparticles have also been investigated for their response to local near-infrared (NIR) light as a stimulus for drug release. In a particular study, gold nanoparticles fuctionalized with double-stranded DNA encapsulating

drug molecules exhibited controlled release upon NIR light irradiationreleasing the drugs at the target site (Xiao et al., 2012; Arruebo, 2011). Due to the well-defined surface properties like higher pore volume, higher surface area and narrower pore diameter distribution, allow the entrapment of drugs, proteins and other biogenic molecules with predictable and reproducible release patterns with inorganic nanoparticles (Vallet-Regí 2006; Wang 2009).

6. Nanoparticle Albumin-bound (nab) Technology

Nanoparticles composed of albumin have emerged as an effective strategy in the clinical research for treating various diseases due to its natural ability to transport hydrophobic particles and transcytose molecules bound to it. The nanoparticle albumin-bound (nab) technology employs the protein albumin as a carrier for hydrophobic chemotherapy drugs through noncovalent binding. (Khakpour et al., 2024)

7. Dendrimers

Dendrimers are highly branched, monodisperse polymeric materials macromolecules. The structure of dendrimers has a significant impact on their physical and chemical properties. Dendrimers, owing to their unique properties, find applicability in a broad spectrum of biomedical and industrial domains. They possess empty internal cavities and numerous functional end groups contributing to high solubility and reactivity. Synthesized through an iterative sequence of reaction steps, each interaction in the process results in a higher generation dendrimer. In the pursuit of creating a delivery vehicle for poorly water-soluble anticancer agents, a collaborative effort between Boston University and the Research Triangle Institute (RTI) has yielded a biocompatible dendrimer. This dendrimer wraps around water-insoluble drugs, offering a promising solution for improving the solubility and delivery of anticancer agents. Polyamidoamine (PAMAM) dendrimers have received much attention for their ability to solubilize water -insoluble drugs and their ability to promote the transport of drugs across biomembranes (Kaurav et al., 2023; Abedi-Gaballu et al., 2018; Almalki et al., 2022; Bohr et al., 2020; Li et al., 2018 ; Prusty 2012).

Role of Nanomaterials in Exploring New Advances and Applications in Biomedicine

Nanomaterials mainly due to their high surface atom ratio, leading to modified physicochemical properties and heightened chemical reactivity, holds immense potential in these domains. CNTs, in particular, have emerged as a formidable tool to advance biomedical methodologies in treating of various diseases. The exceptional capability of CNTs to permeate cell membranes, coupled with the sp2 hybridization of all carbons, facilitates their functionalization with a many of bio molecules or compounds. This versatility enables them to target cells and deliver drugs in response to specific environmental stimuli. The diverse roles of nanomaterials in the 20th century are cited below

i. Theranostic Nanomaterials:

Theranostic is an emerging field that combines therapeutic and diagnostic capabilities in a single entity. Nanomaterials play a crucial role in theranostic by providing a platform for simultaneous disease detection, monitoring, and treatment. Nanoparticles loaded with therapeutic agents and imaging probes enable real-time monitoring of treatment progress, allowing clinicians to adjust therapies as needed (Chen et al., 2014; Jokerst et al., 2011; Xie et al., 2010).

ii. Nanomaterials in Imaging:

In biomedicine, imaging technologies have benefited mainly largely from nanomaterials. Nanomaterials like quantum dots, gold nanoparticles, and superparamagnetic iron oxide have all been employed as contrast agents in various imaging modalities, including fluorescence imaging, magnetic resonance imaging (MRI), and computed tomography (CT). These nanomaterials enhance the sensitivity and resolution of imaging techniques, enabling early disease detection and accurate diagnosis (Han et al., 2019).

iii. Nanomaterials in Regenerative Medicine:

Tissue engineering and regenerative medicine are rapidly advancing fields in today's world. These fields utilize nanomaterials to create biomimetic scaffolds and promote tissue regeneration. Nanofibers, hydrogel, and nanocomposites provide a three-dimensional environment that mimics the extracellular matrix and supports cell growth, differentiation, and tissue formation. Nanomaterials-based scaffolds have been used for bone, cartilage, skin, and nerve tissue regeneration (Arora et al., 2012).

iv. Nanomaterials for Cancer Therapy:

Nanomaterials due to their ability to target and selectively destroy cancer cells, they show immense promise in cancer treatment. Gold nanoparticles, for example, can be functionalized with antibodies to bind to cancer cells specifically. Once targeted, these nanoparticles can generate localized heat upon exposure to near-infrared light, leading to cancer cell death. Nanomaterials can also deliver chemotherapeutic drugs directly to tumor sites, minimizing systemic side effects.

So compared with traditional approach of drug therapy, the discovery and wide range of application of nanomaterials in biomedicine continues to provide better therapeutic effect by reducing toxicity. Though regulatory frameworks for the approval and use of nanomaterials-based products in medicine require careful consideration to ensure their effectiveness and safety, but still the multifunctional property of nanomaterials with integrated diagnostic, therapeutic, and targeting capabilities are expected to become more prevalent. As nanotechnology advances, personalized medicine and patient-tailored therapies will likely be enabled through the use of nanomaterials (Shan et al., 2022 ; Nazarkina et al., 2023 ; Zhou et al., 2023 ; Feng et al., 2022; Dallari et al., 2022; Galić et al., 2022; Feito et al., 2022; Arcos et al., 2023; Jiménez-Holguín et al., 2022).

Role of Nanomaterials in Exploring Novel Innovations and Applications in Drug Delivery

Nanotechnology makes a remarkable transformation in designing and, developing of innovative drug delivery systems (Marovic et al., 2022). Due to their extraordinary chemical diversity, chemical and biological properties with macromolecular specificity and less toxicity, their use as therapeutic agents increased rapidly in comparison to chemicals that are prepared by synthetic sources (Thilakarathna & Rupasinghe 2013 ; Chen et al., 2014; Swierczewska et al., 2016; Chen & Chen 2010; Yhee et al., 2014).

Role

i. Applications in Cancer Therapy

To overcome challenges and side effects associated with traditional therapy involved in treatment of cancer, nanomaterials are proved to be efficient. Lipid-based nanoparticles, such as liposomes and micelles, encapsulate chemotherapeutic drugs, enhancing their solubility and reducing systemic toxicity. Moreover, nanoparticles functionalized with tumor-specific ligands enable targeted drug delivery to cancer cells, minimizing damage to healthy tissues. This approach improves drug accumulation at tumor sites, increasing treatment efficacy.

ii. Innovative Drug Delivery Systems

Innovative nanomaterials-based drug delivery is used mainly in disease treatment to specific target cells. Stimuli-responsive nanoparticles can release drugs in response to changes in pH, temperature, enzyme activity, or other physiological conditions, improving therapeutic outcomes. For example, temperature-sensitive nanoparticles release drugs upon exposure to hyperthermia, a technique used in treating cancer (Liu et al., 2016).

iii. Enhanced Therapeutic Payload

Nanomaterials have enabled the delivery of a wide range of therapeutic agents beyond conventional small molecules, including genes, proteins, and RNA

molecules. Polymeric nanoparticles, for instance, can efficiently encapsulate nucleic acids and protect them from degradation. This capability holds great promise for gene therapy, where nucleic acids are delivered to correct genetic disorders or modulate gene expression to treat diseases.

iv. Overcoming Biological Barriers

Nanomaterials can overcome biological barriers that hinder effective drug delivery. Due to their surface modifications, nanoparticles can deliver medicaments to the brain bypassing the Blood Brain Barrier which will helpful for treating neurodegenerative diseases and brain tumours (Blanco et al., 2015; Maeda et al., 2013).

v. Personalized Medicine and Tailored Therapies

The advent of nanomaterials has paved the way for personalized medicine, where therapies are tailored to individual patients. These particles can carry specific drugs, diagnostics, and targeting ligands based on a patient's genetic profile and disease state. This approach maximizes treatment efficacy while minimizing adverse effects, leading to more precise and effective treatments.

So, the field of nanomaterials in drug delivery is rapidly evolving, with researchers continuously exploring new materials, fabrication techniques, and delivery strategies. Hybrid nanomaterials that combine the properties of multiple components are being developed to further enhance drug delivery efficiency. Integrating artificial intelligence and machine learning can also optimize the design and performance of nanomaterials-based drug delivery systems (Ryu et al., 2014).

Nanomaterials in Pharmaceutical Analysis

Nanomaterials have emerged as a revolutionary tool in pharmaceutical analysis, offering unparalleled opportunities to enhance sensitivity, selectivity, and efficiency in drug testing and quality control. With their unique physicochemical properties, nanomaterials have revolutionized various aspects of pharmaceutical analysis, enabling advancements in drug

detection, quantification, and characterization. This essay explores the recent findings and applications of nanomaterials in pharmaceutical analysis, shedding light on their transformative impact on the industry (Pandit &Zeugolis, 2016; Vertelov et al., 2007; Hernandez-Santos et al., 2002; Li et al., 2012; Kumar et al., 2015; Wolfbeis 2015).

Different Role

i. Nanomaterials in Drug Analysis

Nanomaterials have redefined drug analysis by providing novel platforms for the detection and quantification of pharmaceutical compounds. One significant application is chromatographic separations, where nanoparticles are utilized as stationary phases to improve resolution and selectivity. Using magnetic nanoparticles in sample preparation has also gained prominence, enabling efficient extraction and purification of analytes from complex matrices (Sharma &Chaudhery, 2020; Priscila et al., 2017).

ii. Nanoparticles in Spectroscopic Techniques

Spectroscopic techniques, such as UV-Vis, fluorescence, and Raman spectroscopy, have seen remarkable enhancements by incorporating of nanomaterials. Quantum dots, gold nanoparticles, and carbon nanotubes have been employed as labels or probes to amplify signals and increase sensitivity. Moreover, surface-enhanced Raman scattering (SERS) has leveraged the plasmonic properties of nanoparticles for ultrasensitive detection of drugs, even at trace levels.

iii. Nanomaterials in Mass Spectrometry

Nanomaterials have revolutionized mass spectrometry-based pharmaceutical analysis. Nanoparticles are employed as matrix-assisted laser desorption/ionization (MALDI) matrices, improving analyte ionization and detection. Additionally, nanomaterials such as graphene and metal-organic frameworks have been utilized for selective enrichment of analytes, enhancing detection limits and, reducing matrix interferences (Hecht et al., 2021).

iv. Biosensors and Nanomaterials

Nanomaterials-based biosensors have trans-

formed pharmaceutical analysis by providing rapid, specific, and sensitive detection methods. Nanoparticles are functionalized with bio receptors, such as antibodies or aptamers, to recognize target analytes. These biosensors have applications in detecting drugs, pathogens, and biomarkers, offering point-of-care diagnostics and real-time monitoring.

v. Nanomaterials for Imaging

Nanomaterials have enabled revolutionary advances in pharmaceutical imaging techniques. Various nanoparticles, such as magnetic nanoparticles, quantum dots, and silica nanoparticles, enhance the quality and sensitivity of imaging modalities like magnetic resonance imaging (MRI), computed tomography (CT), and fluorescence imaging. These advances have facilitated non-invasive monitoring of drug distribution, metabolism, and targeting within biological systems.

vi. Nanomaterials in Quality Control

Pharmaceutical quality control relies on rigorous testing to ensure drug safety and efficacy. Nanomaterials have streamlined this process by offering rapid and sensitive analytical methods. Nanoparticles can be used as indicators for colorimetric and electrochemical assays, providing easy-to-read results for pharmaceutical analysis. These tools expedite release testing and batch-to-batch consistency checks (Bhavyasri et al., 2023; Nkanga, 2023).

While integrating nanomaterials in pharmaceutical analysis holds immense potential, challenges persist. Issues related to reproducibility, standardization, and regulatory approval must be addressed. Additionally, nanomaterial's potential toxicity requires careful evaluation to ensure their safe application in pharmaceutical analysis. The future of nanomaterials in pharmaceutical analysis is promising. Continued research and development are expected to yield innovative nanomaterials-based analytical platforms, providing enhanced accuracy, speed, and sensitivity. As nanotechnology continues to evolve, collaborations between researchers, pharmaceutical companies, and regulatory bodies will be crucial to harness its full potential and ensure its safe and effective implementation.

654

CONCLUSIONS

So nanotechnology has led to the creation of a diverse array of nanomaterials with distinct properties, functionalities, and applications in every aspect of drug delivery and biomedicine, which will help in the longevity of human life span. These materials can encapsulate drug molecules, target them, and release therapeutic agents with precision, which has opened new avenues in personalized medicine and improved patient outcomes. Though these miracle particles are front runner in disease treatment, still many areas must have to be addressed and solved related to their stability, biocompatibility, and potential toxicity through thorough evaluation to ensure patient safety. Additionally, the scalability of nanomaterial synthesis and the regulatory approval process require careful consideration to bring these innovative technologies from the lab to clinical practice. As the field of nanomaterials continues to evolve, the pharmaceutical industry stands poised to benefit from their transformative impact, ultimately leading to safer and more effective drugs for patients worldwide.

AUTHOR CONTRIBUTION RATE STATEMENT

Determination of the Subject (AP), Literature Research (AP, SKP), Preparing the Study Text (AP, SKP), Reviewing the Text (AP, SKP)

CONFLICT OF INTEREST

The authors declare that there is no conflict of interest.

REFERENCES

Abedi-Gaballu, F., Dehghan, G., Ghaffari, M., Yekta, R., Abbaspour-Ravasjani, S., Baradaran, B., Dolatabadi, J. E. N., & Hamblin, M. R. (2018). PAMAM dendrimers as efficient drug and gene delivery nanosystems for cancer therapy. *Applied Materials Today*, 12, 177–190.

Alberto, B., Kostas, K., & Maurizio, P. (2005). Applications of carbon nanotubes in drug delivery. *Current Opinion in Chemical Biology, 9(6),* 674–679.

Almalki, Y. E., Ali, M. U., Kallu, K. D., Masud, M., Zafar, A., Alduraibi, S. K., Irfan, M., Basha, M. A. A., Alshamrani, H. A., Alduraibi, A. K., & Aboualkheir, M. (2022). Isolated Convolutional-Neural-Network-Based Deep-Feature Extraction for Brain Tumor Classification Using Shallow Classifier. *Diagnostics (Basel, Switzerland)*, *12*(8), 1793.

Arcos, D., &Portolés, M.T. (2023). Mesoporous Bioactive Nanoparticles for Bone Tissue Applications. *International Journal of Molecular Sciences, 24,* 3249.

Arora, P., Sindhu, A., Dilbaghi, N., Chaudhury, A., Rajakumar, G., &Rahuman, A.A. (2012). Nano-regenerative medicine towards clinical outcome of stem cell and tissue engineering in humans. *Journal of Cellular and Molecular Medicine*, 16(9), 1991- 2000

Arruebo, M. (2011). Drug delivery from structured porous inorganic materials. *Wiley Interdisciplinary Reviews: Nanomedicine and Nanobiotechnology. 4*(1), 16-30.

Ashwin, A.B, Patel, V., Julie, G., Guofeng, Z., Alioscka, A.S., Andrius, S., Richard, D.L., Roberto, W., Silvio, G.J., & James, F.R. (2009). Targeted Killing of Cancer Cells i*n Vivo and in Vitro* with EGF-Directed Carbon Nanotube-Based Drug Delivery. *ACS Nano, 3(2),* 307–316.

Beutler, J.A. (2009). Natural products as a foundation for drug discovery. *Current Protocols in Pharmacology, 46(1),* 9–11.

Bhavyasri, K., Reddy, A.B., Sumakanth, M. (2023). Analytical methods for quality control of nanoformulations-a review. *Asian Journal of Pharmacy and Clinical Research, 16*(10*),* 1-6.

Blanco, E., Shen, H., & Ferrari, M. (2015). Principles of nanoparticle design for overcoming biological barriers to drug delivery. *Natural Biotechnology*, 33(9), 941-51.

Bohr, A., Tsapis, N., Foged, C., Andreana, I., Yang, M., & Fattal, E. (2020). Treatment of acute lung inflammation by pulmonary delivery of anti-TNF-α siRNA with PAMAM dendrimers in a murine model. *European journal of pharmaceutics and biopharmaceutics*, *156*, 114–120.

Bolshakova, O. I., Slobodina, A.D., &Sarantseva, S.V. (2022). Carbon Nanoparticles as Promising Neuroprotectors: Pro et Contra. I. Functionalization and Toxicity. *Nanotechnology Russia, 17*, 132–140.

Cano, A., Ettcheto, M., Chang, J.H., Barroso, E., Espina, M., & Kuhne, B.A. et al. (2019). Dual-drug loaded nanoparticles of Epigallocatechin-3-gallate (EGCG)/Ascorbic acid enhance therapeutic efficacy of EGCG in a APPswe/PS1dE9 Alzheimer's disease mice model. *Journal of Control Release, 301*, 62–75.

Chen, D., Yu, H., Sun, K., Liu, W., & Wang, H. (2014). Dual thermo responsive and pH- responsive self-assembled micellar nanogel for anticancer drug delivery. *Drug Delivery, 21,* 258–264.

Chen, F., Ehlerding, E. B., & Cai, W. (2014). Theranostic nanoparticles. *Journal of Nuclear Medicine*, *55*(12), 1919-22. doi: 10.2967/jnumed.114.146019.

Chen, F., Ehlerding, E.B., Cai, W. (2014). Theranostic nanoparticles. *Journal of Nuclear Medicine, 55*, 1919–22.

Chen, K., Chen, X. (2010). Design and development of molecular imaging probes. *Current Topics in Medicinal Chemistry, 10*, 1227–36.

Contreras-Cáceres, R., Cabeza, L., Perazzoli, G., Díaz, A., López-Romero, J. M., Melguizo, C., & Prados, J. (2019). Electrospun Nanofibers: Recent Applications in Drug Delivery and Cancer Therapy. *Nanomaterials (Basel, Switzerland), 9*(4), 656.

Dallari, C., Innocenti, R., Lenci, E., Trabocchi, A., Pavone, F.S., & Credi, C. (2022). Design and Synthesis of Novel Raman Reporters for Bioorthogonal SERS Nanoprobes Engineering. *International Journal of Molecular Sciences, 23*, 5573.

Din, F. U., Aman, W., Ullah, I., Qureshi, O.S., Mustapha, O., Shafique, S. & Zeb, A. (2017). Effective use of nanocarriers as drug delivery systems for the treatment of selected tumours. *International Journal of Nanomedicine, 12*, 7291-7309.

Doktorovova, S., Souto, E.B., & Silva, A.M. (2014). Nanotoxicology applied to solid lipid nanoparticles and nanostructured lipid carriers—A systematic review of in vitro data. *European Journal of PharmBiopharm, 87*, 1–18.

Egwu CO, Aloke C, Onwe KT, Umoke CI, Nwafor J, Eyo RA, Chukwu JA, Ufebe GO, Ladokun J, Audu DT, et al. (2024). Nanomaterials in Drug Delivery: Strengths and Opportunities in Medicine. *Molecules*, *29*(11), 2584. https://doi.org/10.3390/molecules29112584

Etheridge, M.L., Campbell, S.A., Erdman, A.G, Haynes, C.L., Wolf, S.M., & McCullough, J. (2013). The big picture on nanomedicine: the state of investigational and approved nanomedicine products. *Nanomedicine, 9(1),* 1-14.

Fay, F., Hansen, L., Hectors, S.J.C.G., Sanchez-Gaytan, B.L., Zhao, Y., Tang, J., et al. (2017). Investigating the Cellular Specificity in Tumors of a Surface-Converting Nanoparticle by Multimodal Imaging. *Bioconjugate Chemistry, 28(5),* 1413-1421.

Feito, M.J., Cicuéndez, M., Casarrubios, L., Diez-Orejas, R., Fatiexa, S., Silva, D., Barroca, N., Marques, P.A., &Portolés, M.T. (2022). Effects of Graphene Oxide and Reduced Graphene Oxide Nanostructures on CD4+ Th2 Lymphocytes. *International Journal of Molecular Sciences, 23*, 10625.

Feng, Y., Wang, J., Hou, J., Zhng, X., Gao, Y., & Wang, K. (2022). Facet-Dependent SERS Activity of Co3O4. *International Journal of Molecular Sciences, 23*, 15930. doi: 10.3390/ijms232415930.

Galić, E., Radić, K., Golub, N., Čepo, D.V., Kalćec, N., Vrćek, E., & Vincović, T. (2022). Utilization of Olive Pomace in Green Synthesis of Selenium Nanoparticles: Physico- Chemical Characterization, Bioaccessibility and Biocompatibility. *International Journal of Molecular Sciences*, 9128.

Gupta, P., & Nayak, S. (2019). Theoretical studies on drug delivery using carbon nanotubes. *Journal of Theoretical and Computational Chemistry*, *18*(03).

Hainfeld, J.F., Lin L, Slatkin DN, Avraham Dilmanian F, Vadas T.M. & Smilowitz H. M. (2014). Gold nanoparticle hyperthermia reduces radiotherapy dose. *Nanomedicine, 10(8),* 1609-1617.

Harris PJF. (2009). Carbon Nanotube Science: Synthesis, Properties and Applications. Cambridge University Press.

Han, X., Xu, K., Taratula, O., & Farsad, K. (2019). Applications of nanoparticles in biomedical imaging. *Nanoscale, 11(3)*, 799-819. doi: 10.1039/c8nr07769j.

Hecht, E. S., Scigelova, M. Eliuk, S., & A. Makarov, A. (2019). Fundamentals and Advances of Orbitrap Mass Spectrometry, in Encyclopedia of Analytical Chemistry, ed. R.A. Meyers. https://doi.org/10.1002/9780470027318.a9309.pub2

Hernandez-Santos, D., Gonza lez-García, M.B., García, A.C. (2002). Metal-nanoparticles based electroanalysis. *Electroanalysis.* *14*(18), 1225–1235.

Jawahar, N., & Meyyanathan, S. (2012). Polymeric nanoparticles for drug delivery and targeting: A comprehensive review. *International Journal of Health and Allied Sciences, 1*, 217.

Jiménez-Holguín, J., Arcos, D., Lozano, D., Saiz-Pardo, M., de Pablo, D., Ortega, L., Enciso, S., Fernández,-Tomé, B., Díaz-Güemes, I. & Sánchez-Margallo, F.M. (2022). *In Vitro and In Vivo* Response of Zinc-Containing Mesoporous Bioactive Glasses in a Sheep Animal Model. *International Journal of Molecular Sciences, 23*, 13918.

Jokerst. J.V., & Gambhir, S. S. (2011). Molecular imaging with theranostic nanoparticles. *Accounts of Chemical Research, 44*(10), 1050–1060

Kaurav, M., Ruhi, S., Al-Goshae, H. A., Jeppu, A. K., Ramachandran, D., Sahu, R. K., Sarkar, A. K., Khan, J., & Ashif Ikbal, A. M. (2023). Dendrimer: An update on recent developments and future opportunities for the brain tumors diagnosis and treatment. *Frontiers in Pharmacology, 14*, 1159131.

Khakpour, S., Hosano, N., Moosavi-Nejad, Z., Farajian, A. A., & Hosano, H. (2024). Advancing Tumor Therapy: Development and Utilization of Protein-Based Nanoparticles. *Pharmaceutics*, *16*(7)887. https://doi.org/10.3390/pharmaceutics16070887

Kumar, N., Stephanidis, B., Zenobi, R., Wain, A.J., Roy, D. (2015). Nanoscale mapping of catalytic activity using tip-enhanced Raman spectroscopy. *Nanoscale, 7(16),* 7133– 7137.

Li, J, Liang, H., Liu, J., & Wang, Z. (2018). Poly (amidoamine) (PAMAM) dendrimer mediated delivery of drug and pDNA/siRNA for cancer therapy. *International Journal of Pharmaceutics*, *546*(1-2), 215–225. https://doi.org/10.1016/j.ijpharm.2018.05.045

Li, Y., Jing, C., Zhang, L., Long, Y.T. (2012). Resonance scattering particles as biological nanosensors in vitro and in vivo. *Chemical Society Review, 41(2),* 632–642.

Li, Y., Wang, X., Gao, Y., Zhang, Z., Liu, T., Zhang, Z., Wang, Y., Chang, F., & Yang, M. (2024). Hyaluronic acid-coated polypeptide nanogel enhances specific distribution and therapy of tacrolimus in rheumatoid arthritis. *Journal of Nanobiotechnology*, *22*(1), 547.

Liu, D., Yang, F., Xiong, F., & Gu, N. (2016). The Smart Drug Delivery System and Its Clinical Potential. *Theranostics, 6*(9), 1306-23

Liu, Y., Wang, M., Liu, W., Jing, J., & Ma, H. (2022). Olaparib and Doxorubicin Co-Loaded Polypeptide Nanogel for Enhanced Breast Cancer Therapy. *Frontiers in bioengineering and biotechnology*, *10,* 904344.

Liwei,X., Tongqi, S., Xinyue, X., Lide, Z., Li, S. (2019). Platelets membrane camouflaged irinotecan-loaded gelatin nanogels for in vivo colorectal carcinoma therapy. J. *Drug Deliv. Sci. Technol., 53*, 101190.

Maeda, H., Nakamura, H., & Fang, J. (2013). The EPR effect for macromolecular drug delivery to solid tumors: Improvement of tumor uptake, lowering of systemic toxicity, and distinct tumor imaging in vivo. *Advanced Drug Delivery Reviews*, *65*, 71–79

Marovic, D., Par, M., Tauböck, T., Huegen, H.J., Mandic, V.N., Wüthrich, D., Burrer, P., Zheng, K., Attin, T. &Tarle, Z. (2022). Impact of Copper-Doped Mesoporous Bioactive Glass Nanospheres on the Polymerisation Kinetics and Shrinkage Stress of Dental Resin Composites. *International Journal of Molecular Sciences, 23,* 8195.

Mishra, S., & Sahu, S. (2020). Computational modeling of drug delivery using boron nitride nanotubes. *Journal of Molecular Modeling*, 26(1), 1-10.

Mohanty, S.K., Swamy, M.K., Sinniah, U.R.& Anuradha, M. (2017). Leptadenia reticulata (Retz.) Wight &Arn. (Jivanti): botanical, agronomical, phytochemical, pharmacological, and biotechnological aspects. *Molecules, 22.*

Murphy, E.A., Majeti, B.K., Mukthavaram, R., Acevedo, L.M., Barnes, L.A., &Cheresh, D.A. (2011). Targeted nanogels: A versatile platform for drug delivery to tumors. *Molecular Cancer Therapeutics, 10*, 972–982.

Nazarkina, Z.K., Stepanova, A.O., Chelobanov, B.P., Kvon, R.I., Simonov, P.A., & Karpenko, A.A. et al. (2023). Activated Carbon-Enriched Electrospun-Produced Scaffolds for Drug Delivery/Release in Biological Systems. *International Journal of Molecular Sciences, 24,* 6713.

Nkanga, C.I. (2023). Nanotoxicological profiles of clinically approved nanoplatforms. *Beni- Suef Univ Journal of Basic Appllied Science, 12*, 115. https://doi.org/10.1186/s43088- 023-00458-6

Oh, N.M., Oh, K.T., Baik, H.J., Lee, B.R., Lee, A.H., & Youn, Y.S. et al. (2010). A self- organized 3-diethylaminopropyl-bearing glycol chitosan nanogel for tumor acidic pH targeting: In vitro evaluation. *Colloids Surf B Biointerfaces, 78,* 120–126.

Pandit, A., Zeugolis, D.I. (2016). Twenty-five years of nano-bio-materials: have we revolutionized healthcare? *Future Medicine, 11*(9), 985–7.

Priscila, A., Pedro H.B.A., Leonardo N. F., Alvaro E. A., & Carlos J. L. (2017). Constantino, 3 - Spectroscopic Techniques for Characterization of Nanomaterials, Nanocharacterization Techniques, William Andrew Publishing, Pages 65-98.

Prusty, A. (2012). Dendrimer-The recent drug delivery system. *International Research Journal of Pharmacy*, 3(2), 10-12.

Rodrigues, T., Reker, D., Schneider, P. & Schneider, G. (2016). Counting on natural products for drug design. *Natural Chemistry, 8*, 531.

Rozhin, P., Abdel Monem Gamal, J., Giordani, S., &Marchesan, S. (2022). Carbon Nanomaterials (CNMs) and Enzymes: From Nanozymes to CNM-Enzyme Conjugates and Biodegradation. *Materials (Basel), 15(3),* 103.

Ryu, J.H., Na, J.H., Ko, H.K., You, D.G., Park, S., Jun, E., Yeom, H.J., Seo, D.H., Park, J.H., Jeong, S.Y. (2014). Non-invasive optical imaging of cathepsin B with activatable fluorogenic nanoprobes in various metastatic models. *Biomaterials, 35,* 2302–11.

Sarma, K. N., Thalluri, C., & Mandhadi, J. R. (2024). Nanofibers in Drug Delivery Systems: A Comprehensive Scientific Review of Recent Approaches. *International Journal of Pharmaceutical Investigation*, *14*(3), 633–646. https://doi.org/10.5530/ijpi.14.3.75

Shan, X., Gong, X., Li, J., Wen, J., Li, Y., & Zhang, Z. (2022). Current approaches of nanomedicines in the market and various stage of clinical translation. *Acta Pharmaceutica Sinica B, 12,* 3028–3048.

Sharma, D. &Chaudhery, M. H., (2020). Smart nanomaterials in pharmaceutical analysis. *Arabian Journal of Chemistry, 13*(1), 3319-3343

Siddiqui, A.A., Iram, F., Siddiqui, S. & Sahu, K. (2014). Role of natural products in drug discovery process. *International Journal of Drug Development and Research, 6(2),* 172–204.

Soppimath, K.S., Aminabhavi, T.M., Kulkarni, A.R., & Rudzinski, W.E. (2001). Biodegradable polymeric nanoparticles as drug delivery devices. *Journal of Control Release, 70,* 1–20.

Swamy, M.K. &Sinniah, U.R. (2016). Patchouli (Pogostemoncablin Benth.): botany, agrotechnology and biotechnological aspects. *Industrial Crops and Products, 87,* 161–76.

Swierczewska, M., Han, H., Kim, K., Park, J., Lee, S. (2016). Polysaccharide-based nanoparticles for theranostic nanomedicine. *Advanced Drug DeliveryReview, 99,* 70– 84.

Thakur, P.S., & Sankar, M. (2023). Nanofibers for drug delivery, Advanced and Modern Approaches for Drug Delivery. Academic Press. Pages 493-514.

Thilakarathna, S.H.& Rupasinghe, H. (2013). Flavonoid bioavailability and attempts for bioavailability enhancement. *Nutrients,. 5,* 3367–87.

Vallet-Regí, M. (2006). Ordered Mesoporous Materials in the Context of Drug Delivery Systems and Bone Tissue Engineering. *Chemistry – A European Journal, 12*(23), 5934-5943.

Vertelov, G.K., Olenin, A.Y., Lisichkin, G.V. (2007). Use of nanoparticles in the electrochemical analysis of biological samples. *Journal of Analytical Chemistry, 62*(9), 813–824.

Wang, S. (2009). Ordered mesoporous materials for drug delivery. *Microporous and Mesoporous Materials, 117(1),* 1-9.

Wang, Y., Xu, H., Wang, J., Ge, L., & Zhu, J. (2014). Development of a thermally responsive nanogel based on chitosan-poly (*N*-isopropylacrylamide-co-acrylamide) for paclitaxel delivery. *Journal of Pharmaceutical Sciences, 103,* 2012–2021.

Wilczewska, A.Z., Niemirowicz, K., Markiewicz, K. H. & Car, H. (2012). Nanoparticles as drug delivery systems. *Pharmacological Reports 64*, 1020-1037.

Wolfbeis, O.S. (2015). An overview of nanoparticles commonly used in fluorescent bio imaging. *Chemical Society Review, 44*(14), 4743–4768.

Wu, H.Q., & Wang, C.C. (2016). Biodegradable Smart Nanogels: A New Platform for Targeting Drug Delivery and Biomedical Diagnostics. *Langmuir, 32,* 6211–6225.

Xiao, Z., Ji, C., Shi, J., Pridgen, E.M., Frieder, J., Wu, J., &Farokhzad, O.C. (2012). DNA self-assembly of targeted near-infrared-responsive gold nanoparticles for cancer thermo-chemotherapy. *AngewandteChemie International Edition, 51(47),* 11853-7.

Xie, J., Lee, S., & Chen, X. (2010). Nanoparticle-based theranostic agents. Advanced Drug Delivery Reviews, *62*(11), 1064–1079.

Yhee, J.Y., Son, S., Kim, S.H., Park, K., Choi, K., Kwon, I.C. (2014). Self-assembled glycol chitosan nanoparticles for disease-specific theranostics. *Journal of Controlled Release, 193,* 202–13.

Zhou, Q., Quirk, J.D., Hu, Y., Yan, H., Gaut, J.P., Pham, & C.T.N. et al. (2023). Rapamycin Perfluorocarbon Nanoparticle Mitigates Cisplatin-Induced Acute Kidney Injury. *International Journal of Molecular Sciences, 24,* 6086. doi: 10.3390/ijms24076086.

Zhu, Y., Ang Thiam, P., Keith, C., John, A.M., Narayan, H.S., & Masao, T. (2005). Substituted Carborane-Appended Water-Soluble Single-Wall Carbon Nanotubes: New Approach to Boron Neutron Capture Therapy Drug Delivery". *Journal of the American Chemical Society, 127*(27), 9875–9880.

Zhu, Y.& Narayan, H.S (2017). A Collection of Invited papers at 16th International meeting on Boron Chemistry (IMEBORON-16), Hongkong, 9-13 July 2017.